UNIVERSIDADE DE LISBOA

Faculdade de Medicina de Lisboa

Pathogenesis of Gammaherpesviruses Based upon Structural Data

Sofia Isabel Arriaga Mimoso Cerqueira

Supervisor: Prof. Doutor João Pedro Monteiro e Louro Machado de Simas

Thesis specially elaborated for the degree of Doctor of Philosophy in Biomedical Sciences (Specialization in Microbiology and Parasitology)

2016

As opiniões expressas nesta publicação são da exclusiva responsabilidade do seu autor.

UNIVERSIDADE DE LISBOA

Faculdade de Medicina de Lisboa

Pathogenesis of Gammaherpesviruses Based upon Structural Data

Sofia Isabel Arriaga Mimoso Cerqueira

Supervisor: Prof. Doutor João Pedro Monteiro e Louro Machado de Simas

Thesis specially elaborated for the degree of Doctor of Philosophy in Biomedical Sciences (Specialization in Microbiology and Parasitology)

Júri:

Presidente: Doutor José Augusto Gamito Melo Cristino, Professor Catedrático e Presidente do Conselho Científico da Faculdade de Medicina da Universidade de Lisboa

Vogais:

- Doutora Maria Arménia Abreu Fonseca de Carvalho Teixeira Carrondo, Professora Catedrática do Instituto de Tecnologia Química e Biológica da Universidade Nova de Lisboa
- Doutor Adriano José Alves de Oliveira Henriques, Professor Associado do Instituto de Tecnologia Química e Biológica da Universidade Nova de Lisboa
- Doutor Luís Ricardo Simões da Silva Graça, Professor Associado com Agregação da Faculdade de Medicina da Universidade de Lisboa
- Doutor Nuno Fernando Duarte Cordeiro Correia dos Santos, Professor Associado com Agregação da Faculdade de Medicina da Universidade de Lisboa
- Doutor Mário Nuno Ramos d'Almeida Ramirez, Professor Associado com Agregação da Faculdade de Medicina da Universidade de Lisboa
- Doutor João Pedro Monteiro e Louro Machado de Simas, Professor Associado da Faculdade de Medicina da Universidade de Lisboa (*Orientador*)

The author was recipient of a scholarship from Fundação para a Ciência e a Tecnologia (SFRH/BD/80152/2011)

2016

A impressão desta tese foi aprovada pelo Conselho Científico da Faculdade de Medicina de Lisboa em reunião de 17 de Novembro de 2015.

PREFACE

The current thesis presents data obtained during my PhD research project, developed at Instituto de Medicina Molecular (iMM Lisboa) in the period of January 2012 to April 2015, under the supervision of Professor Doutor João Pedro Simas (Faculdade de Medicina, Universidade de Lisboa). My PhD work was inserted into the project «Pathogenesis of Kaposi's sarcoma herpesvirus LANA», in the scope of Harvard Medical School-Portugal (HMS-PT) Program in Translational Research and Information, from Fundação para a Ciência e a Tecnologia (FCT). This was a project involving three research teams: Prof. Kenneth M. Kaye Laboratory (Harvard Medical School, USA), Prof. Mª Arménia Carrondo and Dr Colin E. McVey Laboratory (Instituto de Tecnologia Química e Biológica, Universidade Nova de Lisboa, Portugal), and Prof. J. Pedro Simas Laboratory (Instituto de Medicina Molecular, Faculdade de Medicina da Universidade de Lisboa, Portugal), the coordinator of the project. The work presented in chapter 5 of this thesis was performed in strict collaboration with Dr Min Tan from Prof. K.M. Kaye Lab and results presented in Figure 5.4 were obtained by him. In addition, the work performed in chapter 6 was developed in collaboration with Dr Imre Berger (European Molecular Biology Laboratory, Grenoble, France), who received me in his laboratory for two weeks during June 2012, where the results presented in Figures 6.3 and 6.4 were generated by me.

This thesis is organized in eight chapters, which are preceded by a summary written in Portuguese and an abstract. Before the description of the results, an introductory review of the subject is provided in chapter 1, followed by the aims of the work. In chapters 2, 3, 4, 5 and 6 the original data obtained during this research project are presented and discussed. Final considerations, which integrate the results presented in previous chapters as well as future directions, are presented in chapter 7. Finally, chapter 8 concerns the description of the materials and methodologies employed to carry out the presented work. The publications that resulted from the research carried out throughout the duration of this project are included in appendix 1 and 2.

Data presented in this dissertation were purely the result of work carried out by me, except for results presented in Figure 5.4, and it is clearly acknowledged in the text whenever data or reagents produced by others were utilized. This work has not been submitted for any degree at this or any university.

PUBLICATIONS

Appendix 1

Correia, B.*, Cerqueira, S.A.*, Beauchemin, C., Pires de Miranda, M., Li, S., Ponnusamy, R., Rodrigues, L., Schneider, T.R., Carrondo, M.A., Kaye, K.M., Simas, J.P., and McVey, C.E. (2013). Crystal structure of the gamma-2 herpesvirus LANA DNA binding domain identifies charged surface residues which impact viral latency. PLoS Pathog. 9, e1003673. *shared first authorship

Construction of recombinant viruses and all animal experiments presented in this publication (Figure 5 and Table 4) were performed by me.

This article was published back to back with two other articles from independent teams, led by Prof. Thomas F. Schulz (Hellert *et al.*, 2013) and Prof. Paul M. Lieberman (Domsic *et al.*, 2013).

Appendix 2

Cerqueira, S.A.*, Tan, M.*, Li, S., Juillard, F., McVey, C.E., Kaye, K.M., and Simas, J.P. LANA E3 ubiquitin-ligase activity impacts gammaherpesvirus latent infection. *In preparation*. *shared first authorship

Data presented in Figures 4, 5 and 7, and Tables 1 and 2 were obtained by me. The MuHV-4 ORF50-deficient recombinant viruses and the cell lines latently infected with these viruses used in Figure 8, panel D were generated by me.

These publications result from the work performed by the consortium in the scope of the HMS-PT Program.

ACKNOWLEDGEMENTS

Em primeiro lugar, quero agradecer ao meu supervisor, Prof. Doutor J. Pedro Simas, pela oportunidade de realizar o meu doutoramento no seu laboratório A sua orientação científica, conselhos, ensinamentos e o interesse demonstrado ao longo do meu doutoramento foram fundamentais. Agradeço-lhe ainda a possibilidade de integrar uma equipa de investigação multidisciplinar, no âmbito do programa «HMS-PT Program in Translational Research and Information» da FCT, que em muito contribuiu para a minha formação científica.

Quero também agradecer à Faculdade de Medicina de Lisboa por me ter aceitado enquanto estudante de doutoramento, bem como ao Instituto de Medicina Molecular por me ter proporcionado as condições apropriadas para o desenvolvimento do meu projecto. Agradeço ainda aos membros do meu comité de tese, Prof. Doutor João Ferreira e Doutor Colin E. McVey, pelas críticas construtivas.

Um agradecimento especial a todos os membros presentes e passados da Unidade de Patogénese Viral pelo apoio, conselhos e amizade. Em particular, agradeço à Lénia Rodrigues, pelos conhecimentos transmitidos, orientação, proteção e, sobretudo, pela grande amizade demonstrada. Obrigada à Marta Miranda e à Sofia Marques por partilharem comigo a sua experiência e conhecimento, à Cristina pelos muitos ensinamentos, pela inspiração e pelos bons momentos no final dos dias trabalhosos, à Diana pela ajuda e enorme cumplicidade, à Inês pela boa disposição, à Ana Lopes por todas as encomendas e confidências, à Teresa por ser “a minha professora preferida”, à Filipa pela rapidez com que me ensinou tanto, à Marta Alenquer e ao Jérémie.

Agradeço também aos investigadores e funcionários do instituto que, pela constante ajuda e disponibilidade, contribuíram para este trabalho. Em particular, agradeço aos membros da Unidade de Citometria de Fluxo e da Unidade de Histologia pelo apoio prestado, e ainda aos membros da Unidade de Reumatologia, pela boa vizinhança e companheirismo.

I would like to thank all the members of HMS-PT team, for great scientific discussion and for the good times we spent. Special thanks should go to Prof. Kenneth M. Kaye, for his invaluable collaboration and for sharing with us his scientific expertise in the field, Dr Min Tan, for his participation in complementing my PhD project, Dr Colin E. McVey, for guiding me through the fascinating world of protein structure, and Dr Rajesh Ponnusamy, for being so helpful in providing me the figures showing mLANA structural features. Further thanks go to Dr Imre Berger, who kindly received me in his laboratory, and to all the members of his team, particularly Fred and Alice.

Por fim, agradeço à minha família e aos meus amigos todo o apoio e motivação. Ao David, por estar sempre ao meu lado e me aceitar como sou. E à minha mãe, pelo amor incondicional que tem suportado a minha vida.

RESUMO

A principal característica dos herpesvírus é a sua capacidade de estabelecerem infeções latentes que persistem durante toda a vida do hospedeiro. Os gamaherpesvírus, em particular, são importantes agentes com potencial oncogénico que estabelecem latência em linfócitos, especialmente células B. Para persistirem no hospedeiro, os gamaherpesvírus exploram o ciclo de vida normal da célula B, induzindo a proliferação de células B latentemente infetadas em centros germinativos e a sua posterior diferenciação em células B de memória de longa duração. Durante a latência, o genoma viral é mantido sob a forma de um episssoma circular extracromossomal no núcleo da célula hospedeira e a expressão de proteínas virais é limitada. Assim, é necessário que os episssomas virais repliquem em sincronia com a divisão celular e que sejam segregados para os núcleos-filhos após a mitose, de modo a persistirem em células em proliferação. Este processo é controlado por proteínas de manutenção do episssoma, codificadas pelos gamaherpesvírus. Os gama-2-herpesvírus, como o vírus associado ao sarcoma de Kaposi (KSHV) ou o herpesvirus de murganho-4 (MuHV-4), expressam uma proteína associada à latência (LANA) que medeia a persistência do episssoma, através da ligação a repetições terminais (TRs) presentes no genoma viral. LANA regula também a transcrição celular através da sua atividade de ubiquitina-ligase E3. A estrutura cristalina do domínio de ligação ao DNA (DBD) de LANA foi recentemente resolvida, revelando várias características estruturais que se encontram associadas a funções específicas da proteína. O estudo dos mecanismos subjacentes às funções de LANA é de extrema importância, uma vez que esta proteína é essencial para o estabelecimento e manutenção da infeção latente *in vivo*. Contudo, a contribuição individual de cada uma das funções atribuídas a LANA no decorrer da infeção natural do hospedeiro encontra-se ainda pouco caracterizada.

A estrita especificidade de hospedeiro dos gamaherpesvírus humanos, o vírus Epstein-Barr (EBV) e o vírus KSHV, tem limitado os estudos *in vivo*. O gamaherpesvírus MuHV-4 é um parasita natural de roedores selvagens, geneticamente relacionado com os gamaherpesvírus humanos e que, à semelhança destes, infeta latentemente células B, induzindo a sua proliferação em centros germinativos e posterior diferenciação em células B de memória, como estratégia para persistir durante toda a vida do hospedeiro. Além disso, a proteína LANA de MuHV-4 (mLANA) apresenta homologia aminoacídica, estrutural e funcional com a proteína LANA de KSHV (kLANA), representando assim um modelo para o estudo da patogénese de LANA *in vivo*, usando um modelo de infeção animal. Esta tese teve como principal objetivo avaliar o papel de determinadas funções de LANA no contexto da infeção latente *in vivo* por gamaherpesvírus, recorrendo à infeção de ratinhos de laboratório com o vírus MuHV-4 como modelo experimental. Com este propósito, foram construídos vírus MuHV-4 recombinantes contendo mutações baseadas na estrutura do DBD de mLANA, de modo a interferir com interfaces específicas da proteína. A capacidade destes recombinantes estabelecerem e manterem uma infeção latente foi analisada após infeção intranasal de ratinhos.

A estrutura cristalina do DBD de mLANA permitiu identificar uma interface de ligação ao DNA, a qual possibilita a interação de mLANA com as sequências TRs do DNA viral. Para avaliar a importância desta interação no contexto da infeção latente *in vivo*, construiu-se um vírus recombinante contendo mLANA incapaz de se ligar às TRs, devido a mutações específicas na interface de ligação ao DNA. Seguidamente, procedeu-se à infeção intranasal de ratinhos com o vírus recombinante e analisou-se o comportamento do mesmo durante o estabelecimento e manutenção da latência. Os resultados obtidos demonstraram que a ligação de mLANA às TRs do DNA viral é essencial para a expansão da latência em células B do centro germinativo, bem como para a persistência do vírus no hospedeiro. Estas experiências validam assim a importância da ligação de mLANA ao DNA viral durante a infeção latente *in vivo*, indicando ainda que a incapacidade do vírus amplificar a latência em células B dos centros germinativos tem consequências severas na manutenção da infeção latente a longo termo, o que suporta o modelo proposto para a infeção por gamaherpesvírus.

No lado oposto à interface de ligação ao DNA de mLANA encontra-se uma região extensa de resíduos carregados positivamente, designada região positiva dorsal. Para investigar o papel funcional desta região na infeção latente *in vivo*, foram construídos vírus MuHV-4 recombinantes contendo mutações na periferia ou na zona central da região positiva dorsal de mLANA. Os vírus foram administrados intranasalmente a ratinhos e o efeito das mutações introduzidas em mLANA no estabelecimento e na manutenção da latência foi avaliado. Os resultados obtidos demonstraram que a região positiva dorsal, particularmente a zona periférica, é necessária para a eficiente expansão da latência em células B do centro germinativo. As mutações na zona central tiveram um impacto menor na latência. Embora estudos anteriores tenham demonstrado que a região positiva dorsal de mLANA está envolvida na ligação à proteína celular Brd4, os resultados obtidos neste estudo não permitiram estabelecer uma relação entre os fenótipos observados e a perda de ligação a Brd4. Deste modo, o mecanismo através do qual a região positiva dorsal de mLANA exerce a sua função permanece desconhecido.

Estudos anteriores realizados no nosso laboratório demonstraram que mLANA promove a formação de um complexo de ubiquitina-ligase através do recrutamento das proteínas celulares ElonguinaB/C e Culina5, de modo a promover a poli-ubiquitinação e consequente regulação de dois fatores de transcrição celulares: o fator nuclear kappa B (NF-κB) e Myc. A interação de mLANA com a ElonguinaB/C e com a Culina5 é mediada pelo motivo supressor da sinalização por citocinas (SOCS-box), presente em mLANA, o qual se localiza perpendicularmente à interface de ligação ao DNA. Para esclarecer a relevância biológica da atividade de ubiquitina-ligase de mLANA, foram construídos vírus MuHV-4 recombinantes contendo mutações na SOCS-box de mLANA. Estas mutações foram introduzidas tendo em conta a estrutura do DBD, de modo a inibir a função de ubiquitina-ligase de mLANA sem interferir com a sua função de manutenção do episssoma viral. Os vírus recombinantes foram administrados intranasalmente a ratinhos e o seu fenótipo foi depois analisado durante o estabelecimento e manutenção da latência. As mutações introduzidas resultaram numa atenuação dos níveis de latência no baço, demonstrando que a atividade de ubiquitina-ligase de mLANA contribui para a amplificação da latência viral *in vivo*.

Embora não tenha sido possível inibir completamente a atividade de ubiquitina-ligase de mLANA, o facto de uma inibição parcial desta função ter sido suficiente para reduzir os níveis de latência sugere que a SOCS-box poderá ser um alvo farmacológico para inibir a atividade de ubiquitina-ligase de mLANA e, consequentemente, controlar a infeção viral.

Durante o estudo do impacto da atividade de ubiquitina-ligase de mLANA *in vivo*, foi identificado um vírus recombinante capaz de expandir a latência em ratinhos apesar de conter mutações em mLANA que comprometiam severamente a ligação às TRs do DNA viral, eliminando assim a persistência do episssoma. Tendo em conta que, conforme demonstrado no presente estudo, a ligação de mLANA às TRs é fundamental para o estabelecimento e manutenção da latência *in vivo*, equacionou-se a hipótese de que este mutante, $mLANA_{V199A/L202A}$, seria capaz de mediar a manutenção do episssoma, mas o ensaio usado para testar esta função não seria suficientemente sensível, devido à presença de um número de cópias de TRs inferior ao número de cópias presente no genoma viral completo. Para determinar se o mutante $mLANA_{V199A/L202A}$ seria capaz de mediar a persistência do episssoma no contexto do genoma viral completo, estabeleceram-se linhas celulares latentemente infetadas com um vírus MuHV-4 deficiente em ORF50, o qual é incapaz de replicação lítica, contendo as mutações V199A/L202A em mLANA ($vORF50^{-}mLANA_{V199A/L202A}$). A presença de episssomas foi posteriormente analisada em gel Gardella. Os resultados obtidos revelaram a presença de episssomas em todas as linhas celulares infetadas com $vORF50^{-}mLANA_{V199A/L202A}$, demonstrando que mLANA é capaz de mediar a persistência do episssoma na presença de mutações que reduzem consideravelmente a sua ligação às TRs, dependendo do número de cópias de TRs existentes nos episssomas. Estes resultados sugerem que a ligação de mLANA a múltiplas cópias de TRs poderá compensar perdas consideráveis na capacidade de ligação ao DNA, de modo a manter eficazmente o episssoma.

Além dos estudos de patogénese anteriormente referidos, no âmbito desta tese testou-se também a possibilidade de expressão de mLANA na sua forma completa em células de inseto, usando baculovírus. Os resultados mostraram que bons níveis de expressão de mLANA podem ser obtidos recorrendo a este sistema de expressão. Esta descoberta poderá contribuir para a futura resolução da estrutura cristalina de mLANA na forma completa, uma vez que apenas a estrutura do seu DBD C-terminal é conhecida, facilitando assim o estudo de outras funções de mLANA *in vivo*, com base em dados estruturais.

Globalmente, os resultados apresentados nesta tese validam o papel essencial de LANA na infeção latente por gamaherpesvírus, evidenciando ainda a vantagem da realização de estudos de patogénese baseados em informação estrutural. Assim, este estudo sugere que a inibição farmacológica de determinadas funções de LANA, usando como alvo características estruturais associadas a funções específicas da proteína, poderá ser uma estratégia para controlar a infeção latente por gamaherpesvírus e as patologias relacionadas.

Palavras-chave: gamaherpesvírus; proteína associada à latência; manutenção do episssoma; região positiva dorsal; ubiquitina-ligase

ABSTRACT

The hallmark of herpesviruses is the establishment of lifelong latent infections in specific cell types. Gammaherpesviruses, a herpesvirus subfamily with causative roles in several malignancies, drive proliferation of latently infected B cells in germinal centres (GCs) to expand latency and to achieve long-term persistence in memory B cells. During latency, the viral genome is maintained as a non-integrated circular episome within the host cell nucleus, and viral protein expression is highly restricted. To persist in proliferating cells, viral episomes must replicate in step with normal cell division and segregate to newly formed nuclei after mitosis. This process is mediated by gammaherpesvirus episome maintenance proteins. In particular, gamma-2-herpesviruses encode a latency-associated nuclear antigen (LANA), which has been shown to mediate episome persistence and is also known as a cellular transcription modulator, including through E3 ubiquitin-ligase activity. Remarkably, the crystal structure of LANA DNA binding domain has been solved and revealed several structural features that are associated with specific LANA functions.

The aim of this thesis was to address the role of particular LANA functions in the context of gammaherpesvirus latent infection *in vivo*, using infection of laboratory mouse with murid herpesvirus-4 (MuHV-4) as an experimental model. To this end, MuHV-4 recombinant viruses harbouring structure-based mutations targeting specific MuHV-4 LANA (mLANA) interfaces were engineered, and the ability of these recombinants to establish and maintain latent infection was analysed upon intranasal infection of mice. These experiments demonstrated that mLANA binding to terminal repeat (TR) elements in viral DNA is essential for latency expansion in GC B cells and persistence in the host. Interestingly, mLANA was capable of mediating episome persistence despite mutations that resulted in considerably reduced TR DNA binding, depending on TR elements number present in episomes. This work also showed that the novel mLANA dorsal positive patch, opposite to the DNA binding interface, is required for efficient latency expansion in GC B cells. In addition, recombinants bearing mutations in mLANA suppressor of cytokine signalling (SOCS)-box, which lies within a loop protruding perpendicular to the DNA binding interface, exhibited an attenuation of latency levels in spleen, demonstrating that mLANA E3 ubiquitin-ligase activity contributes to latency amplification.

Overall, these findings validate LANA as an essential player in gammaherpesvirus latent infection and reveal the advantage of performing pathogenesis studies guided by structural data. Hence, this study constitutes a primer for pharmacological inhibition of LANA functions, through targeting of specific structural features, as a putative strategy to control gammaherpesvirus latent infection and associated pathologies.

Keywords: gammaherpesvirus; latency-associated nuclear antigen; episome maintenance; dorsal positive patch; E3 ubiquitin-ligase

ABBREVIATIONS

AcNPV	*Autographa californica* nuclear polyhedrosis virus
AIDS	acquired immunodeficiency syndrome
AP	alkaline phosphatase
APS	ammonium persulfate
ATP	adenosine triphosphate
BAC	bacterial artificial chromosome
BAFF	B cell-activating factor
BAFF-R	BAFF receptor
BCR	B cell receptor
BET	bromodomain and extra-terminal
BHK	baby hamster kidney
BLAST	Basic Local Alignment Search Tool
bp	base pair
CI	confidence interval
cpe	cytopathic effect
CRL5	Cullin5-RING E3 ubiquitin-ligase
CSR	class switch recombination
CTL	cytotoxic T lymphocyte
DBD	DNA binding domain
DIG	digoxigenin
DMEM	Dulbecco's modified Eagle's medium
DNA	deoxyribonucleic acid
dNTP	deoxynucleotide
dpa	day of proliferation arrest
dpi	days post-infection
DTT	dithiothreitol
EBER	EBV-encoded RNA
EBNA	EBV nuclear antigen
EBV	Epstein-Barr virus
EC_5S	ElonginBC/Cullin5/SOCS
EC_5S^{kLANA}	ElonginBC/Cullin5/SOCS-kLANA
EC_5S^{mLANA}	ElonginBC/Cullin5/SOCS-mLANA
EDTA	ethylenediaminetetraacetic acid
eGFP	enhanced green fluorescent protein
EMBL	European Molecular Biology Laboratory
ERK1	extracellular signal-regulated kinase 1
FACS	flow activated cell sorting

FBS	foetal bovine serum
FC	flow cytometry
FCT	Fundação para a Ciência e a Tecnologia
GC	germinal centre
GFP	green fluorescent protein
GMEM	Glasgow's modified Eagle's medium
GPT	guanosine phosphoribosyl transferase
GSK-3	glycogen synthase kinase-3
h	hour
HCMV	human cytomegalovirus
HECT	homology to E6AP C-terminus
HEK	human embryonic kidney
HHV	human herpesvirus
HIV	human immunodeficiency virus
HMW	high molecular weight
HMS-PT	Harvard Medical School-Portugal
HRP	horseradish peroxidase
HSV	herpes simplex virus
hTERT	human telomerase reverse transcriptase
IgG	class G immunoglobulin
IL-8	interleukin-8
IPTG	isopropyl-β-D-thiogalactopyranoside
ITQB	Instituto de Tecnologia Química e Biológica
κB	kappa B
kDa	kilodaltons
kLANA	KSHV latency-associated nuclear antigen
KS	Kaposi’s sarcoma
KSHV	Kaposi’s sarcoma-associated herpesvirus
LANA	latency-associated nuclear antigen
LB	Luria Bertani
LBS	LANA binding site
LMP	latent membrane protein
Luc	luciferase
MCD	multicentric Castleman’s disease
MCM	mini-chromosomal maintenance protein
MEF	mouse embryonic fibroblast
MHC	major histocompatibility complex
MHV-68	murine gammaherpesvirus-68
min	minute
miRNA	microRNA

mLANA	MuHV-4 latency-associated nuclear antigen
mLBS	MuHV-4 LANA binding site
MPA	mycophenolic acid
MOI	multiplicity of infection
MuHV-4	murid herpesvirus-4
MZ	marginal zone
NBT	nitroblue tetrazolium chloride
NCBI	National Centre for Biotechnology Information
NF-κB	nuclear factor-kappa B
NK	natural killer
nt	nucleotide
NTA	nitrilotriacetic acid
OD	optical density
ON	overnight
ORC	origin recognition complex
ORF	open reading frame
PBS	phosphate-buffered saline
PBS-T	PBS-Tween
PCR	polymerase chain reaction
PEL	primary effusion lymphoma
PFU	plaque forming unit
polyA	polyadenylation
RBL	red blood cell lysis
RBR	RING-between-RING
RFC	replication factor C
RING	really interesting new gene
RNA	ribonucleic acid
rpm	revolutions per minute
RT	room temperature
SAXS	small-angle X-ray scattering
SDS	sodium dodecyl sulfate
SDS-PAGE	SDS-polyacrylamide gel electrophoresis
Sf	*Spodoptera frugiperda*
SHM	somatic hypermutation
SHPM	single-hit Poison Model
SL	soluble lysate
SOCS	suppressor of cytokine signalling
SSC	saline sodium citrate
TAE	Tris-acetate-EDTA
TCR	T cell receptor

TE	Tris-EDTA
TEMED	tetramethylethylenediamine
TNF	tumour necrosis factor
TPB	tryptose phosphate broth
TR	terminal repeat
tRNA	transferRNA
UV	ultraviolet
vFLIP	viral Fas-associated death domain-like interleukin-1β-converting enzyme-inhibitory protein
VHL	von Hippel-Lindau
vIRF-3	viral interferon regulatory factor-3
VZV	varicella-zoster virus
WB	Western-blot
WCE	whole cell extract
WT	wild-type
YFP	yellow fluorescent protein

TABLE OF CONTENTS

INDEX OF FIGURES

INDEX OF TABLES

CHAPTER 1

Introduction

Introduction

Gammaherpesviruses, such as the human viruses Epstein-Barr virus and Kaposi´s sarcoma-associated herpesvirus, establish lifelong latent infections in B lymphocytes and exert causative roles in several malignancies. During latency, the viral genome is maintained as a non-integrated circular episome within the host cell nucleus, and viral protein expression is highly restricted. To persist in proliferating cells, viral episomes must replicate in step with normal cell division and segregate to newly formed nuclei after mitosis. This process is mediated by gammaherpesvirus episome maintenance proteins. Gamma-2-herpesviruses, a genus of gammaherpesvirus, encode a latency-associated nuclear antigen (LANA), which mediates episome persistence. In addition, LANA proteins have been described as cellular transcription modulators. Since LANA is essential for latent infection, understanding the mechanisms underlying its functions offers an opportunity to control gammaherpesvirus infection and associated pathologies. This introductory chapter will mainly focus on the current knowledge on gammaherpesvirus latency and LANA structure and function.

1.1. Herpesvirus

1.1.1. General properties

Herpesviridae is a family of enveloped viruses containing large linear double-stranded DNA genomes (>100 kb) with a vast coding capacity. Herpesviruses are widely disseminated in vertebrate species, with a large spectrum of animals harbouring at least one of these viruses. However, each herpesvirus exhibits a very narrow host range. Herpesviruses are remarkably well-adapted to their hosts, probably due to a long co-evolutionary history. Thus, herpesvirus infection of a natural immunocompetent host is rarely fatal, promoting virus transmission (Barton *et al.*, 2011; Davison, 2002; Wu *et al.*, 2010).

The hallmark of herpesviruses is the establishment of latent infections which persist for the life of the host. During latency, herpesviruses persist as a non-infectious form, from which they periodically reactivate to disseminate to new hosts. Most herpesvirus infections are asymptomatic or cause a mild illness, but effects can be devastating in immunocompromised hosts (Barton *et al.*, 2011; Wu *et al.*, 2010).

Herpesviruses have biphasic life cycles consisting of a lytic and a latent phase. Upon transmission to a naïve host, the virus establishes a productive acute infection at the site of infection, usually the epithelium of a mucosal surface. During this lytic phase, there is a sequential order of viral gene expression and the viral genome is replicated several times, leading to the

production of infectious virion progeny and the death of the infected cell. This primary infection is rapidly resolved by the host immune system and results in effective immunity against reinfection (Stoopler, 2005; Wu *et al.*, 2010).

The lytic infection is followed by a lifelong latent infection in a specific type of cells. The targeted cell type is herpesvirus specific and is usually different from the cell type harbouring the productive infection. During latency, limited gene expression occurs. No virions are produced and viral genome is maintained as a non-integrated circular episome in the nucleus of the infected cell, being replicated by host DNA polymerase and equally distributed to daughter cells, when the latently infected cell divides during the course of cellular growth. The expression of viral proteins is severely reduced to those required for maintenance of viral genome, manipulation of host cell function and evasion of the host immune system. By expressing few proteins during latency, the virus limits the amount of antigen produced, thereby reducing the chance of being detected by the host immune system. A critical aspect of latency is the ability of the virus to sporadically reactivate in response to specific signals, ensuring the transmission of infectious virions to new hosts, as well as reinfection and establishment of latent infection in more cells of the same individual, thereby establishing a reservoir of infection for life (Barton *et al.*, 2011; Wu *et al.*, 2010).

Herpesviridae family is divided into three subfamilies: *Alphaherpesvirinae*, *Betaherpesvirinae* and *Gammaherpesvirinae*. Alphaherpesviruses establish latency mainly in neurons, betaherpesviruses in myeloid cells, and gammaherpesviruses in lymphocytes. Humans are the natural hosts of eight herpesviruses: herpes simplex virus (HSV)-1, HSV-2, and varicella-zoster virus (VZV) (*Alphaherpesvirinae*); human cytomegalovirus (HCMV), human herpesvirus (HHV)-6, and HHV-7 (*Betaherpesvirinae*); Epstein-Barr virus (EBV), and Kaposi's sarcoma-associated herpesvirus (KSHV), also known as HHV-8 (*Gammaherpesvirinae*) (Davison, 2002; Stevenson *et al.*, 2009; Wu *et al.*, 2010). Since the work presented in this thesis is focused on the pathogenesis of gammaherpesvirus latent infection, only this subfamily will be described in detail in the following sections.

1.1.2. The subfamily *Gammaherpesvirinae*

Members of the subfamily *Gammaherpesvirinae* are lymphotropic viruses, with the majority establishing latency in B lymphocytes. Gammaherpesviruses drive the proliferation of latently infected lymphocytes, in order to establish and maintain a large reservoir of latent viral genomes, and thus efficiently colonize the host. However, virus-driven lymphoproliferation is associated with the development of lymphoproliferative diseases, as well as several lymphoid and non-lymphoid cancers, since several gammaherpesviruses are able to induce neoplasia in natural or experimental hosts (Barton *et al.*, 2011; Damania, 2004; Stevenson, 2004).

Gammaherpesvirinae subfamily is further subdivided into four genera, based on DNA homology and genomic organization, being *Lymphocryptovirus* and *Rhadinovirus* the two main genera. Lymphocryptoviruses (or gamma-1-herpesviruses) have only been identified in primates, whereas Rhadinoviruses (or gamma-2-herpesviruses) infect a wide range of mammalian species, including primates (Barton *et al.*, 2011; Davison *et al.*, 2009; Simas and Efstathiou, 1998).

Gammaherpesviruses exhibit a very narrow host tropism, limiting the study of the human gammaherpesviruses EBV and KSHV. For this reason, there has been considerable interest in developing animal models to investigate the pathogenesis of human gammaherpesviruses. In particular, infection of laboratory mice with murid herpesvirus-4 (MuHV-4) has proved to be a good model system (Barton *et al.*, 2011; Nash *et al.*, 2001; Simas and Efstathiou, 1998). The following sections of this thesis will focus on the two known human gammaherpesviruses and then on MuHV-4 as an experimental model for the study of gammaherpesvirus pathogenesis.

1.2. Epstein-Barr virus (EBV)

Epstein-Barr virus (EBV), a gamma-1-herpesvirus, was discovered more than 50 years ago in cultured tumour cells derived from Burkitt's lymphoma tissue (Epstein *et al.*, 1964). This was the first human tumour virus ever described (Thorley-Lawson and Allday, 2008). EBV prevalence in the normal population is extremely high, reaching over 95% of the adult population worldwide (Kutok and Wang, 2006; Lieberman, 2014). Primary EBV infection generally occurs in the first decade of life and is usually asymptomatic. However, if the infection is acquired during adolescence or later, it can result in infectious mononucleosis, a self-limiting lymphoproliferative disease (Henle *et al.*, 1968; Kutok and Wang, 2006). After primary infection, which is rapidly controlled by both cellular and humoral immune mechanisms, EBV persists in a quiescent state in resting memory B lymphocytes that circulate in the peripheral blood for the life of healthy carriers (Babcock *et al.*, 1998; Hislop *et al.*, 2007; Kutok and Wang, 2006). Persistent infection is characterized by stable low levels of latently infected memory B cells, as a consequence of the dynamic equilibrium between virus-driven B cell proliferation and host immune control. A low level of active viral replication continues asymptomatically in EBV carriers, leading to virus secretion into the saliva and transmission from one human to another through the oral route (Hislop *et al.*, 2007; Kutok and Wang, 2006).

Although EBV infection is benign and uneventful in the majority of humans, EBV has been associated with a number of diseases, particularly autoimmunity and cancer. Immunocompromised individuals are at risk for EBV lymphomas that are aggressive and often fatal (Table 1.1). However, EBV-associated malignancies can also develop in immunocompetent individuals (Table 1.1) (Kutok and Wang, 2006; Thorley-Lawson and Gross, 2004).

Table 1.1. EBV-associated diseases (adapted from Kutok and Wang, 2006).

Non-malignant disease		Infectious mononucleosis
		Chronic active infection
		Oral hairy leukoplakia
Malignant disease	Immunocompromised host	Acquired immunodeficiency syndrome (AIDS)-associated B cell lymphomas
		Post-transplant lymphoproliferative disorder
		Severe combined immunodeficiency-associated B cell lymphomas
		X-linked lymphoproliferative disorder-associated B cell lymphomas
	Immunocompetent host	Burkitt's lymphoma
		Classical Hodgkin's lymphoma
		T cell lymphomas
		Lymphoepithelioma-like carcinoma (salivary, thymus, lungs, stomach)

1.2.1. Germinal centre (GC) model of EBV infection

EBV is the best studied gammaherpesvirus and a biological model of EBV infection has been proposed, the germinal centre (GC) model. This model, described below, reveals strategies of infection which are believed to be common to all gammaherpesviruses that persist in B lymphocytes.

The GC model (Figure 1.1), proposed by Thorley-Lawson and co-workers, defends that EBV persists by exploiting normal B cell biology (Thorley-Lawson, 2001). This implies that new latently infected B cells pass through a series of differentiation stages, each employing a discrete viral gene transcription programme. Following oral transmission, EBV establishes a lytic infection in permissive cells of the oropharynx, leading to high levels of virus shedding in saliva. It is thought that both squamous epithelial cells and locally infiltrating B cells support this lytic infection. Thereafter, the virus colonises the general B cell system via growth-transforming latent infection of B cells in local lymphoid tissue such as the tonsil. According to the GC model, EBV directly infects naïve B cells, activating them into proliferating latently infected blasts. At this stage, EBV expresses its latency III or growth transcription programme (Table 1.2), which is characterized by the expression of the full repertoire of viral latent proteins: EBV nuclear antigens (EBNAs) 1, 2, 3A, 3B, 3C and LP, and latent membrane proteins (LMPs) 1, 2A and 2B. These proteins have all the necessary activities to push B cells to become activated blasts without external signalling (Babcock *et al.*, 2000; Joseph *et al.*, 2000; Thorley-Lawson, 2005). In culture, EBV immortalises human resting B cells by expressing the growth programme, driving the establishment of continuously proliferating lymphoblastoid cell lines (growth transformation or immortalisation) (Thorley-Lawson and Mann, 1985).

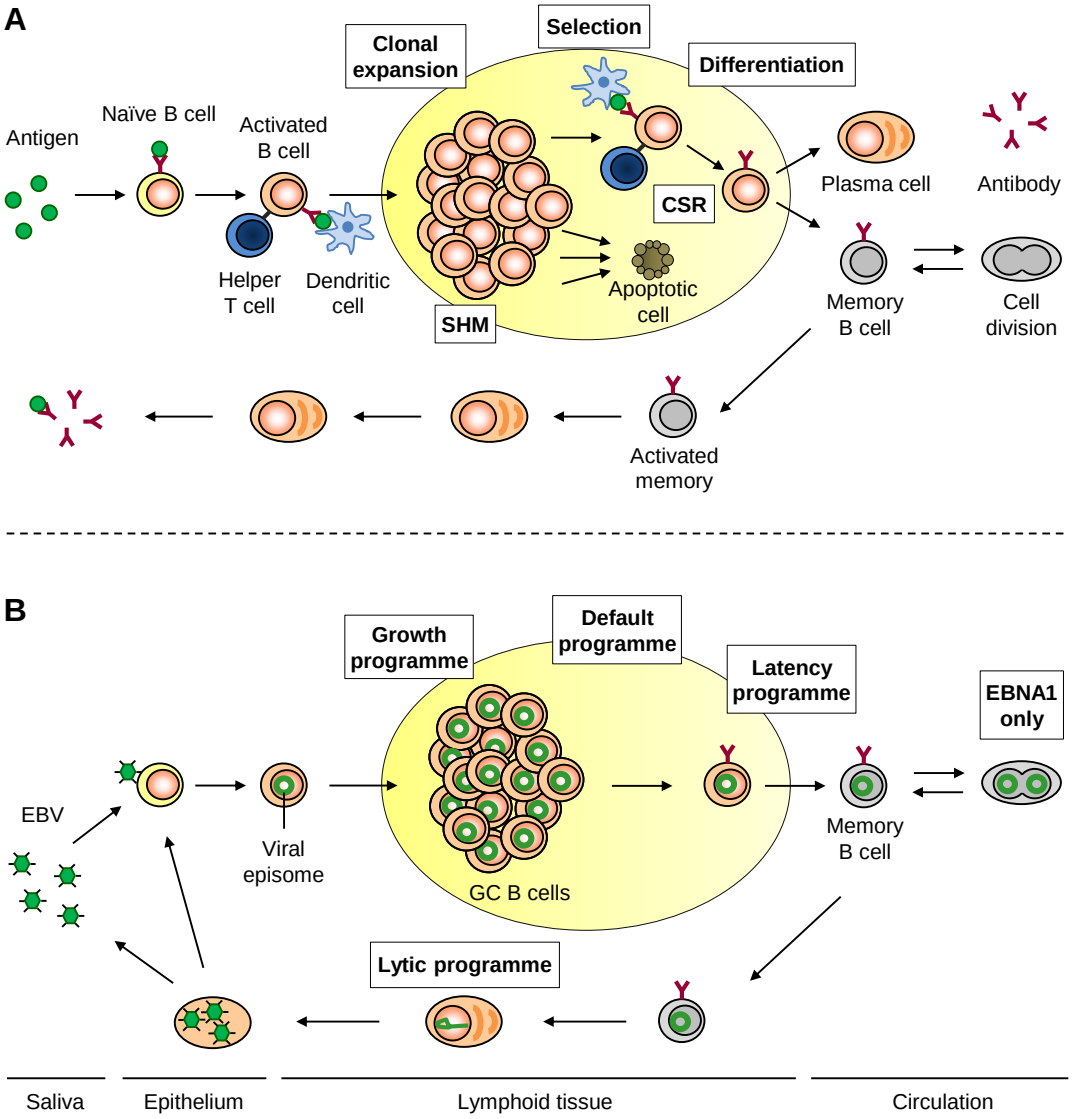

Figure 1.1. Normal B cell response and the parallel with the GC model of EBV persistence. (A) Normal B cell response. The epithelium of the tonsil continuously samples antigens entering the mouth. Underneath the epithelium, naïve B cells that encounter cognate antigen become activated and migrate into a follicle where they receive further activation signals from dendritic cells and helper T cells, and establish a GC reaction. In the GC, the blast undergoes repeated rounds of cell division, proliferating rapidly, in association with somatic hypermutation (SHM) and class switch recombination (CSR), followed by interaction with follicular dendritic cells and T cells to select those blasts that have the highest affinity for the antigen. The later receive further survival and differentiation signals, while the other cells die by apoptosis. The surviving ones differentiate into either a plasma cell or a memory B cell and leave the GC. Upon re-challenge with the antigen, memory B cells are quickly activated and differentiate into antibody producing plasma cells. (B) GC model of EBV persistence. EBV traverses the epithelium and infects a naïve B cell, activating it into a proliferating latently infected blast, as though the cell was responding to antigen, through expression of all nine known latent proteins, the growth transcription programme. These cells migrate to the follicle where the viral transcription programme changes to the more restricted default programme and a GC reaction is established. Subsequently the latently infected cells differentiate into memory B cells that leave the follicle. In the periphery, all viral protein expression is shut down, the latency programme, and the latently infected cells are maintained as normal memory B cells. These

memory B cells can occasionally divide to maintain the pool of latently infected cells and so express the genome tethering protein EBNA1, the EBNA1 only programme. At any time a small subset of latently infected memory B cells initiates lytic replication in association with terminal differentiation signals. Reactivation leads to the production of infectious virus and cell death. These virions can either replicate at a secondary tissue, where they are amplified and shed into saliva for transmission to new hosts, or infect new naïve B cells, thus restarting the cycle of infection (adapted from De Silva and Klein, 2015, Thorley-Lawson, 2005 and Thorley-Lawson *et al.*, 2013).

Table 1.2. Patterns of EBV latent gene expression in normal B cells and tumours (adapted from Thorley-Lawson, 2005).

Transcription programme	Genes expressed[a]	Infected normal B cell type	Function	Infected tumour type
Growth (Latency III)	EBNA1, 2, 3A, 3B, 3C and LP LMP1, 2A and 2B	Naïve	B cell activation	Immunoblastic lymphoma
Default (Latency II)	EBNA1, LMP1 and LMP2A	Germinal centre	Differentiation of activated B cell into memory	Hodgkin's disease
EBNA1 (Latency I)	EBNA1	Dividing memory	Cellular division of latently infected memory B cells	Burkitt's lymphoma
Latency (Latency 0)	None	Resting memory	Allows lifetime persistence	
Lytic	All lytic genes	Plasma cell	Viral replication in plasma cell	

[a]Does not include the non-coding EBER and BART RNAs.

Proliferating latently infected blasts then migrate into a follicle to participate in the GC reaction. Here, EBV expresses the latency II or default transcription programme (Table 1.2), consisting of a more restricted pattern of latent proteins: EBNA1, LMP1 and LMP2A. EBNA1 is required for replication and maintenance of the viral episome, mediating the association of viral genomes with host mitotic chromosomes, whereas LMP1 and LMP2A proteins provide the necessary surrogate signals to drive the differentiation of latently infected B cells into memory B cells that leave the GC and enter the peripheral circulation (Babcock *et al.*, 2000; Caldwell *et al.*, 1998; Casola *et al.*, 2004; Gires *et al.*, 1997; He *et al.*, 2003; Marechal *et al.*, 1999; Panagopoulos *et al.*, 2004; Roughan and Thorley-Lawson, 2009; Sears *et al.*, 2003; Thorley-Lawson, 2001; Yates *et al.*, 1985).

In latently infected memory B cells, EBV expresses either EBNA1 transcription programme (latency I) or latency transcription programme (latency 0) (Table 1.2). During EBNA1 transcription programme, EBV only expresses the viral genome tethering protein EBNA1, so that viral episomal DNA is maintained and segregated when B cells divide. In contrast, in the latency transcription programme no viral proteins are expressed at all. The memory compartment has been considered

the site of long-term persistence, since the virus is quiescent and hence invisible to the immune response (Babcock *et al.*, 2000; Hochberg *et al.*, 2004; Thorley-Lawson, 2001).

In addition to latent proteins, EBV expresses several non-coding RNAs and microRNAs (miRNAs) during latency (Kang and Kieff, 2015). EBV-encoded RNA (EBER) 1 and 2 are small non-coding RNAs abundantly expressed in latently infected cells (Lerner *et al.*, 1981). EBV-encoded miRNAs are expressed from two regions of EBV genome: BART and BHRF1. The EBV genome transcribes at least 25 pre-miRNAs and more than 40 mature miRNAs (Kang and Kieff, 2015; Lopes *et al.*, 2013). Similarly to latent proteins, EBV-encoded miRNAs exhibit distinct patterns of expression according to the EBV latency programme (Qiu *et al.*, 2011).

At any time, a small subset of latently infected memory B cells can reactivate and initiate lytic replication, which is thought to occur in response to the normal physiologic signals that drive terminal differentiation of memory B cells into plasma cells. Reactivation of EBV is subdivided into three phases: immediate early, when the transcription factors initiating viral replication are expressed, early, when the proteins involved in viral DNA replication are produced, and late, when viral DNA and structural proteins are assembled into virions. A crucial role for epithelial cells in amplifying the amount of infectious virus before shedding has been proposed. Released infectious virus can then be shed into saliva for viral spread to new hosts, or infect new naïve B cells, thus completing the cycle (Hadinoto *et al.*, 2009; Laichalk and Thorley-Lawson, 2005; Thorley-Lawson *et al.*, 2013).

Each stage of the cycle of EBV infection has been demonstrated experimentally (Babcock *et al.*, 1998; Babcock *et al.*, 2000; Laichalk and Thorley-Lawson, 2005) and, with the exception of the memory compartment, is potentially regulated by the host immune response (Hislop *et al.*, 2007). The GC model of EBV infection remains the only experimentally validated model that accounts for all the latent and lytic stages of the virus, providing an explanation for the origin and pathogenesis of EBV-associated lymphomas (Thorley-Lawson *et al.*, 2013). However, a quantitative analysis of viral persistence and an understanding of the dynamic interactions between the different components of the GC model and how their regulation by the immune system produces the EBV pattern of persistence has been lacking. Recently, a mathematical description of the GC model has been developed that successfully recapitulates persistent EBV infection, correctly predicting the observed patterns of cytotoxic T lymphocytes (CTLs) regulation and the size of the infected GC and memory B cell populations (Delgado-Eckert and Shapiro, 2011; Hawkins *et al.*, 2013). Importantly, this mathematical model predicts that it is the cycle of infection that explains persistence and provides the stability that allows EBV to persist at extremely low levels, rather than viral quiescence in the memory B cell compartment. This moves the focus away from a single infected stage, the memory B cell compartment, to the entire cycle of infection.

1.3. Kaposi's sarcoma-associated herpesvirus (KSHV)

Kaposi's sarcoma-associated herpesvirus (KSHV) was first discovered in 1994 by Chang and colleagues, from patients with Kaposi's sarcoma (KS) (Chang *et al.*, 1994). KSHV, also known as human herpesvirus-8 (HHV-8), is a gamma-2-herpesvirus with an etiologic role in KS, the most prevalent tumour among human immunodeficiency virus (HIV)/acquired immunodeficiency syndrome (AIDS) patients worldwide (Achenbach *et al.*, 2011). KSHV is also associated with other two human malignancies: primary effusion lymphoma (PEL) and multicentric Castleman's disease (MCD) (Cesarman *et al.*, 1995; Soulier *et al.*, 1995). KS tumours are comprised of KSHV-infected cells of endothelial origin, whereas PEL and MCD are of B cell origin. Furthermore, KSHV was recently associated with an inflammatory cytokine syndrome (Uldrick *et al.*, 2010).

Unlike EBV virus, KSHV is not ubiquitous. Among the general population, the seroprevalence of KSHV infection in northern Europe, Asia and America is less than 10%, but it reaches 30% in Mediterranean regions and over 50% in most of sub-Saharan Africa. The association between the incidence of KSHV-associated malignancies and KSHV seroprevalence is high. However, the presence of KSHV DNA alone in healthy individuals is not sufficient to cause disease, and the existence of cofactors as HIV infection or drug-induced immunosuppression are important for KSHV-associated disease progression. The transmission mode of KSHV has not been completely clarified yet. It is currently thought that KSHV is mainly transmitted through saliva, although transmission through organ transplants, blood and sexual fluids have also been documented (Cai *et al.*, 2010; Edelman, 2005; Mesri *et al.*, 2010; Uldrick and Whitby, 2011; Uppal *et al.*, 2014).

Being a herpesvirus, KSHV exhibits two distinct phases of infection: lytic replication and latency. Latency is characterized by limited gene expression without virion production, and it represents the main strategy used by the virus to escape host immune system, while maintaining its genome in infected cells. Periodically, the latent virus reactivates to enter lytic replication, during which the viral genes are fully expressed in a cascade manner (immediate early, early and late genes), leading to the production of infectious particles and transmission to new hosts. Little is known about KSHV primary infection, but there is evidence that it is benign in immunocompetent individuals, and it results in lifelong latency (Wang *et al.*, 2001; Wu *et al.*, 2012).

1.3.1. KSHV latency

During latency, KSHV genome is maintained as a circular episome within the host cell nucleus with highly restricted protein expression, in order to maintain the genome in the dividing cells and to limit host immune responses, while enhancing cell survival and virus persistence (Uppal *et al.*, 2014). Only a small portion of the viral genome is actively transcribed during latency. The major latency locus includes four viral genes, encoding KSHV latency-associated nuclear antigen

(kLANA)/ORF73, vCyclin/ORF72, viral Fas-associated death domain-like interleukin-1β-converting enzyme-inhibitory protein (vFLIP)/ORF71, and K12/Kaposin family (Kaposin A, B and C), as well as twelve viral pre-miRNAs (Cai *et al.*, 2005; Dittmer *et al.*, 1998). kLANA is the viral episome maintenance protein and, in addition, it exerts transcriptional regulatory activities and affects cell growth, through interaction with several cell proteins (Ballestas and Kaye, 2011). vCyclin, the viral homolog of cellular cyclin D, regulates cell cycle and proliferation, whereas vFLIP, the viral homolog of cellular FLIP, has a role in inhibition of apoptosis (Uppal *et al.*, 2014). The kLANA promoter controls the expression of kLANA, vCyclin and vFLIP, while the Kaposin promoter drives the expression of the three Kaposin transcripts, a bicistronic transcript for vCyclin and vFLIP, and the twelve viral pre-miRNAs which can be processed to yield mature miRNAs (Dittmer *et al.*, 1998; Pearce *et al.*, 2005). The major latency locus is abundantly and consistently transcribed in all latently infected cells (Speck and Ganem, 2010). Additionally, PEL cells, but not KS cells, express a second latency locus encoding viral interferon regulatory factor-3 (vIRF-3), also known as LANA-2, indicating that some latency genes may be lymphoid specific (Rivas *et al.*, 2001; Speck and Ganem, 2010). More recently, a third latency locus encoding K1 protein has been identified (Chandriani and Ganem, 2010). Other viral genes expressed during latency, although at low levels, include viral interleukin-6 (vIL-6) and K15 (Giffin and Damania, 2014).

In vivo, KSHV has been detected in endothelial cells, epithelial cells, B cells and monocytes (Ambroziak *et al.*, 1995; Blasig *et al.*, 1997; Dupin *et al.*, 1999; Pauk *et al.*, 2000). However, the main targets of KSHV long-term latent infection are B cells, particularly the subset expressing the lambda (λ) light chain of B cell receptor (Chadburn *et al.*, 2008; Hassman *et al.*, 2011). KSHV infection drives proliferation of primary B cells (Hassman *et al.*, 2011) and individual KSHV latent genes, specifically the ones encoding kLANA and vFLIP, induce B cell proliferative phenotypes in transgenic mice (Ballon *et al.*, 2011; Sin *et al.*, 2010). B cell specific expression of multiple KSHV latent proteins, including kLANA, vFLIP, vCyclin and Kaposin, as well as the viral miRNAs, leads to sustained hyperplasia, lymphoma and hyper-responsiveness to antigen stimulation in transgenic mice (Sin and Dittmer, 2013).

The mechanisms by which KSHV establishes and maintains latency are not as well understood as for EBV. However, the overall strategy is believed to be the same: subversion of normal B cell developmental pathways to induce cell proliferation and achieve long-term persistence. A putative model of KSHV B cell pathogenesis has been proposed (Dittmer and Damania, 2013). According to this model, the primary infection event drives the infected cell into an activated state. In non-permissive cell subtypes the virus is rapidly lost or the cell dies. In contrast, in cells permissive to the establishment of latency, the virus persists and confers a survival advantage to the infected cell. The molecular nature of this advantage and the exact complement of viral genes which confer it are not well defined. This model suggests that the establishment of KSHV latent infection is analogous to that of EBV, which starts with expressing a more extensive set of genes and then contracts to latency I or latency 0 transcription programmes.

1.4. Murid herpesvirus-4 (MuHV-4)

A major limitation to the study of the human gammaherpesviruses is the absence of a robust small animal model in which to investigate viral pathogenesis, due to the very narrow host tropism exhibited by EBV and KSHV (Barton *et al.*, 2011; Simas and Efstathiou, 1998). The identification of murid herpesvirus-4 (MuHV-4) (archetypal strain murine gammaherpesvirus-68 (MHV-68)) (Blaskovic *et al.*, 1980), a naturally occurring rodent pathogen, offered the possibility of developing a mouse model of gammaherpesvirus pathogenesis.

MuHV-4 was originally isolated from bank voles (*Myodes glareolus*) in Slovakia (Blaskovic *et al.*, 1980). Later studies indicated that this virus is endemic in wood mice (*Apodemus sylvaticus*) in the United Kingdom, suggesting that this may be the natural host species (Blasdell *et al.*, 2003). Like KSHV, MuHV-4 is a gamma-2-herpesvirus. Its genome consists of 118 kb of unique DNA sequence with a G+C content of 46%, flanked by a variable number of 1.2 kb terminal repeat (TR) regions (Efstathiou *et al.*, 1990). It is estimated that MuHV-4 genome contains approximately 80 protein-coding open reading frames (ORFs), the majority of which are collinear and homologous to those of other gammaherpesviruses, particularly KSHV (Virgin *et al.*, 1997). However, MuHV-4 genome harbours a number of genes unique to the virus (*M1-14*).

MuHV-4 readily infects laboratory mice (*Mus musculus*), in which it establishes a lifelong latent infection (Simas and Efstathiou, 1998). Similarly to EBV, MuHV-4 causes an acute infectious mononucleosis syndrome and exploits the normal B cell biology to colonize the host, driving proliferation of latently infected B cells in GC reactions to persist in memory B cells (Barton *et al.*, 2011; Doherty *et al.*, 1997; Flano *et al.*, 2002). Furthermore, persistent infection with MuHV-4 has been associated with increased frequencies of malignancies in mice with defective immune systems, mainly B cell lymphomas (Lee *et al.*, 2009; Sunil-Chandra *et al.*, 1994; Tarakanova *et al.*, 2005). MuHV-4 also provides an *in vivo* infection model in which host immune evasion mechanisms are preserved (Stevenson *et al.*, 2009). In addition, MuHV-4 genome can be readily manipulated, thereby allowing the generation of mutant viruses whose phenotype can be assessed in the mouse (Adler *et al.*, 2000). Therefore, MuHV-4 constitutes a unique experimental model for the study of gammaherpesvirus pathogenesis.

1.4.1. MuHV-4 model of infection

Following intranasal infection of laboratory mice, the primary site of productive virus replication is the lung, specifically alveolar epithelial cells (Figure 1.2) (Sunil-Chandra *et al.*, 1992a). MuHV-4 host entry is co-operative, as virion binding to heparan-expressing alveolar epithelial cells licenses alveolar macrophages infection, and this in turn licenses epithelial cells infection (Lawler *et al.*, 2015). Acute infection in the lung is resolved within 10 to 12 days post-infection (dpi) by host

immune system and is followed by lifelong latent infection in lymphoid tissue. Latency is established predominantly in B cells (Marques *et al.*, 2003; Sunil-Chandra *et al.*, 1992b), but is also established in macrophages, dendritic cells and lung epithelial cells (Flano *et al.*, 2000; Stewart *et al.*, 1998). Latent infection in the spleen is characterized by an initial proliferation of infected B cells and consequent amplification of the latent virus, reaching maximum levels around 14 dpi and decreasing thereafter to low levels, which remain stable throughout the entire life of the host without overt disease (Cardin *et al.*, 1996; Marques *et al.*, 2003; Simas and Efstathiou, 1998; Sunil-Chandra *et al.*, 1992b).

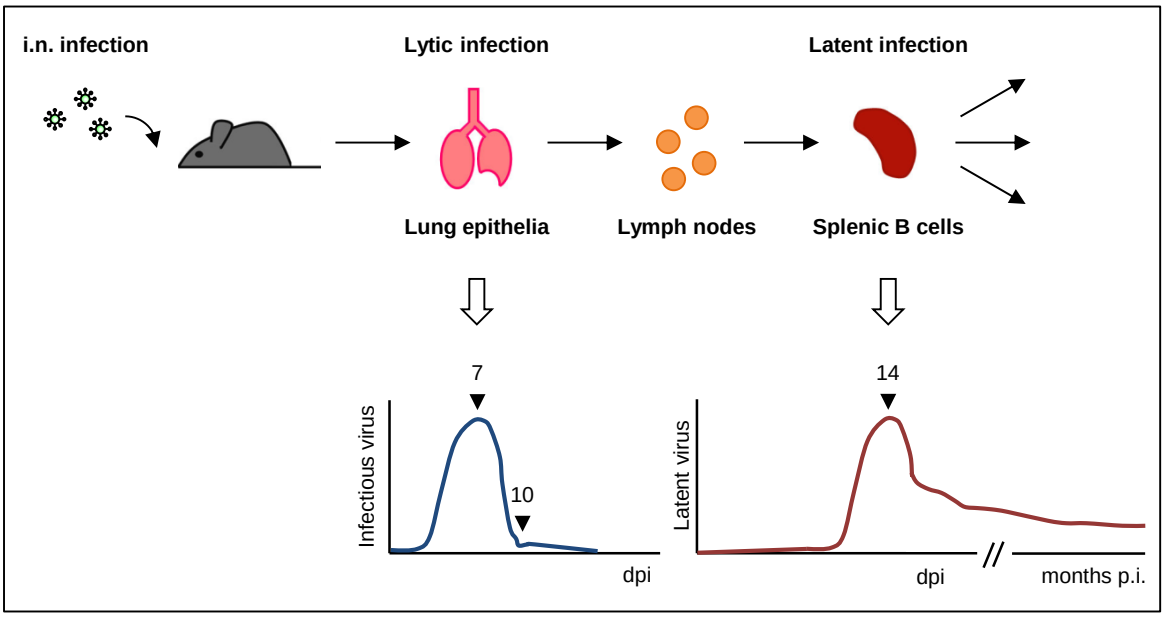

Figure 1.2. Model of MuHV-4 infection. After intranasal (i.n.) infection of inbred mice, MuHV-4 establishes a productive infection in the respiratory tract that peaks at around 4-7 dpi and is cleared to undetectable levels by 10-12 dpi. From the lung, the virus disseminates to the lymphoid tissue, with latent virus being first detected in the lymph nodes and subsequently in the spleen, mainly in B cells. During latent infection in the spleen there is an amplification of latent virus that reaches maximum levels at around 14 dpi and afterwards decreases to reach low steady-state levels of latently infected cells that persist for the lifetime of the host. From the spleen, the virus further disseminates to other sites, probably via infected memory B cells (adapted from (Stevenson *et al.*, 2002)). p.i., post-infection.

The peak of latent infection is accompanied by a transient splenomegaly and lymphadenopathy (Sunil-Chandra *et al.*, 1992a), due to the proliferation of latently infected B cells and to a large increase in $CD4^+$ and $CD8^+$ T cell numbers, dependent on $CD4^+$ T cells (Ehtisham *et al.*, 1993; Usherwood *et al.*, 1996a). This phase of infection is also accompanied by high levels of non-virus-specific antibodies and $CD8^+$ T cells in peripheral blood, thus resembling the infectious mononucleosis caused by EBV (Blackman *et al.*, 2000; Tripp *et al.*, 1997).

In agreement to what has been proposed for EBV, the establishment of MuHV-4 latent infection does not require a prior productive infection. In fact, latency is established in lung B cells as early as 3 days after respiratory inoculation, supporting the hypothesis that infection of B cells is a concurrent event with the ongoing lytic infection of the mucosal epithelium. Moreover, recombinant viruses that cannot undergo lytic replication still establish latency in mice. However, lytic replication is required for virus trafficking and establishment of latency in the spleen (Flano *et al.*, 2005; Moser *et al.*, 2006).

In vitro, MuHV-4 productively infects epithelial cells and fibroblasts from a variety of species, ranging from chickens to primates (Svobodova *et al.*, 1982), and latently infects murine B cell lines (Sunil-Chandra *et al.*, 1993). MuHV-4-positive B cell lines have been established from tumours of infected mice, of which S11 is the best characterized (Usherwood *et al.*, 1996b). Infection of primary B cells with MuHV-4 results in their activation and increased proliferation, however the cells do not become transformed and usually die within two weeks (Dutia *et al.*, 1999; Stevenson and Doherty, 1999). MuHV-4 has been shown to immortalize only foetal B cells *in vitro* (Liang *et al.*, 2011).

1.4.2. MuHV-4 latency

MuHV-4 enters new hosts via the olfactory neuroepithelium (Milho *et al.*, 2012) or genital tract (Francois *et al.*, 2013), dendritic cells take it to lymph nodes (Gaspar *et al.*, 2011), and from there it reaches the spleen. This epithelial/myeloid/lymphoid MuHV-4 infection pathway (Frederico *et al.*, 2012) is thus quite different from the epithelial cell/B cell exchange proposed for EBV (Borza and Hutt-Fletcher, 2002). Then, MuHV-4 enters the spleen by infecting marginal zone (MZ) macrophages, which provide a conduit to MZ B cells. These cells relocate to the white pulp, allowing virus transfer to follicular dendritic cells, which appear to transfer the virus without becoming infected (analogous to their presentation of immune complexes to GC B cells), and from there the virus reaches GC B cells to establish persistent infection. Therefore, MuHV-4 exploits the normal splenic immune communication routes to spread by serial myeloid/lymphoid exchange (Frederico *et al.*, 2014a).

Early in latency, MuHV-4 infection is found in naïve, GC, memory and plasma B cells (Collins *et al.*, 2009; Flano *et al.*, 2002; Marques *et al.*, 2003; Willer and Speck, 2003), as well as in macrophages and dendritic cells (Flano *et al.*, 2000). However, at the peak of latent infection, the majority of latently infected cells correspond to B cells proliferating in GCs. This proliferation leads to the amplification of the pool of latently infected cells**,** which reaches maximal levels at 2 to 3 weeks post-infection (Cardin *et al.*, 1996; Marques *et al.*, 2003; Simas and Efstathiou, 1998). Subsequently, most GCs regress and there is a consequent decline in the latent load to a low steady state that persists for the lifetime of the host. Hence, latency in naïve and GC B cells, as

well as in non-B cell reservoirs, wanes as time progresses, and at late times post-infection viral latency is predominantly maintained in isotype-switched memory B cells (Flano *et al.*, 2002; Willer and Speck, 2003). GC B cell proliferation and differentiation into memory B cells are critical for maintenance of MuHV-4 long-term persistence (Kim *et al.*, 2003; Moser *et al.*, 2005). In fact, although several B cell subsets can be initially infected by the virus, only the ones that access a GC and differentiate into memory B cells are capable of maintaining long-term viral latent infection. Thus, MuHV-4 exploits the normal B cell developmental pathways, taking advantage of the GC reaction to expand the pool of latently infected cells, and later to induce their differentiation into long-lived memory B cells, similarly to what has been proposed for EBV latency.

MuHV-4-driven activation, proliferation and differentiation of latently infected B cells are dependent on $CD4^+$ T cell help (Collins and Speck, 2014; Stevenson and Doherty, 1999; Usherwood *et al.*, 1996a), CD40 ligand (Brooks *et al.*, 1999) and CD40 (Kim *et al.*, 2003), implying that MuHV-4 relies on normal T cell help to enter the GC reaction and differentiate into a memory B cell. In the absence of $CD4^+$ T cells, infected B cells exhibit impaired proliferation in GCs, latency amplification is reduced and splenomegaly is not observed. In addition to $CD4^+$ T cell help, host colonization also requires T cell-independent survival signals provided by the B cell-activating factor (BAFF) receptor (BAFF-R) (Frederico *et al.*, 2014b).

Little is known about how MuHV-4 reactivates from latency and re-enters the lytic cycle. However, similarly to EBV and KSHV, plasma cell differentiation seems to be linked to MuHV-4 reactivation from latently infected B cells, and it has been proposed that the M2 latency-associated protein is involved in this process (Liang *et al.*, 2009; Rangaswamy and Speck, 2014).

A restricted number of MuHV-4 ORFs are transcribed during the establishment of latency in the spleen, including the ones encoding M1, M2, M3, M4, M8, M9, M11 (or vBcl-2), K3, ORF72 (or vCyclin), ORF73 (or MuHV-4 latency-associated nuclear antigen, mLANA) and ORF74 (Marques *et al.*, 2003). Moreover, the pattern of transcription in B cells is selective and dependent on the differentiation stage of the B cell, raising the possibility that, like EBV, MuHV-4 has different latency programmes.

Similarly to EBV and KSHV, MuHV-4 encodes at least 15 miRNAs at the left end of its genome, which are expressed both in lytically and latently infected cells *in vitro* (Pfeffer *et al.*, 2005; Zhu *et al.*, 2010). Recent studies have demonstrated that these miRNAs are dispensable for viral acute replication, but contribute to the establishment of latency and to reactivation *in vivo* (Feldman *et al.*, 2014). MuHV-4 miRNAs are located downstream of viral transfer-RNA (tRNA)-like elements (Pfeffer *et al.*, 2005; Zhu *et al.*, 2010). These uncharged viral tRNAs are expressed in the spleens of latently infected mice and have been used as a marker for latent infection (Bowden *et al.*, 1997; Simas *et al.*, 1999).

Research conducted in our laboratory has focused on the latent phase of MuHV-4 infection. We have been particularly interested in characterizing the biological functions of mLANA and M2 latent proteins, by dissecting the basic molecular mechanisms by which these proteins contribute to the establishment of latency and host colonization, and by clarifying the impact of those mechanisms *in vivo*, using an animal model of infection.

mLANA, also known as ORF73, exhibits homology in sequence, structure and function to KSHV kLANA. In fact, mLANA was shown to mediate viral episome maintenance, and to regulate cellular transcription through E3 ubiquitin-ligase activity (Correia *et al.*, 2013; Fowler *et al.*, 2003; Habison *et al.*, 2012; Hellert *et al.*, 2013; Rodrigues *et al.*, 2009; Rodrigues *et al.*, 2013). Since the work presented in this thesis is focused on the pathogenesis of mLANA on latent infection, the functions of this viral protein will be described in detail in section 1.5.2.

The M2 protein has been shown to function as a modulator of B cell signalling, exhibiting functional homology to EBV LMP2A and KSHV K1 and K15. Biochemical research carried out in our laboratory has identified several intracellular targets of M2, namely Fyn, Lyn, Vav1, NCK1, PLCγ2, PI3K and SHP2, and demonstrated that this viral protein promotes the assembly of B cell signalling complexes downstream of the B cell receptor (BCR) (Pires de Miranda *et al.*, 2008; Pires de Miranda *et al.*, 2013; Rodrigues *et al.*, 2006). Importantly, M2 modulation of B cell signalling was shown to be critical for the efficient entry of latently infected B cells in GC reactions *in vivo* (Herskowitz *et al.*, 2008; Pires de Miranda *et al.*, 2008). Recent studies performed by our research group have shown that M2 promotes the formation of conjugates between the B cell and the helper $CD4^+$ T cell, possibly conferring a competitive advantage to the infected B cell in acquisition of T cell help and initiation of a GC reaction, hence host colonization (Fontinha *et al.*, 2015). Additionally, recent studies from other laboratories have suggested that M2 has also a role in viral reactivation from latently infected B cells, specifically by manipulating plasma cell differentiation (Liang *et al.*, 2009; Rangaswamy and Speck, 2014).

Persistence of gammaherpesviruses relies on a dynamic balance between virus-driven B cell proliferation and control by $CD8^+$ cytotoxic T lymphocytes (CTLs) (Stevenson *et al.*, 2009). Virus-specific $CD8^+$ CTLs recognize viral epitopes through their T cell receptor (TCR). These epitopes are derived from the intracellular processing of viral proteins, and are displayed on the surface of infected cells by major histocompatibility complex (MHC) class I glycoproteins (Tortorella *et al.*, 2000). M2 contains an MHC $H2K^d$ haplotype-restricted epitope that is recognized by $CD8^+$ CTLs from infected BALB/c ($H2^d$) mice (Husain *et al.*, 1999). A study conducted in our laboratory demonstrated that, in these mice, the absence of the M2 epitope results in uncontrolled long-term virus-driven proliferation of latently infected cells in GCs. Therefore, M2 $H2K^d$-restricted $CD8^+$ CTL epitope, in the appropriate host MHC haplotype, renders M2 indirectly responsible for setting the long-term viral load (Marques *et al.*, 2008). Furthermore, a recent work carried out in our group showed that $CD8^+$ CTL control of latency amplification in GC B cells is critically dependent on

strong epitope binding to MHC class I molecules. In contrast, infection control is effective over a broader range of $CD8^+$ CTL functional avidities for the epitope, showing relatively good tolerance for sub-optimal TCR engagement. Therefore, this study identified critical MHC class I and $CD8^+$ T cell engagement thresholds for *in vivo* $CD8^+$ CTL control of virus-driven B cell proliferation, which is fundamental for the development of successful immunotherapies and vaccines (Godinho-Silva *et al.*, 2014).

Another study performed in our laboratory aimed to clarify the role of BCR specificity in B cell susceptibility to MuHV-4 latency and how this is related to B cell activation. This study demonstrated that although viral latency is not restricted to virus-specific B cells, the establishment of latency in B cells is not a stochastic event in terms of BCR specificity, relying on mechanisms that remain to be identified (Decalf *et al.*, 2014).

1.5. Latency-associated nuclear antigen (LANA)

1.5.1. KSHV LANA (kLANA)

KSHV latency-associated nuclear antigen (kLANA), encoded by *ORF73* gene, is one of the few proteins expressed during KSHV latency. kLANA is approximately 1,162 amino acids in length (Figure 1.3). A large repetitive region of acidic and glutamine-rich repeats is contained in the middle of the protein, separating the N- and C-terminal regions. Heterogeneity in the length of this internal repeat region of kLANA has been noted among KSHV isolates. The N-terminal region of kLANA contains a proline-rich region and binds to many chromatin-associated proteins. The C-terminal region contains a unique leucine-rich domain and another repeat region, followed by unique sequence, and associates with a number of host cell proteins and chromosomes. The unique C-terminal region self-associates to bind DNA and recognizes a specific DNA sequence within the TR region of the KSHV genome (Ballestas and Kaye, 2011).

In tumours and latently infected cells, the KSHV genome (~200 kb) persists as a multi-copy (10-50 copies per cell), covalently closed circular extrachromosomal plasmid (episome). To persist in proliferating cells, episomes must segregate to newly formed nuclei after mitosis. kLANA is critical for this process, by simultaneously binding host cell mitotic chromosomes and viral TR DNA sequences, and thus mediating viral episome maintenance in daughter cells (Ballestas *et al.*, 1999; Ballestas and Kaye, 2001, 2011). Binding to TR DNA is mediated by C-terminal kLANA (Kelley-Clarke *et al.*, 2007b). N-terminal kLANA is the dominant chromosome association region (Kelley-Clarke *et al.*, 2009), binding to histones H2A/H2B (Barbera *et al.*, 2006). However, C-terminal kLANA can also bind to chromosomes, with concentration at pericentromeric and peritelomeric regions (Kelley-Clarke *et al.*, 2007a). Interestingly, a number of kLANA-associated proteins localize

in pericentromeric regions of chromosomes or are heterochromatin-associated proteins, including MecP2, Brd4, NuMA, CenpF and Bub1 (Matsumura *et al.*, 2010; Ottinger *et al.*, 2006; Si *et al.*, 2008; Xiao *et al.*, 2010; You *et al.*, 2006), some of which associate with C-terminal kLANA. These interactions are thought to contribute to kLANA tethering of viral genomes to mitotic chromatin.

Another fundamental aspect during proliferation of latently infected cells is the replication of viral episome prior to each cell division, in order to avoid a loss in episome copy number per cell, which would eventually lead to the complete loss of the KSHV genome from proliferating cells. Replication of the KSHV genome is carried out by host cell DNA replication machinery, and kLANA was shown to play an important role in this process (Ballestas and Kaye, 2011; Uppal *et al.*, 2014). C-terminal kLANA binds cooperatively to two adjacent LANA binding sites (LBS) located within each TR unit, a high-affinity site and a low-affinity site (Garber *et al.*, 2002). Near these two binding sites is a 32 bp GC-rich element, and together they form the minimal kLANA DNA replication element (Hu and Renne, 2005). kLANA also recruits host replication factors, including origin recognition complex (ORC) subunits (ORC1-6), mini-chromosomal maintenance proteins (MCMs), topoisomerase IIβ and replication factor C (RFC), to the viral replication element (Purushothaman *et al.*, 2012; Stedman *et al.*, 2004; Sun *et al.*, 2014; Verma *et al.*, 2006). Thus, kLANA mediates replication of the KSHV genome in latently infected cells. Importantly, epigenetic modifications, including DNA methylation, chromatin modifications and nucleosome positioning, control kLANA-mediated KSHV DNA replication during latency (Uppal *et al.*, 2014). Nonetheless, recent studies have suggested that DNA replication can initiate throughout the KSHV genome and that the replication origin of the TRs only exhibits a slight preference for their usage, indicating that kLANA-dependent origin at the TRs plays only a limited role in genome replication (Verma *et al.*, 2011).

kLANA is also known to modulate host cell gene expression by interacting with different transcription factors and chromatin regulatory proteins, and through direct binding to the regulatory regions of the cellular genes (Uppal *et al.*, 2014). In particular, kLANA associates with the Mediator complex, a multi-subunit transcriptional co-activator complex for RNA polymerase II, suggesting that the viral protein can recruit the RNA polymerase II transcriptional machinery to activate transcription (Roupelieva *et al.*, 2010). Consistent with this observation is the association of kLANA with transcriptional activators, including CBP, CREB2, c-jun, KLIP, Myc, Sp1, SRF, Stat3 and Rb (An *et al.*, 2004; Bubman *et al.*, 2007; Lim *et al.*, 2001; Lim *et al.*, 2000; Liu *et al.*, 2007; Muromoto *et al.*, 2006; Pan *et al.*, 2003; Radkov *et al.*, 2000; Roupelieva *et al.*, 2010; Verma *et al.*, 2004). Transcriptional repressors like CIR, I-mfa, Sap30a and Sin3a also interact with kLANA (Krithivas *et al.*, 2000; Kusano and Eizuru, 2010). It has been proposed that these interactions have effects on viral persistence, cellular transcription and growth transformation. However, the actual impact of the association of kLANA with the plethora of reported transcriptional activators and repressors in the context of KSHV life cycle needs to be further elucidated. In addition, kLANA was shown to associate with the promoter region of several cellular genes (Lu *et al.*, 2012), but it remains unclear whether this is sufficient to modulate host gene expression, and coordination with other factors may

be required (Mercier *et al.*, 2014). kLANA also associates with several viral promoters to regulate transcription of viral genes. For instance, kLANA represses the promoter of Rta/ORF50, the KSHV lytic transactivator protein (Lukac *et al.*, 1999), to inhibit its expression, as a mechanism to repress initiation of the viral lytic cycle and thus maintain latency (Lan *et al.*, 2004). kLANA can also auto-regulate its expression by inducing transcription from the kLANA promoter (Jeong *et al.*, 2004).

Control of cell cycle checkpoints and inhibition of apoptosis are hallmarks of proliferating tumour cells, including PEL cells and KS spindle cells. The association of kLANA with many proteins involved in cell cycle regulation suggests that it promotes cell survival. Furthermore, data gathered from protein interaction studies support the role of kLANA in cellular transformation, as certain kLANA-associated proteins can affect cell growth (Ballestas and Kaye, 2011). For example, kLANA represses Brd4-induced activation of the cyclin E promoter, promoting cell cycle progression (Ottinger *et al.*, 2006). In addition, kLANA associates with the tumour suppressors Rb and p53, thereby activating E2F-dependent genes and modulating p53-dependent pathways to prevent cell cycle arrest and apoptosis (An *et al.*, 2005; Cai *et al.*, 2007; Friborg *et al.*, 1999; Katano *et al.*, 2001; Radkov *et al.*, 2000; Si and Robertson, 2006; Wong *et al.*, 2004). kLANA is also an activator of human telomerase reverse transcriptase (hTERT), the enzymatic subunit of telomerase, which has been shown to be an important determinant for cell immortalization (Verma *et al.*, 2004). Moreover, kLANA stabilizes Myc by blocking glycogen synthase kinase-3 (GSK-3)-mediated phosphorylation of Myc at T58 residue and thus its degradation, while independently stimulating extracellular signal-regulated kinase 1 (ERK1)-mediated phosphorylation at S62 residue, an event that stabilizes Myc, thereby promoting its transcriptional activity and growth transformation properties (Liu *et al.*, 2007). Other signalling pathways associated with cancer, such as Notch and Wnt pathways, are affected by kLANA (Fujimuro and Hayward, 2003; Fujimuro *et al.*, 2003; Wang *et al.*, 2014). kLANA effects on cell growth may also be mediated by increases in survivin expression, an inhibitor of apoptosis (Lu *et al.*, 2009). Finally, B cell-specific expression of kLANA in a transgenic mouse model resulted in follicular hyperplasia, increased GC formation, and lymphomas, suggesting that kLANA is a key player in KSHV-associated lymphomagenesis (Fakhari *et al.*, 2006).

In summary, kLANA is a multifunctional protein critical for KSHV latency, with a role in viral episome replication and persistence, regulation of host and viral transcription, and control of cell growth and proliferation. To accomplish this, kLANA interacts with a plethora of host cellular proteins, which are involved in diverse cellular processes. Hence, understanding kLANA role in modifying or adapting host cell protein function may provide an opportunity to control KSHV latent infection and related oncogenesis.

1.5.2. MuHV-4 LANA (mLANA)

Like KSHV, MuHV-4 encodes a latency-associated nuclear antigen (mLANA), which is the product of *ORF73* gene. mLANA is 314 amino acids in length, which is considerably smaller than the 1,162-amino acid kLANA (Figure 1.3) (Virgin *et al.*, 1997). Most of the difference in size is due to the absence of the internal acidic and glutamine-rich repeat elements in mLANA. The N-terminal region of mLANA contains a proline-rich region and it was shown to interact with some host cell proteins (Rodrigues *et al.*, 2013). The C-terminal region of mLANA has amino acid homology to the kLANA DNA binding domain (DBD) and, similarly to the latter, it self-associates to bind DNA and recognizes a specific DNA sequence within the TR region of the MuHV-4 genome (Correia *et al.*, 2013; Grundhoff and Ganem, 2003; Habison *et al.*, 2012; Hellert *et al.*, 2013; Paden *et al.*, 2012).

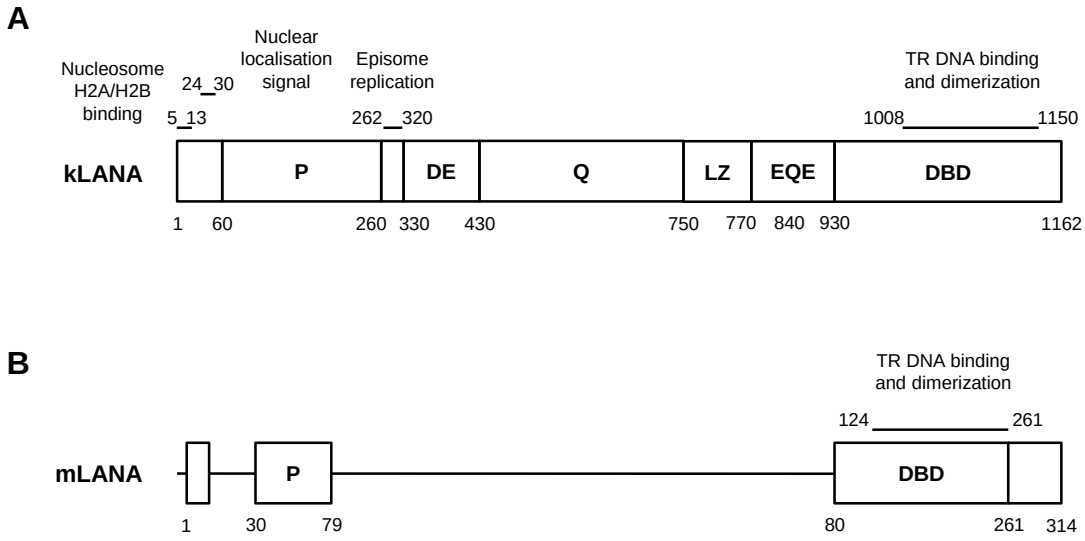

Figure 1.3. Schematic diagram of KSHV LANA (kLANA) and MuHV-4 LANA (mLANA). The proline-rich region (P) and the C-terminal region harbouring the DNA binding domain (DBD) shared by both proteins are indicated. DBD also mediates dimerization and interdimer association of LANA proteins. In kLANA, residues 5 to 13 mediate chromosome association through binding to histones H2A/H2B. The internal region of kLANA, which is absent from mLANA, comprises aspartate-glutamate (DE), glutamine (Q), and glutamine-glutamate (EQE) regions, and also a putative leucine zipper (LZ) region. All these contain repeat elements. The internal unique region of kLANA comprising amino acids 262 to 320 is required for episomal replication (adapted from Ponnusamy *et al.*, 2015).

In contrast to kLANA, mLANA functions can be directly assessed in a mouse model of infection. Previous studies showed that a mLANA-null MuHV-4 virus exhibits a severe latency deficit in splenocytes from infected animals, particularly in GC B cells, thereby demonstrating that mLANA has a critical role in the establishment of latency and virus persistence in the host (Fowler *et al.*, 2003; Moorman *et al.*, 2003).

The role of mLANA in lytic replication is controversial. A study reported that mLANA-null virus displayed normal lytic replication both *in vitro* and *in vivo* (Fowler *et al.*, 2003). In contrast, an independent study found that mLANA-null virus exhibited a modest defect in acute replication in the lungs of infected mice, suggesting that mLANA might play a role in lytic replication *in vivo* (Moorman *et al.*, 2003). Differences in virus inoculum and in mouse strain may account for the divergence between the two published works. Afterwards, a third study reported a multiplicity of infection (MOI)-dependent requirement for mLANA in viral replication in fibroblasts (Forrest *et al.*, 2007), indicating that mLANA might also be involved in lytic replication *in vitro*, which again was not consistent with the work of Fowler *et al.* Possible explanations for the observed discrepancies include differences in the MOI and in the cell line used. Overall, these studies demonstrate that mLANA may have a role in lytic replication *in vitro* and *in vivo*, depending on the virus inoculum and the host. Some authors have speculated that either some aspect of mLANA function is required for virus replication *in vivo* (e.g. a function modulating the innate immune response to MuHV-4 infection), or the establishment of latency in some cell type(s) followed by reactivation contributes to acute virus replication *in vivo* (Moorman *et al.*, 2003). Nonetheless, the exact contribution of mLANA for acute virus replication is unknown, and it is well established that mLANA have a predominant role in latency.

Like the other gammaherpesviruses, the MuHV-4 genome persists as a multi-copy, circularized, extrachromosomal episome in latently infected cells (Usherwood *et al.*, 1996b). mLANA was reported to be required for efficient viral episome maintenance *in vitro* (Fowler *et al.*, 2003). This conclusion was based on the observation that a B cell line infected with the mLANA-null MuHV-4 virus exhibited a significant decrease in viral episomes content compared to the same B cell line infected with the wild-type virus. Furthermore, analysis of viral genome-positive splenocytes from mice infected with the mLANA-null virus revealed the absence of viral episomes, implying that the viral genome was either integrated into the host chromosomes or maintained in a linear state (Paden *et al.*, 2010). Thus, these data suggested that mLANA was involved in the formation and/or maintenance of an extrachromosomal viral episome *in vivo*. However, it was not until recently that the mechanism by which mLANA allows episome persistence was beginning to be elucidated and found to be reminiscent of kLANA-mediated KSHV episome persistence (Habison *et al.*, 2012). In fact, this study demonstrated that mLANA acts on TR DNA sequences of the MuHV-4 genome to mediate viral episome persistence. Moreover, mLANA is broadly distributed throughout the nucleus in interphase and over mitotic chromosomes in episome-deficient cells, but concentrates at dots both in interphase nuclei and along mitotic chromosomes in episome-containing cells. Hence, these dots likely correspond to sites where viral episomes are, supporting the hypothesis that mLANA directly tethers MuHV-4 episomes to mitotic chromosomes to efficiently segregate viral DNA into daughter nuclei, similarly to the tethering mechanism of kLANA. Future work is necessary to clarify the exact molecular mechanism underlying this process and to better understand the similarities and differences between mLANA and kLANA-mediated episome persistence. Unbiased mutagenesis of mLANA revealed a putative DBD, which was

shown to be required for the interaction of mLANA with viral TR DNA *in vitro* and for the establishment of latency *in vivo* (Paden *et al.*, 2012). However, only the determination of the crystal structure of mLANA DBD allowed the identification of specific residues of mLANA involved in binding to DNA (section 1.6.3). The engineering of MuHV-4 recombinant viruses bearing mutations in these residues and the analysis of these DNA binding-deficient mutants in the mouse, thereby combining the structural data with the mouse model of infection, are necessary to provide an unequivocal evidence of the impact of mLANA DNA binding and episome maintenance *in vivo*.

In addition to the episome maintenance function, mLANA is also able to modulate cellular transcription. Research conducted in our laboratory has demonstrated that mLANA assembles an E3 ubiquitin-ligase complex to mediate poly-ubiquitination of host transcription factors nuclear factor-kappa B (NF-κB) and Myc. mLANA promotes the poly-ubiquitination of nuclear p65/RelA, a member of the NF-κB family, targeting it to proteasomal degradation and thereby suppressing NF-κB transcriptional activity (Rodrigues *et al.*, 2009). Hence, mLANA mimics the GC physiological inhibition of NF-kB that prevents premature differentiation of GC B cells (Basso *et al.*, 2004; Heise *et al.*, 2014; Shaffer *et al.*, 2001), suggesting that mLANA promotes the development of MuHV-4-driven GC reactions to expand the host pool of latently infected cells (Rodrigues *et al.*, 2009). In contrast, mLANA stabilizes Myc through heterotypic poly-ubiquitination, thereby prolonging its half-life. Consequently, mLANA increases Myc transcriptional activity and expression of Myc target genes, which are involved in cellular growth and proliferation, thus promoting cell divisions during the expansion of MuHV-4 infected B cells in GCs. Stabilization of Myc by mLANA was demonstrated to be critical for MuHV-4-driven lymphoproliferation, as infected cells exhibit increased expression of Myc target genes and the virus amplifies exclusively in GC B cells containing intact Myc (Rodrigues *et al.*, 2013). Interestingly, mLANA was also found to interact with bromodomain and extra-terminal (BET) proteins, particularly Brd2 and Brd4, to associate with cellular chromatin and activate BET-responsive promoters of G1/S cyclins, thus promoting cell cycle progression (Ottinger *et al.*, 2009). Recent studies have demonstrated that mLANA interaction with BET proteins is important for the establishment of MuHV-4 latency in mice (Hellert *et al.*, 2013). Notably, mLANA is required for MuHV-4 immortalization of murine foetal liver-derived B cells *in vitro* (Liang *et al.*, 2011).

In summary, mLANA exhibits functional homology to kLANA, mediating viral episome persistence and regulating cellular transcription. Therefore, mLANA represents a good model to study LANA pathogenesis *in vivo*, using a mouse model of infection.

1.6. Crystal structure of the DNA binding domain (DBD) of gammaherpesvirus episome maintenance proteins

As mentioned before, during latent infection, gammaherpesvirus genome persists as a multi-copy extrachromosomal plasmid (episome). To ensure episome persistence in proliferating latently infected cells, gammaherpesviruses encode episome maintenance proteins, which are critical for efficient segregation of episomes into daughter nuclei. Gammaherpesvirus episome maintenance proteins include EBV EBNA1, KSHV kLANA and MuHV-4 mLANA.

Episome maintenance proteins must contain a DNA binding domain (DBD) that allows them to bind viral DNA. In fact, the crystal structures of EBV EBNA1, KSHV kLANA and MuHV-4 mLANA DBDs have been solved, and found to exhibit common structural features (Bochkarev *et al.*, 1996; Bochkarev *et al.*, 1995; Correia *et al.*, 2013; Domsic *et al.*, 2013; Hellert *et al.*, 2015; Hellert *et al.*, 2013; Ponnusamy *et al.*, 2015). The resolution of the crystal structure of DBDs provides advantages for pathogenesis studies, enabling the rational design of mutations in the DNA binding interface of episome maintenance proteins that may result in loss of DNA binding and episome persistence properties, with consequent elimination of viable virus in the host.

1.6.1. Crystal structure of EBNA1 DBD

The crystal structure of EBNA1 DBD was solved at 2.5 Å resolution (Bochkarev *et al.*, 1995). Subsequently, the crystal structure of EBNA1 DBD bound to an 18 bp palindromic binding site was solved at 2.4 Å resolution (Bochkarev *et al.*, 1996). These structural studies revealed that EBNA1 DBD binds to its 18 bp palindromic binding site on viral DNA as a dimer. The EBNA1 dimer comprises two domains, the flanking and the core domains. The flanking domain of each monomer (amino acid residues 461-503) includes an α-helix that projects into the major groove of DNA and an extended chain that travels along the minor groove and mediates several sequence-specific contacts with the viral DNA. The core domain (amino acid residues 504-607) comprises the dimerization interface and also has a direct role in DNA recognition (Cruickshank *et al.*, 2000). The structure of EBNA1 core domain contains an eight-stranded anti-parallel β-barrel, which is comprised of four strands from each monomer, and the β-strands in each monomer are connected by two α-helices on the outside of the barrel. The β-barrel is the scaffold of protein and is responsible for the marked stability of the EBNA1 dimer. In addition, EBNA1 is proposed to bend and distort the DNA at the origin of replication (oriP), which contains multiple copies of the 18 bp EBNA1 binding site (Bochkarev *et al.*, 1996; Hsieh *et al.*, 1993).

1.6.2. Crystal structure of kLANA DBD

The crystal structure of kLANA C-terminal DBD was not solved until recently (Domsic *et al.*, 2013; Hellert *et al.*, 2013). Interestingly, the structure shares the overall fold of EBNA1 DBD, despite the very little amino acid sequence homology shared between the two proteins. A central, anti-parallel β-sheet forms a hydrophobic core through which two protein subunits form a dimer. kLANA dimers are stabilized by an eight-stranded anti-parallel β-barrel to which each monomer contributes four β-strands. In addition to the stabilization by the hydrogen bonding network of the β-barrel, hydrophobic amino acid side chains project into the core and form a tightly packed hydrophobic cluster. The β-barrel is flanked by two α-helices of each monomer, α2 and α3. The N-terminal helix, α1, is packed against the two other helices and is not in direct contact with the central β-barrel. Remarkably, the crystal structure of kLANA DBD revealed a higher-ordered assembly comprised of five dimers interacting end-to-end, forming a decameric ring with an exterior DNA binding surface. The inter-dimer interactions are mediated by helices α1 and α3 facing the equivalent helices in the second dimer. The oligomeric interface between kLANA dimers is dispensable for single site DNA binding, but is required for cooperative DNA binding, replication function, and episome maintenance. The crystal structure also identified an N-terminal arm, which is crucial for DNA interaction and, based on homology to EBNA1, likely wraps around the minor groove of the cognate DNA, providing for high affinity binding.

Opposite to the DNA binding site, kLANA DBD harbours a characteristic lysine-rich positively charged surface patch (Domsic *et al.*, 2013; Hellert *et al.*, 2013), which is absent in EBNA1. This lysine patch contains key residues involved in interactions with cellular BET proteins Brd2 and Brd4, which have been shown to mediate kLANA function in chromosome binding, transcription regulation and cell cycle control (Ottinger *et al.*, 2006; Viejo-Borbolla *et al.*, 2005). A recent published work has demonstrated that the lysine patch exerts a key role in kLANA-mediated DNA replication and consequent episome persistence, likely acting through a host cell partner(s) other than a BET protein or by inducing specific structures or complexes (Li *et al.*, 2015).

Previous experiments demonstrated that kLANA cooperatively binds to two sites within the KSHV TR DNA, LBS1 and LBS2 (Garber *et al.*, 2002). However, a third kLANA binding site, LBS3, was recently described (Hellert *et al.*, 2015). All three sites are located in a region of the KSHV TR subunit previously recognized as a minimal replicator. LBS1 is a high-affinity site, whereas LBS2 and LBS3 correspond to low-affinity sites. The crystal structure of kLANA DBD in complex with LBS1 has also been solved (Hellert *et al.*, 2015), providing the basis for a plausible model to describe the arrangement of three kLANA dimers on the KSHV minimal replicator. In contrast to EBNA1, kLANA binds to the minimal replicator in an asymmetric manner. Binding of three kLANA dimers is facilitated by the presence of three kLANA binding sites and, in this assembly, the protein complex presumably follows the shape of a semicircle, with the lysine patches of the individual dimers oriented towards the centre. One helix α2 per dimer interacts with the major groove of DNA.

Intriguingly, it was shown that kLANA DBD can coat DNA of arbitrary sequence by virtue of its characteristic lysine patch, assembling into supermolecular spirals around DNA by self-association of kLANA (Hellert *et al.*, 2015). It has been proposed that the KSHV minimal replicator may act as a structural template for the nucleation of kLANA spirals in *trans*. Such spirals may assemble on remote sites in the viral genome that are not directly defined by their DNA sequence. Once formed, this nucleator complex may recruit more free and/or LBS-bound kLANA dimers to cooperatively assemble a spiral of unknown length. Functionally, this self-assembly of kLANA oligomers may be involved in the formation of the latent subnuclear KSHV microdomains (kLANA speckles), which can be visualized by fluorescence microscopy and are a hallmark of KSHV latency (Gao *et al.*, 1996; Kedes *et al.*, 1996; Simpson *et al.*, 1996). These microdomains possibly also contain a plethora of cellular proteins, many of which are known to directly interact with kLANA (Hu *et al.*, 2014; Kaul *et al.*, 2007). In addition, an oligomer might also incorporate kLANA binding sites in the host genome, which would further contribute to the physical link between virus and host chromatin (Mercier *et al.*, 2014). Alternatively, the minimal replicator may induce kLANA spiral assembly directly on unspecific host DNA, which would have a similar effect.

Another crystal form of kLANA DBD was shown to form dimer and bent tetramer assemblies (Ponnusamy *et al.*, 2015). Interestingly, kLANA tetramer is intrinsically bent both in the free and bound state to LBS1-2 DNA. This bent conformation is driven by the core of hydrophobic residues in kLANA that are located at one end of both helices α1 and α3 at the dimer-dimer interface. kLANA DBD bent tetramer can adopt different bend angles, thereby facilitating kLANA cooperative binding and bending of DNA. This rotational flexibility is conferred by a hydrophobic pivot point located at the dimer-dimer assembly interface. The LBS1 and LBS2 sites are each expected to bind one kLANA dimer, hence formation of tetramer is required for binding with LBS1-2 DNA. In solution, kLANA maintains a bent conformation when bound to LBS1-2, but additionally assembles into an octamer ring with two LBS1-2 bound. Alterations in the arrangement of LBS within TR or at the tetramer assembly interface have a drastic effect on the ability of kLANA binding.

In summary, the studies on kLANA DBD crystal structure have demonstrated that kLANA oligomerizes into different assemblies: a dimer, a tetramer, an octameric or decameric ring, and an infinitive number of dimers joined to form a spiral conformation. These assemblies may each have designated functions for KSHV, and the versatility of kLANA functions may be attributed to the different observed quaternary structures (Ponnusamy *et al.*, 2015)**.**

1.6.3. Crystal structure of mLANA DBD

The crystal structure of mLANA C-terminal DBD was recently solved by our consortium in the scope of the Harvard Medical School-Portugal (HMS-PT) Program (Correia *et al.*, 2013), and by others (Hellert *et al.*, 2013). Reminiscent of EBNA1, the tertiary structure of mLANA DBD exhibits

an α+β ferredoxin-like fold which assembles to form a dimeric eight-stranded anti-parallel β-barrel that is central to its functional architecture. Each monomer contributes an anti-parallel four-stranded β-sheet ‘‘half-barrel’’ from which helices α2 and α3 pack onto the plaited sheet with their axis parallel to the strands of the sheet. The core of the barrel is occupied by large hydrophobic surface that contributes to the stability of mLANA. The flanking helix α1 caps this helical arrangement and lies perpendicular to the central β-barrel. mLANA DBD dimer forms a tetramer to cooperatively bind adjacent TR DNA binding sites. mLANA dimers pack so that the DNA-binding flanking helix α1 in each dimer is in position to interact with both the flanking helix α1 and helix α3 from the adjacent dimer.

Similarly to kLANA, mLANA DBD exhibits an electrostatic surface with a ventral (top) and a dorsal (bottom) face, corresponding to the opposite sides of the β-barrel core (Correia *et al.*, 2013; Hellert *et al.*, 2013). A representation of mLANA ventral and dorsal faces is shown in the introductions of chapter 2 (Figure 2.1) and chapter 3 (Figure 3.1), respectively. The ventral face of mLANA DBD contains a cluster of positively charged residues and was identified as the DNA binding interface, since disruption of targeted residues on the ventral surface abolishes DNA binding. Helix α2 is the predicted DNA recognition helix. Similarly to kLANA, mLANA cooperatively binds to two adjacent high and low-affinity TR DNA binding sites, MuHV-4 LANA binding site 1 (mLBS1) and mLBS2, respectively. mLANA tetramers and octamers bound to mLBS1-2 have been described, but not rings or spiral-like structures (Ponnusamy *et al.*, 2015). Remarkably, mLANA oligomers adopt a rigid linear conformation upon binding to DNA, rather than the bent conformation of kLANA tetramer. Interestingly, regardless of the binding modes, both kLANA and mLANA bind to reciprocal DNA, suggesting that it might be feasible to substitute mLANA with kLANA within MuHV-4 virus in order to explore kLANA function in a mouse model of infection.

Protruding perpendicular to the ventral face of mLANA DBD lies a partially disordered β2-β3 loop (amino acid residues 199-215) that harbours a motif required for the interaction of mLANA with the components of the E3 ubiquitin-ligase complex (Correia *et al.*, 2013; Rodrigues *et al.*, 2009). In addition, electrostatic surface analysis of mLANA DBD revealed an extensive positive patch on its dorsal side, opposite to the DNA binding interface, which is present in kLANA but absent in EBNA1 (Correia *et al.*, 2013; Hellert *et al.*, 2013). This dorsal face encompasses the identified ^{226}QAKKLK^{231} motif that is involved in binding to BET proteins, particularly Brd2 and Brd4 (Ottinger *et al.*, 2009).

In conclusion, MuHV-4 mLANA shares not only functional homology (section 1.5.2) but also structural homology to KSHV kLANA, emphasising the use of mLANA as a model for the study of kLANA pathogenesis in the mouse and even for testing pharmacological inhibitors of LANA functions through targeting of key structural features of the DNA binding domain.

1.7. E3 ubiquitin-ligase complexes assembled by LANA proteins

In addition to their critical function in episome persistence, LANA proteins are able to assemble E3 ubiquitin-ligase complexes to modulate ubiquitination and thus control cellular pathways. Ubiquitination is a post-translational modification in which the small protein ubiquitin is attached to a protein substrate (Kerscher *et al.*, 2006). Ubiquitin is covalently attached to a substrate lysine and one ubiquitin molecule is conjugated to the next through one of its seven lysines, leading to the formation of different types of poly-ubiquitin chains (Berndsen and Wolberger, 2014). The tagging of substrates with particular types of poly-ubiquitin chains determines their fate in the cell (Komander and Rape, 2012). Thus, ubiquitination is an essential regulatory mechanism in eukaryotes, controlling a wide range of cellular pathways. Ubiquitination occurs through a three-enzyme cascade (Figure 1.4), involving an E1 ubiquitin-activating enzyme, an E2 ubiquitin-conjugating enzyme and an E3 ubiquitin-ligase enzyme (Berndsen and Wolberger, 2014). First, ubiquitin is activated by the E1 activating enzyme, in an adenosine triphosphate (ATP)-dependent reaction, resulting in the formation of a thioester bond between the E1 active site cysteine and the ubiquitin C-terminus. Ubiquitin is then transferred to the active site cysteine of the E2 conjugating enzyme, yielding an E2~ubiquitin thioester intermediate. Finally, the E3 ubiquitin-ligase binds to the E2~ubiquitin intermediate and the substrate, catalysing the transfer of ubiquitin to the substrate target lysine (or, in some cases, to the substrate N-terminus). Distinct classes of E3 ubiquitin-ligases have been identified, including really interesting new gene (RING) E3s, which catalyse the direct transfer of ubiquitin from the E2 enzyme to the substrate, in a one-step reaction. In particular, Cullin5-RING E3 ubiquitin-ligases (CRL5), also known as ElonginBC/Cullin5/suppressor of cytokine signalling (SOCS) (EC_5S) E3 ubiquitin-ligases, are multisubunit complexes containing a scaffold protein (Cullin5) attached to a RING finger protein (Rbx) (Cullin5-Rbx module), an adaptor heterodimer (ElonginB/C), and a substrate recognition protein (SOCS-box protein). The latter component bridges the substrate of ubiquitination to the E3 ubiquitin-ligase complex, by interacting with ElonginB/C and Cullin5 through its SOCS-box (Lydeard *et al.*, 2013; Skaar *et al.*, 2013; Yoshimura *et al.*, 2007).

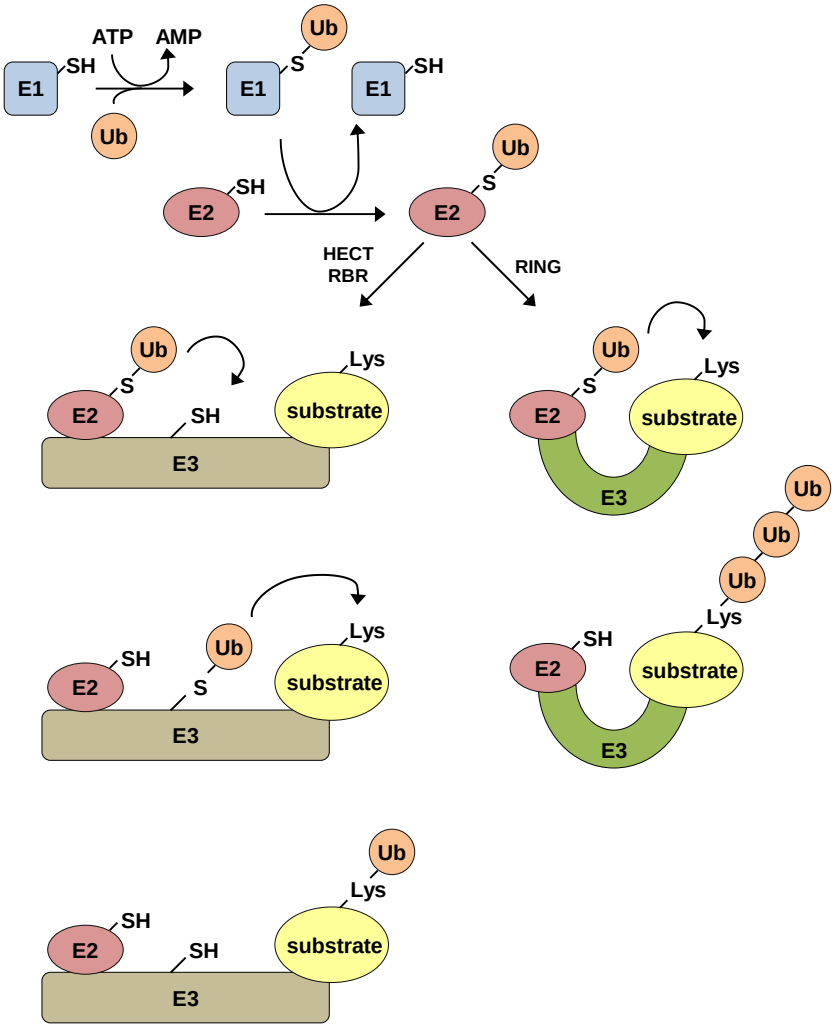

Figure 1.4. The ubiquitination cascade. The ubiquitination cascade begins with ATP-dependent charging of the E1 activating enzyme and results in formation of a thioester bond between the ubiquitin C-terminus and the E1 active site cysteine. Ubiquitin is then transferred to the active site cysteine of the E2 conjugating enzyme in a transthioesterification reaction. An E3 ubiquitin-ligase catalyses the transfer of the ubiquitin from the active site cysteine of the E2 to a primary amine on a lysine side chain or protein N-terminus. There are three classes of E3 ubiquitin-ligases: the really interesting new gene (RING), the homology to E6AP C-terminus (HECT) and the RING-between-RING (RBR). RING E3s bind to both E2~Ub thioester and substrate, catalysing the attack of the substrate lysine on the thioester. HECT and RBR E3s both have active site cysteines and catalyse substrate ubiquitination in a two-step reaction involving formation of a thioester with the HECT or RBR E3, followed by attack of the substrate lysine or N-terminus on the E3~Ub thioester to form an isopeptide (or peptide) linkage between the ubiquitin C-terminus and lysine (or the protein N-terminus) (adapted from Berndsen and Wolberger, 2014).

kLANA assembles an E3 ubiquitin-ligase complex by recruiting ElonginB/C and Cullin5, through an unconventional SOCS-box motif, in order to target the tumour suppressors p53 and von Hippel-Lindau (VHL) for degradation, potentially providing a favourable environment for cell growth (Cai *et al.*, 2006). Recent studies have demonstrated that the E3 ubiquitin-ligase complex

assembled by kLANA also targets the NF-κB family member p65/RelA for degradation, resulting in a reduction of interleukin-8 (IL-8) expression and neutrophil chemotaxis (Li *et al.*, 2011). However, the relevance of kLANA E3 ubiquitin-ligase activity within the physiological context of KSHV latent infection *in vivo* remains to be clarified.

Similarly to kLANA, mLANA assembles an E3 ubiquitin-ligase complex, EC_5S^{mLANA}, by recruiting ElonginB/C and Cullin5 (Figure 1.5), through an unconventional SOCS-box motif (amino acid residues 199-206) present in mLANA C-terminal domain (Rodrigues *et al.*, 2009). mLANA also acts as the substrate recognition component of the EC_5S^{mLANA} complex, interacting with cellular substrates through motifs independent of the SOCS-box, as yet unidentified (Rodrigues *et al.*, 2009; Rodrigues *et al.*, 2013). Two cellular targets of mLANA E3 ubiquitin-ligase activity are known: NF-κB and Myc. mLANA mediates poly-ubiquitination-dependent proteasomal degradation of the NF-κB family member p65, thus inhibiting NF-κB transcriptional activity (Rodrigues *et al.*, 2009). In contrast, mLANA stabilizes Myc through heterotypic poly-ubiquitination, thus increasing Myc transcriptional activity (Rodrigues *et al.*, 2013). Mutation of four key residues on mLANA SOCS-box (^{199}VSCLPLVP^{206}, underlined residues mutated to alanine) prevents mLANA binding to ElonginC, therefore abrogating mLANA E3 ubiquitin-ligase activity, and a recombinant MuHV-4 virus containing these mutations (vSOCS) exhibits a severe latency deficit, being unable to expand in GC B cells and persist in mice (Rodrigues *et al.*, 2009). However, recent unpublished results demonstrated that the four mutations introduced in mLANA SOCS-box disrupt not only mLANA E3 ubiquitin-ligase activity but also its ability to bind viral TR DNA and to mediate episome persistence (Tan *et al.*, unpublished data). Therefore, the severe latency deficit of vSOCS recombinant virus cannot be exclusively attributed to the suppression of mLANA E3 ubiquitin-ligase activity, and the contribution of this function of mLANA for latent infection remains to be elucidated.

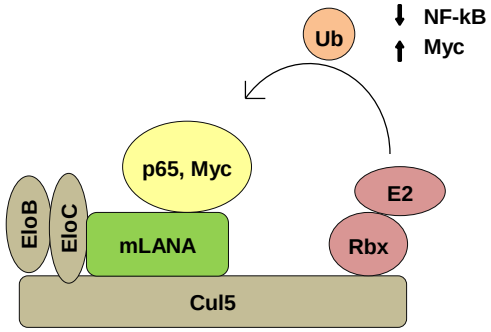

Figure 1.5. E3 ubiquitin-ligase complex assembled by mLANA (EC_5S^{mLANA}). mLANA recruits ElonginB/C and Cullin5, through a SOCS-box motif, to assemble an E3 ubiquitin-ligase complex. In addition, mLANA is also the substrate recognition component of the complex, interacting with p65 and Myc through motifs independent of the SOCS-box. EC_5S^{mLANA} complex mediates poly-ubiquitination-dependent proteasomal degradation of the NF-κB family member p65, thus inhibiting NF-κB transcriptional activity. In contrast, EC_5S^{mLANA} stabilizes Myc through heterotypic poly-ubiquitination, thus increasing Myc transcriptional activity. EloB, ElonginB; EloC, ElonginC, Cul5, Cullin5; Ub, ubiquitin.

1.8. Aims

During latency, the gammaherpesvirus genome is maintained as a non-integrated circular episome within the host cell nucleus. To persist in proliferating cells, viral episomes must replicate in step with normal cell division and segregate to newly formed nuclei after mitosis. LANA protein has been shown to mediate episome persistence, through binding to the TR sequences in viral genome. In addition, LANA regulates cellular transcription, including through E3 ubiquitin-ligase activity. Remarkably, the crystal structure of LANA DNA binding domain has been solved and revealed several structural features that are associated with specific LANA functions. The study of the mechanisms underlying LANA functions is crucial, since this protein is essential for the establishment and maintenance of latent infection *in vivo*. However, the individual contribution of each function assigned to LANA during the natural infection remains largely uncharacterized.

As mentioned in the preface, this work was inserted into the project «Pathogenesis of Kaposi's sarcoma herpesvirus LANA» of the HMS-PT Program from FCT, gathering the expertise of three research teams in KSHV LANA (Prof. K.M. Kaye group), structural biology (Prof. M.A. Carrondo and Dr C.E. McVey group) and in the murine model of MuHV-4 infection (Prof. J.P. Simas group). The aim of this thesis was to address the role of particular LANA functions in the context of gammaherpesvirus latent infection *in vivo*, combining LANA structural data, obtained by Carrondo and McVey group, with the animal model of infection with MuHV-4, in which our group is expert. MuHV-4 LANA, mLANA, was used as a model to investigate LANA pathogenesis in mice. To this end, MuHV-4 recombinant viruses harbouring structure-based mutations targeting specific mLANA interfaces were engineered, and the ability of these recombinants to establish and maintain latent infection was analysed upon intranasal infection of mice.

CHAPTER 2

mLANA binding to TR DNA is essential for gammaherpesvirus latency expansion in GC B cells and persistence in the host

mLANA binding to TR DNA is essential for gammaherpesvirus latency expansion in GC B cells and persistence in the host

2.1. Introduction

During expansion of latency in GC B cells, MuHV-4 genomes (episomes) must replicate in step with normal cell division and segregate to daughter nuclei, in order to persist in proliferating cells. mLANA mediates viral episome persistence by binding to TR DNA sequences of the MuHV-4 genome and tethering viral episomes to mitotic chromosomes, thus ensuring segregation of the viral DNA into daughter nuclei (Habison *et al.*, 2012).

The crystal structure of C-terminal mLANA DBD was recently solved by Prof. M.A. Carrondo and Dr C.E. McVey laboratory, and by others (Correia *et al.*, 2013; Hellert *et al.*, 2013). The structure uncovered an electrostatic surface with a ventral and a dorsal face. The ventral face contains a cluster of positively charged residues, identified as the DNA binding interface (Figure 2.1, panel A). The structural basis for DNA recognition was inferred from the observed phosphate binding pattern, which revealed that five of the seven phosphate ions located at the surface of mLANA DBD are situated on the ventral face. This analysis demonstrated that histidine (H) 186 and lysine (K) 187 residues, in the predicted DNA recognition helix α2 (Figure 2.1, panel B), are involved in interactions with phosphate ions of DNA. Notably, mutations at these residues ($mLANA_{H186D/K187E}$) disrupt mLANA binding to TR DNA (Correia *et al.*, 2013).

To validate *in vivo* the DNA binding structural data, a MuHV-4 recombinant virus containing mLANA mutations H186D/K187E ($vmLANA_{H186D/K187E}$) was engineered in the scope of this thesis. This recombinant virus was intranasally administered to C57BL/6 mice and its phenotype was analysed during the establishment and maintenance of latency by three independent, although complementary assays. *Ex vivo* reactivation assays were performed in total splenocytes to determine latent load in spleen. Limiting dilution coupled to real-time PCR to detect viral DNA-positive cells (Marques *et al.*, 2003) was applied to quantify the frequency of infection in total splenocytes and in GC B cells. Finally, *in situ* hybridization of splenic sections with viral tRNAs/miRNAs (Bowden *et al.*, 1997; Simas *et al.*, 1999) was performed to identify infected cells within the spleen.

Data presented in this chapter is included in the publication in Appendix 1 (Correia *et al.*, 2013), in which I am first co-author. During the development of this work, two independent teams led by Prof. Thomas F. Schulz (Hellert *et al.*, 2013) and Prof. Paul M. Lieberman (Domsic *et al.*, 2013) were also working on LANA structure. For this reason, the three articles were published back to back.

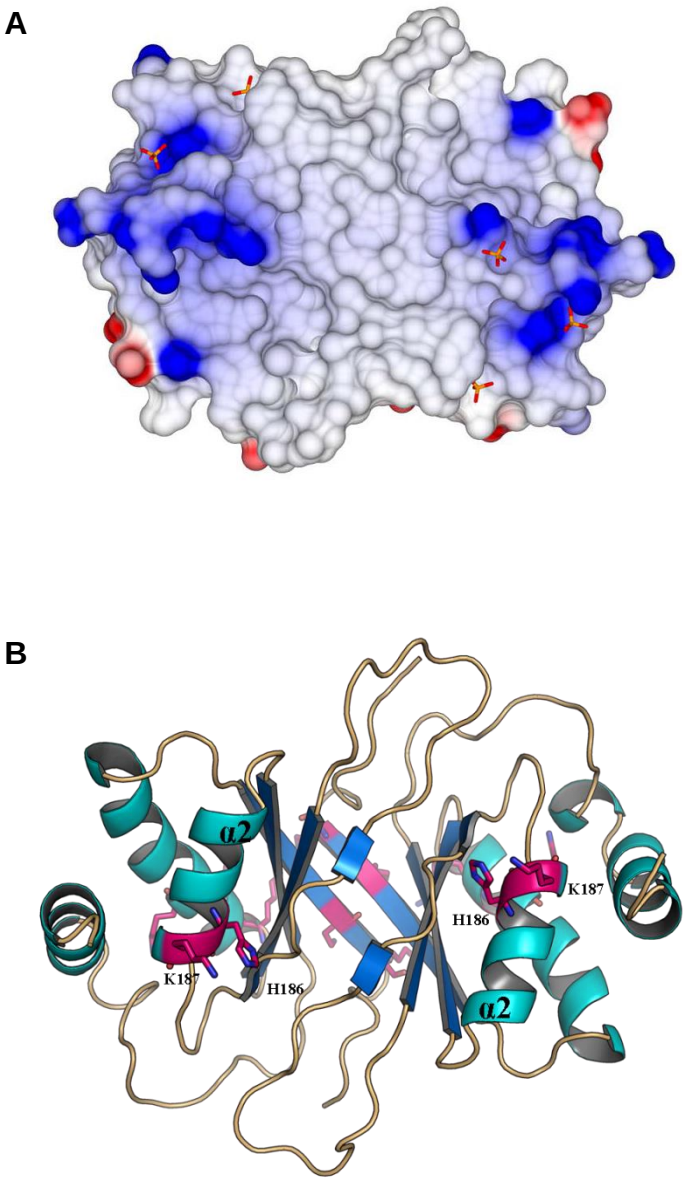

Figure 2.1. The ventral face of mLANA DBD. (A) Electrostatic surface potential representation showing the ventral side of mLANA dimer DBD. The five phosphate binding sites that trace DNA interactions are highlighted. The surface potentials displayed scale from -0.5 V (red, negatively charged) to +0.5 V (blue, positively charged) (Correia *et al.*, 2013). (B) Ribbon representation of mLANA dimer in the same orientation as in (A). Residues H186 and K187, in the predicted DNA recognition helix α2, are highlighted. This panel was kindly provided by Dr Rajesh Ponnusamy from Dr C.E. McVey's laboratory (Instituto de Tecnologia Química e Biológica (ITQB), Universidade Nova de Lisboa, Portugal).

2.2. Results

2.2.1. Generation of a MuHV-4 recombinant virus harbouring mutations on mLANA ventral face

To evaluate the importance of mLANA binding to viral TR DNA in MuHV-4 latent infection, a recombinant virus containing mLANA residues histidine (H) 186 and lysine (K) 187 substituted by aspartate (D) and glutamate (E), respectively, was engineered (vmLANA$_{H186D/K187E}$ virus).

The MuHV-4 recombinant was generated by mutagenesis of the viral genome cloned as a bacterial artificial chromosome (BAC) (Adler *et al.*, 2000), as described in detail in Materials and Methods, section 8.2.5. This technique allows the maintenance of the viral genome as a BAC in *Escherichia coli* and the site-directed mutagenesis of the genome by homologous recombination (Adler *et al.*, 2003). Verification of the introduced mutations was carried out by sequencing across *ORF73* gene in the BAC vector. The genomic structure of generated virus was verified by examination of restriction enzyme digestion profiles of *E. coli*-derived BAC DNA.

Infectious viruses were reconstituted by transfection of BAC DNA into baby hamster kidney (BHK)-21 fibroblasts. Since MuHV-4 containing BAC sequences is attenuated *in vivo* compared to the wild-type virus (Adler *et al.*, 2001), these sequences were removed by propagating the viruses in NIH-3T3 fibroblasts expressing Cre recombinase (Stevenson *et al.*, 2002). In MuHV-4 BAC, the BAC sequences are flanked by *loxP* sites and the expression of Cre recombinase from the cellular genome results in efficient excision of the BAC sequences during growth.

The stability of the introduced mutations was checked in viruses recovered from latently infected spleens, by sequencing *ORF73* gene in viral high molecular weight (HMW) DNA extracted from frozen-thawed splenocyte suspensions of infected mice. This analysis confirmed the retention of the engineered point mutations following *in vivo* infection.

2.2.2. vmLANA$_{H186D/K187E}$ recombinant virus displays normal lytic replication kinetics *in vitro* and *in vivo*

In vitro lytic replication kinetics of vmLANA$_{H186D/K187E}$ recombinant virus was compared to that of the vWT virus by a multi-step growth curve in permissive BHK-21 fibroblasts. Cells were infected at a low MOI and virus titres were determined at 0, 24, 48, 72, 96 and 120 hours post-infection. vmLANA$_{H186D/K187E}$ replicated to higher levels than vWT for the first 48 hours post-infection, followed by a growth plateau, while vWT virus reached a slightly higher growth plateau at 96 hours post-infection (Figure 2.2, panel A). Despite these differences, the lytic replication kinetics *in vitro* was essentially preserved for vmLANA$_{H186D/K187E}$ virus.

The course of MuHV-4 infection upon intranasal inoculation is characterized by the establishment of a productive infection in alveolar epithelial cells that peaks at 4 to 7 dpi and is then resolved to undetectable levels by 10 to 12 dpi (Sunil-Chandra *et al.*, 1992a). *In vivo* acute phase replication kinetics of vmLANA$_{H186D/K187E}$ recombinant virus was determined and compared to that of vWT virus in lung tissue of infected C57BL/6 mice. Following intranasal inoculation of C57BL/6 mice, lungs were removed at 3, 7 and 14 dpi, and the titre of infectious viruses was determined in frozen-thawed lung homogenates by plaque assay. At the peak of lytic infection, vmLANA$_{H186D/K187E}$ virus exhibited a deficit of about 10-fold compared to vWT virus (Figure 2.2, panel B). However, the lytic replication kinetics of vmLANA$_{H186D/K187E}$ *in vivo* was similar to that of vWT, with peak titres at around 7 dpi and clearance by day 14 (Figure 2.2, panel B).

Taken together, these results demonstrate that vmLANA$_{H186D/K187E}$ recombinant virus displays normal lytic replication kinetics *in vitro* and *in vivo*, consistent with mLANA having a predominant role in latency (Fowler *et al.*, 2003; Marques *et al.*, 2003).

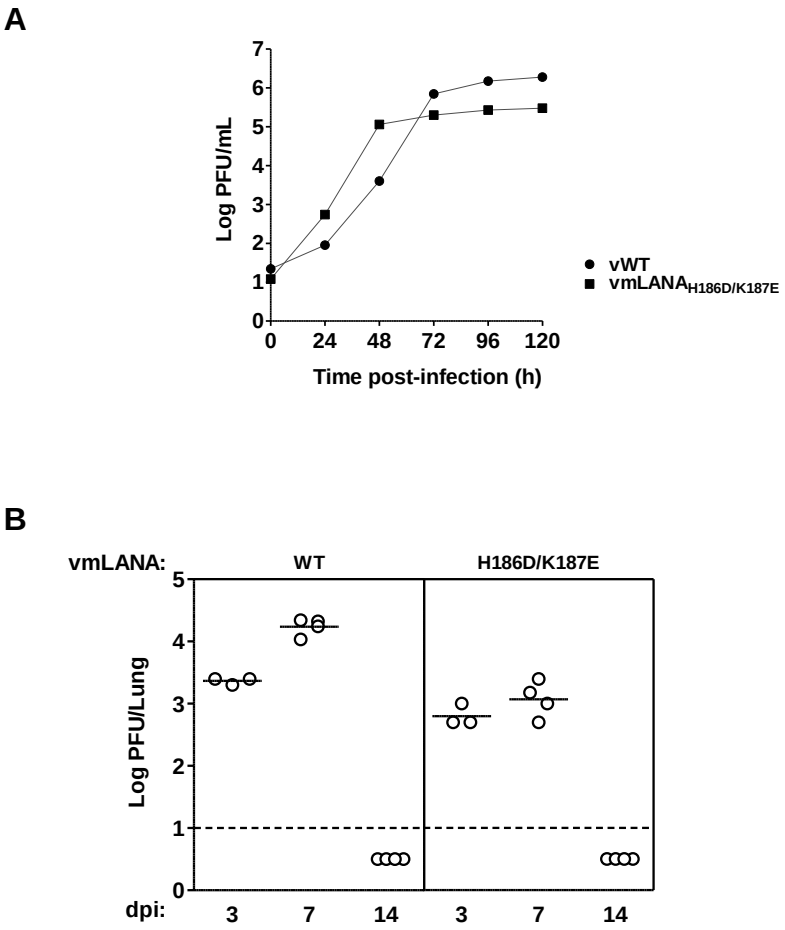

Figure 2.2. vmLANA$_{H186D/K187E}$ recombinant virus displays normal lytic replication kinetics *in vitro* and *in vivo*. (A) Multi-step growth curves were constructed by infection of BHK-21 cells with the indicated viruses at low MOI (0.01 plaque forming units (PFU)/cell). At the indicated times post-infection, samples were harvested and virus titres were determined by plaque assay of frozen-thawed samples. (B) C57BL/6 mice were intranasally infected with 10^4 PFU of the indicated viruses. At 3, 7 and 14 days post-infection, lungs were removed and infectious viruses were titrated by plaque assay of frozen-thawed lung homogenates. Each point shows the titre of an individual mouse. Horizontal lines indicate arithmetic means. The dashed line represents the limit of detection of the assay.

2.2.3. mLANA binding to viral TR DNA is required for the establishment and maintenance of MuHV-4 latency

Following lytic replication in the lung, MuHV-4 disseminates to the lymphoid tissue, namely the spleen and lymph nodes, where it establishes a latent infection (Sunil-Chandra *et al.*, 1992a). Latent infection in the spleen is characterized by an initial proliferation of infected B cells and consequent amplification of the latent virus, reaching maximum levels around 14 dpi and decreasing thereafter to low levels, which remain stable throughout the entire life of the host (Cardin *et al.*, 1996; Flano *et al.*, 2003; Marques *et al.*, 2003; Simas and Efstathiou, 1998; Sunil-Chandra *et al.*, 1992b).

To evaluate the importance of mLANA binding to viral TR DNA in MuHV-4 latent infection, C57BL/6 mice were intranasally infected with vmLANA$_{H186D/K187E}$ recombinant virus and latent load in spleen was determined by quantification of *ex vivo* reactivation-competent viruses in total splenocytes by infectious centre assay. For comparative purposes, vWT virus, expressing a fully functional mLANA, was also included in the experiments.

Infectious centre assay (Marques *et al.*, 2003; Sunil-Chandra *et al.*, 1992a), also known as *ex vivo* reactivation assay, is a well-established assay in which single cell suspensions are prepared from the harvested spleens, serially diluted and co-cultured with permissive fibroblast cells. The presence of latent virus in the splenocyte population is revealed by the observation of cytopathic effect (cpe) – plaques of cell lysis – in fibroblast monolayers. Viral plaques are counted and infectious centres titre is expressed as the number of plaque forming units (PFU) per spleen, considering that a viral plaque is originated by a single PFU. Unless preformed infectious viruses are present at the time of harvest, cpe can only result from viral reactivation from latency. Thus, to confirm that the results obtained for each virus truly reflect latent infection, spleen samples must also be analysed for the presence of preformed infectious viruses. To this end, replicate samples are subjected to freeze-thawing to disrupt the cells and, consequently, any possibility of reactivation from latency, without inactivating preformed infectious virus. Replicating viruses are then detected by incubation with permissive cells, which are later examined for the presence of cpe.

vmLANA$_{H186D/K187E}$ recombinant virus was examined at 14 and 21 dpi for its ability to establish and expand latent infection in the spleen, and at 50 dpi for its ability to maintain long-term persistence. The results obtained are shown in Figure 2.3, panel A. vWT virus presented the expected peak of infection at 14 dpi, with latent infection subsiding at 21 dpi to reach low long-term latency levels at 50 dpi (Figure 2.3, panel A). In contrast, vmLANA$_{H186D/K187E}$ virus exhibited a marked defect in *ex vivo* reactivation assay, being barely detectable beyond the limit of detection of the assay as soon as 14 dpi (Figure 2.3, panel A). Analysis of vmLANA$_{H186D/K187E}$ infection at 21

and 50 dpi revealed that virus persistence in mice was severely compromised (Figure 2.3, panel A).

Not every latently infected cell necessarily reactivates its virus *ex vivo*. Therefore, the *ex vivo* reactivation assay was complemented with limiting dilution coupled to real-time PCR to detect viral DNA-positive cells (Marques *et al.*, 2003), as a second measure of the frequency of infection of total splenocytes.

To this end, C57BL/6 mice intranasally infected with vWT or vmLANA$_{H186D/K187E}$ viruses were analysed at 14, 21 and 50 dpi. Total splenocytes were subjected to 2-fold serial dilutions, with 8 replicates per dilution, and lysed. Cell lysates were then analysed by real-time PCR for the presence of viral genomes, using the fluorescent TaqMan methodology with primers and probe specific for MuHV-4 *M9* gene. Further details are described in Materials and Methods, section 8.2.10.

The results obtained are in agreement with results from *ex vivo* reactivation assay. At 14 dpi, the peak of latency amplification, the frequency of vmLANA$_{H186D/K187E}$ DNA-positive total splenocytes was two orders of magnitude lower in comparison with vWT infection (Figure 2.3, panel B and Table 2.1). The incapability of vmLANA$_{H186D/K187E}$ to amplify latency resulted in a severe deficit of virus persistence at 21 and 50 dpi when compared to vWT (Figure 2.3, panel B and Table 2.1).

Altogether, these data demonstrate that mLANA binding to viral TR DNA is required for the establishment and maintenance of MuHV-4 latency.

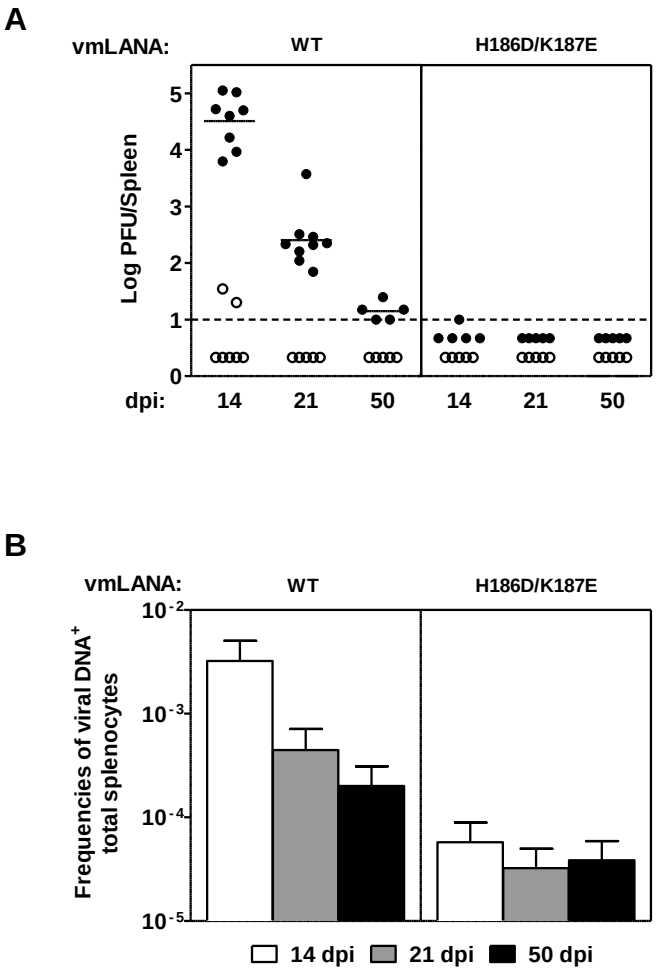

Figure 2.3. mLANA binding to viral TR DNA is required for the establishment and maintenance of MuHV-4 latency. (A) Quantification of latent infection in spleen by *ex vivo* reactivation assay. C57BL/6 mice were intranasally infected with 10^4 PFU of the indicated viruses. At days 14, 21 and 50 post-infection, latent viruses in spleens were titrated by infectious centre assay (closed circles). Titres of preformed infectious viruses were determined in frozen-thawed splenocyte suspensions (open circles). Each circle represents the titre of an individual mouse. Horizontal bars show arithmetic means. The dashed line represents the limit of detection of the assay. (B) Quantification of viral DNA-positive cells in total splenocytes. C57BL/6 mice were intranasally infected with 10^4 PFU of the indicated viruses. At days 14, 21 and 50 post-infection, reciprocal frequencies of viral infection in total splenocytes were determined by limiting dilution and real-time PCR. Data were obtained from pools of five spleens per group. Bars represent the frequency of viral DNA-positive cells with 95% confidence intervals.

Table 2.1. Frequency of MuHV-4 latent infection in total splenocytes[a].

Virus	Dpi	Reciprocal frequency[b] of viral DNA$^+$ cells (95% CI)	
vWT	14	310	(198-707)
	21	2243	(1405-5545)
	50	4976	(3220-10952)
$vmLANA_{H186D/K187E}$	14	17377	(11229-38406)
	21	30949	(20094-67314)
	50	25919	(16901-55571)

[a]Data were obtained from pools of 5 spleens.

[b]Frequencies were calculated by limiting dilution coupled to real-time PCR, with 95% confidence intervals (CI).

2.2.4. mLANA binding to viral TR DNA is essential for MuHV-4 latency expansion in GC B cells

During the establishment of latent infection in the spleen, MuHV-4 colonizes multiple cell types. However, the main target of latent infection is B lymphocytes (Flano *et al.*, 2000; Marques *et al.*, 2003). To assess whether the deficit in the establishment of latency exhibited by $vmLANA_{H186D/K187E}$ recombinant virus reflected a phenotype in GC B cells, the frequency of viral DNA-positive cells in this subpopulation was determined by limiting dilution combined with real-time PCR (Marques *et al.*, 2003).

C57BL/6 mice were intranasally infected with vWT or $vmLANA_{H186D/K187E}$ viruses and spleens were harvested at 14 dpi. Splenocyte suspensions were prepared and stained with three cell surface markers: anti-CD19, anti-CD95 and anti-GL7 T and B cell activation marker. GC B cells were purified by flow activated cell sorting (FACS), through enrichment for $CD19^+CD95^{hi}GL7^{hi}$ cells. The purity of the sorted GC B cell population was higher than 95%. Purified GC B cells were 2-fold serially diluted and 8 replicates of each dilution were analysed by real-time PCR for the presence of viral genomes, using a set of primers and probe specific for MuHV-4 *M9* gene. Further details are described in Materials and Methods, section 8.2.10.

The results obtained are shown in Figure 2.4 and Table 2.2. The frequency of $vmLANA_{H186D/K187E}$ infection in GC B cells at 14 dpi was three orders of magnitude lower comparing to vWT infection. This result shows that the severe latency deficit in spleen reported earlier for $vmLANA_{H186D/K187E}$ recombinant virus (section 2.2.3) reflects a marked impairment in the ability of the virus to drive latency expansion in GC B cells.

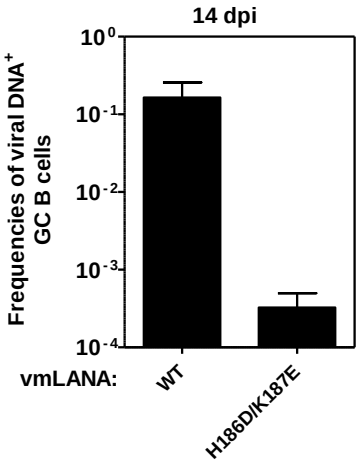

Figure 2.4. mLANA binding to viral TR DNA is essential for MuHV-4 latency expansion in GC B cells. Quantification of viral DNA-positive cells in GC B cells. C57BL/6 mice were intranasally infected with 10^4 PFU of the indicated viruses. At day 14 post-infection, reciprocal frequencies of viral infection in FACS-purified GC B cells ($CD19^+CD95^{hi}GL7^{hi}$) were determined by limiting dilution and real-time PCR. Data were obtained from pools of five spleens per group. Bars represent the frequency of viral DNA-positive cells with 95% confidence intervals.

Table 2.2. Frequency of MuHV-4 latent infection in GC B cells[a].

Virus	Dpi	Reciprocal frequency[b] of viral DNA^+ cells (95% CI)	
vWT	14	6	(4-14)
$vmLANA_{H186D/K187E}$		3079	(2006-6619)

[a]Data were obtained from pools of 5 spleens. The purity of sorted cells was determined by FACS analysis and was always greater 95%.

[b]Frequencies were calculated by limiting dilution coupled to real-time PCR, with 95% confidence intervals (CI).

2.2.5. Loss of mLANA-mediated TR DNA binding abolishes MuHV-4 colonization of splenic follicles

To complement the data of frequencies of infection in GC B cells during acute virus-driven lymphoproliferation, the ability of vmLANA$_{H186D/K187E}$ virus to colonize splenic follicles and to induce latency expansion in GCs was assessed by *in situ* hybridization, using a probe specific for MuHV-4 tRNAs and miRNAs (Bowden *et al.*, 1997; Pfeffer *et al.*, 2005). These transcripts are abundantly expressed in the GC and constitute an important marker for latency, allowing the analysis of the colonization and expansion of latent infection in GCs (Bowden *et al.*, 1997; Simas *et al.*, 1999).

C57BL/6 mice were intranasally infected with vWT or vmLANA$_{H186D/K187E}$ viruses and at 14 dpi spleens were dissected, fixed and paraffin-embedded. Spleen sections were made and processed for *in situ* hybridization with viral tRNAs/miRNAs specific riboprobes (details in Materials and Methods, section 8.2.11). Three spleens and six sections per spleen were analysed per virus. Pictures of representative spleen sections from each group of animals were taken.

Mice infected with vWT virus exhibited the typical large clusters of infected cells within GCs at 14 dpi (Figure 2.5, panel a) (Simas *et al.*, 1999). These clusters correspond to cellular proliferation and consequent expansion of the latently infected cell pool. In contrast, *in situ* hybridization showed that vmLANA$_{H186D/K187E}$ virus had a severe impairment in GC colonization, with consequent abolishment of the proliferation of latently infected cells within splenic follicles (Figure 2.5, panel b).

In situ hybridization results are consistent with the previous data, demonstrating that loss of mLANA-mediated TR DNA binding during latent infection severely compromises host GC colonization.

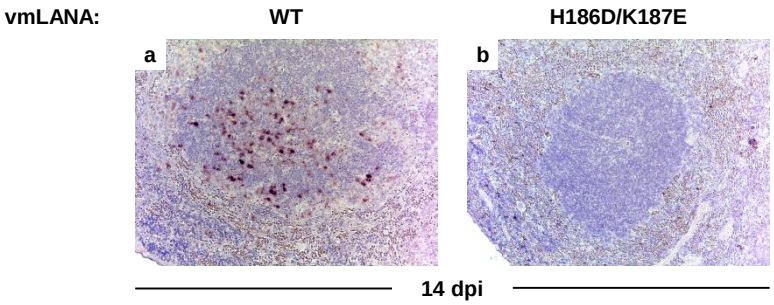

Figure 2.5. Loss of mLANA-mediated TR DNA binding abolishes MuHV-4 colonization of splenic follicles. C57BL/6 mice were intranasally infected with 10^4 PFU of the indicated viruses. At 14 days post-infection, spleens were dissected and processed for *in situ* hybridization with a viral tRNA/miRNA-specific riboprobe. Panels show representative spleen sections from each group of animals. Dark staining indicates cells positive for virally encoded tRNAs/miRNAs. All sections are magnified x200 and counterstained with haematoxylin.

2.2.6. Phenotypic changes in vmLANA$_{H186D/K187E}$ recombinant virus are intrinsic to *ORF73* locus and not the consequence of mutations elsewhere in MuHV-4 genome

To ensure that the phenotypic alterations observed in vmLANA$_{H186D/K187E}$ recombinant virus were due to the mutations introduced in mLANA, which disrupted binding to viral TR DNA, and not the consequence of mutations introduced elsewhere in MuHV-4 genome during mutagenesis, a revertant virus (vmLANA$_{H186D/K187E}$-R) was generated. In this revertant virus, the *ORF73* locus was restored to the wild-type status, by mutagenesis of the viral genome cloned as a BAC (Adler *et al.*, 2000), as described in detail in Materials and Methods, section 8.2.5.

C57BL/6 mice were intranasally infected with vWT virus or vmLANA$_{H186D/K187E}$-R revertant virus and latent load in spleen was determined by quantification of *ex vivo* reactivation-competent viruses in total splenocytes by infectious centre assay.

vmLANA$_{H186D/K187E}$-R revertant virus was examined at 14 dpi for its ability to establish and expand latent infection in the spleen. Infectious centre assay showed that vmLANA$_{H186D/K187E}$-R virus established normal latency levels in spleen (Figure 2.6).

These results demonstrate that vmLANA$_{H186D/K187E}$ phenotype is reverted to the wild-type phenotype when *ORF73* locus is restored to the wild-type status. Thus, these data confirm that the phenotypic changes observed with vmLANA$_{H186D/K187E}$ recombinant virus result from the mutations in mLANA which disrupted DNA binding, and not from mutations elsewhere in the viral genome.

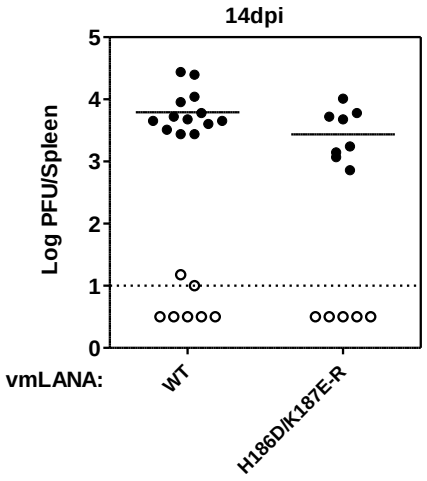

Figure 2.6. Phenotypic changes in vmLANA$_{H186D/K187E}$ recombinant virus are intrinsic to *ORF73* locus and not the consequence of mutations elsewhere in MuHV-4 genome. Quantification of latent infection in spleen by *ex vivo* reactivation assay. C57BL/6 mice were intranasally infected with 10^4 PFU of the indicated viruses. At day 14 post-infection, latent viruses in spleens were titrated by infectious centre assay (closed

circles). Titres of preformed infectious viruses were determined in frozen-thawed splenocyte suspensions (open circles). Each circle represents the titre of an individual mouse. Horizontal bars show arithmetic means. The dashed line represents the limit of detection of the assay.

2.3. Discussion

This work demonstrates the essential role of mLANA DNA binding interface in gammaherpesvirus latent infection, as a MuHV-4 recombinant virus containing mLANA abolished for DNA binding was severely compromised in its ability to establish latent infection in mice.

mLANA binding to viral TR DNA was shown to be required for the establishment of MuHV-4 latency. At 14 dpi, the peak of viral latent infection (Cardin *et al.*, 1996; Marques *et al.*, 2003), vmLANA$_{H186D/K187E}$ recombinant virus harbouring mLANA abolished for DNA binding exhibited a severe deficit in latency levels in the spleen, as assessed by *ex vivo* reactivation assay and quantification of the frequency of infection in total splenocytes. This deficit resulted from a marked impairment of virus-driven latency expansion in GC B cells, which severely compromised the colonization of splenic follicles. Hence, mLANA binding to viral TR DNA is critical for viral persistence in proliferating GC B cells. These data validate earlier studies with mLANA-null virus, which reported a requirement of mLANA for efficient viral episome maintenance *in vitro* (Fowler *et al.*, 2003) and for the maintenance of an extrachromosomal viral episome *in vivo* (Paden *et al.*, 2010). In addition, these results are consistent with the finding that virus containing mLANA incapable of binding DNA was highly deficient for establishment of latency *in vivo* (Paden *et al.*, 2012). Notwithstanding, the work presented in this chapter is novel in the sense that the mutations introduced in mLANA were based on structural data and thus specific for DNA binding (Correia *et al.*, 2013), in contrast to the random mutagenesis strategy previously used to identify DNA binding-deficient mutants (Paden *et al.*, 2012). The structural basis for DNA recognition was inferred from the observed phosphate binding pattern, which demonstrated that residues H186 and K187 were involved in interactions with phosphate ions of DNA (Correia *et al.*, 2013). Therefore, the phenotypic alterations of vmLANA$_{H186D/K187E}$ recombinant virus can be specifically attributed to the loss of mLANA-mediated DNA binding. The resolution of the crystal structure of mLANA DBD complexed with viral TR DNA, revealing the residues bound to DNA, would be the unequivocal demonstration that vmLANA$_{H186D/K187E}$ recombinant virus contains mutations in the residues of mLANA directly involved in DNA binding.

Disruption of targeted residues on mLANA ventral face abolishing DNA binding also severely compromised virus persistence, as assessed at 21 and 50 dpi, demonstrating that mLANA binding to viral TR DNA is also required for maintenance of MuHV-4 latency. Moreover, these data suggest that the virus incapability to amplify latency in GC B cells has a great impact on long-term

maintenance of latency. These findings support the proposed model in which MuHV-4 expansion of latent infection in GC B cells as a strategy to access persistence in long-lived memory B cells is vital for host colonization, reminiscent of the strategy employed by EBV (Flano *et al.*, 2002; Thorley-Lawson, 2001).

The ability of LANA proteins to bind TR DNA is important for both viral DNA replication and episome persistence (Ballestas and Kaye, 2011; Habison *et al.*, 2012; Uppal *et al.*, 2014). Although a role of mLANA in the replication of the MuHV-4 genome is not formally demonstrated, it is reasonable to think that, given its functional homology to KSHV kLANA, mLANA is involved in viral DNA replication. Hence, the phenotypic alterations observed for vmLANA$_{H186D/K187E}$ recombinant virus can be ascribed both to a loss of mLANA-mediated episome persistence and to a lack of mLANA-mediated DNA replication. However, kLANA-dependent origin of replication at the TRs was shown to play only a limited role in KSHV genome replication (Verma *et al.*, 2011), supporting the hypothesis that the deficiency of mLANA episome maintenance function exerts a major contribution to make latency unviable compared to the impairment of genome replication function.

Although the kinetics of lytic replication was essentially preserved for vmLANA$_{H186D/K187E}$ recombinant virus compared to vWT virus, vmLANA$_{H186D/K187E}$ exhibited a 10-fold reduction in lytic replication levels in the lungs of infected mice, similar to the phenotype reported before for mLANA-null virus in C57BL/6 mice (Moorman *et al.*, 2003). This result suggests that mLANA binding to viral TR DNA may have a minor role in lytic replication *in vivo*. For instance, if virus reactivation from some latently infected cell types contributes to lytic replication *in vivo*, as previously proposed by Moorman *et al.*, mLANA binding to DNA may be important for the establishment of that early latency.

In conclusion, the resolution of the crystal structure of mLANA DBD enabled the rational design of mutations in the DNA binding interface that resulted in loss of DNA binding and consequently severely compromised virus-associated GC B cell proliferation and persistence of viable virus in the host. Hence, this work highlights the importance of combining structural data with an animal model of infection to investigate gammaherpesvirus pathogenesis.

CHAPTER 3

mLANA dorsal positive patch is required for efficient expansion of gammaherpesvirus latency in GC B cells

mLANA dorsal positive patch is required for efficient expansion of gammaherpesvirus latency in GC B cells

3.1. Introduction

The crystal structure of mLANA DBD revealed an extensive positive patch on its dorsal side (Figure 3.1, panel A), opposite to the DNA binding interface. This dorsal positive patch, unique to LANA proteins, includes lysine (K) residues 224, 225, 228, 229, 231, 251 and 253, and arginine (R) residues 156 and 232 of mLANA. Notably, four key lysine residues are conserved in both mLANA (K228, K229, K251 and K253) and kLANA (K1113, K1114, K1138 and K1140). mLANA residues K228 and K229 are located at the periphery of the positive patch, whereas K251 and K253 are in the central region of the positive patch (Figure 3.1, panel B) (Correia *et al.*, 2013; Domsic *et al.*, 2013; Hellert *et al.*, 2013).

Interestingly, mLANA dorsal positive patch harbours the identified ^{226}QAKKLK^{231} motif that is involved in binding to BET proteins, particularly Brd2 and Brd4 (Correia *et al.*, 2013; Hellert *et al.*, 2013; Ottinger *et al.*, 2009). Previous studies demonstrated that mLANA interacts with BET proteins to associate with cellular chromatin and activate BET-responsive promoters of G1/S cyclins, thus promoting cell cycle progression (Ottinger *et al.*, 2009).

To investigate if the dorsal positive patch exerts a functional role *in vivo*, MuHV-4 recombinant viruses containing mLANA mutations that targeted either the central or the peripheral regions of the dorsal positive patch were engineered. Recombinant viruses were intranasally administered to C57BL/6 mice and the effect of the engineered mLANA mutations on establishment and maintenance of latent infection was assessed by three complementary assays. Latent load in spleen was determined by quantification of *ex vivo* reactivation-competent viruses in total splenocytes by infectious centre assay. Limiting dilution coupled to real-time PCR to detect viral DNA-positive cells (Marques *et al.*, 2003) was applied to quantify the frequency of infection of total splenocytes and of GC B cells. *In situ* hybridization of splenic sections with viral tRNAs/miRNAs (Bowden *et al.*, 1997; Simas *et al.*, 1999) was performed to identify infected cells within the spleen.

Data presented in this chapter is included in the publication in Appendix 1 (Correia *et al.*, 2013).

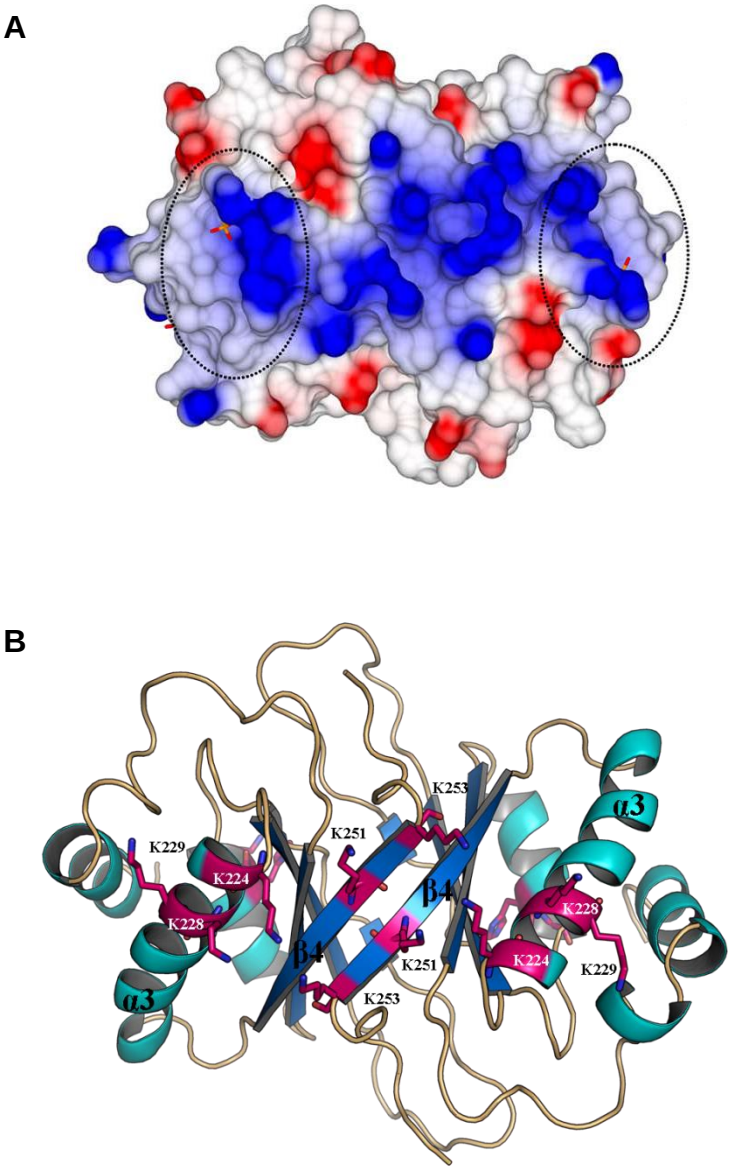

Figure 3.1. The dorsal positive patch of mLANA DBD. (A) Electrostatic surface potential representation showing the dorsal side of mLANA dimer DBD. Residues R156, K224, K225, K228, K229, K231 and R232, which run along the spine of the dorsal face, contribute to the positive electrostatic potential. The QAKKLK motif is highlighted. The surface potentials displayed scale from -0.5 V (red, negatively charged) to +0.5 V (blue, positively charged) (Correia *et al.*, 2013). (B) Ribbon representation of mLANA dimer in the same orientation as in (A). Residues K224, K228 and K229, at the periphery of the dorsal positive patch, and residues K251 and K253, in the central region, are highlighted. Helix α3 is identified. This figure was gently provided by Dr Rajesh Ponnusamy from Dr C.E. McVey's laboratory (ITQB, Universidade Nova de Lisboa, Portugal).

3.2. Results

3.2.1. Generation of a MuHV-4 recombinant virus harbouring mutations on mLANA dorsal positive patch

To clarify the role of mLANA dorsal positive patch in MuHV-4 latent infection, four recombinant viruses were engineered. vmLANA$_{K224A/K228A/K229A}$ and vmLANA$_{K224E/K228E/K229E}$ recombinants harboured lysine (K) residues 224, 228 and 229, at the periphery of mLANA positive patch, substituted by alanine (A) or glutamate (E), respectively, whereas vmLANA$_{K251A/K253A}$ and vmLANA$_{K251E/K253E}$ recombinants contained similar substitutions in residues K251 and K253, which are located in the central region of the positive patch (Figure 3.1, panel B). K228, K229, K251 and K253 are conserved between LANA proteins, suggesting that they might be important for LANA function. K224 is not a conserved residue, but it was also mutated since it is exposed on the surface of helix α3, similarly to K228 and K229 (Figure 3.1, panel B) (Correia *et al.*, 2013; Domsic *et al.*, 2013; Hellert *et al.*, 2013).

MuHV-4 recombinants were generated by mutagenesis of the viral genome cloned as a BAC (Adler *et al.*, 2000), as described in detail in Materials and Methods, section 8.2.5. Verification of the introduced mutations was carried out by sequencing across *ORF73* gene in the BAC vector. The genomic structure of generated virus was verified by examination of restriction enzyme digestion profiles of *E. coli*-derived BAC DNA. Infectious viruses were reconstituted by transfection of BAC DNA into BHK-21 fibroblasts and BAC sequences were removed by propagating the viruses in NIH-3T3 fibroblasts expressing Cre recombinase (Stevenson *et al.*, 2002). The stability of the introduced mutations was checked in viruses recovered from latently infected spleens, by sequencing *ORF73* gene in viral HMW DNA extracted from frozen-thawed splenocyte suspensions of infected mice. This analysis confirmed the retention of the engineered point mutations following *in vivo* infection.

3.2.2. Recombinant viruses containing mutations on mLANA dorsal positive patch display normal lytic replication kinetics *in vitro* and *in vivo*

In vitro lytic replication kinetics of recombinant viruses containing mutations on mLANA dorsal positive patch was compared to that of the vWT virus by a multi-step growth curve in permissive BHK-21 fibroblasts. Cells were infected at a low MOI and virus titres were determined at 0, 24, 48, 72, 96 and 120 hours post-infection. vmLANA$_{K224E/K228E/K229E}$, vmLANA$_{K251A/K253A}$ and vmLANA$_{K251E/K253E}$ viruses exhibited an *in vitro* growth kinetics equivalent to the vWT virus (Figure 3.2, panel A), with increasing levels of replication until 96 hours post-infection, when a growth plateau was established. vmLANA$_{K224A/K228A/K229A}$ replicated to higher levels than vWT for the first 72 hours post-infection, followed by a growth plateau until 96 hours post-infection, when lytic replication started to decline (Figure 3.2, panel A). Despite these differences, the lytic replication kinetics *in vitro* was essentially preserved for vmLANA$_{K224A/K228A/K229A}$ virus.

Next, *in vivo* acute phase replication kinetics of recombinant viruses was determined and compared to that of vWT virus in lung tissue of infected C57BL/6 mice. Following intranasal inoculation of C57BL/6 mice, lungs were removed at 3, 7 and 14 dpi, and the titre of infectious viruses was determined in frozen-thawed lung homogenates by plaque assay. Recombinant viruses showed identical lytic replication kinetics in the lungs of infected mice (Figure 3.2, panel B), with peak titres at 7 dpi and clearance at 14 dpi.

Taken together, these results demonstrate that the mutations introduced on mLANA dorsal positive patch did not affect viral lytic replication kinetics *in vitro* and *in vivo*, consistent with mLANA having a predominant role in latency (Fowler *et al.*, 2003; Marques *et al.*, 2003).

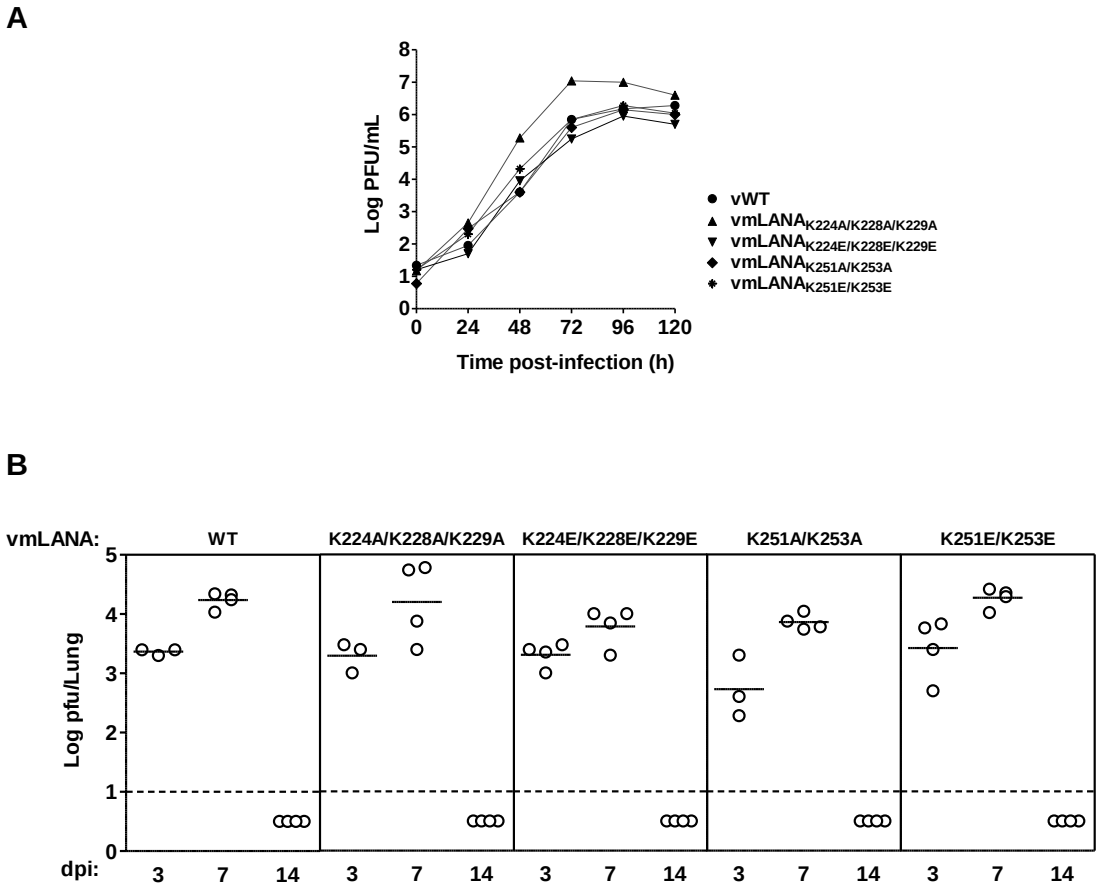

Figure 3.2. Recombinant viruses containing mutations on mLANA dorsal positive patch display normal lytic replication kinetics *in vitro* and *in vivo*. (A) Multi-step growth curves were constructed by infection of BHK-21 cells with the indicated viruses at low MOI (0.01 PFU/cell). At the indicated times post-infection, samples were harvested and virus titres were determined by plaque assay of frozen-thawed samples. (B) C57BL/6 mice were intranasally infected with 10^4 PFU of the indicated viruses. At 3, 7 and 14 days post-infection, lungs were removed and infectious viruses were titrated by plaque assay of frozen-thawed lung homogenates. Each point shows the titre of an individual mouse. Horizontal lines indicate arithmetic means. The dashed line represents the limit of detection of the assay.

3.2.3. The positive patch periphery of mLANA dorsal face is required for efficient expansion of MuHV-4 latency

To investigate the role of mLANA dorsal positive patch in MuHV-4 latent infection, C57BL/6 mice were intranasally infected with the recombinant viruses described in section 3.2.1. vWT virus was included in the experiments for comparative purposes. Latent load in spleen was then determined by quantification of *ex vivo* reactivation-competent viruses in total splenocytes by infectious centre assay at 14, 21 and 50 dpi.

The results obtained are shown in Figure 3.3. vmLANA$_{K224A/K228A/K229A}$ and vmLANA$_{K224E/K228E/K229E}$ viruses, bearing mutations at the positive patch periphery of the dorsal surface of mLANA, exhibited a substantial deficit in latency at 14 dpi (Figure 3.3, panel A). In contrast, vmLANA$_{K251A/K253A}$ and vmLANA$_{K251E/K253E}$ viruses, containing mutations in the central region of the dorsal positive patch, showed a mild attenuation of latency levels at 14 dpi (Figure 3.3, panel A). Similarly to vWT virus, the latent load of all recombinant viruses declined at 21 dpi (Figure 3.3, panel A) and was barely detected at 50 dpi (Figure 3.3, panel A).

Infectious centre assays were then complemented with limiting dilution coupled to real-time PCR to detect viral DNA-positive cells (Marques *et al.*, 2003), as a second measure of the frequency of infection of total splenocytes. To this end, total splenocytes of C57BL/6 mice intranasally infected with vWT or recombinant viruses were analysed at 14, 21 and 50 dpi by real-time PCR, using the fluorescent TaqMan methodology with primers and probe specific for MuHV-4 *M9* gene (Marques *et al.*, 2003) (Materials and Methods, section 8.2.10).

The results obtained are consistent with results from infectious centre assays. At 14 dpi, the peak of latency amplification, the frequency of vmLANA$_{K224A/K228A/K229A}$ and vmLANA$_{K224E/K228E/K229E}$ DNA-positive total splenocytes was approximately 10-fold lower than vWT infection (Figure 3.3, panel B and Table 3.1). In contrast, the frequency of vmLANA$_{K251A/K253A}$ and vmLANA$_{K251E/K253E}$ infection in total splenocytes was similar to that of vWT virus (Figure 3.3, panel B and Table 3.1). Frequencies of infection for all recombinant viruses declined at 21 dpi (Figure 3.3, panel B and Table 3.1), reaching low levels of long-term persistence at 50 dpi (Figure 3.3, panel B and Table 3.1).

Altogether, these data demonstrate that residues at the charged patch periphery of mLANA dorsal face are required for efficient expansion of MuHV-4 latent infection, whereas substitution of residues in the central region have little effect.

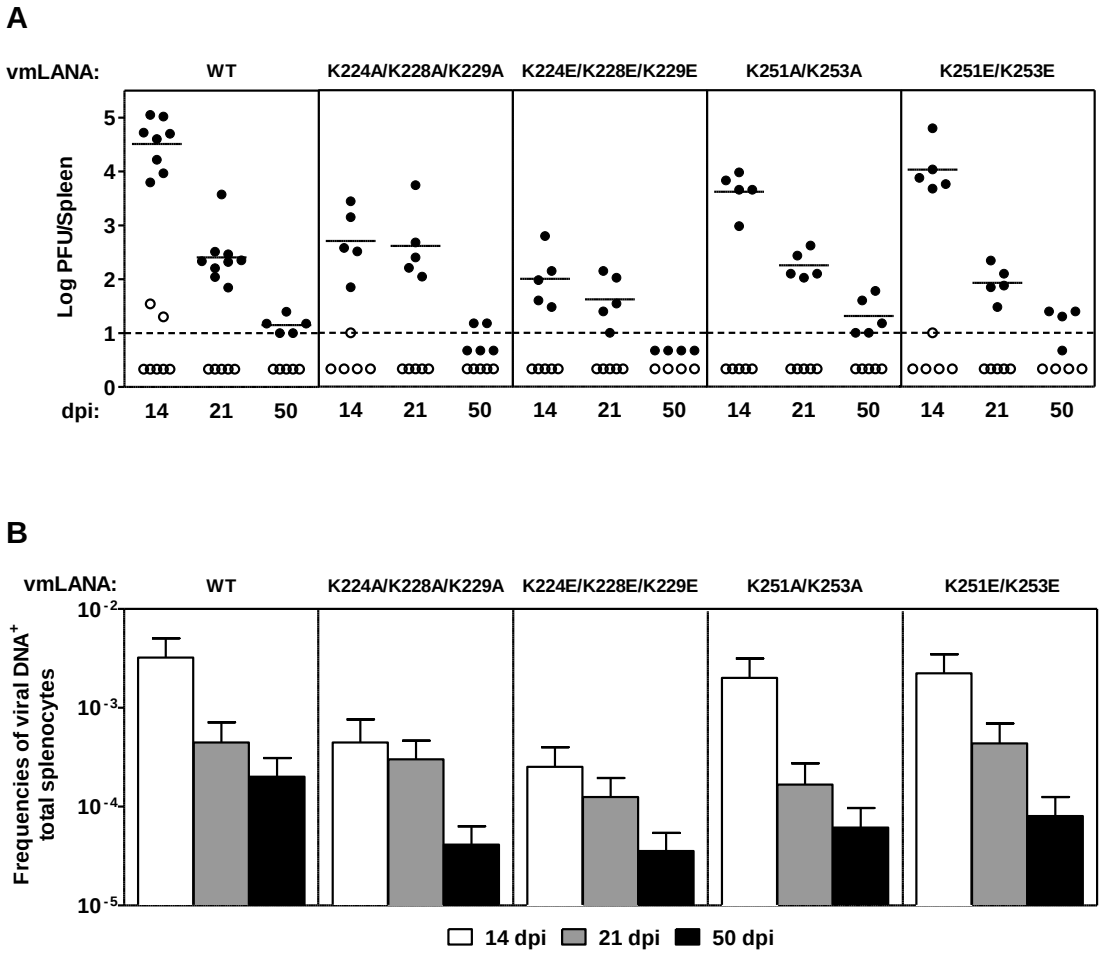

Figure 3.3. The positive patch periphery of mLANA dorsal face is required for efficient expansion of MuHV-4 latency. (A) Quantification of latent infection in spleen by *ex vivo* reactivation assay. C57BL/6 mice were intranasally infected with 10^4 PFU of the indicated viruses. At days 14, 21 and 50 post-infection, latent viruses in spleens were titrated by infectious centre assay (closed circles). Titres of preformed infectious viruses were determined in frozen-thawed splenocyte suspensions (open circles). Each circle represents the titre of an individual mouse. Horizontal bars show arithmetic means. The dashed line represents the limit of detection of the assay. (B) Quantification of viral DNA-positive cells in total splenocytes. C57BL/6 mice were intranasally infected with 10^4 PFU of the indicated viruses. At days 14, 21 and 50 post-infection, reciprocal frequencies of viral infection in total splenocytes were determined by limiting dilution and real-time PCR. Data were obtained from pools of five spleens per group. Bars represent the frequency of viral DNA-positive cells with 95% confidence intervals.

Table 3.1. Frequency of MuHV-4 latent infection in total splenocytes[a].

Virus	Dpi	Reciprocal frequency[b] of viral DNA$^+$ cells (95% CI)	
vWT	14	310	(198-707)
	21	2243	(1405-5545)
	50	4976	(3220-10952)
$vmLANA_{K224A/K228A/K229A}$	14	2242	(1311-7712)
	21	3322	(2148-7334)
	50	24175	(15796-51478)
$vmLANA_{K224E/K228E/K229E}$	14	3953	(2502-9373)
	21	7985	(5134-17955)
	50	28081	(18461-58638)
$vmLANA_{K251A/K253A}$	14	499	(317-1170)
	21	5979	(3653-16461)
	50	16282	(10332-38380)
$vmLANA_{K251E/K253E}$	14	448	(287-1019)
	21	2296	(1442-5630)
	50	12444	(8010-27880)

[a]Data were obtained from pools of 5 spleens.

[b]Frequencies were calculated by limiting dilution coupled to real-time PCR, with 95% confidence intervals (CI).

3.2.4. The positive patch periphery of mLANA dorsal face is required for efficient MuHV-4 colonization of GC B cells

To assess whether the deficit in the establishment of latency exhibited by recombinant viruses bearing mutations at the positive patch periphery of mLANA dorsal face reflected an impairment of latency amplification in GC B cells, the frequency of viral DNA-positive cells in this subpopulation was determined by limiting dilution combined with real-time PCR (Marques *et al.*, 2003).

To this end, GC B cells from C57BL/6 mice intranasally infected with vWT or recombinant viruses were FACS-purified at 14 dpi, by enriching for $CD19^+CD95^{hi}GL7^{hi}$ cells. The purity of the sorted GC B cell population was higher than 95%. Purified GC B cells were then analysed by real-time PCR for the presence of viral genomes, using a set of primers and probe specific for MuHV-4 *M9* gene (Marques *et al.*, 2003) (Materials and Methods, section 8.2.10).

The results obtained are shown in Figure 3.4 and Table 3.2. The frequency of infection in GC B cells at 14 dpi was one order of magnitude lower for $vmLANA_{K224A/K228A/K229A}$ and two orders of magnitude lower for $vmLANA_{K224E/K228E/K229E}$, comparing to vWT infection. The frequency of $vmLANA_{K251A/K253A}$ and $vmLANA_{K251E/K253E}$ infection in GC B cells was similar to that of vWT virus.

These data show that the latency deficit of vmLANA$_{K224A/K228A/K229A}$ and vmLANA$_{K224E/K228E/K229E}$ recombinants correlates with an impairment in latency expansion in GC B cells. Therefore, K224, K228 and K229 residues, located at the periphery of the dorsal positive patch of mLANA, are required for MuHV-4 to efficiently colonize GC B cells and expand latent infection, whereas the central region of mLANA dorsal positive patch has little impact on latency amplification in GC B cells.

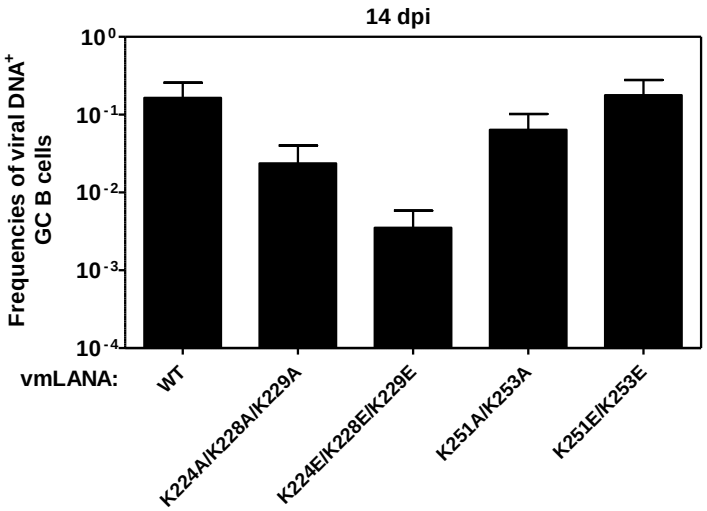

Figure 3.4. The positive patch periphery of mLANA dorsal face is required for efficient MuHV-4 colonization of GC B cells. Quantification of viral DNA-positive cells in GC B cells. C57BL/6 mice were intranasally infected with 10^4 PFU of the indicated viruses. At day 14 post-infection, reciprocal frequencies of viral infection in FACS-purified GC B cells ($CD19^+CD95^{hi}GL7^{hi}$) were determined by limiting dilution and real-time PCR. Data were obtained from pools of five spleens per group. Bars represent the frequency of viral DNA-positive cells with 95% confidence intervals.

Table 3.2. Frequency of MuHV-4 latent infection in GC B cells[a].

Virus	Dpi	Reciprocal frequency[b] of viral DNA$^+$ cells (95% CI)	
vWT		6	(4-14)
vmLANA$_{K224A/K228A/K229A}$		30	(20-59)
vmLANA$_{K224E/K228E/K229E}$	14	284	(171-841)
vmLANA$_{K251A/K253A}$		16	(10-39)
vmLANA$_{K251E/K253E}$		6	(4-13)

[a]Data were obtained from pools of 5 spleens. The purity of sorted cells was determined by FACS analysis and was always greater 95%.

[b]Frequencies were calculated by limiting dilution coupled to real-time PCR, with 95% confidence intervals (CI).

3.2.5. The positive patch periphery of mLANA dorsal face is required for efficient MuHV-4 latency amplification in splenic follicles

To confirm the role of the mutations introduced on mLANA dorsal positive patch in the formation of infected GCs, the ability of recombinant viruses to colonize splenic follicles and to induce latency expansion in GCs was assessed by *in situ* hybridization, using a probe specific for MuHV-4 tRNAs and miRNAs (Bowden *et al.*, 1997; Pfeffer *et al.*, 2005; Simas *et al.*, 1999).

Spleen sections from C57BL/6 mice intranasally infected with vWT or recombinant viruses were prepared at 14 dpi and processed for *in situ* hybridization (Materials and Methods, section 8.2.11). Mice infected with vmLANA$_{K224A/K228A/K229A}$ and vmLANA$_{K224E/K228E/K229E}$ viruses showed a reduction in the number of infected cells within positive follicles in comparison to vWT (Figure 3.5, panels b and c, respectively). In contrast, the pattern of splenic follicles colonization exhibited by vmLANA$_{K251A/K253A}$ and vmLANA$_{K251E/K253E}$ was similar to that of vWT virus, with large clusters of infected cells within GCs (Figure 3.5, panels d and e, respectively).

Consistent with the previous data, these results demonstrate that mutations at the periphery of the positive patch of mLANA dorsal face impair GC colonization and consequent expansion of the latently infected cell pool within splenic follicles, whereas mutations in the central region of mLANA dorsal positive patch have little effect on splenic follicle colonization.

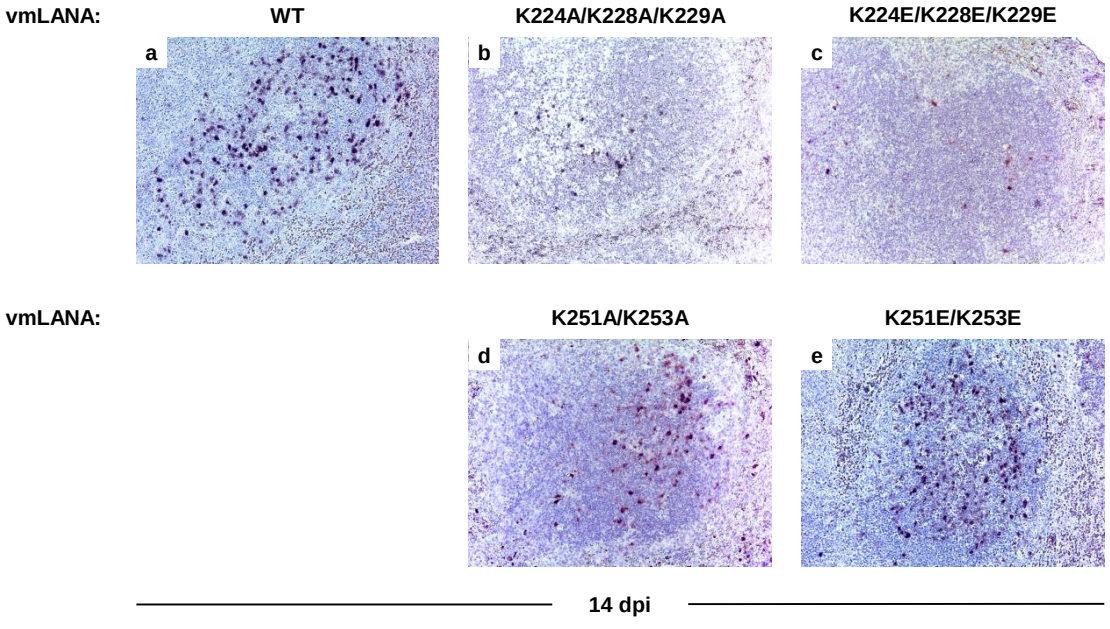

Figure 3.5. The positive patch periphery of mLANA dorsal face is required for efficient MuHV-4 latency amplification in splenic follicles. C57BL/6 mice were intranasally infected with 10^4 PFU of the indicated viruses. At 14 days post-infection, spleens were dissected and processed for *in situ* hybridization with a viral tRNA/miRNA-specific riboprobe. Panels show representative spleen sections from each group of animals.

Dark staining indicates cells positive for virally encoded tRNAs/miRNAs. All sections are magnified x200 and counterstained with haematoxylin.

3.2.6. Phenotypic changes in dorsal recombinant viruses are intrinsic to *ORF73* locus and not the consequence of mutations elsewhere in MuHV-4 genome

To ensure that the phenotypic alterations observed for vmLANA$_{K224A/K228A/K229A}$ and vmLANA$_{K224E/K228E/K229E}$ recombinant viruses reflected the mutations introduced in mLANA and were not the consequence of mutations introduced elsewhere in MuHV-4 genome during mutagenesis, the *ORF73* locus was restored to the wild-type status. To this end, revertant viruses (vmLANA$_{K224A/K228A/K229A}$-R and vmLANA$_{K224E/K228E/K229E}$-R) were generated from the respective mutant viral genomes cloned as a BAC (Materials and Methods, section 8.2.5). A revertant of vmLANA$_{K251A/K253A}$ virus (vmLANA$_{K251A/K253A}$-R) was also constructed, as a control of mutations introduced in the central region of the dorsal positive patch of mLANA.

C57BL/6 mice were intranasally infected with vWT or revertant viruses and latent load in spleen was determined by quantification of *ex vivo* reactivation-competent viruses in total splenocytes by infectious centre assay at 14 dpi. All revertant viruses were able to establish normal latency levels in spleen (Figure 3.6).

Therefore, these results confirm that the phenotypic changes observed for recombinant viruses result from the mutations introduced in mLANA, and not from mutations introduced elsewhere in the viral genome.

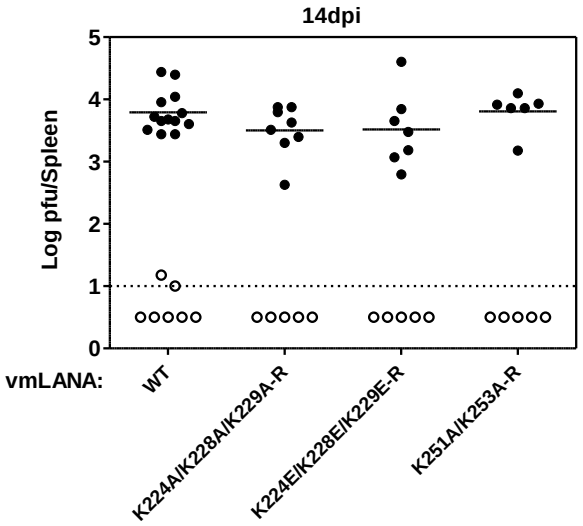

Figure 3.6. Phenotypic changes in dorsal recombinant viruses are intrinsic to *ORF73* locus and not the consequence of mutations elsewhere in MuHV-4 genome. Quantification of latent infection in spleen by *ex vivo* reactivation assay. C57BL/6 mice were intranasally infected with 10^4 PFU of the indicated viruses. At day 14 post-infection, latent viruses in spleens were titrated by infectious centre assay (closed circles). Titres of preformed infectious viruses were determined in frozen-thawed splenocyte suspensions (open circles). Each circle represents the titre of an individual mouse. Horizontal bars show arithmetic means. The dashed line represents the limit of detection of the assay.

3.3. Discussion

The work presented in this chapter highlights the importance of mLANA dorsal positively charged patch for the expansion of MuHV-4 latency in GC B cells. MuHV-4 recombinant viruses containing mutations at the periphery of mLANA dorsal patch displayed a substantial deficit in latency establishment, whereas recombinants with mutations in the central region of the dorsal patch exhibited only a mild attenuation of latency levels in spleen. However, the mechanisms by which mLANA dorsal patch exerts its function remain to be clarified.

The finding that mutations in the peripheral region of mLANA dorsal positive patch resulted in a substantially latency deficit is supported by other work (Hellert *et al.*, 2013). In fact, Hellert and colleagues found that a MuHV-4 recombinant virus harbouring mLANA mutations K228A/K229A/L230A/K231A exhibited a pronounced reduction of latency levels in the spleen of infected mice. mLANA dorsal positive patch harbours the identified ^{226}QAKKLK^{231} motif, which was previously shown to bind to BET proteins, specifically Brd2 and Brd4 (Ottinger *et al.*, 2009). BET proteins are important regulators of cellular transcription, interacting via their bromodomains with acetylated histones and recruiting transcriptional regulatory complexes to acetylated chromatin (Shi

and Vakoc, 2014; Wang and Filippakopoulos, 2015). Brd2 and Brd4, in particular, have been implicated in cell cycle control, and their deregulation has been associated with cancer (Prinjha *et al.*, 2012). Previous studies demonstrated that mLANA interacts with BET proteins to associate with cellular chromatin and activate BET-responsive promoters of G1/S cyclins, thus promoting cell cycle progression (Ottinger *et al.*, 2009). Notably, substitution of positively charged for negative residues in mLANA$_{K224E/K228E/K229E}$ reduced Brd4 binding, although substitution with neutral residues in mLANA$_{K224A/K228A/K229A}$ did not, as demonstrated elsewhere (Correia *et al.*, 2013). Similarly, mLANA$_{K251E/K253E}$, but not mLANA$_{K251A/K251A}$, was reduced for Brd4 binding, suggesting possible electrostatic inhibition when positively charged residues were substituted for ones with a negative charge. Therefore, the deficit in latency of vmLANA$_{K224A/K228A/K229A}$ and vmLANA$_{K224E/K228E/K229E}$ recombinant viruses observed in the present study does not correlate with binding to Brd4 protein, since mLANA$_{K224A/K228A/K229A}$ bound Brd4 normally. Moreover, mLANA$_{K251E/K253E}$ showed substantially reduced Brd4 binding but vmLANA$_{K251E/K253E}$ recombinant only exhibited mild latency attenuation. Altogether, these data indicate that the charged patch periphery of mLANA dorsal face contributes to the expansion of latency in GC B cells through a mechanism independent of Brd4. Nonetheless, it remains a possibility that mLANA dorsal patch periphery acts through interaction with Brd2, since binding of the mLANA dorsal mutants to this host protein has not been tested. Alternatively, the dorsal positive patch of mLANA may interact with other host protein(s) necessary for efficient latency expansion in GC B cells, as a replication factor or a chromosome-binding protein, thereby facilitating episome replication and persistence in proliferating cells.

The dorsal positive patch is a common feature of both MuHV-4 mLANA and KSHV kLANA (Correia *et al.*, 2013; Domsic *et al.*, 2013; Hellert *et al.*, 2013). Although the role of kLANA dorsal positive patch in the context of KSHV infection *in vivo* has not been formally demonstrated, kLANA dorsal positive patch, particularly the peripheral region, was recently shown to facilitate viral DNA replication and episome persistence in latently infected cells in culture (Domsic *et al.*, 2013; Li *et al.*, 2015). Experiments with kLANA dorsal mutants revealed that reductions in episome maintenance were independent of BET protein binding, but closely correlated with DNA replication deficiencies, suggesting that the replication defects account for the reduced episome persistence. The reduced DNA replication was not due to inability of kLANA to efficiently bind TR DNA. Given these findings and since mLANA mediates MuHV-4 episome persistence using mechanisms similar to kLANA (Habison *et al.*, 2012), it is likely that the disruption of mLANA dorsal positive patch, specially the peripheral region, impacts on viral DNA replication and episome persistence. This could explain the reductions in latency observed for the MuHV-4 recombinant viruses described in this chapter. Interestingly, all mLANA dorsal mutants used here bound to TR DNA, similarly to kLANA dorsal mutants (Correia *et al.*, 2013).

The dorsal positive patch of kLANA was recently shown to mediate interaction with DNA of arbitrary sequence, allowing the assembly into supermolecular spirals around DNA by self-association of kLANA (Hellert *et al.*, 2015). These spiral structures may also contain a plethora of

cellular proteins interacting with kLANA. To date, no spiral-like structures have been described for mLANA. However, mLANA has been shown to oligomerize (Correia *et al.*, 2013; Hellert *et al.*, 2013; Ponnusamy *et al.*, 2015) and the possibility that its dorsal positive patch is involved in the formation of supermolecular structures, with possible roles in viral DNA replication, may not be excluded.

In summary, mLANA dorsal positive patch could be divided into two regions with different functional effects, a central region and a peripheral region. Although the former had little effect on MuHV-4 latency establishment, the latter was required for efficient latency expansion in GC B cells. Future work should elucidate whether the dorsal positive patch exerts its effects through interactions with a particular host cell partner(s) other than Brd4 or through another mechanism, such as interacting with DNA in a sequence-independent manner to induce the formation of specific complexes required for episome replication and maintenance.

CHAPTER 4

mLANA E3 ubiquitin-ligase activity impacts on gammaherpesvirus latency amplification

mLANA E3 ubiquitin-ligase activity impacts on gammaherpesvirus latency amplification

4.1. Introduction

E3 ubiquitin-ligases control a broad range of cellular pathways, through ubiquitination of target proteins (Lydeard *et al.*, 2013). Previous studies in our laboratory demonstrated that mLANA assembles an E3 ubiquitin-ligase complex (EC_5S^{mLANA}) by recruiting cellular ElonginB/C and Cullin5, through an unconventional SOCS-box motif (amino acid residues 199-206) present in mLANA C-terminal domain (Rodrigues *et al.*, 2009). mLANA also acts as the substrate recognition component of the EC_5S^{mLANA} complex, interacting with cellular substrates through motifs independent of the SOCS-box, as yet unidentified (Rodrigues *et al.*, 2009; Rodrigues *et al.*, 2013). Two cellular targets of mLANA E3 ubiquitin-ligase activity are known: NF-κB and Myc. mLANA mediates poly-ubiquitination-dependent proteasomal degradation of the NF-κB family member p65, thus inhibiting NF-κB transcriptional activity (Rodrigues *et al.*, 2009). In contrast, mLANA stabilizes Myc through heterotypic poly-ubiquitination, thereby increasing Myc transcriptional activity (Rodrigues *et al.*, 2013).

The crystal structure of mLANA C-terminal domain revealed that the SOCS-box lies within a loop (β2-β3 loop, residues 199-215), which protrudes perpendicular to the DNA binding interface (Figure 4.1) (Correia *et al.*, 2013). mLANA-SOCS mutant, containing mutations of four SOCS-box residues (^{199}VSCLPLVP^{206}, underlined residues mutated to alanine), fails to bind to ElonginC, therefore abrogating mLANA E3 ubiquitin-ligase activity (Rodrigues *et al.*, 2009). A recombinant MuHV-4 virus bearing these mutations (vSOCS) exhibits a severe latency deficit, being unable to expand in GC B cells and persist in mice (Rodrigues *et al.*, 2009). However, recent studies have shown that mLANA-SOCS mutant is unable to bind viral TR DNA and to mediate episome persistence (Tan *et al.*, unpublished data), demonstrating that mutations introduced in mLANA-SOCS mutant compromised not only mLANA E3 ubiquitin-ligase activity, but also its function as DNA binding and episome maintenance protein. Since binding of mLANA to TR DNA is critical for viral latency expansion in GC B cells and virus persistence in mice, as demonstrated in the present study (chapter 2), the severe latency deficit of vSOCS recombinant virus cannot be exclusively attributed to the suppression of mLANA E3 ubiquitin-ligase activity. Therefore, the contribution of mLANA E3 ubiquitin-ligase activity for latent infection remains unclear.

To clarify the biological relevance of mLANA E3 ubiquitin-ligase activity for gammaherpesvirus pathogenesis, a structure-based (Correia *et al.*, 2013) mutagenesis approach was employed to generate MuHV-4 recombinant viruses containing mutations in mLANA SOCS-box. These mutations were designed so that E3 ubiquitin-ligase activity was impaired without compromising

episome maintenance function of mLANA. Recombinant viruses were intranasally administered to BALB/c mice and their phenotype was analysed during the establishment and maintenance of latency by *ex vivo* reactivation assay to determine latent load in spleen and limiting dilution coupled to real-time PCR to quantify the frequency of viral DNA-positive cells in total splenocytes (section 4.2.5).

Data presented in this chapter is included in the manuscript in Appendix 2, which is being prepared for submission.

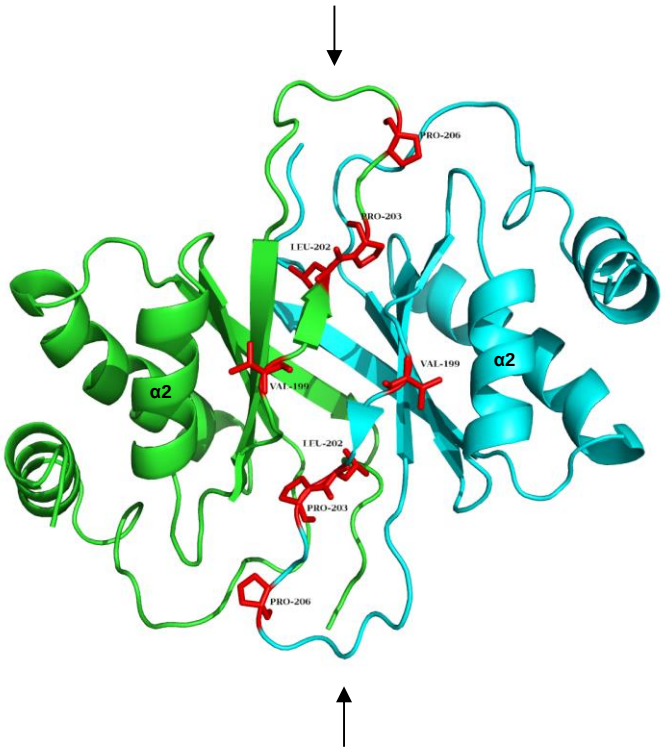

Figure 4.1. β2-β3 SOCS-box loop of mLANA. The mLANA dimer interface on the ventral side is represented. The β2-β3 SOCS-box loop (indicated by arrows) protrudes perpendicular to the DNA binding interface. V199, L202, P203 and P206 residues in the SOCS-box are coloured in red. α2 is the predicted recognition helix. This figure was kindly provided by Dr Rajesh Ponnusamy from Dr C.E. McVey's laboratory (ITQB, Universidade Nova de Lisboa, Portugal).

4.2. Results

4.2.1. $mLANA_{V199A}$, $mLANA_{V199A/L202A}$ and $mLANA_{P203A/P206A}$ mutants exhibit impaired ability to inhibit NF-κB and to activate Myc transcriptional activities

mLANA-SOCS mutant contained valine (V) 199, leucine (L) 202, proline (P) 203 and proline (P) 206 residues substituted by alanine (A) (V199A, L202A, P203A and P206A) (Rodrigues *et al.*, 2009). To minimize the interference with DNA binding interface, six mLANA constructs containing different combinations of these mutations were generated: $mLANA_{V199A}$, $mLANA_{L202A}$, $mLANA_{V199A/L202A}$, $mLANA_{P203A}$, $mLANA_{P206A}$ and $mLANA_{P203A/P206A}$ (Figure 4.1). First, E3 ubiquitin-ligase activity of mLANA mutants towards NF-κB and Myc was evaluated, through reporter gene assays. Human embryonic kidney (HEK) 293T cells were transiently transfected with a NF-κB or Myc reporter plasmid containing tandem copies of kappa B (κB) or E-box consensus sequences (respectively) regulating the expression of luciferase (Brostjan *et al.*, 1997), and a plasmid encoding mLANA (WT or mutants). Tumour necrosis factor (TNF)-α was used as a stimulus leading to NF-κB activation. Luciferase activity was correlated with the amount of luciferase produced, which in turn depended on the amount of NF-κB or MYC molecules bound to the consensus sequences regulating luciferase expression. Therefore, NF-κB and MYC transcriptional activities could be quantified by measuring luciferase activity in each experimental condition.

NF-κB reporter assays showed that mLANA-WT inhibited TNF-driven NF-κB activation, while mLANA-SOCS mutations reverted this phenotype (Figure 4.2, panel A), reproducing the results of earlier studies (Rodrigues *et al.*, 2009). $mLANA_{V199A}$, $mLANA_{V199A/L202A}$ and $mLANA_{P203A/P206A}$ mutants exhibited impaired ability to inhibit TNF-driven NF-κB activation (Figure 4.2, panel A). In contrast, $mLANA_{L202A}$, $mLANA_{P203A}$ and $mLANA_{P206A}$ mutants behaved similarly to mLANA-WT, inhibiting NF-κB transcriptional activity (Figure 4.2, panel A). Myc reporter assays demonstrated that mLANA-WT promoted Myc transcriptional activity, whereas mLANA-SOCS mutant was unable to modulate Myc (Figure 4.2, panel B), as previously described (Rodrigues *et al.*, 2013). $mLANA_{V199A}$, $mLANA_{V199A/L202A}$ and $mLANA_{P203A/P206A}$ mutants exhibited impaired ability to increase Myc transcriptional activity, while $mLANA_{L202A}$, $mLANA_{P203A}$ and $mLANA_{P206A}$ mutants behaved similarly to mLANA-WT (Figure 4.2, panel B). Importantly, the levels of expression of mLANA mutants were similar (Figure 4.2, panel B, bottom panel). Taken together, these data demonstrate that mutations at residues V199, V199/L202 or P203/P206 compromise mLANA E3 ubiquitin-ligase activity.

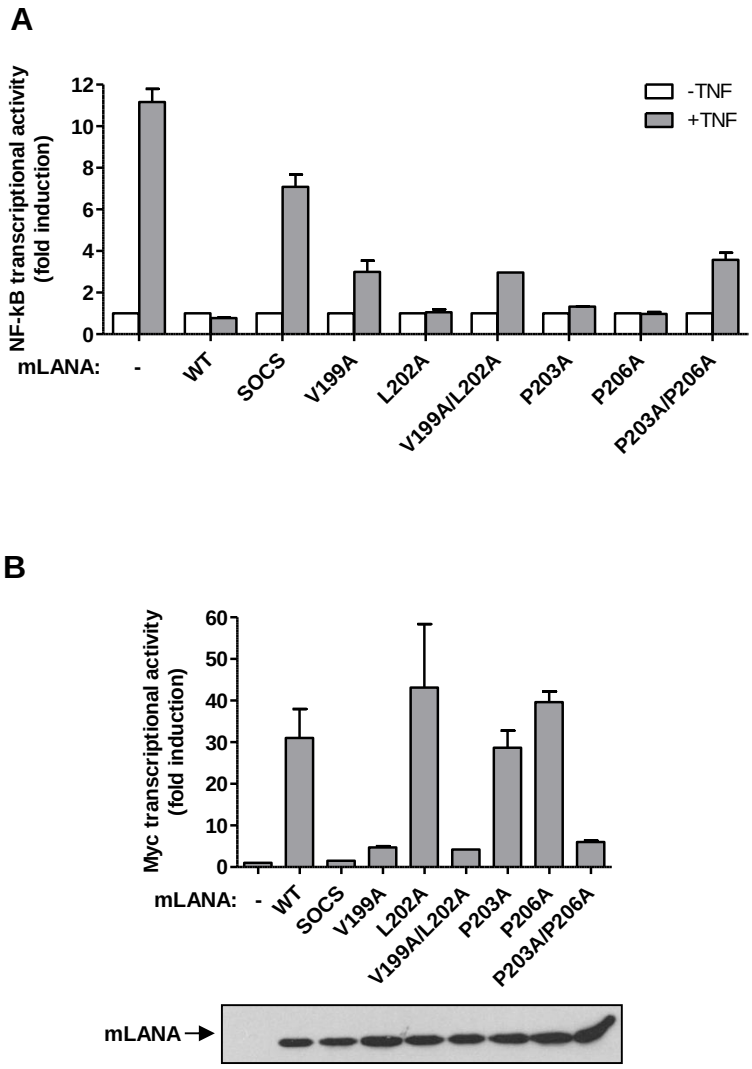

Figure 4.2. mLANA$_{V199A}$, mLANA$_{V199A/L202A}$ and mLANA$_{P203A/P206A}$ exhibit impaired ability to inhibit NF-κB and to activate Myc transcriptional activities. HEK 293T cells were transiently transfected with a NF-κB (A) or Myc (B) luciferase reporter vector and a plasmid encoding mLANA (WT or mutants), as indicated at the bottom. In (A), transfected cells were either stimulated with 50 ng/ml of TNF (filled bars) or left unstimulated (open bars). NF-κB (A) and Myc (B) transcriptional activities associated with each sample were assayed using a luminometer. Results are shown as the fold induction relative to luciferase activity measured in unstimulated cells (A) or in cells that did not express mLANA (B). Error bars represent SEM from triplicates from two independent transfection experiments. In addition, representative aliquots of the total cellular lysates were used to detect appropriate expression of mLANA (bottom panel).

4.2.2. mLANA$_{V199A}$, mLANA$_{V199A/L202A}$ and mLANA$_{P203A/P206A}$ mutants exhibit diminished capability to promote p65 and Myc poly-ubiquitination

mLANA targets nuclear p65 for poly-ubiquitination and subsequent proteasomal degradation, leading to a downmodulation of NF-κB transcriptional activity (Rodrigues *et al.*, 2009). In contrast, mLANA stabilizes Myc through heterotypic poly-ubiquitination, thereby promoting Myc transcriptional activity (Rodrigues *et al.*, 2013). Therefore, poly-ubiquitination assays were performed in order to investigate whether modulation of NF-κB and Myc mediated by mLANA mutants was dependent on the mechanism of substrate poly-ubiquitination. To accomplish this, HEK 293T cells were transiently transfected with expression plasmids encoding p65 or Myc, mLANA (WT or mutants) and His-tagged ubiquitin. His-tagged ubiquitin is incorporated into poly-ubiquitin chains, hence poly-ubiquitinated proteins are His-tagged. Ni-NTA beads have high affinity for His-tagged proteins, allowing their purification from an expression system. Thus, ubiquitinated proteins were pulled-down using Ni-NTA beads and the levels of ubiquitinated p65 and Myc present in each condition were analysed by Western-blot.

Poly-ubiquitination assays revealed that, similarly to mLANA-SOCS mutant, mLANA$_{V199A}$, mLANA$_{V199A/L202A}$ and mLANA$_{P203A/P206A}$ had diminished capability to promote both p65 (Figure 4.3, panel A) and Myc (Figure 4.3, panel B) poly-ubiquitination. In contrast, mLANA$_{L202A}$, mLANA$_{P203A}$ and mLANA$_{P206A}$ mutants enhanced p65 (Figure 4.3, panel A) and Myc (Figure 4.3, panel B) poly-ubiquitination as efficiently as mLANA-WT. These data demonstrate that the defective modulation of NF-κB and Myc transcriptional activities observed for mLANA$_{V199A}$, mLANA$_{V199A/L202A}$ and mLANA$_{P203A/P206A}$ mutants can be attributed to inefficient substrate poly-ubiquitination mediated by these mutants.

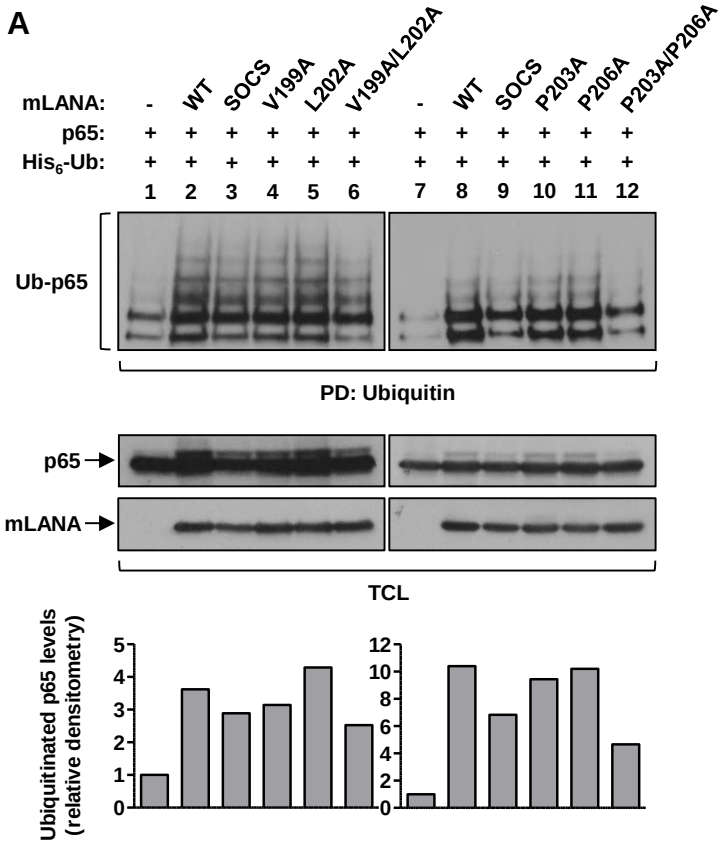
A
mLANA: - WT SOCS V199A L202A V199A/L202A - WT SOCS P203A P206A P203A/P206A
p65: + + + + + + + + + + + +
His6-Ub: + + + + + + + + + + + +
1 2 3 4 5 6 7 8 9 10 11 12
Ub-p65
PD: Ubiquitin
p65
mLANA
TCL
Ubiquitinated p65 levels (relative densitometry)
0 1 2 3 4 5
0 2 4 6 8 10 12

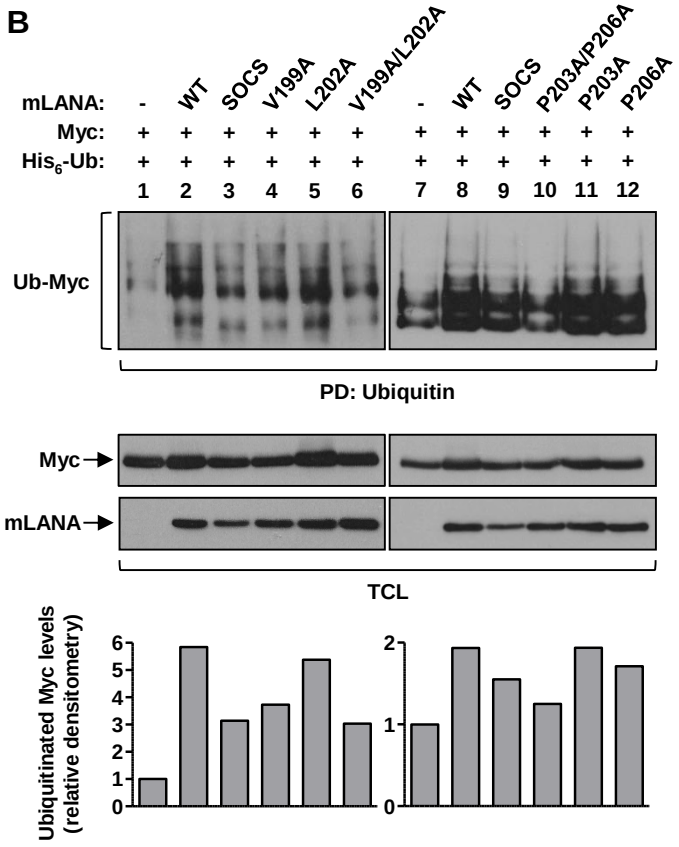
B
mLANA: - WT SOCS V199A L202A V199A/L202A - WT SOCS P203A/P206A P203A P206A
Myc: + + + + + + + + + + + +
His6-Ub: + + + + + + + + + + + +
1 2 3 4 5 6 7 8 9 10 11 12
Ub-Myc
PD: Ubiquitin
Myc
mLANA
TCL
Ubiquitinated Myc levels (relative densitometry)
0 1 2 3 4 5 6
0 1 2

Figure 4.3. mLANA$_{V199A}$, mLANA$_{V199A/L202A}$ and mLANA$_{P203A/P206A}$ exhibit diminished capability to promote p65 and Myc poly-ubiquitination. HEK 293T cells were transiently transfected with plasmids encoding mLANA (WT or mutants), p65 (A) or Myc (B) and histidine-tagged ubiquitin, as indicated on top. After 48 h, total cellular lysates were subjected to a Ni-NTA pull-down, allowing the purification of ubiquitinated proteins. The levels of ubiquitinated p65 (A) or Myc (B) in each condition were assayed using an anti-p65 or anti-Myc antibody (first panel), respectively. Representative aliquots of the total cellular lysates were used to detect the appropriate expression of p65 (A) or Myc (B) (second panel) and mLANA (third panel). Graphs at the bottom show densitometry analysis of ubiquitinated p65 (A) and ubiquitinated Myc (B) levels present in each experimental condition, expressed as fold induction relative to cells not expressing mLANA. -, without; +, with; PD, pull-down; TCL, total cellular lysates; Ub, ubiquitinated.

4.2.3. mLANA$_{V199A}$, mLANA$_{V199A/L202A}$ and mLANA$_{P203A/P206A}$ mutants weakly associate with ElonginC and Cullin5

To investigate whether poly-ubiquitination activity of mLANA mutants relied on the reconstitution of an E3 ubiquitin-ligase complex, their ability to associate with ElonginC and Cullin5 was tested by co-immunoprecipitation experiments. HEK 293T cells were transiently transfected with expression plasmids encoding ElonginC or Cullin5 and mLANA (WT or mutants). Cell lysates were incubated with antibodies to ElonginC or Cullin5 and immunecomplexes were recovered by incubation with beads coupled to Protein G, which binds to the Fc region of class G immunoglobulin (IgG) from several mammalian species (Akerstrom *et al.*, 1985). The presence of mLANA in immunecomplexes was then analysed by Western-blot, using the appropriate antibodies.

As reported previously (Rodrigues *et al.*, 2009), mLANA-WT associated with ElonginC and Cullin5 (Figure 4.4, panels A and B, respectively), and mutations introduced at mLANA-SOCS resulted in loss of binding to those proteins (Figure 4.4). mLANA$_{V199A}$, mLANA$_{V199A/L202A}$ and mLANA$_{P203A/P206A}$ mutants were unable to recruit ElonginC (Figure 4.4, panel A) and weakly associated with Cullin5 (Figure 4.4, panel B), whereas mLANA$_{L202A}$, mLANA$_{P203A}$ and mLANA$_{P206A}$ efficiently recruited both ElonginC (Figure 4.4, panel A) and Cullin5 (Figure 4.4, panel B). These results demonstrate that mLANA$_{V199A}$, mLANA$_{V199A/L202A}$ and mLANA$_{P203A/P206A}$ mutants have impaired ability to assemble an E3 ubiquitin-ligase complex, thereby compromising their poly-ubiquitination activity towards p65 and Myc.

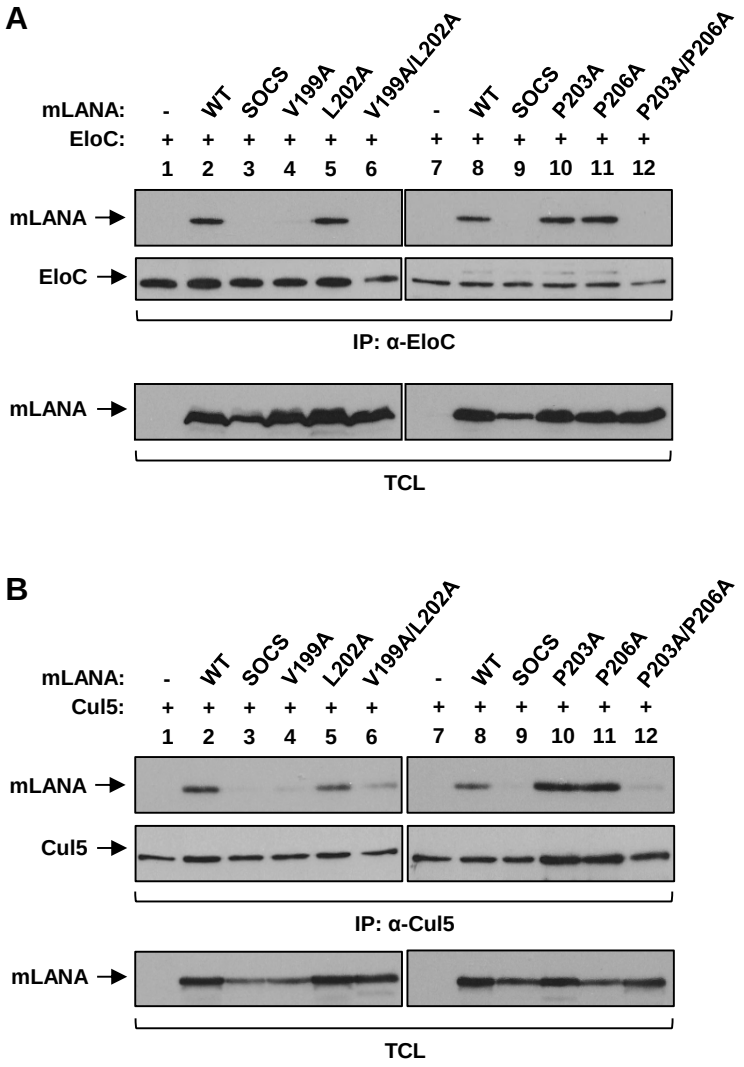

Figure 4.4. mLANA$_{V199A}$, mLANA$_{V199A/L202A}$ and mLANA$_{P203A/P206A}$ weakly associate with ElonginC and Cullin5. HEK 293T cells were transiently transfected with plasmids encoding mLANA (WT or mutants) and ElonginC (A) or Cullin5 (B), as indicated on top. After 48 h, cells were lysed and total cellular lysates were subjected to immunoprecipitation using an anti-ElonginC (A) or anti-Cullin5 (B) antibody. Immunoprecipitates were analysed by Western-blot (first and second panels). Representative aliquots of the total cellular lysates were used to detect the appropriate expression of mLANA (third panel). -, without; +, with; α, anti; IP, immunoprecipitation; TCL, total cellular lysates; EloC, ElonginC; Cul5, Cullin5.

Taken together, the data obtained indicate that mutations at residue V199, residues V199/L202 and residues P203/P206 of mLANA disrupt recruitment of ElonginC and, to a lower extent, Cullin5, thus impairing the formation of EC_5S^{mLANA} E3 ubiquitin-ligase complex and, consequently, mLANA function as a mediator of p65 and Myc poly-ubiquitination. Hence, mutations at these residues impair mLANA E3 ubiquitin-ligase activity, which impacts on its ability to modulate NF-κB and Myc transcriptional activities.

4.2.4. Generation of MuHV-4 recombinant viruses harbouring mutations in mLANA SOCS-box

To assess whether the mutations introduced in SOCS-box impacted on episome maintenance function of mLANA, our collaborator Dr Min Tan from Prof. K.M. Kaye's laboratory (Harvard Medical School, USA) further characterized these mutants regarding their ability to bind TR DNA and maintain viral episome (Tan *et al.*, unpublished data). His experiments demonstrated that mLANA$_{V199A}$, mLANA$_{L202A}$, mLANA$_{P203A}$, mLANA$_{P206A}$, and mLANA$_{P203A/P206A}$ mutants were able to maintain episomes, despite only mLANA$_{L202A}$ and mLANA$_{P206A}$ exhibited strong binding to TR DNA. mLANA$_{V199A/L202A}$ mutant showed a severe DNA binding deficiency and failed to maintain episomes.

To assess the impact of mLANA E3 ubiquitin-ligase impairment in the physiological context of latency *in vivo*, two MuHV-4 recombinant viruses containing E3 ubiquitin-ligase deficient mLANA with mutation V199A (vmLANA$_{V199A}$) or mutations P203A/P206A (vmLANA$_{P203A/P206A}$) were generated. Recombinant viruses bearing mLANA mutations P203A (vmLANA$_{P203A}$), which exerted WT E3 ubiquitin-ligase activity, or V199A/L202A (vmLANA$_{V199A/L202A}$), which was E3 ubiquitin-ligase deficient and did not maintain episome persistence, were generated as controls.

MuHV-4 recombinants were generated by mutagenesis of the viral genome cloned as a BAC (Adler *et al.*, 2000), as described in detail in Materials and Methods, section 8.2.5. Verification of the introduced mutations was carried out by restriction enzyme digestion and sequencing across *ORF73* gene in the BAC vector. The genomic structure of generated viruses was verified by examination of restriction enzyme digestion profiles of *E. coli*-derived BAC DNA. Infectious viruses were reconstituted by transfection of BAC DNA into BHK-21 fibroblasts and BAC sequences were removed by propagating the viruses in NIH-3T3 fibroblasts expressing Cre recombinase (Stevenson *et al.*, 2002). The stability of the introduced mutations was checked in viruses recovered from latently infected spleens, by sequencing *ORF73* gene in viral HMW DNA extracted from frozen-thawed splenocyte suspensions of infected mice. This analysis confirmed the retention of the engineered point mutations following *in vivo* infection.

Previous work in our laboratory found that vSOCS recombinant virus displayed normal lytic replication kinetics *in vitro* and *in vivo* (Rodrigues *et al.*, 2009), demonstrating that the mutations introduced in mLANA SOCS-box did not affect virus lytic replication. Since the recombinant viruses engineered in this section harboured different combinations of vSOCS mutations, it is reasonable to assume that they also exhibit normal lytic replication.

4.2.5. Impairment of mLANA E3 ubiquitin-ligase activity impacts on MuHV-4 latency amplification

To clarify the biological relevance of mLANA E3 ubiquitin-ligase activity for gammaherpesvirus latency, MuHV-4 recombinant viruses described in section 4.2.4 were used to intranasally infect BALB/c mice. vWT virus was included in the experiments for comparative purposes. The effect of the engineered mLANA mutations on latent infection was then assessed by two complementary experiments. Latent load in spleen was examined by quantification of *ex vivo* reactivation-competent viruses by infectious centre assay. Limiting dilution combined with real-time PCR to detect viral DNA-positive cells (Marques *et al.*, 2003) was applied to determine the frequency of infection of total splenocytes.

All viruses were evaluated at 14 and 21 dpi for their ability to establish and expand a latent load in spleen. The results obtained are shown in Figure 4.5. vWT virus presented the expected peak of infection at 14 dpi (Figure 4.5, panel A), with latent infection subsiding at 21 dpi (Figure 4.5, panel C), as previously described (Cardin *et al.*, 1996; Flano *et al.*, 2003; Marques *et al.*, 2003; Simas and Efstathiou, 1998; Sunil-Chandra *et al.*, 1992b). In contrast, vmLANA$_{V199A}$ and vmLANA$_{P203A/P206A}$ viruses exhibited an attenuation of latency at 14 dpi (Figure 4.5, panel A). Consistent with this result, the frequency of vmLANA$_{V199A}$ and vmLANA$_{P203A/P206A}$ infection in total splenocytes at 14 dpi was about 10-fold lower than vWT infection (Figure 4.5, panel B, and Table 4.1). At 21 dpi, levels of latent infection were similar for vmLANA$_{V199A}$, vmLANA$_{P203A/P206A}$ and vWT (Figure 4.5, panel C). No preformed infectious viruses were detected at any time point by suspension assay of frozen-thawed spleen homogenates, showing that splenic infection was only latent (Figure 4.5, panels A and C, open circles). Altogether, these data demonstrate that the impairment of mLANA E3 ubiquitin-ligase activity impacts on MuHV-4 latency amplification.

The splenic latency levels established by vmLANA$_{P203A}$ virus at 14 dpi were identical to vWT (Figure 4.5, panel A), declining at 21 dpi (Figure 4.5, panel C). This is in good agreement with the previous observation that E3 ubiquitin-ligase and episome maintenance functions of mLANA$_{P203A}$ mutant were intact.

Unexpectedly, vmLANA$_{V199A/L202A}$ virus only exhibited an attenuation of latency at 14 dpi (Figure 4.5, panel A), which is not in agreement with the observation that mLANA$_{V199A/L202A}$ does not mediate episome maintenance (Tan *et al.*, unpublished data). As demonstrated in chapter 2, a virus containing mLANA unable to bind to viral TR DNA, and hence unable to mediate episome persistence, is severely compromised in establishment of latent infection in mice. Therefore, it was expected that vmLANA$_{V199A/L202A}$ virus would be incapable of viable latency in mice. These findings gave rise to a new set of experiments, described in chapter 5. For this reason, these results will not be analysed in the discussion below, but rather in the next chapter of this thesis.

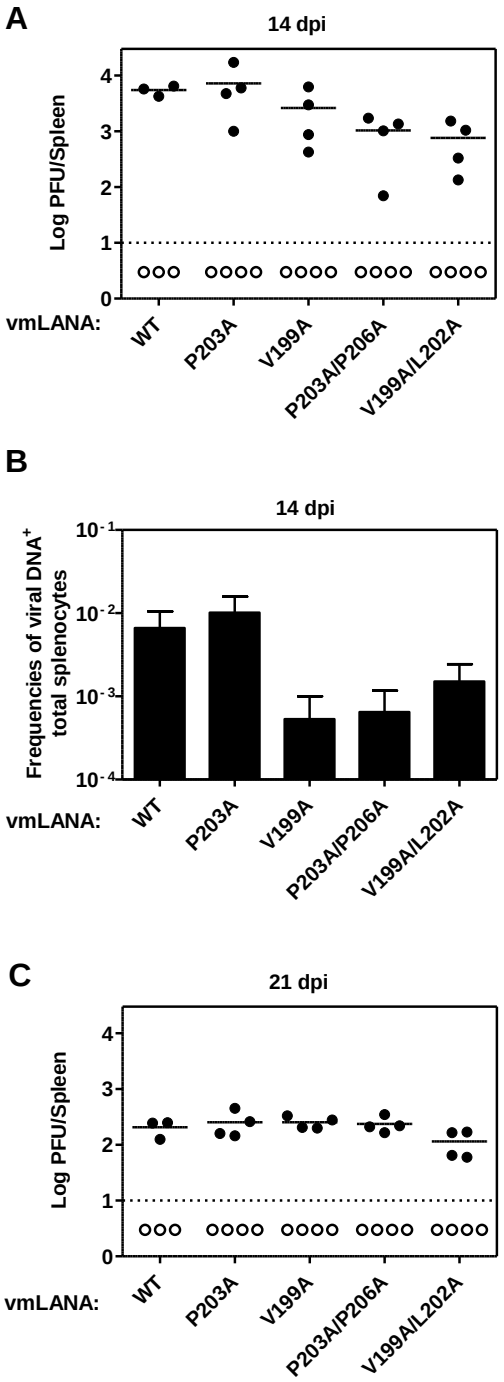

Figure 4.5. Impairment of mLANA E3 ubiquitin-ligase activity impacts on MuHV-4 latency amplification. (A and C) Quantification of latent infection in spleen by *ex vivo* reactivation assay. BALB/c mice were intranasally infected with 10^4 PFU of the indicated viruses. At days 14 (A) and 21 (C) post-infection, latent viruses in spleens were titrated by infectious centre assay (closed circles). Titres of preformed infectious viruses were determined in frozen-thawed splenocyte suspensions (open circles). Each circle represents the titre of an individual mouse. Horizontal bars show arithmetic means. The dashed line represents the limit of detection of the assay. (B) Quantification of viral DNA-positive cells in total splenocytes. BALB/c mice were intranasally infected with 10^4 PFU of the indicated viruses. At 14 dpi, reciprocal frequencies of viral infection in total splenocytes were determined by limiting dilution and real-time PCR. Data were obtained from pools of

three to four spleens per group. Bars represent the frequency of viral DNA-positive cells with 95% confidence intervals.

Table 4.1. Frequency of MuHV-4 latent infection in total splenocytes[a].

Virus	Dpi	Reciprocal frequency[b] of viral DNA$^+$ cells (95% CI)	
vWT		151	(95-367)
vmLANA$_{P203A}$		98	(63-219)
vmLANA$_{V199A}$	14	1877	(998-15734)
vmLANA$_{P203A/P206A}$		1544	(855-7916)
vmLANA$_{V199A/L202A}$		663	(411-1710)

[a]Data were obtained from pools of 3-4 spleens.

[b]Frequencies were calculated by limiting dilution coupled to real-time PCR, with 95% confidence intervals (CI).

4.3. Discussion

E3 ubiquitin-ligases control a broad range of cellular pathways, through ubiquitination of target proteins (Lydeard *et al.*, 2013). This study established a link between the E3 ubiquitin-ligase activity of mLANA viral protein and murid gammaherpesvirus pathogenesis *in vivo*. MuHV-4 recombinant viruses with mutations in mLANA SOCS-box compromising E3 ubiquitin-ligase activity, without abrogating episome maintenance function, exhibited an attenuation of latency. Therefore, mLANA E3 ubiquitin-ligase activity contributes to gammaherpesvirus latency expansion.

Myc is central to GC biology, being essential for the formation and maintenance of GCs (Basso and Dalla-Favera, 2015; Calado *et al.*, 2012; De Silva and Klein, 2015; Dominguez-Sola *et al.*, 2012). mLANA modulates Myc through heterotypic poly-ubiquitination, increasing protein stability and prolonging its half-life (Rodrigues *et al.*, 2013). Therefore, mLANA increases Myc transcriptional activity and expression of Myc target genes, promoting cell divisions during the expansion of MuHV-4 infected B cells in GCs. In the current study, mLANA E3 ubiquitin-ligase activity was impaired, thus inhibiting mLANA-mediated Myc modulation. Hence, the impairment of mLANA E3 ubiquitin-ligase activity may have decreased the proliferative potential of latently infected B cells within GCs, attenuating viral latency amplification. Furthermore, centroblasts – the proliferating GC B cells – do not display NF-kB activation, suggesting that NF-kB signalling needs to be switched off during GC proliferation in order to prevent premature differentiation into plasma and memory B cells (Basso *et al.*, 2004; Heise *et al.*, 2014; Shaffer *et al.*, 2001). Previous research conducted in our laboratory indicated that mLANA mimics the GC physiological inhibition of NF-kB

to promote the development of virus-driven GC reactions to expand the host pool of latently infected cells (Rodrigues *et al.*, 2009). Hence, the partial loss of mLANA-mediated NF-kB inhibition observed in the present study may have impaired the proliferation of latently infected GC B cells, thus contributing to a deficit in viral latency expansion. In addition, mLANA may target other cellular proteins for poly-ubiquitination, so that impairing E3 ubiquitin-ligase activity may hamper mLANA-mediated modulation of other proteins relevant to MuHV-4 latency expansion. Quantification of infection in GC B cells for recombinant viruses containing mLANA deficient for E3 ubiquitin-ligase activity would be required to establish a definitive link between mLANA E3 ubiquitin-ligase activity and latency expansion in GCs.

The results of the *in vivo* experiments performed in this study showed that the impairment of mLANA E3 ubiquitin-ligase activity did not eliminate latency amplification. This result likely reflects the fact that the mutations introduced in mLANA SOCS-box did not completely abolish the E3 ubiquitin-ligase activity of mLANA. Therefore, the remaining activity may have sufficed to enable the virus to modulate NF-kB and Myc, although less efficiently, and thus to expand latency in GC B cells. To demonstrate an unequivocal effect of mLANA E3 ubiquitin-ligase activity on viral latency, a complete ablation of this function would be required. However, despite several efforts in our laboratory to identify residues in mLANA SOCS-box which are essential to E3 ubiquitin-ligase activity, it has not been possible to find a set of mutations that completely disrupt E3 ubiquitin-ligase activity without compromising episome maintenance function. In fact, the mLANA-SOCS mutant (V199A/L202A/P203A/P206A) reported earlier (Rodrigues *et al.*, 2009) exhibited an ablation of E3 ubiquitin-ligase activity, but could not bind TR DNA nor maintain viral episome, as demonstrated in the current study. The crystal structure of mLANA C-terminal domain revealed that the SOCS-box lies within a loop (β2-β3 loop, residues 199-215), which protrudes perpendicular to the DNA binding interface (Correia *et al.*, 2013). Given the spatial proximity of these two functional regions, it is possible that the introduction of certain mutations in SOCS-box impacts on the predicted DNA recognition helix α2, disrupting DNA binding interface and, consequently, mLANA-mediated episome persistence. Current structural studies on mLANA-ElonginB/C-Cullin5 complex are being performed in our laboratory, since determining the structure of mLANA in complex with its ligands may reveal key interacting residues in mLANA SOCS-box. In any case, the finding that deficient mLANA E3 ubiquitin-ligase activity reduced viral latency suggests that complete inhibition of this activity could result in an even more severe effect on the ability of the virus to establish latent infection, perhaps abolishing it.

KSHV kLANA is also able to assemble an EC_5S ubiquitin-ligase complex (EC_5S^{kLANA}) through a SOCS-box motif (Cai *et al.*, 2006). EC_5S^{kLANA} complex promotes poly-ubiquitination of p53, VHL and p65, targeting these substrates for degradation (Cai *et al.*, 2006; Li *et al.*, 2011). In addition, kLANA stabilizes Myc through two mechanisms which do not involve its E3 ubiquitin-ligase activity (Liu *et al.*, 2007). kLANA blocks GSK-3-mediated phosphorylation of Myc at T58 residue and thus Myc degradation, while independently stimulating ERK1-mediated phosphorylation of Myc at S62

residue, an event that stabilizes Myc (Liu *et al.*, 2007; Sears *et al.*, 2000). Therefore, similarly to mLANA, kLANA inhibits NF-kB and promotes Myc stabilization, highlighting the importance of the modulation of these cellular transcription factors for gammaherpesvirus latency.

The property of a viral protein assembling an EC_5S E3 ubiquitin-ligase complex through a SOCS-box motif is not unique to LANA proteins. However, the biological significance of such a mechanism for viral pathogenesis *in vivo* remains largely unknown. A recent study showed that HIV-1 Vif-mediated degradation of APOBEC3 proteins, the targets of Vif E3 ubiquitin-ligase activity, is important for viral propagation *in vivo* (Sato *et al.*, 2014). The authors infected a humanized mouse model with HIV-1 mutants, which contained mutations in Vif motifs involved in interaction with APOBEC3 proteins. Although those mutations did not specifically inhibit Vif E3 ubiquitin-ligase activity, since they were introduced in Vif substrate binding motifs rather than in its SOCS-box, this study points out the importance of Vif E3 ubiquitin-ligase activity *in vivo*, at least on APOBEC3 proteins. However, the work presented in this thesis is novel in the sense that it assesses the impact of the assembly of an E3 ubiquitin-ligase complex by a gammaherpesvirus protein during latency *in vivo*.

Given the importance of the ubiquitin system, it is not surprising that gammaherpesviruses have developed a strategy to hijack host proteins involved in the ubiquitination pathway. This work provides evidence for the *in vivo* importance of the E3 ubiquitin-ligase complex, through which mLANA modulates at least two cellular proteins whose regulation is critical for GC reaction, NF-kB and Myc, thus promoting virus expansion during latency. Although mLANA E3 ubiquitin-ligase activity was not completely ablated, the partial impairment of this function was sufficient to reduce viral latency levels. Thus, pharmacological inhibition of LANA E3 ubiquitin-ligase activity through targeting of SOCS-box motifs is a putative strategy to control gammaherpesvirus infection.

CHAPTER 5

DNA binding-deficient mLANA mediates episome persistence in the context of multiple TR elements

DNA binding-deficient mLANA mediates episome persistence in the context of multiple TR elements

5.1. Introduction

Chapter 2 of this study demonstrated that mLANA binding to viral TR DNA is critical for the establishment and maintenance of MuHV-4 latency *in vivo*. However, vmLANA$_{V199A/L202A}$ recombinant virus, engineered in chapter 4, was able to expand latency in mice (Figure 4.5, panel A) despite mutations in mLANA which severely compromised DNA binding and abolished episome persistence. Hence, it was reasonable to consider the hypothesis that mLANA$_{V199A/L202A}$ likely mediated MuHV-4 episome maintenance although no viral episomes were detected in the presence of this mLANA mutant, as assessed by our collaborator Dr M. Tan from Prof. K.M. Kaye's laboratory (Harvard Medical School, USA) (Tan *et al.*, unpublished data).

In episome maintenance assays, performed by Dr M. Tan, a plasmid containing mLANA$_{V199A/L202A}$ coding sequence and four TR elements was transfected into mouse embryonic fibroblast (MEF) cells (Tan *et al.*, unpublished data). mLANA acts on TR elements to mediate episome persistence, thereby allowing the maintenance of the transfected plasmid, whose presence is then detected in Gardella gels (Gardella *et al.*, 1984; Habison *et al.*, 2012). The number of TR elements in MuHV-4 genome is unknown. If MuHV-4 genome contains approximately 40 TR elements, similarly to KSHV (Lagunoff and Ganem, 1997), it is possible that this number may be necessary for mLANA episome maintenance function and that mLANA$_{V199A/L202A}$ may exert episome maintenance function in the setting of a higher number of TR elements. In fact, it was previously shown that mLANA episome maintenance efficiency was increased with eight compared to two or four TR elements (Habison *et al.*, 2012).

To investigate whether mLANA$_{V199A/L202A}$ could mediate MuHV-4 episome persistence in a whole-virus context, an *in vitro* system was set up during this study, using a MuHV-4 ORF50-deficient virus previously described (Milho *et al.*, 2009). MuHV-4 ORF50-deficient virus (MuHV-4 M3-Luc/ORF50^{-}eGFP) contains a deletion of *ORF50* exon 2 (Figure 5.1), preventing the expression of ORF50, the major lytic transactivator protein of MuHV-4 (Pavlova *et al.*, 2003; Wu *et al.*, 2000). As a consequence, when ORF50-deficient virus infects a permissive cell, it is unable to go through lytic replication and hence remains latent in the infected cell, persisting as an episome. This enables the establishment of cell lines latently infected with MuHV-4 and analysis of their content in viral episomes.

Data presented in this chapter is included in the manuscript in Appendix 2, which is being prepared for submission.

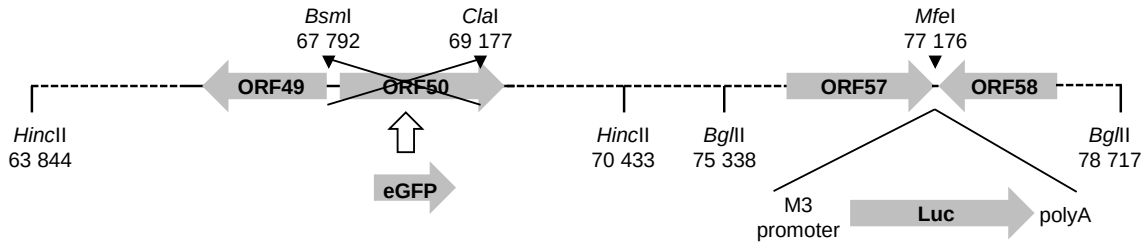

Figure 5.1. Schematic diagram of MuHV-4 ORF50-deficient virus (MuHV-4 M3-Luc/ORF50$^-$eGFP). eGFP was inserted in place of the removed ORF50 gene, and a M3 promoter-luciferase-polyA cassette was inserted between ORFs 57 and 58 (Milho *et al.*, 2009). Relevant restrictions sites are shown. eGFP, enhanced green fluorescent protein; Luc, luciferase.

5.2. Results

5.2.1. Generation of MuHV-4 ORF50-deficient recombinant viruses harbouring mutations in mLANA SOCS-box

To test the episome maintenance function of mLANA$_{V199A/L202A}$ mutant in a whole-virus context, an ORF50-deficient recombinant virus containing mLANA V199A/L202A mutation in the background of MuHV-4 ORF50-deficient genome (vORF50$^-$mLANA$_{V199A/L202A}$) was generated. mLANA-SOCS mutant was also tested using this approach, since it was previously characterized as being unable to bind viral TR DNA and to mediate episome persistence (Tan *et al.*, unpublished data), similarly to mLANA$_{V199A/L202A}$ mutant. Thus, an ORF50-deficient recombinant virus bearing mLANA V199A/L202A/P203A/P206A mutations (vORF50$^-$mLANA-SOCS) was constructed. ORF50-deficient virus containing mLANA-WT (vORF50$^-$mLANA-WT) was used as a positive control for episome maintenance.

MuHV-4 ORF50-deficient recombinants were generated by mutagenesis of MuHV-4 M3-Luc/ORF50$^-$eGFP genome cloned as a BAC (Milho *et al.*, 2009), as described in detail in Materials and Methods, section 8.2.5. MuHV-4 M3-Luc/ORF50$^-$eGFP contains a deletion of *ORF50* exon 2 (Figure 5.1), preventing the expression of ORF50. The coding sequence of eGFP is cloned in place of the removed fragment and a cassette consisting of the M3 promoter driving luciferase transcription is inserted between ORF57/58 (Figure 5.1).

Verification of the introduced mLANA mutations in the background of MuHV-4 ORF50-deficient genome was carried out by restriction enzyme digestion and sequencing across *ORF73* gene in the BAC vector. The genomic structure of generated viruses was verified by examination of restriction enzyme digestion profiles of *E. coli*-derived BAC DNA. Infectious viruses were

reconstituted by transfection of BAC DNA into 3T3-ORF50 complementing cell lines (Milho *et al.*, 2009) and treating cells with doxycycline. 3T3-ORF50 complementing cell lines express ORF50 under a doxycycline-inducible promoter. Thus, by treating infected cells with doxycycline, ORF50-deficient virus reactivates from latency and viral replication occurs, allowing the production of virus working stocks (Milho *et al.*, 2009).

5.2.2. Generation of cell lines latently infected with MuHV-4 ORF50-deficient recombinant viruses

To generate latently infected cell lines, MEF-1 cells were infected with MuHV-4 ORF50-deficient recombinant viruses at a MOI of 3 PFU per cell, to ensure that nearly all cells were infected. Cells were seeded at low density, to generate individual clones, and placed under drug selection with mycophenolic acid (MPA) and xanthine (Figure 5.2).

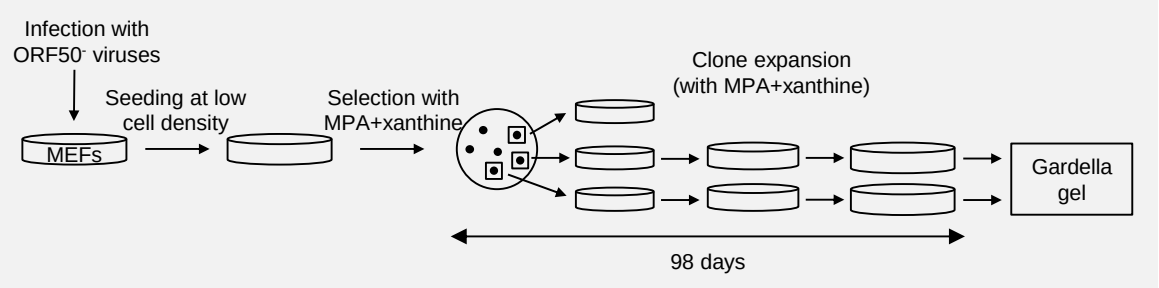

Figure 5.2. Experimental strategy to establish cell lines latently infected with MuHV-4 ORF50-deficient recombinant viruses. MEF-1 cells were infected with ORF50-deficient recombinant viruses at a MOI of 3 PFU per cell. Two days after infection, cells were trypsinised, counted and seeded at low cell density. Fresh medium containing MPA and xanthine was added. Resistant clones were picked, expanded under continued drug selection and analysed in Gardella gels for the presence of viral genomes. MPA, mycophenolic acid.

MPA inhibits *de novo* synthesis of cellular purines, thereby inhibiting nucleic acid synthesis and preventing cell growth (Franklin and Cook, 1969; Mulligan and Berg, 1981). However, cells expressing *E. coli* enzyme guanosine phosphoribosyl transferase (GPT) can grow under these conditions, since this enzyme is able to synthesize purine precursors from xanthine (Mulligan and Berg, 1981). BAC-derived MuHV-4 ORF50-deficient viruses retain the BAC cassette (Milho *et al.*, 2009), which contains *gpt* gene from *E. coli* (Adler *et al.*, 2000), encoding GPT enzyme (Figure 5.3). Therefore, *gpt* acted as a selective marker, allowing selection of cells latently infected with ORF50-deficient viruses in the presence of MPA and xanthine. Since mLANA is essential for viral episome maintenance (Habison *et al.*, 2012), only MEF cells latently infected with an ORF50-deficient virus containing mLANA able to mediate episome persistence are expected to efficiently persist under drug selection.

Figure 5.3. Schematic diagram of the left end of BAC-cloned MuHV-4 genome. Viral terminal repeats and the *gpt* gene, BAC sequences and *gfp* gene, flanked by *loxP* sites, are shown, as described by Adler *et al.*, 2000. TR, terminal repeats; *gpt*, guanosine phosphoribosyl transferase; BAC, bacterial artificial chromosome; *gfp*, green fluorescent protein.

The same number of MEF cells was infected with each virus. Infection with vORF50$^-$mLANA-SOCS resulted in only five MPA-resistant clones, whereas the number of MPA-resistant clones for vORF50$^-$mLANA-WT or vORF50$^-$mLANA$_{V199A/L202A}$ was too numerous to count (Table 5.1). The high rate of MPA outgrowth for vORF50$^-$mLANA$_{V199A/L202A}$, similar to vORF50$^-$mLANA-WT, suggested that mLANA$_{V199A/L202A}$ mediated episome maintenance, whereas the low outgrowth of vORF50$^-$mLANA-SOCS was consistent with absence of episome maintenance. Ten vORF50$^-$mLANA-WT or vORF50$^-$mLANA$_{V199A/L202A}$ clones, and all five vORF50$^-$mLANA-SOCS clones were picked for expansion under drug selection with MPA and xanthine in order to establish stable cell lines latently infected with MuHV-4 ORF50-deficient viruses.

Six of ten vORF50$^-$mLANA-WT and eight of ten vORF50$^-$mLANA$_{V199A/L202A}$ clones could be expanded after 98 days (Table 5.1). In contrast, all five vORF50$^-$mLANA-SOCS clones failed to expand and cells died (Table 5.1). These results are consistent with mLANA-WT and mLANA$_{V199A/L202A}$, but not mLANA-SOCS, efficiently maintaining viral episomes.

5.2.3. mLANA$_{V199A/L202A}$ mutant efficiently mediates episome persistence in a whole-virus context

To confirm the presence of episomal DNA, MPA-resistant cells were assessed by Gardella gel analysis (Gardella *et al.*, 1984). These experiments were performed by Dr M. Tan from Prof. K.M. Kaye's laboratory (Harvard Medical School, USA) and data presented in this section were produced by him, using cell lines latently infected with MuHV-4 ORF50-deficient viruses obtained by me.

Five million cells of each cell line were loaded into Gardella gels and lysed *in situ* as electrophoresis occurred. DNA was then transferred to a nylon membrane and detected with a TR probe to detect viral DNA. Gardella gel analysis showed that all six vORF50$^-$mLANA-WT and all eight vORF50$^-$mLANA$_{V199A/L202A}$ cell lines contained episomes (Figure 5.4 and Table 5.1). Therefore, mLANA$_{V199A/L202A}$ mediates MuHV-4 episome persistence.

The finding that mLANA$_{V199A/L202A}$ mediates episome persistence is consistent with the previous observation that vmLANA$_{V199A/L202A}$ recombinant virus was able to establish viable latency in mice (Figure 4.5, panel A). Notably, mLANA$_{V199A/L202A}$ mediated episome persistence as efficiently as did mLANA-WT. Therefore, the attenuation of latency expansion exhibited by vmLANA$_{V199A/L202A}$ can be attributed to the impairment of mLANA E3 ubiquitin-ligase activity (chapter 4).

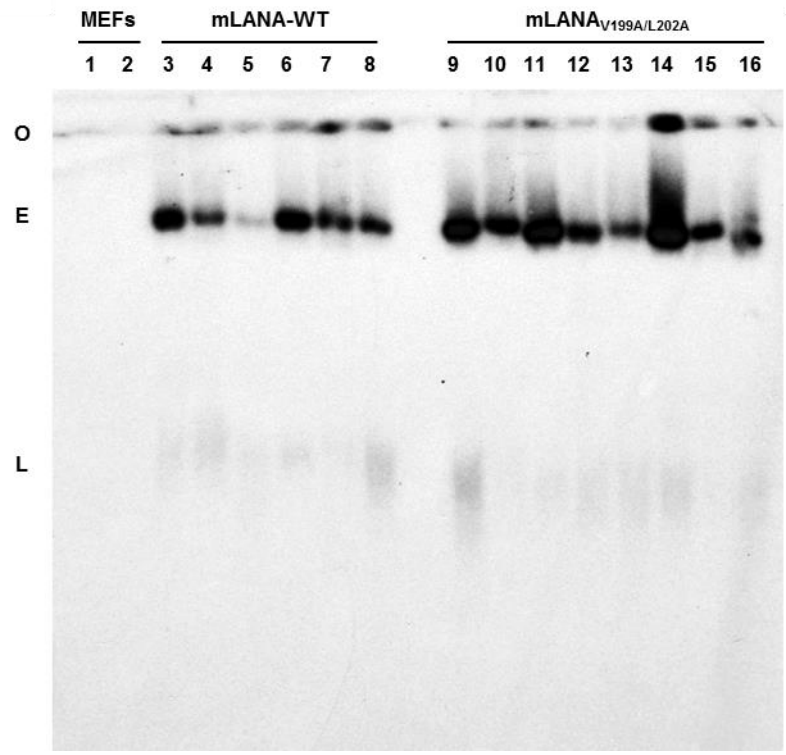

Figure 5.4. mLANA$_{V199A/L202A}$ efficiently mediates MuHV-4 episome persistence. After 98 days of MPA selection, approximately 5x10^6 cells were loaded per lane for Gardella gel analysis. DNA was then transferred to a nylon membrane and detected with a TR probe to detect viral DNA. Gardella gel contained uninfected MEF cells (lanes 1-2), vORF50$^-$mLANA-WT (lanes 3-8) or vORF50$^-$mLANA$_{V199A/L202A}$ (lanes 9-16) infected MEF cells. O, gel origin, E, episomal DNA, L, linear MuHV-4 DNA resulting from low level lytic replication. These data were obtained by Dr Min Tan from Prof. K.M. Kaye Lab (Harvard Medical School, USA).

Table 5.1. Number of resistant clones obtained from infection of MEF cells with ORF50-deficient viruses.

Virus	Number of resistant clones	Number of resistant clones after 98 days of drug selection	Number of resistant clones containing episomes
vORF50$^-$mLANA-WT	TNTC	6/10	6/6
vORF50$^-$mLANA-SOCS	5	0/5	NA
vORF50$^-$mLANA$_{V199A/L202A}$	TNTC	8/10	8/8

TNTC, Too Numerous To Count; NA, Not Applicable.

5.3. Discussion

This work demonstrates that mLANA is capable of episome maintenance despite mutations that result in considerably reduced TR DNA binding, depending on the number of TR elements present in episomes. Moreover, given the finding that mLANA$_{V199A/L202A}$ mutant actually mediates episome persistence, the attenuation of latency expansion exhibited by vmLANA$_{V199A/L202A}$ recombinant virus reported in chapter 4 can be attributed to the impairment of mLANA E3 ubiquitin-ligase activity.

It is particularly noteworthy that despite a severe TR DNA binding deficiency and the failure to mediate episome maintenance with four TR elements, mLANA$_{V199A/L202A}$ efficiently mediated episome persistence in the setting of a full complement of TRs in MuHV-4. It is likely that cooperative binding in the context of multiple TR elements compensates for mLANA DNA binding deficiencies. However, such compensation by an increased TR number is not without limit, as MuHV-4 with mLANA-SOCS or other mLANA mutants that are completely abolished for DNA binding cannot establish viable latent infection (Correia *et al.*, 2013; Paden *et al.*, 2012; Rodrigues *et al.*, 2009). It was previously observed that episome persistence efficiency increased with eight TR elements as compared to two or four TR elements (Habison *et al.*, 2012). Remarkably, mLANA or kLANA plasmids containing up to eight TR elements increased in size when maintained as episomes in transfected cells, compared to the input plasmids (Ballestas and Kaye, 2001; De Leon Vazquez and Kaye, 2011; Habison *et al.*, 2012). This increase in episome size was found to be due to TR duplication and recombination of input plasmids into multimers. KSHV genome contains approximately 40 TR elements (Lagunoff and Ganem, 1997) and MuHV-4 may contain a similar number. Therefore, it is likely that there is strong selection for recombination events that lead to a TR number similar to that in the virus. A recent study reported that at least 16 TR elements are necessary for optimal KSHV episome maintenance (Shrestha and Sugden, 2014).

As mentioned before, the dorsal positive patch of kLANA DBD was shown to interact with DNA of arbitrary sequence and assemble into supermolecular spirals around DNA by self-association of kLANA (Hellert *et al.*, 2015). Since mLANA has a similar positively charged patch (Correia *et al.*, 2013; Hellert *et al.*, 2013), it is possible that higher order mLANA structures may form and exert compensatory roles to overcome DNA binding deficiency.

Overall, these data reveal that deficiencies in mLANA binding to TR DNA are tolerated to some extent without disruption of episome maintenance function, possibly through cooperative binding of mLANA to multiple TR elements in the MuHV-4 genome. Further investigation is necessary to clarify this compensatory mechanism.

CHAPTER 6

Full-length mLANA is expressed in insect cells using baculovirus MultiBac system

Full-length mLANA is expressed in insect cells using baculovirus MultiBac system

6.1. Introduction

The resolution of the crystal structure of C-terminal mLANA enabled the rational design of mutations targeting specific functions of the viral protein, as demonstrated in chapters 2, 3 and 4 of this thesis. Therefore, determining the crystal structure of full-length mLANA would likely provide an opportunity to investigate thoroughly mLANA functions *in vivo*, and hence identify other motifs in this protein that could be used as putative pharmacological targets to control viral infection. However, the crystal structure of full-length mLANA remains undetermined, mainly due to the failure in obtaining appropriate protein expression levels.

Prokaryotic hosts, in particular *E. coli*, have been the systems of choice for recombinant protein expression, due to their simplicity, versatility and low cost (Vincentelli and Romier, 2013). However, the expression levels of full-length mLANA achieved using *E. coli* were very poor (Pires de Miranda *et al.*, unpublished data). Therefore, it was necessary to find an alternative system which allowed good expression levels of full-length mLANA.

Eukaryotic hosts, including yeast, insect cells and mammalian cells, have been successfully used for production of recombinant proteins (Bieniossek *et al.*, 2012). In particular, the use of insect cell cultures infected with a recombinant baculovirus, carrying the gene of interest, has become an important tool in recombinant protein expression.

Dr Imre Berger's laboratory (EMBL, Grenoble, France) has developed MultiBac system (Berger *et al.*, 2004; Bieniossek *et al.*, 2008; Trowitzsch *et al.*, 2010; Vijayachandran *et al.*, 2011), in which an engineered *Autographa californica* nuclear polyhedrosis virus (AcNPV) baculoviral genome, containing the heterologous gene, is used to infect cells of the caterpillar *Spodoptera frugiperda*. Dr I. Berger's team at EMBL Grenoble is very experienced in protein expression and runs the Eukaryotic Expression Facility, where visitors receive specific training in MultiBac system.

To investigate whether full-length mLANA could be expressed in insect cells using baculovirus, two recombinant baculoviruses containing the *ORF73* gene were generated using the MultiBac system. The feasibility study of mLANA expression in insect cells was performed by me at the Eukaryotic Expression Facility at EMBL Grenoble, under the supervision of Dr I. Berger, Frederic Garzoni and Alice Aubert. Chronologically, these experiments were performed before the ones presented in the previous chapters, and were also included in the consortium of HMS-PT Program.

6.2. Results

6.2.1. Construction of transfer plasmids for integration of *ORF73* gene into baculovirus genome

To achieve higher levels of mLANA expression in *Spodoptera frugiperda* 21 (Sf21) insect cells, the *ORF73* gene sequence was optimized for codon usage in insect cells. Codon optimization was performed by GenScript company, using OptimumGene algorithm. 63% of *ORF73* codons were modified (data not shown). Two codon optimized *ORF73* constructs were engineered (Figure 6.1): GST-His-mLANA and His-mLANA, encoding mLANA with a N-terminus GST-8xHis-tag or 8xHis-tag, respectively, followed by a PreScission protease cleavage site. These tags were introduced to allow subsequent purification of mLANA from insect cells.

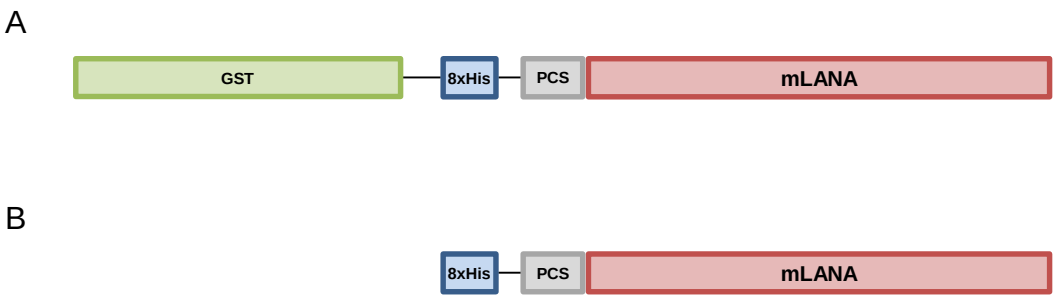

Figure 6.1. Schematic diagram of mLANA constructs for expression in insect cells. GST-His-mLANA (A) and His-mLANA (B) constructs encode mLANA with a N-terminus GST-8xHis-tag or 8xHis-tag, followed by a PreScission protease cleavage site (PCS). mLANA coding sequence was codon optimized for expression in insect cells.

GST-His-mLANA and His-mLANA coding sequences were then subcloned into pPBac transfer plasmid (Vijayachandran *et al.*, 2011) (details in Materials and Methods, section 8.2.3.3). pPBac contains the expression cassette, where the heterologous genes are inserted, flanked by Tn7L and Tn7R DNA sequences, thus allowing Tn7-mediated integration of the genes of interest into the baculovirus genome (section 6.2.2).

6.2.2. Generation of recombinant baculoviruses expressing full-length mLANA

Recombinant baculoviruses were derived from yellow fluorescent protein (YFP)-expressing AcNPV baculovirus genome cloned as a BAC (EMBacY) (Bieniossek *et al.*, 2008; Trowitzsch *et al.*, 2010). EMBacY contains a Tn7 attachment site embedded in a *lacZα* gene for integrating foreign genes into the baculovirus genome, via transfer plasmids. Therefore, successful integration of the expression cassette disrupts *lacZα* gene, allowing selection of positive clones by blue/white screening. In addition, EMBacY contains a YFP coding gene elsewhere in the genome that allows a tracking of infection.

Transfer plasmids harbouring GST-His-mLANA or His-mLANA coding sequences were transformed into an *E. coli* strain containing EMBacY plasmid (Bieniossek *et al.*, 2008; Trowitzsch *et al.*, 2010). Positive clones, with mLANA coding sequences integrated into the baculovirus genome, were then selected. Recombinant baculoviruses were reconstituted by transfection of the recombinant EMBacY plasmid into Sf21 insect cells. Each transfection was performed in duplicate. Further details are described in Materials and Methods, sections 8.2.6.3 and 8.2.6.4.

For production of the initial baculovirus stocks (V_0), supernatants of Sf21 cell cultures transfected with the recombinant EMBacY plasmids were harvested, after incubation for 48 h (Figure 6.2).

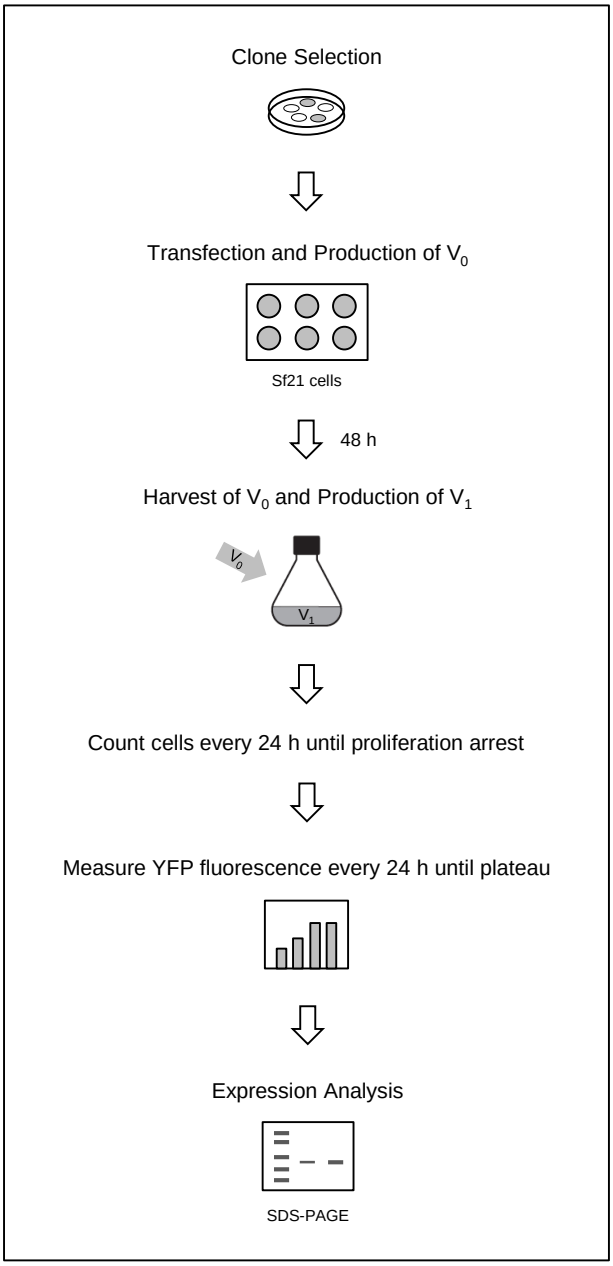

Figure 6.2. Protocol for gene expression test in insect cells using MultiBac system. Transfer plasmids harbouring the heterologous gene(s) are integrated into EMBacY baculoviral DNA via Tn7 transposition. Positive clones are identified by blue/white screening. Recombinant baculoviral DNA is isolated from cultures of single colonies and used to transfect Sf21 cells in 6-well plate format. Two clones obtained with the same construct are processed in parallel. After 48 h, media containing initial virus (V_0) is harvested from the wells and used to infect a new insect cell culture (25 ml volume) in an Erlenmeyer shaker flask. Infected cell cultures are counted every 24 h and split as needed until cell proliferation arrest occurs. After proliferation arrest, $1x10^6$ cells are sampled every 24 h for measuring YFP fluorescence. Media containing amplified virus (V_1) is removed 48 h after proliferation arrest, and fresh medium is replenished instead. Cells are harvested when the YFP signal has reached a plateau (typically after 3-4 days). Protein production is then analysed by sodium dodecyl sulfate-polyacrylamide gel electrophoresis (SDS-PAGE) (adapted from Trowitzsch *et al.*, 2010).

6.2.3. Small-scale expression of full-length mLANA

To assess expression of mLANA constructs in insect cells, a small-scale protein expression test was performed. V_0 stocks were added to fresh Sf21 cells and infected cell cultures were grown. YFP fluorescence was then measured every day after cell proliferation arrest occurred, until YFP fluorescence reached a plateau. At that point, cells were harvested and mLANA expression was analysed by sodium dodecyl sulfate-polyacrylamide gel electrophoresis (SDS-PAGE), followed by Coomassie Blue staining and Western-blot (Figure 6.2).

The YFP coding gene, inserted into *loxP* site of EMBacY plasmid, is under control of polyhedrin promoter, as heterologous genes (Bieniossek *et al.*, 2008; Trowitzsch *et al.*, 2010). Dr I. Berger's group observed that when YFP expression reaches a plateau, the expression of heterologous proteins under the same promoter also reach their peak production. Therefore, heterologous protein production levels can be monitored by following YFP expression. As observed in Figure 6.3, YFP levels increased for all the constructs for the first 96 h after proliferation arrest. Since at this time point the YFP levels for one of the constructs, His-mLANA #2, (Figure 6.3, panel D) nearly reached a plateau, cells were harvested for analysis of mLANA expression.

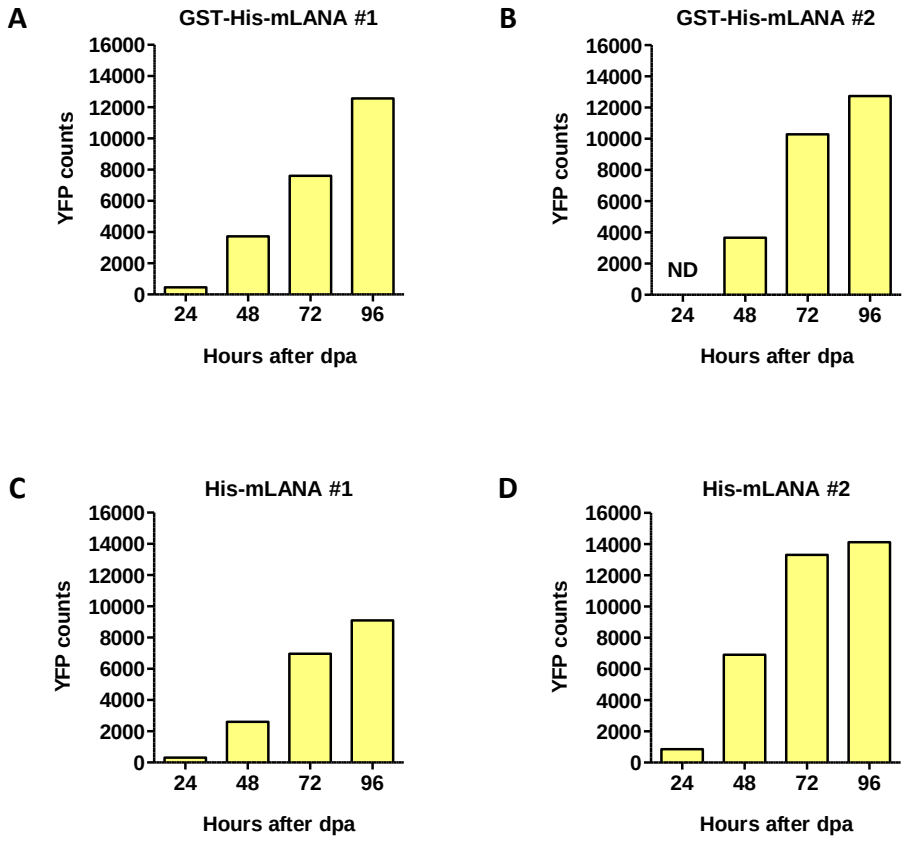

Figure 6.3. Yellow fluorescent protein (YFP) expression from recombinant EMBacY baculoviral DNA. Samples from infected cell cultures were briefly sonicated and, following centrifugation, the supernatant was

used for YFP fluorescence measurement, using a fluorescence spectrophotometer. YFP fluorescence was measured every day after cell proliferation arrest occurred, until YFP levels reached a plateau. At that point, cells were harvested and mLANA expression was analysed. Two clones for each construct were processed in parallel (#1 and #2). dpa, day of proliferation arrest; ND, not determined.

The harvested cells were then analysed by SDS-PAGE, followed by Coomassie Blue staining and Western-blot, to assess mLANA expression. GST-His-mLANA (≈75 kDa) was detected both in Coomassie staining (Figure 6.4, top panel, lanes 1-4, asterisks) and in Western-blot (Figure 6.4, bottom panel, lanes 1-4). The band below 75 kDa detected for this samples in the Western-blot (Figure 6.4, bottom panel, lanes 1-4) likely correspond to degradation of GST-His-mLANA constructs. In contrast, His-mLANA (≈50 kDa) was only detected by Western-blot (Figure 6.4, bottom panel, lanes 5-8), but it is possible that it is masked in the Coomassie by other proteins of the same size.

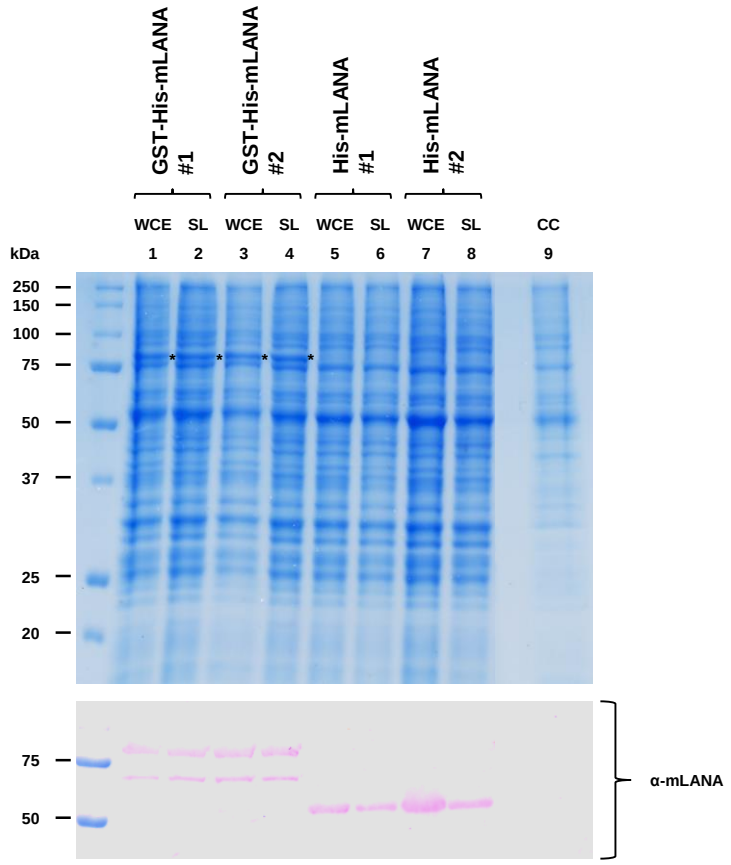

Figure 6.4. Full-length mLANA is expressed in insect cells using baculovirus MultiBac system. Samples from infected cell cultures were harvested at 96 h after cell proliferation arrest and sonicated. An aliquot of sonicated sample was removed for whole cell extract (WCE) analysis. The remaining sample was centrifuged and an aliquot of supernatant was removed for soluble lysate (SL) analysis. WCE and SL samples were boiled in Laemmli's sample buffer, resolved by SDS-PAGE and either stained with Coomassie Blue (top panel), or transferred to nitrocellulose and immunoblotted with anti-mLANA antibody to detect expression of

mLANA constructs (bottom panel). A sample of non-infected Sf21 cells was processed in parallel as control (cell control, CC). Approximately 2.5 x 10^4 cells were loaded in each well. Asterisks mark the band corresponding to GST-His-mLANA construct.

To amplify baculovirus stocks expressing GST-His-mLANA and His-mLANA, cell cultures infected with V_0 were centrifuged 48 h after proliferation arrest, and supernatants were harvested, constituting the V_1 stock (Figure 6.2). V_1 corresponds to a stock of amplified virus, which can be used to infect larger volumes of Sf21 cultures to produce mLANA in large scale.

Overall, these results show that full-length mLANA can be expressed in insect cells using baculovirus MultiBac system.

6.3. Discussion

The feasibility study of mLANA expression in insect cells using baculovirus demonstrated that the full-length protein can be successfully expressed with this system. Remarkably, the achieved levels of expression were good, particularly for GST-His-mLANA construct, as this protein was readily detected in the Coomassie staining. However, it is a possibility that His-mLANA construct is masked in the Coomassie by other proteins of the same size (≈50 kDa).

The crystal structure of full-length mLANA remains unknown. Although the determination of the crystal structure requires the surmounting of several critical steps, the accomplishment of good levels of protein expression is a major contribute to obtain good quality structural data (Aloy and Russell, 2006). Therefore, the use of MultiBac system for expression in insect cells as an approach to express mLANA may be an important tool for structural studies on full-length mLANA. Subsequent experiments performed by Dr Marta Miranda in our laboratory succeeded in purifying mLANA from the frozen pellets obtained in section 6.2.3, and large-scale expression in insect cells has been started, using the V_1 amplified baculovirus stock. The first structural studies on full-length mLANA using small-angle X-ray scattering (SAXS) are being performed by Dr C.E. McVey's team (Instituto de Tecnologia Química e Biológica (ITQB), Universidade Nova de Lisboa, Portugal). Importantly, SAXS analysis allows the determination of low-resolution structure of proteins in solution, with no need for crystals. For instance, the binding modes of mLANA and kLANA C-terminal DBDs to viral TR DNA were recently inferred from SAXS low-resolution structural analysis of mLANA/kLANA-DNA complexes in solution (Ponnusamy *et al.*, 2015).

Notably, the resolution of the crystal structure of mLANA DBD enabled the rational design of mutations targeting specific functions of the viral protein (Correia *et al.*, 2013; Hellert *et al.*, 2013). Hence, structural data on full-length mLANA will likely provide an invaluable contribution to mLANA pathogenesis studies, and the finding that mLANA can be successfully expressed in insect cells using the MultiBac system of EMBL Grenoble is a major achievement. Future work on the three-dimensional structure of full-length mLANA complexed with its cellular partners so far identified may also be relevant. Moreover, the expression of full-length mLANA using this expression system may also be useful for other studies that require pure full-length protein, for instance binding studies.

CHAPTER 7

Final Considerations

Final Considerations

Gammaherpesviruses drive proliferation of latently infected B cells in GCs to expand latency and to achieve long-term persistence in memory B cells. During latency, the viral genome is maintained as an extrachromosomal circular episome within the host cell nucleus. To persist in proliferating cells, viral episomes must replicate in step with normal cell division and segregate to newly formed nuclei after mitosis. This process is mediated by gammaherpesvirus episome maintenance proteins, which include EBV EBNA1, KSHV kLANA and MuHV-4 mLANA (Ballestas *et al.*, 1999; Ballestas and Kaye, 2001, 2011; Habison *et al.*, 2012; Yates *et al.*, 1985). The crystal structures of the DNA binding domains (DBDs) of these proteins were solved and revealed a common overall fold, containing a dimeric central eight-stranded anti-parallel β-barrel, with four β-strands contributing from each monomer and flanked on either side by three α-helices (Bochkarev *et al.*, 1996; Bochkarev *et al.*, 1995; Correia *et al.*, 2013; Domsic *et al.*, 2013; Hellert *et al.*, 2015; Hellert *et al.*, 2013; Ponnusamy *et al.*, 2015). The DBD allows episome maintenance proteins to bind to viral DNA. LANA proteins, in particular, cooperatively bind to multiple sites within the TR sequences of the viral genome through their DBD and tether viral episomes to host cell mitotic chromosomes, thereby promoting efficient segregation of episomes into daughter nuclei. Other LANA structural features associated with specific functions were also revealed by the crystal structure of DBD. The study of the mechanisms underlying LANA functions is crucial, since this protein is essential for the establishment and maintenance of latent infection *in vivo*. However, the individual contribution of each function assigned to LANA during the natural infection remains largely uncharacterized.

A major limitation to the study of the human gammaherpesviruses is the absence of a robust small animal model in which to investigate viral pathogenesis, due to the very narrow host tropism exhibited by EBV and KSHV (Barton *et al.*, 2011; Simas and Efstathiou, 1998). The identification of MuHV-4 (Blaskovic *et al.*, 1980) offered the possibility of developing a mouse model of gammaherpesvirus pathogenesis. Remarkably, MuHV-4 mLANA shares structural and functional homology to KSHV kLANA (Correia *et al.*, 2013; Fowler *et al.*, 2003; Habison *et al.*, 2012; Hellert *et al.*, 2013; Rodrigues *et al.*, 2009; Rodrigues *et al.*, 2013), particularly in the DBD, thereby emphasising the use of mLANA as a model to study kLANA pathogenesis in the mouse and to potentially test pharmacological inhibitors of LANA functions through targeting of key structural features of the DBD.

The work presented in this thesis was inserted into the project «Pathogenesis of Kaposi's sarcoma herpesvirus LANA» of the HMS-PT Program from FCT, gathering the expertise of three research teams in KSHV LANA (Prof. K.M. Kaye group), structural biology (Prof. M.A. Carrondo and Dr C.E. McVey group) and in the murine model of MuHV-4 infection (Prof. J.P. Simas group).

The aim of this thesis was to address the importance of particular LANA functions in the context of gammaherpesvirus latent infection *in vivo*, integrating LANA structural data and the animal model of infection with MuHV-4. mLANA was used as a model to investigate LANA pathogenesis in mice. To this end, MuHV-4 recombinant viruses harbouring structure-based mutations targeting specific mLANA interfaces were engineered, and the ability of these recombinants to establish and maintain latent infection was analysed upon intranasal infection of mice. The results presented in this study support a critical role of LANA in gammaherpesvirus latency, particularly due to its function as a DNA binding protein. Other LANA functions, as E3 ubiquitin-ligase activity or dorsal positive patch-associated functions, were also shown to contribute to latency expansion.

The crystal structure of mLANA DBD allowed the identification of a DNA binding interface containing a cluster of positively charged residues. In particular, residues H186 and K187, in the predicted DNA recognition helix α2, were found to be involved in interactions with phosphate ions of DNA and mutations at these residues disrupted mLANA binding to TR DNA (Correia *et al.*, 2013). To validate *in vivo* the DNA binding structural data, a MuHV-4 recombinant virus containing mLANA mutations H186D/K187E (vmLANA$_{H186D/K187E}$) was engineered in the scope of this thesis (chapter 2). mLANA binding to the TR elements in viral genome was found to be essential for latency expansion in GC B cells and persistence in the host, thereby validating the importance of mLANA binding to viral DNA during latent infection *in vivo*. This is consistent with mLANA acting on TR elements to mediate episome persistence (Habison *et al.*, 2012). Interestingly, deficiencies in mLANA binding to TR DNA were tolerated to some extent without abrogation of episome maintenance function (chapter 5), possibly due to cooperative binding of mLANA to multiple TR elements in the MuHV-4 genome. Further investigation is necessary to clarify this compensatory mechanism.

The crystal structure of mLANA DBD also revealed an extensive positive patch on its dorsal side, opposite to the DNA binding interface. This dorsal positive patch harbours the ^{226}QAKKLK^{231} motif, which is involved in binding to BET proteins, particularly Brd2 and Brd4 (Correia *et al.*, 2013; Hellert *et al.*, 2013; Ottinger *et al.*, 2009). To investigate if the dorsal positive patch exerted a functional role *in vivo*, MuHV-4 recombinant viruses containing mLANA mutations that targeted either the central (K251, K253) or the peripheral (K224, K228, K229) regions of the patch were engineered (chapter 3). The work presented in this thesis demonstrated that the dorsal positive patch of mLANA, particularly the peripheral region, is required for efficient latency expansion in GC B cells, exerting its functions through an unknown mechanism. Interestingly, the deficit in latency for some recombinant viruses did not correlate with binding to Brd4 protein. It is possible that the dorsal positive patch associates with a host cell partner(s) other than Brd4 or, alternatively, interacts with viral DNA in a sequence-independent manner to induce the formation of specific complexes required for episome replication and maintenance. This is an important question that should be addressed in future experiments. Notably, KSHV kLANA exhibits a similar dorsal positive

patch, which was recently shown to facilitate viral DNA replication and episome persistence in latently infected cells in culture (Domsic *et al.*, 2013; Li *et al.*, 2015).

LANA proteins are also known as modulators of cellular transcription, particularly due to their E3 ubiquitin-ligase activity (Cai *et al.*, 2006; Li *et al.*, 2011; Rodrigues *et al.*, 2009; Rodrigues *et al.*, 2013). The crystal structure of mLANA DBD showed that the SOCS-box, through which mLANA recruits cellular ElonginB/C and Cullin5 in order to assemble the E3 ubiquitin-ligase complex, lies within a loop protruding perpendicular to the DNA binding interface (Correia *et al.*, 2013). To clarify the biological relevance of mLANA E3 ubiquitin-ligase activity for gammaherpesvirus pathogenesis, MuHV-4 recombinant viruses containing mutations in mLANA SOCS-box which impaired E3 ubiquitin-ligase activity without compromising episome maintenance function were generated (chapter 4). The results obtained in this study revealed that the impairment of mLANA E3 ubiquitin-ligase activity results in an attenuation of latency levels in spleen, demonstrating that this function of mLANA contributes to latency expansion. Quantification of infection in GC B cells would be necessary to establish a definitive link between mLANA E3 ubiquitin-ligase activity and latency expansion in GCs. mLANA has two known cellular targets for poly-ubiquitination, NF-κB and Myc (Rodrigues *et al.*, 2009; Rodrigues *et al.*, 2013). Given that mLANA acts as the substrate recognition component of the E3 ubiquitin-ligase complex, interacting with the NF-κB family member p65 and with Myc through motifs independent from the SOCS-box, as yet unidentified, it could be a possibility that the dorsal positive patch of mLANA would be the binding site to these substrates. However, previous experiments performed in our laboratory mapped interactions with p65 and Myc to N-terminal mLANA (residues 1-140) (Rodrigues *et al.*, unpublished data), thereby rejecting the hypothesis that the C-terminal dorsal positive patch could be involved in these interactions. Remarkably, KSHV kLANA is also able to assemble an E3 ubiquitin-ligase complex through a SOCS-box motif, promoting the poly-ubiquitination of p53, VHL and p65, and targeting these substrates for degradation, thereby potentially providing a favourable environment for cell growth (Cai *et al.*, 2006; Li *et al.*, 2011). Hence, although kLANA substrates are different from the ones of mLANA, it is likely that targeting the E3 ubiquitin-ligase function of kLANA will have an impact on KSHV latency in the host.

Overall, this thesis reinforces the overview of LANA as a multifunctional protein and addresses the contribution of several LANA functions to gammaherpesvirus latent infection *in vivo*, using MuHV-4 mLANA as a model. One of the hallmarks of herpesvirus latency is the highly restricted pattern of viral protein expression, in order to reduce the chance of being detected by the host immune system (Wu *et al.*, 2010). Therefore, by concentrating several critical functions in the same viral protein, the virus limits the amount of antigen produced while efficiently maintaining latency. Interestingly, mLANA was shown to reduce the presentation of an MHC class I-restricted epitope linked to it in *cis*, suggesting that mLANA exerts a mechanism to limit its presentation to CTLs, similarly to EBV EBNA1 (Bennett *et al.*, 2005).

Furthermore, this work provides evidence that it is quite advantageous to perform pathogenesis studies guided by protein structural data, as several structural features are associated with specific functions of the protein, thereby enabling the rational design of mutations targeting a particular function. In this sense, determining the crystal structure of full-length mLANA, which is currently unknown, would likely provide an opportunity to investigate thoroughly mLANA functions *in vivo*. This project revealed that full-length mLANA can be successfully expressed in insect cells using baculovirus (chapter 6). This is a first step towards the resolution of mLANA full-length structure, which may allow novel structure-guided pathogenesis studies with mLANA.

Herein, the impact of disruption of several mLANA structural interfaces was evaluated. Three possible targets to control gammaherpesvirus infection were identified: the DNA binding interface, the dorsal positive patch and the SOCS-box. The DNA binding interface is likely the best candidate, as a virus bearing mutations abrogating TR DNA binding was severely compromised in establishment of latency in mice. Notably, KSHV kLANA exhibits a DNA binding interface similar to mLANA (Domsic *et al.*, 2013; Hellert *et al.*, 2015; Hellert *et al.*, 2013; Ponnusamy *et al.*, 2015), and mutation of residues P1065, Y1066 and G1067, in the DNA recognition helix α2, abolishes binding of kLANA to the LBS sites in the KSHV TRs (Han *et al.*, 2010; Kelley-Clarke *et al.*, 2007b). Therefore, these residues are likely candidates to disrupt episome persistence and, consequently, KSHV latency in the natural context of infection. Future work using small molecule inhibitors targeting these structural features is necessary to clarify whether the pharmacological disruption of such structures is an effective strategy to control gammaherpesvirus latent infection and associated pathologies.

Other latent DNA viruses maintain genomes as extrachromosomal circular episomes within the nuclei of infected cells. Virus-encoded *cis*- and *trans*-acting genome maintenance functions seem to be dispensable when latency is established in non-dividing cell populations, as is the case of neurotropic herpes simplex virus (HSV) (Nicoll *et al.*, 2012). In contrast, episome maintenance proteins assume a prominent role when latency is established within proliferating cells, and this is not exclusive to lymphotropic gammaherpesviruses. For instance, papillomavirus encodes a DNA binding protein, the E2 protein, which was shown to mediate virus episome persistence through a mechanism resembling the tethering mechanism of gammaherpesvirus EBNA1 and LANA. The papillomavirus E2 protein contains a DBD which allows it to bind to specific sites in the viral genome, while other regions of E2 interact with chromosomal proteins, thereby tethering viral episome to mitotic chromosomes in the proliferating basal cells (Bastien and McBride, 2000; Ilves *et al.*, 1999; Lehman and Botchan, 1998; McBride, 2013; Piirsoo *et al.*, 1996; Skiadopoulos and McBride, 1998). Notably, the crystal structure of E2 DBD exhibits great structural homology to the EBNA1 and LANA DBDs, despite the absence of sequence homology to these gammaherpesvirus proteins (Bochkarev *et al.*, 1995; Correia *et al.*, 2013; Dell *et al.*, 2003; Domsic *et al.*, 2013; Hegde *et al.*, 1992; Hellert *et al.*, 2013). Therefore, virus-encoded DBD-containing episome maintenance proteins that bind to specific DNA sequences in the viral genome and tether it to mitotic

chromosomes likely represent an overall strategy employed by episomal DNA viruses to ensure that the virus is not lost during cell division. This emphasizes the perspective of episome maintenance proteins as putative targets to disrupt viral latency.

Gammaherpesvirus latent infection is characterized by stable low levels of latently infected memory B cells, as a consequence of the dynamic equilibrium between virus-driven B cell proliferation and host immune control. However, when the virus-host equilibrium is disrupted, latently infected B cells can proliferate unchecked, leading to the development of lymphoproliferative diseases (Cesarman, 2014; Kutok and Wang, 2006; Thorley-Lawson and Gross, 2004). EBV is aetiologically linked to three B cell malignancies, Burkitt's lymphoma, Hodgkin's lymphoma and post-transplant lymphoproliferative disorder, to a subset of T and natural killer (NK) cell lymphomas, and to an epithelial tumour, nasopharyngeal carcinoma (Cesarman, 2014; Kutok and Wang, 2006). KSHV is similarly associated with B cell lymphoproliferative diseases, such as primary effusion lymphoma (PEL) and multicentric Castleman's disease (MCD), and to a tumour of endothelial origin, Kaposi's sarcoma (KS) (Cesarman *et al.*, 1995; Chang *et al.*, 1994; Soulier *et al.*, 1995). These malignancies are characterized by uncontrolled proliferation of latently infected cells expressing EBNA1 or kLANA. Although other functions of these proteins have been hypothesised to contribute to oncogenesis, it is their episome maintenance function that has been linked to the successful persistence strategy of gammaherpesvirus, avoiding viral episomes to be lost during cell division in proliferating tumour cells (Ballestas and Kaye, 2011; Barton *et al.*, 2011; Cesarman, 2014; Gramolelli and Schulz, 2015; Kang and Kieff, 2015; Schulz and Cesarman, 2015). This places episome maintenance proteins at the centre of gammaherpesvirus pathogenesis. The work presented in this thesis demonstrated that disruption of LANA DNA binding interface severely impairs viral persistence in proliferating B cells *in vivo* (chapter 2), reinforcing the use of episome maintenance proteins DBD as a pharmacological target to disrupt latency and thus control gammaherpesvirus-associated pathologies. In fact, recent studies have shown that EBNA1 DBD can be targeted by small molecules identified by high-throughput cell-based screens, resulting in inhibition of EBNA1 binding to its cognate DNA, progressive loss of EBV episome, and limited growth of EBV-infected lymphoblastoid cell lines or Burkitt's lymphoma cells (Lee *et al.*, 2014). The use of mLANA in the context of the MuHV-4 mouse model of infection may add insightful contribution to these screenings.

CHAPTER 8

Materials and Methods

Materials and Methods

8.1. Materials

8.1.1. General reagents

Analytical or molecular biology grade chemicals were obtained from Bio-Rad, Calbiochem, Invitrogen, Merck, NZYTech, Roche and Sigma-Aldrich. Molecular biology reagents and enzymes were obtained from Agilent, Fermentas, Invitrogen, New England Biolabs, NZYTech, Promega and Roche. Synthetic oligonucleotides were synthesized by Thermo Scientific. Protein methods reagents were obtained from Bio-Rad, Fujifilm, GE Healthcare, Promega, Qiagen, Roche, Sigma-Aldrich and Thermo Scientific. Tissue culture reagents and supplements were obtained from Gibco.

8.1.2. Antibodies

8.1.2.1. Primary antibodies

Anti-mLANA mouse monoclonal antibody (Rodrigues *et al.*, 2013) was raised against the C-terminal domain (residues 140-314) of purified GST-mLANA protein. The antibodies against this region of mLANA were generated at the Monoclonal Antibodies Core Facility, European Molecular Biology Laboratory (EMBL). This antibody was used in Western-blot experiments.

Anti-mLANA rabbit polyclonal serum (Rodrigues *et al.*, 2009) was generated by immunization of New Zealand white rabbits (Abcam) with purified GST-mLANA protein. This antibody was used in immunoprecipitation experiments.

The other primary antibodies used in this study are commercially available and are described in Table 8.1:

Table 8.1. Primary antibodies (commercially available) used in this study.

Name (Clone)	Assay	Type	Species	Supplier
c-Myc (9E10)	WB	Monoclonal IgG1	Mouse	Clontech
HA (16B12)	WB	Monoclonal IgG1	Mouse	Covance
FLAG (M2)	WB	Monoclonal IgG1	Mouse	Sigma-Aldrich
p65 (F-6)	WB	Monoclonal IgG1	Mouse	Santa Cruz Biotechnology
c-Myc (N-262)	WB	Polyclonal	Rabbit	Santa Cruz Biotechnology
EloC (R-20)	WB	Polyclonal	Goat	Santa Cruz Biotechnology
Cul5 (H-300)	WB	Polyclonal	Rabbit	Santa Cruz Biotechnology
Actin (A2066)	WB	Polyclonal	Rabbit	Sigma-Aldrich
CD16/32 (2.4G2)	FC	Monoclonal IgG2b, κ	Rat	BD Pharmingen (BD Biosciences)
CD19-APC-H7 (1D3)	FC	Monoclonal IgG2a, κ	Rat	BD Pharmingen (BD Biosciences)
CD95-PE (Jo2)	FC	Monoclonal IgG2, λ2	Hamster	BD Pharmingen (BD Biosciences)
GL7-eFluor660 (GL7)	FC	Monoclonal IgM	Rat	eBioscience
Dig-AP	ISH	Polyclonal	Sheep	Roche

WB, Western-blot; FC, Flow Cytometry; ISH, *In Situ* Hybridization.

8.1.2.2. Secondary antibodies

Horseradish peroxidase (HRP)-conjugated secondary antibodies against mouse or goat class G immunoglobulins (IgGs) were purchased from Jackson Immunoresearch. HRP-conjugated secondary antibody against rabbit IgGs was purchased from GE Healthcare. These secondary antibodies were used in Western-blot experiments.

8.1.3. Cell lines

Baby hamster kidney (BHK)-21 fibroblast cells were used for growing and titrating viral stocks, *in vitro* growth curves, *ex vivo* reactivation, plaque assays and analysis of mLANA expression.

NIH-3T3-CRE mouse fibroblast cells were kindly provided by Dr Philip Stevenson (Sir Albert Sakzewski Virus Research Centre, School of Chemistry and Molecular Biosciences,

University of Queensland and Royal Children's Hospital, Australia) and were used during the construction of murid herpesvirus-4 (MuHV-4) recombinant viruses, for removing the *lox*P-flanked bacterial artificial chromosome (BAC) cassette. This cell line was established by transduction of NIH-3T3 cells with a retrovirus derived from Phoenix-ecotropic cells transfected with pMSCV-CRE-NEO (*cre* of bacteriophage P1 cloned into the *Eco*RI-*Xho*I sites of pMSCV-NEO) and selection with 1mg/mL of G418 (Stevenson *et al.*, 2002).

3T3-ORF50 mouse fibroblast cells were a kind gift by Dr Stacey Efstathiou (Division of Virology, Department of Pathology, University of Cambridge, UK) and Dr P. Stevenson, and were used to grow and titrate MuHV-4 ORF50-deficient recombinant viruses. This cell line was established by serially transducing NIH-3T3 cells with three retroviruses: one expressing ORF50 from a promoter with doxycycline-responsive (TRE) promoter, one expressing constitutively a transcriptional suppressor with doxycycline-inactivated TRE-binding, and one expressing constitutively a transcriptional activator with doxycycline-activated TRE-binding, thus allowing doxycycline-inducible ORF50 expression. ORF50 coding sequence was amplified by polymerase chain reaction (PCR) from infected cell cDNA and cloned into pREV-TRE. TRE-binding transcriptional suppressor was excised from pTET-tTS with *Eco*RI/*Cla*I, *Cla*I site was blunted with T4 DNA polymerase and the fragment was ligated into *Eco*RI-blunted *Xho*I sites of pMSCV-IRES-PURO. TRE-binding transcriptional activator was from pREV-TET-ON. Each plasmid was transfected into human embryonic kidney (HEK) 293T cells together with pEQPAM3 packaging plasmid. Retroviruses were collected after 48 and 72 h, and added to cells with 6 µg/mL of polybrene. Triply transduced cells were selected with puromycin, hygromycin and G418 (Milho *et al.*, 2009).

Mouse embryonic fibroblast (MEF-1) cells were used for episome maintenance assays with MuHV-4 ORF50-deficient recombinant viruses.

Human embryonic kidney (HEK) 293T epithelial cells were used for reporter gene assays, poly-ubiquitination assays and immunoprecipitation assays.

Spodoptera frugiperda 21 (Sf21) insect cells were a kind gift from Dr Imre Berger (EMBL, Grenoble, France) and were used for propagation of recombinant baculovirus stocks and production of full-length mLANA.

8.1.4. Bacterial strains

Escherichia coli strain DH5α (Invitrogen), genotype F^- Φ80*lac*ZΔM15 Δ(*lac*ZYA-*arg*F) U169 *rec*A1 *end*A1 *hsd*R17(r_K^-, m_K^+) *pho*A *sup*E44 *thi*-1 *gyr*A96 *rel*A1 λ-, was used to grow high-copy plasmids.

E. coli strain XL10-Gold Ultracompetent (Agilent Technologies), genotype Tet^{r}Δ(*mcr*A)*183* Δ(*mcr*CB-*hsd*SMR-*mrr*)*173* *end*A1 *sup*E44 *thi*-1 *rec*A1 *gyr*A96 *rel*A1 *lac* Hte [F´ *pro*AB *lac*I^{q}ZΔM15 Tn*10*(Tet^r) Amy Cam^r], was used to grow plasmids generated by PCR mutagenesis and shuttle vector derived plasmids.

E. coli strain DH10B (Invitrogen), genotype F$^-$ *mcr*A Δ(*mrr-hsd*RMS-*mcr*BC) Φ80*lac*ZΔM15 Δ*lac*X74 *rec*A1 *end*A1 *ara*D139 Δ (*ara*, *leu*)7697 *gal*U *gal*K λ$^-$ *rps*L (Str^r) *nup*G, containing the MuHV-4 BAC pHA3 (Adler *et al.*, 2000), was provided by Dr Heiko Adler (Helmholtz Zentrum Munich, German Research Center for Environmental Health, Germany) and Dr Ulrich Koszinowski (Max von Pettenkofer-Institut, Ludwig-Maximilians-Universität, Munich, Germany) and was used for mutagenesis of MuHV-4 BAC pHA3.

E. coli strain DH10B containing the MuHV-4 M3-Luc/ORF50$^-$eGFP BAC (Milho *et al.*, 2009) was a kind gift from Dr S. Efstathiou and Dr P. Stevenson, and was used for mutagenesis of MuHV-4 M3-Luc/ORF50$^-$eGFP BAC.

E. coli DH10EMBacY, containing the yellow fluorescent protein (YFP)-expressing *Autographa californica* nuclear polyhedrosis virus (AcNPV) baculoviral genome cloned as a BAC (EMBacY) (Bieniossek *et al.*, 2008; Trowitzsch *et al.*, 2010), was gently provided by Dr I. Berger and was used for generation of recombinant baculoviruses. In addition, *E. coli* DH10EMBacY contains a helper plasmid (tetracycline-resistance marker) that expresses the Tn7 transposon complex upon induction with isopropyl-β-D-thiogalactopyranoside (IPTG).

8.1.5. Plasmids

8.1.5.1. Plasmids for transient expression in mammalian cells

pCMV-Myc, a commercial plasmid (Clontech), was used for transient expression of proteins in fusion with Myc epitope or as a transfection control.

pCMV-HA, a commercial plasmid (Clontech), was used for transient expression of proteins in fusion with HA epitope or as a transfection control.

pCMV-Myc-mLANA was used for transient expression of mLANA wild-type (WT) viral protein. This plasmid was constructed by Dr Lénia Rodrigues (Instituto de Medicina Molecular, Faculdade de Medicina da Universidade de Lisboa, Portugal) (Rodrigues *et al.*, 2009).

pCMV-Myc-mLANA-SOCS was used for transient expression of a mutant version of mLANA viral protein (mLANA-SOCS), containing valine (V) residue 199, leucine (L) residue 202, proline (P) residue 203 and proline (P) residue 206 substituted by alanine (A). This plasmid was constructed by Dr L. Rodrigues (Rodrigues *et al.*, 2009).

pCMV-Myc-mLANA$_{H186D/K187E}$ was used for transient expression of a mutant version of mLANA viral protein (mLANA$_{H186D/K187E}$), containing histidine (H) residue 186 and lysine (K) residue 187 substituted by aspartate (D) and glutamate (E), respectively. This plasmid was constructed in this study by site-directed mutagenesis, using QuikChange II XL Site-Directed Mutagenesis Kit (Agilent Technologies) according to the manufacturer's instructions. The oligonucleotides used in PCR are described in Table 8.2.

pCMV-Myc-mLANA$_{K224A/K228A/K229A}$ was used for transient expression of a mutant version of mLANA viral protein (mLANA$_{K224A/K228A/K229A}$), containing lysine (K) residues 224, 228 and 229 substituted by alanine (A). This plasmid was constructed in this study by site-directed mutagenesis, using QuikChange II XL Site-Directed Mutagenesis Kit (Agilent Technologies) according to the manufacturer's instructions. The oligonucleotides used in PCR are described in Table 8.2.

pCMV-Myc-mLANA$_{K224E/K228E/K229E}$ was used for transient expression of a mutant version of mLANA viral protein (mLANA$_{K224E/K228E/K229E}$), containing lysine (K) residues 224, 228 and 229 substituted by glutamate (E). This plasmid was constructed in this study by site-directed mutagenesis, using QuikChange II XL Site-Directed Mutagenesis Kit (Agilent Technologies) according to the manufacturer's instructions. The oligonucleotides used in PCR are described in Table 8.2.

pCMV-Myc-mLANA$_{K251A/K253A}$ was used for transient expression of a mutant version of mLANA viral protein (mLANA$_{K251A/K253A}$), containing lysine (K) residues 251 and 253 substituted by alanine (A). This plasmid was constructed in this study by site-directed mutagenesis, using QuikChange II XL Site-Directed Mutagenesis Kit (Agilent Technologies) according to the manufacturer's instructions. The oligonucleotides used in PCR are described in Table 8.2.

pCMV-Myc-mLANA$_{K251E/K253E}$ was used for transient expression of a mutant version of mLANA viral protein (mLANA$_{K251E/K253E}$), containing lysine (K) residues 251 and 253 substituted by glutamate (E). This plasmid was constructed in this study by site-directed mutagenesis, using QuikChange II XL Site-Directed Mutagenesis Kit (Agilent Technologies) according to the manufacturer's instructions. The oligonucleotides used in PCR are described in Table 8.2.

pCMV-Myc-mLANA$_{V199A}$ was used for transient expression of a mutant version of mLANA viral protein (mLANA$_{V199A}$), containing valine (V) residue 199 substituted by alanine (A). This plasmid was constructed in this study by site-directed mutagenesis, using QuikChange II XL Site-Directed Mutagenesis Kit (Agilent Technologies) according to the manufacturer's instructions. The oligonucleotides used in PCR are described in Table 8.2.

pCMV-Myc-mLANA$_{L202A}$ was used for transient expression of a mutant version of mLANA viral protein (mLANA$_{L202A}$), containing leucine (L) residue 202 substituted by alanine (A). This

plasmid was constructed by Dr L. Rodrigues, by site-directed mutagenesis, using QuikChange II XL Site-Directed Mutagenesis Kit (Agilent Technologies) according to the manufacturer's instructions. The oligonucleotides used in PCR are described in Table 8.2.

pCMV-Myc-mLANA$_{V199A/L202A}$ was used for transient expression of a mutant version of mLANA viral protein (mLANA$_{V199A/L202A}$), containing valine (V) residue 199 and leucine (L) residue 202 substituted by alanine (A). This plasmid was constructed in this study by site-directed mutagenesis, using QuikChange II XL Site-Directed Mutagenesis Kit (Agilent Technologies) according to the manufacturer's instructions. The oligonucleotides used in PCR are described in Table 8.2.

pCMV-Myc-mLANA$_{P203A}$ was used for transient expression of a mutant version of mLANA viral protein (mLANA$_{P203A}$), containing proline (P) residue 203 substituted by alanine (A). This plasmid was constructed by Dr L. Rodrigues, by site-directed mutagenesis, using QuikChange II XL Site-Directed Mutagenesis Kit (Agilent Technologies) according to the manufacturer's instructions. The oligonucleotides used in PCR are described in Table 8.2.

pCMV-Myc-mLANA$_{P206A}$ was used for transient expression of a mutant version of mLANA viral protein (mLANA$_{P206A}$), containing proline (P) residue 206 substituted by alanine (A). This plasmid was constructed by Dr L. Rodrigues, by site-directed mutagenesis, using QuikChange II XL Site-Directed Mutagenesis Kit (Agilent Technologies) according to the manufacturer's instructions. The oligonucleotides used in PCR are described in Table 8.2.

pCMV-Myc-mLANA$_{P203A/P206A}$ was used for transient expression of a mutant version of mLANA viral protein (mLANA$_{P203A/P206A}$), containing proline (P) residue 203 and proline (P) residue 206 substituted by alanine (A). This plasmid was constructed in this study by site-directed mutagenesis, using QuikChange II XL Site-Directed Mutagenesis Kit (Agilent Technologies) according to the manufacturer's instructions. The oligonucleotides used in PCR are described in Table 8.2.

pCMV-Myc-p65 was used for transient expression of p65 protein. This plasmid was described earlier (Anrather *et al.*, 1999).

pCMV-HA-Myc was used for transient expression of Myc protein. This plasmid was constructed by Dr L. Rodrigues (Rodrigues *et al.*, 2013).

pEBB-FLAG-EloC was used for transient expression of FLAG-tagged ElonginC protein. This plasmid was kindly offered by Dr Ezra Burstein (Department of Internal Medicine and Department of Molecular Biology, University of Texas Southwestern Medical Center, USA).

VR1012-Cul5-Myc was used for transient expression of Myc-tagged Cullin5 protein. This plasmid was kindly offered by Dr Xiao-Fang Yu (Department of Molecular Microbiology and

Immunology, Johns Hopkins Bloomberg School of Public Health, Baltimore, USA) and it was described earlier (Yu *et al.*, 2003).

His_6-ubiq was used for transient expression of 6xhistidine-tagged ubiquitin. This plasmid was kindly offered by Dr Dirk Bohmann (Department of Biomedical Genetics, University of Rochester Medical Center, USA).

pC45 (κB -Luc), containing three copies of kappa B (κB) consensus sequence regulating the expression of firefly luciferase (Luc), was used as a nuclear factor-kappa B (NF-κB) reporter plasmid. This plasmid was described earlier (Brostjan *et al.*, 1997).

pMyc-TA-Luc, containing six tandem copies of the E-box consensus sequence driving the expression of firefly luciferase, was used as a Myc reporter plasmid. This plasmid was purchased from Clontech.

Renilla plasmid was used for transient expression of *Renilla* luciferase. This plasmid was kindly offered by Dr Xosé R. Bustelo (Centro de Investigación del Cáncer and Instituto de Biología Molecular y Celular del Cáncer, University of Salamanca, Spain).

8.1.5.2. Plasmids for construction of MuHV-4 recombinant viruses

pACYC184-BamG (pBamG) is a pACYC184 (New England Biolabs) based plasmid in which the *Bam*HI-G MuHV-4 genomic fragment (coordinates 101,654 to 106,903) (Efstathiou *et al.*, 1990), containing ORF73 coding and flanking regions, was cloned into the *Bam*HI site, and a *Bsp*HI restriction site on the pACY184 backbone was removed by overlapping PCR. This plasmid was kindly provided by Dr P. Stevenson.

pST76K-SR (shuttle vector) (Adler *et al.*, 2000) was a kind gift from Dr H. Adler and Dr U. Koszinowski.

*Bam*HI-G shuttle plasmid, constructed by Dr Sofia Marques (Instituto de Medicina Molecular, Faculdade de Medicina da Universidade de Lisboa, Portugal), is the *Bam*HI-G genomic fragment of MuHV-4 (coordinates 101,654 to 106,903) cloned in the pST76K-SR plasmid. This plasmid was used to insert the desired mutations in the BAC plasmid, by homologous recombination in *E. coli*.

pHA3 is the MuHV-4 genome cloned as a BAC (Adler *et al.*, 2000) and was kindly provided by Dr H. Adler and Dr U. Koszinowski.

M3-Luc/ORF50$^-$eGFP BAC is the MuHV-4 M3-Luc/ORF50$^-$eGFP genome cloned as a BAC (Milho *et al.*, 2009) (Figure 5.1) and was a kind gift from Dr S. Efstathiou and Dr P. Stevenson. The luciferase coding sequence plus polyadenylation (polyA) signal were removed from pGL4.10 (Promega) by digestion with *Bgl*II/*Sal*I and cloned into the *Bam*HI/*Sal*I sites of pSP73 (Promega), downstream of a 500 bp MuHV-4 M3 promoter (May *et al.*, 2005). M3-luciferase-

polyA was then excised with *Bgl*II/*Sal*I, blunted with Klenow fragment DNA polymerase and cloned into the blunted *Mfe*I site (genomic coordinate 77,176) of a *Bgl*II MuHV-4 genomic clone (coordinates 75,338 to 78,717) in pSP73. The expression cassette plus genomic flanks were subcloned into the *Bam*HI site of the pST76K-SR shuttle vector and recombined into a MuHV-4 BAC (Adler *et al.*, 2000). An ORF50-deficient derivative was made by cloning a *Hinc*II genomic fragment (coordinates 63,844 to 70,433) into the *Hinc*II site of pUC9 (New England Biolabs), with the *Bam*HI site of pUC9 at the 70,433 end of the insert. This was cut with *Bsm*I (67,792) and *Cla*I (69,177) to remove most of ORF50 exon 2 (67,661 to 69,376), blunted and dephosphorylated with Antarctic alkaline phosphatase (New England Biolabs). The enhanced green fluorescent protein (eGFP) coding sequence from pEGFP-N3 (Clontech) was ligated in place of the removed fragment. eGFP plus its genomic flanks were then excised using a genomic *Kpn*I site (66,120) and the *Bam*HI site in pUC9, cloned into the *Bam*HI/*Kpn*I sites of pST76K-SR, and recombined into the MuHV-4 M3-Luc BAC.

8.1.5.3. Plasmids for *in situ* hybridization

pEH1.4 is a pBluescript based plasmid containing the 1.4 kb *Hind*III-*Eco*RI subfragment of the *Hind*III-E MuHV-4 genomic fragment (nt 107 to 1518) cloned in an antigenomic orientation. It contains viral tRNA 1 to 4 and viral miRNA miR-M1-1 to 6, 10 and 11 transcripts. This plasmid was used to generate the digoxigenin (DIG)-labelled probe used to detect viral tRNA 1 to 4 and viral miRNA miR-M1-1 to 6, 10 and 11 transcripts by ISH. Plasmid was linearized with *Hind*III and DIG-labelled antisense probes were synthesized by *in vitro* transcription with T7 RNA polymerase via the T7 phage promoter. This plasmid was constructed by Dr Rory Bowden (Bowden *et al.*, 1997).

8.1.5.4. Plasmids for baculovirus studies

pUC57-GST-His-mLANA is a plasmid encoding mLANA with a N-terminus GST-8xHis-tag. The tag is preceded by a TEV cleavage site and followed by a PreScission protease cleavage site. *ORF73* gene encoding mLANA was codon optimized at GenScript for expression in insect cells (section 8.2.6.1).

pUC57-His-mLANA is a plasmid encoding mLANA with a N-terminus 8xHis-tag. The tag is preceded by a TEV cleavage site and followed by a PreScission protease cleavage site. *ORF73* gene encoding mLANA was codon optimized at GenScript for expression in insect cells (section 8.2.6.1).

pPBac is a transfer plasmid used for integration of the genes of interest into EMBacY plasmid (Vijayachandran *et al.*, 2011) and was a kind gift from Dr I. Berger. pPBac contains a resistance marker (gentamicin-resistance) and an expression cassette flanked by a polyhedrin promoter and a terminator derived from the SV40 polyA signal sequence. The

cassette harbours an ORF encoding TEV protease, followed by a short linker DNA sequence with a *Bst*EII restriction site and a *Rsr*II restriction site, which are used to clone the genes of interest into pPBac. The resistance marker and the expression cassette are flanked by Tn7L and Tn7R DNA sequences, which are recognised by Tn7 transposase, allowing integration of heterologous genes into the Tn7 attachment site of EMBacY plasmid.

pPBac-GST-His-mLANA is the GST-His-tagged mLANA coding sequence cloned into pPBac. This plasmid was constructed in this study and it was used to integrate GST-His-tagged mLANA DNA sequence into EMBacY plasmid (section 8.2.6.3).

pPBac-His-mLANA is the His-tagged mLANA coding sequence cloned into pPBac. This plasmid was constructed in this study and it was used to integrate His-tagged mLANA DNA sequence into EMBacY plasmid (section 8.2.6.3).

EMBacY is the YFP-expressing AcNPV baculovirus genome cloned as a BAC (Bieniossek *et al.*, 2008; Trowitzsch *et al.*, 2010) and was kindly provided by Dr I. Berger. EMBacY contains a resistance marker (kanamycin-resistance), a F-factor for single-copy replication and a *lacZα* blue/white selection cassette harbouring a Tn7 attachment site. In addition, EMBacY contains a YFP coding gene under the control of the polyhedrin promoter into a *loxP* site, allowing monitorization of virus performance during infection.

8.1.6. Viruses

8.1.6.1. MuHV-4 viruses

MuHV-4 used in this study belongs to the strain murine herpesvirus-68 (MHV-68) that was originally isolated by Prof. Dusan Blaskovic (Blaskovic *et al.*, 1980). Clone G2.4 was isolated from virus grown in BHK-21 cells by Dr S. Efstathiou (Efstathiou *et al.*, 1990).

Wild-type virus (vWT) used in animal experiments was derived from a genomic BAC and was a kind gift from Dr H. Adler and Dr U. Koszinowski. This virus is essentially MHV-68 clone G2.4 but contains a single *lox*P site (Adler *et al.*, 2001; Adler *et al.*, 2000).

vmLANA$_{H186D/K187E}$ recombinant virus was engineered in this study by mutagenesis of the virus genome in *E. coli* using the MuHV-4 BAC pHA3 (Adler *et al.*, 2000) as described in detail in section 8.2.5. It contains histidine (H) residue 186 and lysine (K) residue 187 of mLANA substituted by aspartate (D) and glutamate (E), respectively.

vmLANA$_{K224A/K228A/K229A}$ recombinant virus was engineered in this study by mutagenesis of the virus genome in *E. coli* using the MuHV-4 BAC pHA3 (Adler *et al.*, 2000) as described in detail in section 8.2.5. It contains lysine (K) residues 224, 228 and 229 of mLANA substituted by alanine (A).

vmLANA$_{K224E/K228E/K229E}$ recombinant virus was engineered in this study by mutagenesis of the virus genome in *E. coli* using the MuHV-4 BAC pHA3 (Adler *et al.*, 2000) as described in detail in section 8.2.5. It contains lysine (K) residues 224, 228 and 229 of mLANA substituted by glutamate (E).

vmLANA$_{K251A/K253A}$ recombinant virus was engineered in this study by mutagenesis of the virus genome in *E. coli* using the MuHV-4 BAC pHA3 (Adler *et al.*, 2000) as described in detail in section 8.2.5. It contains lysine (K) residues 251 and 253 of mLANA substituted by alanine (A).

vmLANA$_{K251E/K253E}$ recombinant virus was engineered in this study by mutagenesis of the virus genome in *E. coli* using the MuHV-4 BAC pHA3 (Adler *et al.*, 2000) as described in detail in section 8.2.5. It contains lysine (K) residues 251 and 253 of mLANA substituted by glutamate (E).

vmLANA$_{P203A}$ recombinant virus was engineered in this study by mutagenesis of the virus genome in *E. coli* using the MuHV-4 BAC pHA3 (Adler *et al.*, 2000) as described in detail in section 8.2.5. It contains proline (P) residue 203 of mLANA substituted by alanine (A).

vmLANA$_{P203A/P206A}$ recombinant virus was engineered in this study by mutagenesis of the virus genome in *E. coli* using the MuHV-4 BAC pHA3 (Adler *et al.*, 2000) as described in detail in section 8.2.5. It contains proline (P) residues 203 and 206 of mLANA substituted by alanine (A).

vmLANA$_{V199A}$ recombinant virus was engineered in this study by mutagenesis of the virus genome in *E. coli* using the MuHV-4 BAC pHA3 (Adler *et al.*, 2000) as described in detail in section 8.2.5. It contains valine (V) residue 199 of mLANA substituted by alanine (A).

vmLANA$_{V199A/L202A}$ recombinant virus was engineered in this study by mutagenesis of the virus genome in *E. coli* using the MuHV-4 BAC pHA3 (Adler *et al.*, 2000) as described in detail in section 8.2.5. It contains valine (V) residue 199 and leucine (L) residue 202 of mLANA substituted by alanine (A).

vmLANA$_{H186D/K187E}$-R revertant virus was engineered in this study by mutagenesis of the virus genome in *E. coli* using the mutant MuHV-4-mLANA$_{H186D/K187E}$ BAC pHA3 as described in detail in section 8.2.5. It contains the mLANA$_{H186D/K187E}$ locus restored to the wild-type status.

vmLANA$_{K224A/K228A/K229A}$-R revertant virus was engineered in this study by mutagenesis of the virus genome in *E. coli* using the mutant MuHV-4-mLANA$_{K224A/K228A/K229A}$ BAC pHA3 as described in detail in section 8.2.5. It contains the mLANA$_{K224A/K228A/K229A}$ locus restored to the wild-type status.

vmLANA$_{K224E/K228E/K229E}$-R revertant virus was engineered in this study by mutagenesis of the virus genome in *E. coli* using the mutant MuHV-4-mLANA$_{K224E/K228E/K229E}$ BAC pHA3 as described

in detail in section 8.2.5. It contains the mLANA$_{K224E/K228E/K229E}$ locus restored to the wild-type status.

vmLANA$_{K251A/K253A}$-R revertant virus was engineered in this study by mutagenesis of the virus genome in *E. coli* using the mutant MuHV-4-mLANA$_{K251A/K253A}$ BAC pHA3 as described in detail in section 8.2.5. It contains the mLANA$_{K251A/K253A}$ locus restored to the wild-type status.

vORF50^{-} mLANA-WT recombinant virus was derived from a genomic MuHV-4 M3-Luc/ORF50^{-}eGFP BAC (Milho *et al.*, 2009), as described in detail in section 8.1.5.4, and was a kind gift from Dr S. Efstathiou and Dr P. Stevenson. This virus retains the *loxP*-flanked BAC cassette (Adler *et al.*, 2000), since it was not passed through NIH-3T3-CRE cells.

vORF50^{-} mLANA-SOCS recombinant virus was engineered in this study by mutagenesis of the virus genome in *E. coli* using the mutant MuHV-4 M3-Luc/ORF50^{-}eGFP BAC pHA3 (Milho *et al.*, 2009) as described in detail in section 8.2.5. It contains valine (V) residue 199, leucine (L) residue 202, proline (P) residue 203 and proline (P) residue 206 of mLANA substituted by alanine (A). This virus retains the *loxP*-flanked BAC cassette (Adler *et al.*, 2000), since it was not passed through NIH-3T3-CRE cells.

vORF50^{-} mLANA$_{V199A/L202A}$ recombinant virus was engineered in this study by mutagenesis of the virus genome in *E. coli* using the mutant MuHV-4 M3-Luc/ORF50^{-}eGFP BAC pHA3 (Milho *et al.*, 2009) as described in detail in section 8.2.5. It contains valine (V) residue 199 and leucine (L) residue 202 of mLANA substituted by alanine (A). This virus retains the *loxP*-flanked BAC cassette (Adler *et al.*, 2000), since it was not passed through NIH-3T3-CRE cells.

8.1.6.2. Baculoviruses

Baculoviruses used in this study were derived from YFP-expressing AcNPV baculovirus genome cloned as a BAC (EMBacY) (Bieniossek *et al.*, 2008; Trowitzsch *et al.*, 2010) (section 8.1.5.4).

vEMBacY-GST-His-mLANA recombinant virus was engineered in this study using MultiBac system, developed by Dr I. Berger at EMBL Grenoble (Berger *et al.*, 2004; Bieniossek *et al.*, 2008; Trowitzsch *et al.*, 2010; Vijayachandran *et al.*, 2011), as described in detail in section 8.2.6. This baculovirus contains the GST-His-tagged mLANA coding sequence integrated into its genome.

vEMBacY-His-mLANA recombinant virus was engineered in this study using MultiBac system, developed by Dr I. Berger at EMBL Grenoble (Berger *et al.*, 2004; Bieniossek *et al.*, 2008; Trowitzsch *et al.*, 2010; Vijayachandran *et al.*, 2011), as described in detail in section 8.2.6. This baculovirus contains the His-tagged mLANA coding sequence integrated into its genome.

8.1.7. Mice

BALB/c and C57BL/6 mice used in this study were from Charles Rivers Laboratories International. Animals were housed and subjected to experimental procedures in specific pathogen-free conditions, at Instituto de Medicina Molecular animal facility, Lisbon, Portugal.

8.2. Methods

8.2.1. Isolation and analysis of DNA

8.2.1.1. High molecular weight (HMW) cellular/viral DNA extractions

High molecular weight (HMW) DNA was extracted from frozen-thawed splenocyte suspensions of infected mice. To this end, frozen-thawed splenocyte suspensions were centrifuged at 500 x g for 5 min. The pellet was resuspended in 750 µl of Tris-ethylenediaminetetraacetic acid (TE) lysis buffer (10 mM Tris-HCl pH 8.0, 50 mM ethylenediaminetetraacetic acid (EDTA), 0.5% sodium dodecyl sulfate (SDS) and 20 µg/ml Proteinase K) and incubated overnight (ON) at 37ºC. DNA samples containing proteins and salts were purified by deproteinization using phenol/chloroform extraction and concentrated by ethanol precipitation. An equal volume of TE-buffered phenol:chroloform:isoamyl alcohol (25:24:1) was added to the DNA solution, mixed well by vigorous shaking or vortexing, incubated for 5 min at room temperature (RT) and centrifuged at 10,500 x g for 5 min at RT. The upper aqueous phase containing DNA was transferred to a clean tube and re-extracted twice with an equal volume of chloroform. DNA was precipitated using 0.1 volumes of 3 M KOAc or NaOAc (pH 5.5) and 2.5 volumes of 100% ethanol. Samples were gently mixed well, left for 10 min at RT and HMW DNA was extracted by spooling onto a glass Pasteur pipette. DNA was washed with cold 70% ethanol, left for 10-20 min at RT to air-dry and then resuspended in MilliQ water or TE.

8.2.1.2. Plasmid DNA isolation

Plasmid DNA was isolated from plasmid-containing *E. coli* strains (section 8.1.4) grown in Luria Bertani (LB) broth (tryptone 1%, yeast extract 0.5%, NaCl 1%) containing the appropriate antibiotic(s), using an alkaline lysis method modified accordingly to the scale of the preparation and plasmid size. Antibiotics were used at the following concentrations: 100 µg/ml ampicillin, 17 µg/ml chloramphenicol, 30 µg/ml kanamycin (or 50 µg/ml for EMBacY-containing bacteria), 24 µg/ml tetracycline and 10 µg/ml gentamicin.

Small scale plasmid preparation

For small scale plasmid preparations (plasmid minipreps), 3-10 mL of LB broth cultures containing the appropriate antibiotic(s) were inoculated from single bacterial colonies and incubated with vigorous shaking 12-18 h at 37 or 30ºC. Cultures were pelleted by centrifugation for 5 min at 3,000 x g. Plasmid DNA was obtained using the Wizard Plus SV Minipreps DNA Purification System (Promega), by column purification of DNA prepared by alkaline lysis, according to manufacturer's instructions. DNA was eluted in 50-100 µl of MilliQ water and stored at -20ºC.

Large scale plasmid preparation

For large scale plasmid preparations (plasmid maxipreps), cultures of plasmid-containing bacteria were prepared by inoculation of 200 mL of LB broth cultures containing the appropriate antibiotic(s) from single colonies and incubation with shaking 12-18 h at 37 or 30ºC. Bacterial cultures were pelleted by centrifugation at 6,000 x g for 15 min at 4ºC and DNA was purified using the LFU / Plasmid Purification MAXI Kit (JETSTAR), following manufacturer's instructions. DNA was resuspended in 200-600 µl of MilliQ water and stored at -20ºC.

Small scale BAC plasmid preparation

For small scale BAC plasmid preparations (BAC plasmid minipreps), 10 ml of LB broth containing chloramphenicol were inoculated from single bacterial colonies and incubated with vigorous shaking 12-18 h at 37ºC. Bacteria were pelleted by centrifugation at 2,500 x g for 10 min at 4ºC. Pellet was thoroughly resuspended in 200 µl of buffer S1 (50 mM Tris-HCl pH 8.0, 10 mM EDTA; from NucleoBond BAC 100 Kit, Macherey-Nagel) plus 100 µg/ml RNase A. 300 µl of buffer S2 (200 mM NaOH, 1% SDS; from NucleoBond BAC 100 Kit, Macherey-Nagel) were promptly added and the suspension was mixed by gentle inversion and left at RT for 5 min. 300 µl of chilled buffer S3 (2.8 M KAc pH 5.1; from NucleoBond BAC 100 Kit, Macherey-Nagel) were added, tube was gently inverted to mix solution, incubated on ice for 15 min and centrifuged for 10 min at 18,000 x g and 4ºC. Supernatant was transferred to a new tube and 1 ml of phenol/chloroform (1:1) was added and mixed by inversion. Mixture was left 5 min at RT and then centrifuged 10 min at 18,000 x g and 4ºC. Aqueous phase was recovered and precipitated with 0.7 volumes of isopropanol and left at RT for 5 min. BAC plasmid DNA was pelleted by centrifugation for 20 min at 18,000 x g and 4ºC. Supernatant was discharged and the pellet was washed with 100 µl of 70% ethanol, centrifuged another 10 min, drained and air dried. DNA was resuspended in 60 µl of TE (10 mM Tris, 1 mM EDTA, pH 8.0) supplemented with RNase A (10 µg/ml) and stored at 4ºC.

Large scale BAC plasmid preparation

For large scale BAC plasmid preparations (BAC plasmid maxipreps), cultures of BAC plasmid-containing bacteria were prepared by inoculation of 400 ml of LB broth supplemented with chloramphenicol from single colonies and incubation with shaking 12-18 h at 37ºC. Bacteria were pelleted by centrifugation at 6,000 x g for 15 min at 4ºC. BAC plasmid DNA was isolated using

NucleoBond BAC 100 plasmid purification kit (Macherey-Nagel), according to manufacturer's instructions. BAC DNA was resuspended in 100-200 µl of MilliQ water and stored at 4ºC.

Small scale EMBacY plasmid preparation

For small scale EMBacY plasmid preparations (EMBacY plasmid minipreps), 2 ml of LB broth containing kanamycin, tetracycline and gentamicin were inoculated from single bacterial colonies and incubated with vigorous shaking ON at 37ºC. Bacteria were pelleted by centrifugation at 2,500 x g for 10 min at 4ºC. Pellet was thoroughly resuspended in 300 µl of buffer P1 (50 mM Tris-HCl pH 8.0, 10 mM EDTA; from Qiagen Large-Construct Kit) plus 100 µg/ml RNase A. 300 µl of buffer P2 (200 mM NaOH, 1% SDS; from Qiagen Large-Construct Kit) were added and the suspension was mixed by gentle inversion and left at RT for 5 min. 300 µl of chilled buffer P3 (3 M KAc pH 5.5; from Qiagen Large-Construct Kit) were added, tube was gently inverted to mix solution, incubated on ice for 10 min and centrifuged for 10 min at 18,000 x g and 4ºC. Supernatant was transferred to a new tube and centrifuged again for 3 min at 18,000 x g and 4ºC. Supernatant was transferred to a new tube and DNA was precipitated with 700 µl of isopropanol and pelleted by centrifugation for 10 min at 18,000 x g and 4ºC. Supernatant was discharged and the pellet was washed with 200 µl of 70% ethanol and centrifuged another 5 min. Supernatant was discharged and the pellet was washed again with 50 µl of 70% ethanol. Ethanol was removed in a sterile hood and the pellet was air dried for 10 min. DNA was gently resuspended in 30 µl of filter sterilized water.

8.2.1.3. Quantification of DNA

DNA was quantified by ultraviolet (UV) spectrophotometry using a Nanodrop (ND-1000) spectrophotometer.

8.2.1.4. Restriction endonuclease digestion

Restriction endonuclease digestion of plasmids or PCR products was used either to prepare linear or insert purified DNA, or to screen DNA for a desired digestion profile or for the presence of inserts cloned in expression vectors. Restriction enzyme assays were performed using the appropriate restriction endonucleases and correspondent reaction buffers, according to manufacturer's instructions. The volume of the reaction as well as the amount of DNA and enzymes used depended on purpose of the assay. Typically, digestion of plasmids or PCR products for subsequent ligation and cloning was performed for 1-4 h, with 1-5 µg of DNA and 0.1-10 U of restriction endonuclease per µg of DNA, using the manufacturer's recommended conditions in a volume of 50-60 µl. Diagnosis digestion was performed with 1 µg of DNA, 1-10 U of restriction endonuclease, using manufacturer´s recommended conditions, in a volume of 20-50 µL for 1-2 h. Multiple digestions of the same DNA were performed when possible with the same buffer; otherwise salt conditions were adjusted for subsequent digestion steps or DNA was re-purified in column. Restriction profile and completeness of the digestion were assessed by analytical agarose gel electrophoresis.

8.2.1.5. Analysis and isolation of DNA by gel electrophoresis

Linear DNA was size fractioned and visualized on agarose gels stained with GelRed (Biotium) or RedSafe (iNtRON Biotechnology), according to manufacturer's instructions. Gels were prepared using 0.8-1.5% agarose in 1x Tris-acetate-EDTA (TAE) (40 mM Tris-acetate, 1 mM EDTA, pH 8.0). DNA samples were mixed with the appropriate volume of DNA loading buffer (10 mM EDTA, 5% glycerol, 0.025% bromophenol blue and 0.025% xylene cyanol) prior to loading into the gel. Samples were electrophoresed at 0.5-5.0 V/cm in 1x TAE buffer. DNA was visualized by UV transillumination. The size of DNA bands was estimated by comparison with linear DNA standards of known molecular weight (1 Kb plus DNA ladder, Invitrogen) run along with samples.

Following analysis of DNA by agarose gel electrophoresis, the DNA fragments of interest were purified by excision of the resolved bands from the gel and recovered on High Pure PCR Product Purification Kit columns (Roche), according to manufacturer´s instructions. Typically, DNA was eluted in 50 µl of MilliQ water and a fraction of the purified samples (1/10 of the total volume of the eluate) was re-run on an agarose gel, in order to check the DNA purification.

8.2.1.6. DNA sequencing

The integrity of the plasmids constructed in this study was confirmed by sequencing the PCR-generated inserts. During recombinant virus construction, identification of mutant BAC clones was performed by sequencing across *ORF73* in the BAC vector. Recombinant viruses were also sequenced in the region subjected to mutagenesis to confirm the retention of the engineered point mutations following *in vivo* infection.

DNA was sequenced at STAB VIDA according to the Sanger method and using an automatic DNA sequencer (ABI 3730XL). DNA sequences were analysed and compared to sequences deposited in the National Centre for Biotechnology Information (NCBI) database using the Basic Local Alignment Search Tool (BLAST) and Multiple Sequence Alignment with Hierarchical Clustering – MultAlin software.

8.2.2. Polymerase Chain Reaction (PCR)

PCR was used for different purposes.

During construction of pCMV-Myc plasmids encoding mLANA mutants, mutations in *ORF73* gene were introduced by PCR using pCMV-Myc-mLANA plasmid as a template. The mutagenic primers used are described in Table 8.2. PCR was performed using the QuikChange II XL Site-Directed Mutagenesis Kit (Agilent Technologies), according to manufacturer´s instructions.

Table 8.2. Primers used to generate pCMV-Myc-mLANA mutants.

mLANA mutations	mLANA template	Oligonucleotide sequence (5'-3')
H186D/K187E	WT	CACATCCCTACACTTTGAATAAACTTGACGAGTGTATCCAAAGCAAACATG
K224A	WT	ACTATTTACTTTCATTTGTTGAAGACGCGAAACAGGCCAAAAAACTAAAAAGGG
K224A/K228A/K229A	K224A	TTGTTGAAGACGCGAAACAGGCCGCAGCACTAAAAAGGGTTGTCTTGGCCT
K224E	WT	CTATTTACTTTCATTTGTTGAAGACGAGAAACAGGCCAAAAAACTAAAAAG
K224E/K228E/K229E	K224E	TTTGTTGAAGACGAGAAACAGGCCGAGGAGCTAAAAAGGGTTGTCTTGGCCTAC
K251A/K253A	WT	AGCAGCGTAGAAGGTACTATAGTCGCGGCAGCGCCTTATTTTCCCTTACCAGAG
K251E/K253E	WT	GCGTAGAAGGTACTATAGTCGAGGCAGAGCCTTATTTTCCCTTA
V199A	WT	TGTACTCTCAACACCAGCTAGCTGTTTACCCTTGG
L202A	WT	TGTACTCTCAACACCAGTTAGCTGTGCACCCTTGGTACCA
V199A/L202A	V199A	TGTACTCTCAACACCAGCTAGCTGTGCACCCTTGGTACCA
P203A	WT	CACCAGTTAGCTGTTTAGCCTTGGTACCAGGC
P206A	WT	AGTTAGCTGTTTACCCTTGGTAGCAGGCACAACAC
P203A/P206A	WT	CAACACCAGTTAGCTGTTTAGCCTTGGTAGCAGGCACAACA

Mutations introduced in template mLANA DNA sequence are underlined. WT, wild-type.

ORF73 region was amplified by PCR from BAC plasmid or HMW DNA for subsequent verification of the introduced mutations in recombinant viruses by restriction endonuclease digestion (section 8.2.1.4) or DNA sequencing (section 8.2.1.6). The primers designed were specific for *ORF73* gene and generated a fragment of 966 bp (Table 8.3). PCR was performed using GoTaq Flexi DNA Polymerase (Promega). PCR mixes were prepared in a total volume of 50 µl (made up in sterile MilliQ water) and consisted of 300 nM of each primer, 1x GoTaq Flexi buffer (Promega), 2 mM of $MgCl_2$, 200 µM of each deoxynucleotide (dNTP), 1.25 U of GoTaq Flexi DNA polymerase (Promega) and <100 ng of template DNA. DNA was amplified on a MyCycler thermal cycler (Bio-Rad), under the following conditions: an initial melting step of 95ºC for 5 min followed by 30 cycles of amplification, composed of denaturation at 95ºC for 45 sec, annealing at 59ºC for 45 sec (depending on the optimal annealing temperature for each specific set of primers) and extension at 72ºC for 1 min; a final extension step was performed at 72ºC for 5 min. PCR products were purified with High Pure PCR Product Purification Kit (Roche) (section 8.2.1.5), according to manufacturer´s instructions.

Table 8.3. Primers used to amplify *ORF73* gene.

Oligonucleotide	Sequence (5'-3')	Amplicon (bp)
Upper primer	AAAGGATCCTATGCCCACATCCCCAC	966
Lower primer	AAAGCGGCCGCTTATGTCTGAGACCCTTGTC	966

8.2.3. Cloning procedures

8.2.3.1. Cloning of inserts into pBamG vector

pCMV-Myc constructs encoding mLANA$_{K224A/K228A/K229A}$, mLANA$_{K224E/K228E/K229E}$, mLANA$_{K251A/K253A}$, mLANA$_{K251E/K253E}$, mLANA$_{P203A}$, mLANA$_{V199A}$, mLANA$_{P203A/P206A}$ and mLANA$_{V199A/L202A}$ were digested with *Hind*III and *Pci*I restriction endonucleases (section 8.2.1.4) to isolate the fragments harbouring the desired mutations. pCMV-Myc construct encoding mLANA$_{H186D/K187E}$ was digested with *BstE*II and *Pci*I restriction endonucleases. Digested inserts were isolated by gel electrophoresis and purified from agarose gel using the High Pure PCR Product Purification Kit (Roche) (section 8.2.1.5), according to manufacturer's instructions. pBamG plasmid (pACYC184-BamG), containing the *Bam*HI-G MuHV-4 genomic fragment (coordinates 101,654 to 106,903) (section 8.1.5.2), was digested with *Hind*III and *Pci*I, or *BstE*II and *Pci*I restriction endonucleases, creating compatible cohesive ends with the insert. Digested vector was isolated by gel electrophoresis and purified from agarose gel using the High Pure PCR Product Purification Kit (Roche). Prepared insert and vector were ligated as described in section 8.2.3.4 and ligations were transformed into *E. coli* DH5α competent cells (section 8.2.3.5). DNA was isolated from colonies by plasmid miniprep (section 8.2.1.2) and plasmid structure was screened by restriction analysis with the appropriate endonucleases (section 8.2.1.4).

8.2.3.2. Subcloning of inserts into the shuttle vector

Inserts in pBamG constructs described in section 8.2.3.1 were subcloned into a *Bam*HI-G MuHV-4 genomic fragment (coordinates 101,654 to 106,903) cloned into pST76K-SR plasmid (*Bam*HI-G shuttle plasmid). Both plasmids were digested with *Bam*HI restriction enzyme, creating compatible cohesive ends. Digested vector was dephosphorylated with 2 U of alkaline phosphatase (Roche) per µg of DNA, for 30 min at 37ºC. Digested insert and vector were then isolated by gel electrophoresis and purified from agarose gel using the High Pure PCR Product Purification Kit (Roche) (section 8.2.1.5). Insert and vector were ligated as described in section 8.2.3.4 and ligations were transformed into XL10-Gold Ultracompetent cells (Agilent Technologies) (section 8.2.3.5). DNA was isolated from colonies by plasmid miniprep (section 8.2.1.2) and plasmid structure was screened by restriction analysis with the appropriate endonucleases (section 8.2.1.4).

8.2.3.3. Subcloning of GST-His-mLANA and His-mLANA inserts into pPBac plasmid

GST-His-mLANA and His-mLANA coding sequences cloned into pUC57 (section 8.1.5.4) were subcloned into pPBac plasmid. Both plasmids were digested with *BstE*II and *Rsr*II restriction enzymes, creating compatible cohesive ends. Digested insert and vector were then isolated by gel electrophoresis and purified from agarose gel using the High Pure PCR Product Purification Kit (Roche) (section 8.2.1.5). Insert and vector were ligated as described in section 8.2.3.4 and ligations were transformed into *E. coli* strain DH5α (section 8.2.3.5). DNA was isolated from colonies by plasmid maxiprep (section 8.2.1.2) and plasmid structure was screened by restriction analysis with *BstE*II and *Rsr*II restriction endonucleases (section 8.2.1.4).

8.2.3.4. DNA ligation

Digested inserts and vectors were ligated using T4 DNA ligase (Roche). Approximately 100 ng of vector DNA was ligated with 1-3 fold excess of insert in 20 µl reactions (made up in sterile MilliQ water), containing 1x ligase buffer (Roche) and 1U of T4 DNA ligase. Cohesive-end ligations were performed ON at 14ºC.

8.2.3.5. Bacterial transformation

Preparation of chemically competent cells

Competent *E. coli* strains DH5α and DH10B (containing the MuHV-4 BAC plasmid) were prepared by the Inoue modified method (Inoue *et al.*, 1990). *E. coli* glycerol stock was streaked into a LB agar plate supplemented with the appropriate antibiotic(s) and grown ON at 37ºC. On the next day, a single colony was inoculated into 10 ml of LB broth supplemented with the appropriate antibiotic(s) and incubated with vigorous shaking 12-18 h at 37ºC. 10 ml of the resulting culture were inoculated into 400 ml of fresh LB broth supplemented with the appropriate antibiotic(s) and incubated at 37ºC with vigorous shaking, until the bacterial culture reached an optical density $(OD)_{600nm}$ of 0.6. Cells were cooled on ice and centrifuged at 3,500 x g for 15 min at 4ºC. Cell pellet was gently resuspended in 100 ml of ice-cold sterile solution A (0.03 M KCH_3COO, 0.05 M $MnCl_2$, 0.01 M $CaCl_2$, 0.1 M KCl and 15% glycerol in sterile MilliQ water). Cells were centrifuged again at 3,500 x g for 8 min at 4ºC and the pellet was resuspended in 20 ml of ice-cold sterile solution B (0.01 M NaMOPS pH 7.0, 0.075 M $CaCl_2$, 0.01 M KCl and 15% glycerol in sterile MilliQ water). 100 µl and 300 µl aliquots were made. Each aliquot was quickly frozen by transferring the vials to dry ice immersed in ethanol. Competent cells were stored at -80ºC until further use.

Preparation of electrocompetent cells

E. coli DH10EMBacY glycerol stock was streaked into a LB agar plate supplemented with kanamycin (50 µg/ml), tetracycline (24 µg/ml), X-Gal (100 µg/ml) and IPTG (1 mM) and grown ON at 37ºC. On the following day, three blue colonies were inoculated into 100 ml of LB broth

supplemented with kanamycin and tetracycline and incubated with vigorous shaking 12-18 h at 37ºC. This preculture was then inoculated into 1 l of fresh LB broth supplemented with kanamycin and tetracycline and incubated at 37ºC with vigorous shaking, until the bacterial culture reached an OD_{600nm} of 0.5. Cells were cooled on ice for 15 min and centrifuged four times at 3,500 x g for 15 min at 4ºC. Cell pellet was gently resuspended in 500, 250, 50 and 2 ml of ice-cold sterile 10% glycerol solution after first to fourth centrifugation, respectively. 100 µl aliquots were made, quickly frozen in dry ice immersed in ethanol and stored at -80ºC until further use. Competent cells were tested by streak out on LB agar containing kanamycin, tetracycline, X-Gal and IPTG to confirm that all colonies were blue.

Transformation of chemically competent cells

Chemically competent *E. coli* was transformed by the heat shock method.

100 µl of competent *E. coli* DH5α and DH10B (containing MuHV-4 BAC) were incubated on ice for 30 min with 100 ng of plasmid DNA or 5 µl of ligation mix. Cells were heat shocked for 45 sec at 42ºC and subsequently chilled on ice for 2 min. 500 µl of SOC medium (2% tryptone, 0.5% yeast extract, 10 mM NaCl, 2.5 mM MgCl2, 10 mM $MgSO_4$, 20 mM glucose) were added to each vial and cells were incubated for 1 h at 37 or 30ºC, with vigorous shaking. Cells were then spread onto LB agar plates containing the appropriate antibiotic(s) and incubated ON at 37 or 30ºC. Ampicillin was used at 100 µg/ml, chloramphenicol at 17 µg/ml, kanamycin at 30 µg/ml and gentamicin at 10 µg/ml.

When using XL10-Gold Ultracompetent cells (Agilent Technologies), 2 µl of β-mercaptoethanol mix provided with the kit were added to 45 µl of cells and incubated on ice for 10 min before adding the DNA. 5 µl of DNA was then added to cells and incubated on ice for 30 min. Cells were heat shocked for 30 sec at 42ºC and subsequently chilled on ice for 2 min. 500 µl of preheated (42ºC) SOC medium were added to each vial and cells were incubated for 1 h at 37ºC, with vigorous shaking. Cells were then spread onto LB agar plates containing the appropriate antibiotic(s) and incubated ON at 37ºC.

Transformation of electrocompetent cells

Electrocompetent *E. coli* DH10EMBacY was transformed by electroporation. First, 0.1 cm electroporation cuvettes (Bio-Rad) were placed at -20ºC and electrocompetent cells were put on ice. 100 µl of cells were incubated with 1 µg of plasmid DNA for 1 min on ice and then the mix was carefully transferred into a cuvette, avoiding the formation of bubbles. The cuvette was placed in an electroporator (Gene Pulser Xcell – Bio-Rad) and cells were electroporated at 1,800 V, 25 µF and 200 Ω. 600 µl of SOC medium were added to cells immediately after electroporation and the mix was transferred into a 1.5 ml tube and incubated ON at 37ºC with vigorous shaking.

8.2.4. Cell culture and transfections

8.2.4.1. Media and culture conditions

BHK-21 cells were cultured in Glasgow's modified Eagle's medium (GMEM) supplemented with 10% foetal bovine serum (FBS), 2 mM L-glutamine, 100 U/ml penicillin-streptomycin and 10% tryptose phosphate broth (TPB).

NIH-3T3-CRE, 3T3-ORF50, MEF-1 and HEK 293T cells were cultured in Dulbecco's modified Eagle's medium (DMEM) supplemented with 10% FBS, 2 mM L-glutamine and 100 U/ml penicillin-streptomycin.

Sf21 cells were cultured in HyClone SFM4Insect medium (Thermo Scientific), at a cell density of 0.5-2x10^6 cells/ml. Since Sf21 cells double approximately every 24 h, cells were split every day and seeded at 0.5-1x10^6 cells/ml.

BHK-21, NIH-3T3-CRE, 3T3-ORF50, MEF-1 and HEK 293T cell cultures were grown in a humidified tissue culture incubator at 37ºC under 5% CO_2. Sf21 cell cultures were grown at 27ºC with shaking at 90 rpm, in a non-humidified, air regulated, non-CO_2 atmosphere.

8.2.4.2. Transfections

Transient transfections were performed using FuGENE 6 or X-tremeGENE HP DNA Transfection Reagent (Roche), according to manufacturer's instructions.

On the day before transfection, 10^6 BHK-21 cells were plated in 6 cm cell culture dishes and grown to 70-90% confluency. 1 µg of BAC DNA was added to 500 µl of non-supplemented GMEM and gently mixed. 2 µl of X-tremeGENE HP were subsequently added and the mix was incubated for 15 min at RT. The obtained solution was added dropwise to cells and these cultures were incubated in a tissue culture incubator at 37ºC with 5% CO_2, until approximately 50% of cytopathic effect (cpe) was visible (3-5 days).

5x10^5 3T3-ORF50 cells were plated in 6 cm dishes on the day before transfection and grown to 70-90% confluency. 1 µg of BAC DNA was added to 500 µl of non-supplemented DMEM and gently mixed. 2 µl of X-tremeGENE HP were subsequently added and the mix was incubated for 15 min at RT. The obtained solution was added dropwise to cells and cultures were treated with doxycycline (1 µg/ml). Cells were incubated in a tissue culture incubator at 37ºC with 5% CO_2, until approximately 50% cpe was visible (3-5 days).

HEK 293T cells were plated on the day before transfection and grown to 70-90% confluency. Approximately 24 h later, the appropriate amount of expression plasmids was added to non-supplemented DMEM and gently mixed. The transfection reagent was added in a ratio of 2:1 (2µl of X-tremeGENE HP DNA Transfection Reagent per µg of DNA) and the mix was incubated for 15 min at RT. The obtained solution was added dropwise to cells and these cultures were incubated in a tissue culture incubator at 37ºC with 5% CO_2, for 48 h. The number of plated cells, the amount of expression plasmids and the volume of non-supplemented DMEM were dependent on the assay performed and are described in detail in sections 8.2.13.1, 8.2.13.2 and 8.2.13.3.

0.5-1x10^6 Sf21 cells were plated per well in 6-well plates, in 3 ml of HyClone medium, and allowed to adhere 15 min at 27ºC to form monolayers. For each EMBacY plasmid to be transfected, 10 µl of Fugene 6 were incubated with 100 µl of HyClone medium. This mix was added to EMBacY plasmid diluted in 200 µl of HyClone medium and the transfection mix was incubated for 15 min at 27ºC. Finally, 150 µl of transfection mix were added to each well containing cells (2 wells per plasmid). A well containing untransfected cells and a well containing medium only were included as negative controls. Cell cultures were incubated at 27ºC for 48 h.

8.2.5. Construction of MuHV-4 recombinant viruses

MuHV-4 recombinants were derived from a BAC-cloned MuHV-4 pHA3 (Adler *et al.*, 2001; Adler *et al.*, 2000). Revertant viruses were obtained from mutant MuHV-4 BAC pHA3. ORF50-deficient recombinants were derived from MuHV-4 M3-Luc/ORF50$^-$eGFP BAC pHA3 (Milho *et al.*, 2009). Site-directed mutagenesis of MuHV-4-BAC genome was performed by homologous recombination in *E. coli*, using a two-step replacement procedure (Adler *et al.*, 2003). Chloramphenicol was used at 17 µg/ml and kanamycin at 30 µg/ml. Viral progeny was reconstituted by transfection of the recombinant BAC plasmid into eukaryotic cells.

8.2.5.1. Shuttle vector cloning

The first step in the generation of recombinant viruses is the construction of a recombination plasmid (shuttle plasmid) containing the desired mutation(s) flanked by sequences homologous to the integration site (2 to 3 kb on each side). Mutations in *ORF73* gene were introduced by PCR (section 8.2.2) using pCMV-Myc-mLANA plasmid as a template. pCMV-Myc constructs encoding mLANA mutants were digested with the appropriate restriction endonucleases (section 8.2.3.1.) to isolate the fragments harbouring the desired mutations. These fragments were inserted into the *Bam*HI-G MuHV-4 genomic fragment (coordinates 101,654 to 106,903) cloned in pBamG plasmid (section 8.1.5.2), digested with the same restriction endonucleases as the insert. Inserts in pBamG constructs were then subcloned into a *Bam*HI-G MuHV-4 genomic fragment cloned in pST76K-SR plasmid (*Bam*HI-G shuttle plasmid), using *Bam*HI restriction sites (section 8.2.3.2).

8.2.5.2. BAC mutagenesis in *E. coli*

Recombinant shuttle plasmids were transformed into *E. coli* strain DH10B containing MuHV-4 BAC (Adler *et al.*, 2000) or MuHV-4 M3-Luc/ORF50$^-$eGFP BAC (Milho *et al.*, 2009). To generate revertant viruses, the wild-type *Bam*HI-G pST76K-SR shuttle plasmid was transformed into DH10B cells containing each of the mutant BAC genomes. Bacteria were plated on LB plates containing kanamycin (shuttle plasmid resistance marker) and chloramphenicol (BAC plasmid resistance marker) and incubated ON at 30ºC, since shuttle vector has a temperature-sensitive replication mode. The shuttle plasmid encodes the RecA protein, which promotes complete integration of the

shuttle plasmid into the viral BAC genome by homologous recombination (Adler *et al.*, 2003). Bacteria containing the cointegrate were selected by incubation ON at 43ºC on LB plates containing kanamycin and chloramphenicol. Clones were replated on LB plates containing chloramphenicol and grown for one day at 30ºC. Under these conditions, cointegrates can spontaneously resolve by homologous recombination (bacteria are RecA+ at 30ºC) to either wild-type or mutant BAC plasmid. Bacteria harbouring resolved cointegrates were selected by replating on LB plates containing chloramphenicol and 5% sucrose (counterselection against SacB encoded by the shuttle plasmid) and grown at 30ºC (selection for sucrose-resistance works best at 30ºC). Finally, colonies were plated in parallel on kanamycin and chloramphenicol-containing LB plates and grown ON at 37ºC. Chloramphenicol-resistant kanamycin-sensitive clones were characterized by PCR and subsequent sequencing or restriction endonuclease digestion to identify the mutant clones (sections 8.2.1.4, 8.2.1.6 and 8.2.2). BAC plasmids from mutant clones were isolated by small or large scale BAC plasmid preparations (section 8.2.1.2). The structure and integrity of the viral genome was verified by digestion of BAC DNA with *Bam*HI and *Eco*RI restriction enzymes (section 8.2.1.4) and analysis of the resulting restriction patterns by agarose gel electrophoresis (section 8.2.1.5).

8.2.5.3. Virus reconstitution

Mutant or revertant BAC DNA was transfected into BHK-21 cells using X-tremeGENE HP DNA Transfection Reagent (Roche) (section 8.2.4.2). ORF50-deficient recombinant viruses were reconstituted by transfection of BAC DNA into 3T3-ORF50 complementing cell lines (section 8.1.3) using X-tremeGENE HP DNA Transfection Reagent (section 8.2.4.2) and treating cells with doxycycline (1µg/ml). When approximately 50% cpe was visible (after 3-5 days), cells and media were harvested and subjected to a freeze-thawing cycle to disrupt the cells. 1 ml aliquots were made and stored at -80ºC until further use. The obtained viral aliquots constituted the BAC^+ virus master stock.

8.2.5.4. Removal of BAC sequences

BAC cassette contains a *gfp* gene (Adler *et al.*, 2000), thus the screening of virus containing BAC sequences can be performed using green fluorescent protein (GFP) as a marker. $5x10^5$ NIH-3T3-CRE cells were infected with 0.3-10 µl of the obtained BAC^+ master stock diluted in 750 µl of complete DMEM (section 8.2.8.1) to remove the *lox*P-flanked BAC cassette. Virus was allowed to adsorb to cells in 6-well plates for 1 h at 37ºC and then 2 ml of complete DMEM was added. Cell cultures were incubated at 37ºC until viral plaques appeared (3-4 days). Viral plaques were analyzed by fluorescence microscopy and, if GFP-negative, cells and media were harvested by cell scraping and frozen-thawed. The obtained $BAC^{+/-}$ master stock was then used to infect fresh NIH-3T3-CRE cells as described above. Wells containing only GFP-negative viral plaques were selected and cells and media were harvested by cell scraping and frozen-thawed. 800 µl aliquots were made and constituted the recombinant virus BAC^- master stock.

ORF50-deficient recombinant viruses were not passed through NIH-3T3-CRE cells, therefore retaining the *loxP*-flanked BAC cassette.

8.2.6. Construction of recombinant baculoviruses

Recombinant baculoviruses were derived from YFP-expressing AcNPV baculovirus genome cloned as a BAC (EMBacY) (Bieniossek *et al.*, 2008; Trowitzsch *et al.*, 2010) (section 8.1.5.4). Recombinant baculoviruses were engineered using MultiBac system, a Tn7 transposition-based approach, developed by Dr I. Berger at EMBL Grenoble (Berger *et al.*, 2004; Bieniossek *et al.*, 2008; Trowitzsch *et al.*, 2010; Vijayachandran *et al.*, 2011). Kanamycin was used at 50 µg/ml, tetracycline at 24 µg/ml, gentamicin at 10 µg/ml, X-Gal at 100 µg/ml and IPTG at 1 mM. Baculoviruses were reconstituted by transfection of the recombinant EMBacY plasmid into Sf21 insect cells.

8.2.6.1. Codon optimization of *ORF73* gene

To achieve higher levels of mLANA expression in Sf21 cells, the *ORF73* gene sequence was optimized for codon usage in insect cells. Codon optimization was performed by GenScript company, using OptimumGene algorithm. 63% of *ORF73* codons were modified and the optimized gene was delivered in pUC57 plasmid. Two codon optimized *ORF73* constructs were engineered (Figure 6.1): pUC57-GST-His-mLANA and pUC57-His-mLANA, encoding mLANA with a N-terminus GST-8xHis-tag or 8xHis-tag, respectively. Each tag is preceded by a TEV cleavage site and followed by a PreScission protease cleavage site. Both plasmids contain engineered *BstE*II and *Rsr*II restriction sites upstream and downstream of the optimized sequence, respectively.

8.2.6.2. Subcloning of GST-His-mLANA and His-mLANA inserts into pPBac plasmid

GST-His-mLANA and His-mLANA coding sequences cloned into pUC57 were subcloned into pPBac plasmid (section 8.1.5.4), using *BstE*II and *Rsr*II restriction sites, as described in detail in section 8.2.3.3.

8.2.6.3. Generation of recombinant EMBacY plasmids

pPBac-GST-His-mLANA or pPBac-His-mLANA plasmids were transformed into *E. coli* DH10EMBacY containing baculovirus genome cloned as a BAC (EMBacY) (Bieniossek *et al.*, 2008; Trowitzsch *et al.*, 2010). Transformation was performed by electroporation, as described in section 8.2.3.5, and bacteria were incubated ON at 37ºC with vigorous shaking. On the following day, bacteria were streaked into LB agar plates supplemented with kanamycin, tetracycline, gentamicin, X-Gal and IPTG in 10-fold dilution series (1:1 to 1:1000), plating 135 µl of each dilution.

Inoculated plates were incubated ON at 37ºC and, on the next day, white and blue colonies were obtained. White colonies contain the region between Tn7L and Tn7R of pPBac plasmid (including the heterologous insert and gentamicin-resistance marker) inserted into the Tn7 attachment site, thereby disrupting the *lacZα* gene in EMBacY and resulting in loss of blue colour phenotype. For each transformation, eight white colonies and one control blue colony were picked, streaked into LB agar plates supplemented with kanamycin, tetracycline, gentamicin, X-Gal and IPTG and incubated ON at 37ºC to confirm the colour. Two white colonies per transformation were separately inoculated into 2 ml of LB broth containing kanamycin, tetracycline and gentamicin, and recombinant EMBacY plasmids were isolated as described in section 8.2.1.2.

8.2.6.4. Baculovirus reconstitution

Recombinant baculoviruses were reconstituted by transfection of recombinant EMBacY DNA into Sf21 cells, using FuGENE 6 DNA Transfection Reagent (Roche) (section 8.2.4.2). Transfected Sf21 cell cultures were incubated at 27ºC for 48 h and then supernatants were harvested. This constituted the V_0 stock, which was stored at 4ºC protected from light until further use.

8.2.7. Animal experiments

8.2.7.1. Ethics statement

This study was carried out in strict accordance with the recommendations of the Portuguese official Veterinary Directorate (Portaria 1005/92). The Portuguese Experiments on Animal Act strictly comply with the European Directive 2010/63/EU and follow the Federation of European Laboratory Animal Science Associations (FELASA) guidelines on laboratory animal welfare. Animal experiments were approved by the Portuguese official veterinary department for welfare licensing (protocol AEC_2010_017_PS_Rdt_General) and by the Instituto de Medicina Molecular Animal Ethics Committee.

8.2.7.2. Mice infection

Female BALB/c and C57BL/6 mice (Charles Rivers Laboratories International) were delivered to Instituto de Medicina Molecular animal facility at least four days before infections were carried out. 6 to 8-week old mice were inoculated intranasally with 10^4 plaque forming units (PFU) of MuHV-4 or MuHV-4 recombinants. All virus inoculations were performed in 20 µl of phosphate-buffered saline (PBS) under the effect of isofluorane anaesthesia. At different time points after infection, mice were sacrificed by CO_2 inhalation, and lungs or spleens were removed and processed for subsequent analysis.

8.2.8. MuHV-4 virus assays

8.2.8.1. Viral infection of cell cultures

Cells were seeded in tissue culture flasks or plates and grown to semi-confluence for low multiplicity of infection (MOI) or to confluence for high MOI. Cell monolayers were adsorbed with virus suspension in 20% of the final volume of culture medium for 1 h at 37ºC, then covered with the remaining 80% of medium and incubated in a tissue culture incubator at 37ºC with 5% CO_2, for the appropriate time.

For infection with ORF50-deficient recombinant viruses, 3T3-ORF50 cells were seeded in tissue culture flasks or plates and grown to semi-confluence. Cell monolayers were adsorbed with virus suspension in 20% of the final volume of culture medium for 2 h at 37ºC, then covered with the remaining 80% of medium (DMEM complete containing doxycycline at 1 µg/ml of the final volume of culture medium) and incubated in a tissue culture incubator at 37ºC with 5% CO_2, for the appropriate time.

8.2.8.2. Virus working stocks

Virus working stocks were grown by infection of BHK-21 cells at low MOI (0.001 PFU/cell) in 175 cm^2 culture flasks. When approximately 50% cpe was visible (4-5 days), cells and supernatants were transferred to 50 ml tubes and centrifuged at 500 x g for 5 min at 4ºC. Cell-associated virus was resuspended in 2 ml of supernatant, subjected to freeze-thawing, and kept at -80ºC in 200 µl aliquots. Supernatant-associated virus was centrifuged at 15,000 x g for 2 h at 4ºC and pellet was resuspended in 2 ml of fresh complete GMEM medium. 100 µl aliquots were made and stored at -80ºC. Virus titres were determined in duplicates by suspension assay (section 8.2.8.4).

ORF50-deficient recombinant viruses working stocks were grown by infection of 3T3-ORF50 cells at low MOI (0.01 PFU/cell) in 175 cm^2 culture flasks (4 flasks per virus), in the presence of doxycycline (1 µg/ml). When approximately 60% or more cpe was visible (4-5 days), the flasks were frozen at -80ºC, then thawed and centrifuged at 500 x g for 5 min at 4ºC to remove cell debris. The supernatant was then centrifuged at 16,000 x g for 1 h 30 min at 4ºC to pellet the virus, and the pellet was resuspended in 1.5 ml of fresh complete DMEM medium. 100 µl aliquots were made and stored at -80ºC. Virus titres were determined in duplicates by suspension assay (section 8.2.8.4).

8.2.8.3. *In vitro* multi-step growth curves

Low MOI growth curves were performed on confluent cell monolayers in 24-well plates. One day prior to infection, $5x10^4$ BHK-21 cells were plated per well in a 24 well-plate. BHK-21 cells were infected at a MOI of 0.01 PFU/cell, in 200 µl of complete GMEM, and virus was allowed to adsorb for 1 h at 37ºC. Cells were washed in PBS and 1 ml of fresh complete GMEM was added. At each

time point after infection (0, 24, 48, 72, 96 and 120 h), cells and supernatants were harvested, subjected to freeze-thawing and kept at -80ºC. Virus titres were determined in duplicates by suspension assay (section 8.2.8.4).

8.2.8.4. Plaque assay (suspension assay)

Virus stocks, *in vitro* multi-step growth curves and infectious virus in the lung and spleen of infected mice were titrated by plaque assay (or suspension assay). Lungs and spleens were dissected into 15 ml tubes containing 5 ml of complete GMEM. Frozen-thawed lungs were homogenized in a glass homogenizer and frozen at -80ºC. Spleens were processed as described below (section 8.2.8.5) and frozen at -80ºC. Thawed lung homogenates, splenocyte suspensions, virus working stocks and each time point of *in vitro* multi-step growth curves were 10-fold serially diluted in 1 ml of complete GMEM. All dilutions were performed in duplicate. $5x10^5$ BHK-21 cells were added to the serial 10-fold dilutions of virus suspensions in 1 ml of complete GMEM and adsorbed for 1 h at 37ºC with shaking. 3 ml of complete GMEM were added and then the suspension was plated out into 6 cm cell culture dishes. After 4 days of incubation at 37ºC with 5% CO_2 in a humidified incubator, cell monolayers were fixed with 10% formaldehyde in PBS and stained with 0.05% toluidine blue. Viral plaques were counted using a magnifier lenses (Olympus SZ51 zoom stereo microscope) and virus titres were calculated from the number of viral plaques on duplicate dishes.

ORF50-deficient recombinant viruses stocks were 10-fold serially diluted in 1 ml of complete DMEM (in duplicate). $5x10^5$ 3T3-ORF50 cells were added to the serial 10-fold dilutions of virus suspensions in 1 ml of complete DMEM and adsorbed for 2 h at 37ºC with shaking. 3 ml of complete DMEM with doxycycline (1 µg/ml of the final volume of culture medium) were added and then the suspension was plated out into 6 cm cell culture dishes. After 5 days of incubation at 37ºC with 5% CO_2 in a humidified incubator, cell monolayers were fixed with 10% formaldehyde in PBS and stained with 0.05% toluidine blue. Viral plaques were counted using a magnifier lenses (Olympus SZ51 zoom stereo microscope) and virus titres were calculated from the number of viral plaques on duplicate dishes.

8.2.8.5. Infectious centre assay

Spleens were dissected from mice into 5 ml of complete GMEM and kept on ice during the procedure. Single cell suspensions were obtained by mechanical disruption and cell debris was removed by filtering through a 100 µl cell strainer. Cells were pelleted by centrifugation at 300 x g for 5 min at 4ºC. Red blood cells were lysed by incubation with 1 ml of red blood cell lysis (RBL) (154 mM NH_4Cl, 14 mM $NaHCO_3$, 1 mM EDTA pH 7.3) for 5 min on ice. 10 ml of complete GMEM were added, cells were centrifuged at 300 x g for 5 min at 4ºC and resuspended in 5 ml of fresh medium. Cell suspensions were 10-fold serially diluted in 1 ml of complete GMEM (in duplicate) and added to 6 cm cell culture dishes containing $5x10^5$ BHK-21 cells in 4 ml of medium. Assays were incubated for 5 days at 37ºC in a humidified incubator with 5% CO_2. Cell monolayers were

fixed with 10% formaldehyde in PBS and stained with 0.05% toluidine blue. Viral plaques were counted using a magnifier lenses (Olympus SZ51 zoom stereo microscope) and infectious centres were determined from duplicate dishes.

8.2.9. Flow cytometry

8.2.9.1. Staining of splenocytes

Spleens were pooled from 4-5 animals into 5 ml of 2% FBS in PBS (PBS+2%FBS) and kept on ice until mechanical disruption to obtain single splenocyte suspensions. Cell debris was removed by filtering through a 100 µl cell strainer and cells were pelleted by centrifugation at 300 x g for 5 min at 4ºC. Red blood cells were lysed by incubation with RBL for 5 min on ice. Cell suspensions were washed in PBS+2%FBS and centrifuged at 300 x g for 5 min at 4ºC. Blocking was performed by incubation with anti-CD16/32 (clone 2.4G2) (BD Pharmingen) for 3 min at 4ºC. After washing in PBS+2%FBS and centrifugation, splenocytes were stained by incubation for 30 min, at 4ºC, in the dark, with the appropriated antibodies diluted in PBS+2%FBS (Table 8.1). Unbound antibodies were removed by washing with PBS+2%FBS and centrifugation. Cells were resuspended in PBS+2%FBS, filtered through a 40 µl cell strainer and purified by flow cytometry (section 8.2.9.2).

8.2.9.2. Purification of germinal centre (GC) B cell populations

Single cell suspensions of 5 pooled spleens stained with anti-CD19 (clone 1D3) APC-H7 (BD Pharmingen), anti-CD95 (clone Jo2) PE (BD Pharmingen) and anti-GL7 T and B cell activation marker (clone GL7) eFluor660 (eBioscience) were enriched for the germinal centre (GC) B cell population $CD19^{+}CD95^{hi}GL7^{hi}$ using a BD FACSAria Flow Cytometer (BD Biosciences). Cells were recovered into 50% FBS in PBS and kept on ice until further use.

8.2.10. Limiting dilution analysis of infected splenocytes

The frequency of viral genome-positive cells was determined by limiting dilution combined with real-time PCR. Total single cell splenocyte suspensions or flow activated cell sorting (FACS)-purified GC B cells (section 8.2.9.2) were 2-fold serially diluted in PBS+2%FBS and 8 replicates were made per dilution. Cells were lysed by incubation in lysis buffer (10 mM Tris-HCl pH 8.3, 0.45% Tween-20, 0.45% NP-40, 3 mM $MgCl_2$, 50 mM KCl and 0.5 mg/mL Proteinase K) at 37ºC ON. On the next day, Proteinase K was inactivated by incubation at 95ºC for 5 min. Samples were analysed by real-time PCR (section 8.2.10.2) with primer/probe sets specific for *M9* viral gene. For each dilution, the number of negative PCR reactions, corresponding to a failure to obtain an amplification curve during the PCR cycles, was determined.

8.2.10.1. Statistical analysis of limiting dilution assay

Statistical analysis of limiting dilution assay to estimate the frequency of virus DNA$^+$ cells was performed according to the method developed by Dr S. Marques (Marques *et al.*, 2003). The frequency of virus DNA$^+$ cells (*f*) was calculated according to the single-hit Poison Model (SHPM) by maximum likelihood estimation (Bonnefoix *et al.*, 2001). This model assumes that one limiting cell of one cell subset is necessary and sufficient for generating a positive response. To evaluate the fit of the SHPM to our limiting dilution experiments, a method developed by Bonnefoix *et al.*, (2001) was employed. This method consists in modelling the limiting dilution data according to the linear log-log regression model fitting the SHPM ($-log(log(\mu_i)) = log(f) + log(x_i)$), where μ_i is the theoretical fraction of negative wells and x_i is the number of cells plated in each replicate well and checking this model by an appropriate slope test. Being *f* the frequency of virus DNA$^+$ cells, the maximum likelihood of *f* is the value of *f* that maximizes the following function:

$$log(L) = \sum_{i=1}^{k} \left[log\left(\frac{n_i!}{r_i!\,(n_i! - r_i!)}\right) + r_i\, log(P_i) + (n_i - r_i)\, log\left(1 - P_i^k\right) \right]$$

where $log(L)$ is the natural logarithm of the likelihood function *L*, P_i is given by $P_i = exp(-f x_i)$ according to the SHPM. k is the number of groups of replicate PCR reactions, numbered $i = 1,2,3, \ldots, k$; n_i is the number of replicate reactions and r_i is the number of observed negative PCR reactions. The standard error of *f* was calculated as the square root of the negative reciprocal of the second derivate of $log(L)$:

$$SE(f) = \sqrt{\frac{-1}{d^2\, log(L)/df^2}}$$

The 95% confidence interval (CI) of *f* was calculated as $95\%\ CI(f) = f \pm 1.96SE(f)$.

8.2.10.2. Real-time PCR

Real-time PCR was performed on a Rotor Gene 6000 (Corbett Life Science) according to manufacturer's instructions, using the fluorescent Taqman methodology. Primer/probe sets specific for MuHV-4 *M9* gene were used (Table 8.4). Reactions were performed in a final volume of 25 µl, containing 2.5 µl of cell lysate, 200 µM of each primer, 300 µM of probe, 1x Platinum Quantitative PCR SuperMix-UDG (Invitrogen), 5 mM of $MgCl_2$ and 1x Rox reference dye. Samples were subjected to a melting step of 95ºC for 10 min followed by 40 cycles of 15 s at 95ºC and 1 min at 60ºC. Real-time PCR results were analysed on the Rotor Gene 6000 software.

Table 8.4. Primers and probe specific for *M9* gene used to detect MuHV-4 DNA.

Oligonucleotide	Sequence (5'-3')	Genomic coordinates[a]
Upper primer	GCCACGGTGGCCCTCTA	94,176 – 94,192
Lower primer	CAGGCCTCCCTCCCTTTG	94,140 – 94,157
Probe	6-FAM-CTTCTGTTGATCTTCC-MGB[b]	94,159 – 94,174

[a]According to GenBank accession no NC_001826.

[b]Oligonucleotide with fluorophore (6FAM) and quencher (MGB) covalently attached to the 5´- and 3´-ends, respectively.

8.2.11. *In situ* hybridization

8.2.11.1. Generation of digoxigenin (DIG) UTP-labelled riboprobes

Riboprobe used in this study was *in vitro* transcribed from pEH1.4 plasmid using the DIG RNA labelling kit T7/SP6 (Roche), according to manufacturer´s instructions. Briefly, 1 µg of *Hind*III-linearized plasmid was transcribed in a 20 µl reaction containing 2 µl of 10x transcription buffer, 2 µl of 10x NTP labelling mixture, 1 µl of Protector RNase inhibitor and 2 µl of T7 RNA polymerase. After 2 h of incubation at 37ºC, template DNA was removed by addition of 2 µl of DNase and incubation for 15 min at 37ºC. Reaction was stopped by adding 2 ml of 0.2 M EDTA (pH 8.0). RNA was precipitated by addition of 2.5 µl of 4 M LiCl and 75 µl of ice-cold 100% ethanol, and incubation at -80ºC for at least 30 min. RNA was centrifuged at 18,000 x g and 4ºC for 15 min, supernatant was discarded and pellet was washed with 50 µl of ice-cold 70% ethanol. Pellet was resuspended in 100 µl MilliQ water and incubated for 30 min at 37ºC. 20 µl aliquots were made and stored at -80ºC until required. Concentration of labelled RNA was analysed by spot test assay, according to instructions provided in the DIG RNA labelling kit manual (Roche).

8.2.11.2. Preparation of tissue for *in situ* hybridization

Spleens for *in situ* hybridization were dissected from groups of mice and fixed in 10% formalin, ON, at RT. Spleens were then embedded in paraffin in the Histology and Comparative Pathology Laboratory of Instituto de Medicina Molecular. Serial 5 µm sections were cut on a Minot Microtome Leica RM 2145 and mounted on Superfrost Plus slides (Menzel-Glaser).

8.2.11.3. *In situ* hybridization

In situ hybridization was performed as described by Simas *et al.*, 1999. Sections were dewaxed in xylene for 20 min, rehydrated through graded ethanol solutions (100% for 5 min, 90%, 70% and 50% for 2 min each) and finally PBS for 5 min. Sections were then fixed in 0.1% v/v glutaraldehyde in PBS for 30 min at 4ºC, washed twice in PBS for 5 min and then digested with 100 µg/ml of Proteinase K in 20 mM Tris pH 7.5 and 2 mM $CaCl_2$ in dH_2O for 8-10 min at 37ºC. Sections were rinsed in PBS for 2 min at RT, re-fixed in 0.1% v/v glutaraldehyde for 15 min at 4ºC,

rinsed in PBS again for 2 min at RT, then acetylated with fresh 0.25% v/v acetic anhydride in 0.1 M triethanolamine pH 8.0 while being stirred for 10 min at RT. Sections were washed in 2x saline sodium citrate (SSC) (300 mM NaCl and 30 mM tri-sodium-citrate) for 5 min at 4ºC before being dehydrated through graded ethanol (50% to 100%) and left to air dry.

For 100 µl of probe mix, 2 µl of DIG-labelled riboprobe were mixed with 50 µl of formamide, 5 µl of sonicated salmon sperm (10 mg/ml) and 5 µl of tRNA (10 mg/ml). Mix was denatured by heating for 5 min at 80ºC and then quenched for 5 min on ice. 20 µl of 5x hybridization buffer, 1 µl of dithiothreitol (DTT) (100 mM) and 100 U of Protector RNase inhibitor were added with MilliQ water to a final volume of 100 µl. 50 µl of probe mix were added to each section, covered with parafilm and incubated ON at 55ºC in a humidified incubator.

After hybridization, probes were washed in 2x SSC and 10 mM Tris pH 7.5 for 15 min at RT with stirring and then in 0.1x SSC and 10 mM Tris pH 7.5 for additional 15 min. The stringency wash was performed in 30% formamide, 0.1x SSC and 10 mM Tris pH 7.5, for 30 min, at 58ºC. Finally sections were rinsed in 0.1x SSC and 10 mM Tris pH 7.5 for 5 min at RT with stirring. Hybridized probe was detected with alkaline phosphatase (AP)-conjugated anti-DIG antibody (Roche). Sections were rinsed for 5 min, while stirring, in buffer 1 (100 mM Tris pH 7.5 and 150 mM NaCl in dH_2O), then blocked by incubation in blocking buffer (1% Boehringer Blocking Reagent, Roche, in buffer 1) for 30 min at RT. Sections were then dried around the edges and incubated with 120 µl of anti-DIG-AP antibody (1:750 in blocking buffer) for 1 h at RT in a humidified chamber. Unbound antibody was removed by washing twice with buffer 1 for 15 min at RT.

Bound antibody was revealed by colorimetric detection with nitroblue tetrazolium chloride (NBT). Sections were rinsed in buffer 3 (100 mM Tris pH 9.5, 100 mM NaCl and 50 mM $MgCl_2$ in dH_2O) for 10 min at RT. Colour development was performed in the dark by incubation of sections with NBT and X-Phos (Roche) in buffer 3 for at least 2 h. Reaction was stopped by rising in dH_2O. Sections were counterstained with 10% Mayer´s Haemalum, rinsed in tap H_2O and mounted with Aquatex (Merck).

8.2.12. Episome maintenance assays

MEF-1 cells were infected with MuHV-4 ORF50-deficient recombinant viruses at a MOI of 3 PFU per cell in 10-cm dishes at about 80% confluence. Two days after infection, cells were trypsinised, counted and seeded at $2x10^4$ or $2x10^5$ cells in a 10-cm dish. On the next day, fresh DMEM medium containing mycophenolic acid (MPA) (25 µM) and xanthine (25 µM) was added. Resistant clones were picked and, after expansion under continued drug selection, their content in viral genomes was analysed in Gardella gels.

8.2.13. Protein methods

8.2.13.1. Reporter gene assays

For NF-κB reporter gene assays, $2x10^5$ HEK 293T cells were plated per well in 12-well cell culture plates, in 1 ml of complete DMEM. On the next day, cells were transiently transfected with 150 ng of reporter plasmid (pC45) and 1 µg of plasmid encoding mLANA (WT or mutants). A *Renilla* luciferase expression plasmid (20 ng) was used to normalize luciferase activity. Transfections were performed in triplicate. After 48 h in culture, cells were left unstimulated or stimulated with tumour necrosis factor (TNF)-α (50 ng/ml) for 7 h. Cells were washed in PBS and lysed in 200 µl of passive lysis buffer (Promega). Firefly luciferase and *Renilla* luciferase activities were assayed using Dual-Luciferase Reporter Assay System (Promega). Light emission in each sample was quantified in a luminometer. Results are shown as fold induction relative to luciferase activity measured in unstimulated cells. SEM was calculated from triplicates from two independent experiments.

For Myc reporter gene assays, $2x10^5$ HEK 293T cells were plated per well in 12-well plates, in 1 ml of complete DMEM. On the next day, cells were transiently transfected with 500 ng of reporter plasmid (pMyc-TA-Luc) and 1 µg of plasmid encoding mLANA (WT or mutants). A *Renilla* luciferase expression plasmid (20 ng) was used to normalize luciferase activity. Transfections were performed in triplicate. After 48 h in culture, cells were washed in PBS and lysed in 200 µl of passive lysis buffer (Promega). Firefly luciferase and *Renilla* luciferase activities were assayed using Dual-Luciferase Reporter Assay System (Promega). Light emission in each sample was quantified in a luminometer. Results are shown as fold induction relative to luciferase activity measured in cells not expressing mLANA. SEM was calculated from triplicates from two independent experiments.

In all reporter gene assays, representative aliquots of the total cellular lysates were used to detect appropriate expression of mLANA by Western-blot (section 8.2.13.6).

8.2.13.2. Immunoprecipitations

$3x10^6$ HEK 293T cells were plated in 10 cm cell culture dishes, in 10 ml of complete DMEM. On the next day, cells were transiently transfected with expression plasmids encoding ElonginC (2 µg) or Cullin5 (4 µg), and mLANA (WT or mutants) (2 µg). After 48 h in culture, cells were rinsed in ice-cold PBS and disrupted in 500 µl of ice-cold lysis buffer containing 10 mM Tris–HCl (pH 7.5), 150 mM NaCl, 1% Triton X-100, 1 mM NaF, 100 mM Na_3VO_4 and a cocktail of protease inhibitors (cOmplete, Roche). Lysates were harvested by cell scraping, incubated on ice for 10 min and clarified by centrifugation at 18,000 x g for 15 min at 4ºC. Supernatants were harvested into new tubes and 50 µl were removed for analysis of protein expression in total cellular lysates. The remaining volume of supernatant (approximately 450 µl) was incubated with 1 µg of antibodies to ElonginC or Cullin5 for 2 h at 4ºC, with rotation. Immunecomplexes were recovered by incubation with Protein G-Conjugated Sepharose Beads (GE Healthcare) (50 µl of beads:lysis buffer slurry) for

1 h at 4ºC, with rotation. Next, samples were centrifuged at 18,000 x g for 3 min at 4ºC and supernatants were discarded. Beads were washed with 1 ml of ice-cold lysis buffer and harvested by centrifugation at 18,000 x g for 1 min at 4ºC. After three washes, beads were collected by centrifugation at 18,000 x g for 3 min at 4ºC. Proteins were eluted in reducing Laemmli's sample buffer (section 8.2.13.4) by incubation at 100ºC for 10 min, resolved by sodium dodecyl sulfate-polyacrylamide gel electrophoresis (SDS-PAGE) (section 8.2.13.4), transferred to nitrocellulose (section 8.2.13.5), and immunoblotted with the appropriate antibodies (section 8.2.13.6).

8.2.13.3. Poly-ubiquitination assays

Levels of ubiquitinated p65 or Myc were determined by pull-down using Ni-nitrilotriacetic acid (NTA) agarose beads (Qiagen). $3x10^6$ HEK 293T cells were plated in 10 cm dishes, in 10 ml of complete DMEM. On the following day, cells were transiently transfected with expression plasmids encoding p65 (2 µg) or Myc (2 µg), mLANA (WT or mutants) (2 µg), and His_6-ubiquitin (4 µg). After 48 h in culture, cells were rinsed in ice-cold PBS and lysed in 750 µl of ice-cold urea lysis buffer containing 8 M urea, 50 mM Tris-HCl (pH 7.5), 300 mM NaCl, 1% Triton X-100, 10 mM imidazole, 1 mM Na_3VO_4 and a cocktail of protease inhibitors (cOmplete, Roche). Lysates were harvested by cell scraping, incubated on ice for 10 min and clarified by centrifugation at 18,000 x g for 30 min at 4ºC. Cell debris was discarded and 50 µl of supernatant was removed for analysis of protein expression in total cellular lysates. The remaining volume of supernatant was incubated with 50 µl of Ni-NTA beads:lysis buffer slurry for 2 h at 4ºC, with rotation. After incubation, samples were centrifuged at 18,000 x g for 3 min at 4ºC and supernatants were discarded. Beads were washed with 1 ml of ice-cold urea lysis buffer and harvested by centrifugation at 18,000 x g for 1 min at 4ºC. After three washes, beads were collected by centrifugation at 18,000 x g for 3 min at 4ºC. Proteins were eluted in reducing Laemmli's sample buffer (section 8.2.13.4) by incubation at 100ºC for 10 min, resolved by SDS-PAGE (section 8.2.13.4), transferred to nitrocellulose (section 8.2.13.5), and immunoblotted with the appropriate antibodies (section 8.2.13.6).

8.2.13.4. Sodium dodecyl sulfate-polyacrylamide gel electrophoresis (SDS-PAGE)

Protein samples prepared in Laemmli's sample buffer (50 mM Tris-HCl pH 6.8, 10% glycerol, 2% SDS, 5% β-mercaptoethanol, 0.1% bromophenol blue) and heated at 100ºC for 5-10 min were separated through sodium dodecyl sulfate-polyacrylamide gel electrophoresis (SDS-PAGE in 0.75-1.5 mm mini-slab gels of Bio-Rad Miniprotean II Electrophoresis System. Resolving gel was prepared with 8-12% polyacrylamide (acrylamide:bis-acrylamide 37.5:1, Bio-Rad), 375 mM Tris-HCl pH 8.8, 0.1% SDS, 0.1% ammonium persulfate (APS) and 0.04% tetramethylethylenediamine (TEMED). Stacking gel was prepared with 5% polyacrylamide, 125 mM Tris-HCl pH 6.8, 0.1% SDS, 0.1% APS and 0.1% TEMED. Electrophoresis was performed in running buffer (25 mM Tris-base, 192 mM glycine and 0.1% SDS), at 120 V until maximal resolution of protein bands.

8.2.13.5. Transfer of proteins into nitrocellulose membranes

After separation by SDS-PAGE as described above, proteins were transferred to a nitrocellulose membrane (Protran, GE Healthcare) using a Trans-Blot Cell (Bio-Rad), assembled according to manufacturer's instructions. Transfer was performed in standard transfer buffer (25 mM Tris-base, 200 mM glycine and 20% methanol) for 1 h 30 min at constant current of 250 mA. Transferred proteins in the membrane were stained with Ponceau S (Sigma-Aldrich) for 1 min and then the membrane was washed with PBS-Tween (PBS-T) (PBS with 0.05% Tween 20) for 5-10 min with stirring to remove Ponceau S.

8.2.13.6. Western-blot

Following transfer, the membrane was incubated with blocking buffer (5% skimmed milk powder in PBS-T) for 1 h at RT on a rocking platform. The protein of interest was detected by incubating the membrane with the appropriate primary antibody (Table 8.1), diluted in blocking buffer according to manufacturer's instructions, for 1-2 h at RT or ON at 4ºC, on a rocking platform. The membrane was then washed with PBS-T (three washes, each involving 5-10 min incubation on a rocking platform at RT) to remove unbound primary antibody. Protein-primary antibody interactions were detected by incubation of the membrane with a HRP-conjugated secondary antibody specific for the species where primary antibody was produced (Table 8.1 and section 8.1.2.2), diluted 1:5000 in blocking buffer, for 30 min-1 h at RT on a rocking platform. The membrane was then washed as described above, and the protein bands were visualized by chemiluminescence using the SuperSignal West Pico Chemiluminescent Substrate (Thermo Scientific), according to the manufacturer's recommendations. Light signal was detected on an autoradiography film (Fujifilm) exposed for the appropriate time and revealed using Curix 60 (Agfa).

8.2.14. mLANA expression in insect cells using baculovirus (feasibility study)

The feasibility study of mLANA expression in insect cells using baculovirus MultiBac system (Berger *et al.*, 2004; Bieniossek *et al.*, 2008; Trowitzsch *et al.*, 2010; Vijayachandran *et al.*, 2011) was performed by me at Eukaryotic Expression Facility at EMBL Grenoble, under the supervision of Dr I. Berger, Frederic Garzoni and Alice Aubert.

8.2.14.1. Processing of samples for SDS-PAGE and YFP fluorescence measurement

Samples were sonicated for 2-5 sec at medium setting and 50 µl of sonicated sample were removed for whole cell extract (WCE) analysis. The remaining sample was centrifuged for 3 min at 18,000 x g and 4ºC, and 50 µl of supernatant were removed for soluble lysate (SL) analysis. The remaining supernatant (approximately 400 µl) was used for YFP fluorescence measurement, using a fluorescence spectrophotometer. WCE and SL samples were boiled in Laemmli's sample buffer

at 95ºC for 10 min. Samples were then resolved by SDS-PAGE (section 8.2.13.4) and either stained with Coomassie Blue (section 8.2.14.2) or transferred to nitrocellulose (section 8.2.13.5) and immunoblotted (section 8.2.13.6) with anti-mLANA antibody to detect expression of GST-His-mLANA and His-mLANA.

8.2.14.2. Coomassie Blue staining

To visualize proteins directly in polyacrylamide gels, gels were covered with a Coomassie Blue solution (0.1% Coomassie brilliant blue R-250, 40% methanol and 10% acetic acid) for 30 min to 3 h at RT, with stirring. Staining solution was removed and gels were rinsed in destaining solution (30% methanol, 10% acetic acid) for 10-15 min at RT, with stirring, until excess stain was removed. Destaining solution was changed and left at RT, with stirring, until proper level of destaining was achieved.

8.2.14.3. Baculovirus amplification and small-scale protein expression

To amplify baculovirus stocks expressing GST-His-mLANA and His-mLANA, 3 ml of V_0 stock were added to flasks containing 25 ml of Sf21 cells at $0.5x10^6$ cells/ml. Infected suspension cultures were maintained at 27ºC with shaking at 90 rpm and cells were counted every 24 h using a hemocytometer. If cell density was lower than $1x10^6$ cells/ml, cell culture was not diluted; if cell density was higher than $1x10^6$ cells/ml, cell culture was diluted at $0.5\text{-}1x10^6$ cells/ml in fresh HyClone medium, filling cell culture flasks with no more than 10% of the total volume of the flask to allow sufficient aeration for optimal cell growth. One day after cell proliferation arrest occurred, $1x10^6$ cells were harvested and centrifuged for 2 min at 18,000 x g and 4ºC. Supernatant was discarded and cell pellet was resuspended in 500 µl of PBS by pipetting up and down. Samples were processed for YFP fluorescence measurement as described in section 8.2.14.1. 48 h after proliferation arrest, cell culture was centrifuged at 120 x g for 3 min at 27ºC and supernatant was harvested, constituting the V_1 amplified virus stock. V_1 stock was stored at 4ºC protected from light and cell pellet was gently resuspended in 50 ml of fresh medium. Cells were kept in culture at 27ºC with shaking at 90 rpm and $1x10^6$ cells were sampled every 24 h until YFP fluorescence reached a plateau (typically after 3-4 days). At that point, cell culture was centrifuged at 120 x g for 3 min, supernatant was discarded and cell pellet was stored at -20ºC. mLANA expression was then analysed by SDS-PAGE, followed by Coomassie Blue staining and Western-blot (section 8.2.14.1). A schematic diagram of this small-scale protein expression protocol is shown in Figure 6.2.

CHAPTER 9

References

References

Achenbach, C.J., Cole, S.R., Kitahata, M.M., Casper, C., Willig, J.H., Mugavero, M.J., and Saag, M.S. (2011). Mortality after cancer diagnosis in HIV-infected individuals treated with antiretroviral therapy. AIDS 25, 691-700.

Adler, H., Messerle, M., and Koszinowski, U.H. (2001). Virus reconstituted from infectious bacterial artificial chromosome (BAC)-cloned murine gammaherpesvirus 68 acquires wild-type properties in vivo only after excision of BAC vector sequences. J. Virol. 75, 5692-5696.

Adler, H., Messerle, M., and Koszinowski, U.H. (2003). Cloning of herpesviral genomes as bacterial artificial chromosomes. Rev. Med. Virol. 13, 111-121.

Adler, H., Messerle, M., Wagner, M., and Koszinowski, U.H. (2000). Cloning and mutagenesis of the murine gammaherpesvirus 68 genome as an infectious bacterial artificial chromosome. J. Virol. 74, 6964-6974.

Akerstrom, B., Brodin, T., Reis, K., and Bjorck, L. (1985). Protein G: a powerful tool for binding and detection of monoclonal and polyclonal antibodies. J. Immunol. 135, 2589-2592.

Aloy, P., and Russell, R.B. (2006). Structural systems biology: modelling protein interactions. Nat. Rev. Mol. Cell Biol. 7, 188-197.

Ambroziak, J.A., Blackbourn, D.J., Herndier, B.G., Glogau, R.G., Gullett, J.H., McDonald, A.R., Lennette, E.T., and Levy, J.A. (1995). Herpes-like sequences in HIV-infected and uninfected Kaposi's sarcoma patients. Science 268, 582-583.

An, F.Q., Compitello, N., Horwitz, E., Sramkoski, M., Knudsen, E.S., and Renne, R. (2005). The latency-associated nuclear antigen of Kaposi's sarcoma-associated herpesvirus modulates cellular gene expression and protects lymphoid cells from p16 INK4A-induced cell cycle arrest. J. Biol. Chem. 280, 3862-3874.

An, J., Sun, Y., and Rettig, M.B. (2004). Transcriptional coactivation of c-Jun by the KSHV-encoded LANA. Blood 103, 222-228.

Anrather, J., Csizmadia, V., Soares, M.P., and Winkler, H. (1999). Regulation of NF-kappaB RelA phosphorylation and transcriptional activity by p21(ras) and protein kinase Czeta in primary endothelial cells. J. Biol. Chem. 274, 13594-13603.

Babcock, G.J., Decker, L.L., Volk, M., and Thorley-Lawson, D.A. (1998). EBV persistence in memory B cells in vivo. Immunity 9, 395-404.

Babcock, G.J., Hochberg, D., and Thorley-Lawson, A.D. (2000). The expression pattern of Epstein-Barr virus latent genes in vivo is dependent upon the differentiation stage of the infected B cell. Immunity 13, 497-506.

Ballestas, M.E., Chatis, P.A., and Kaye, K.M. (1999). Efficient persistence of extrachromosomal KSHV DNA mediated by latency-associated nuclear antigen. Science 284, 641-644.

Ballestas, M.E., and Kaye, K.M. (2001). Kaposi's sarcoma-associated herpesvirus latency-associated nuclear antigen 1 mediates episome persistence through cis-acting terminal repeat (TR) sequence and specifically binds TR DNA. J. Virol. 75, 3250-3258.

Ballestas, M.E., and Kaye, K.M. (2011). The latency-associated nuclear antigen, a multifunctional protein central to Kaposi's sarcoma-associated herpesvirus latency. Future Microbiol. 6, 1399-1413.

Ballon, G., Chen, K., Perez, R., Tam, W., and Cesarman, E. (2011). Kaposi sarcoma herpesvirus (KSHV) vFLIP oncoprotein induces B cell transdifferentiation and tumorigenesis in mice. J. Clin. Invest. 121, 1141-1153.

Barbera, A.J., Chodaparambil, J.V., Kelley-Clarke, B., Joukov, V., Walter, J.C., Luger, K., and Kaye, K.M. (2006). The nucleosomal surface as a docking station for Kaposi's sarcoma herpesvirus LANA. Science 311, 856-861.

Barton, E., Mandal, P., and Speck, S.H. (2011). Pathogenesis and host control of gammaherpesviruses: lessons from the mouse. Annu. Rev. Immunol. 29, 351-397.

Basso, K., and Dalla-Favera, R. (2015). Germinal centres and B cell lymphomagenesis. Nat. Rev. Immunol. 15, 172-184.

Basso, K., Klein, U., Niu, H., Stolovitzky, G.A., Tu, Y., Califano, A., Cattoretti, G., and Dalla-Favera, R. (2004). Tracking CD40 signaling during germinal center development. Blood 104, 4088-4096.

Bastien, N., and McBride, A.A. (2000). Interaction of the papillomavirus E2 protein with mitotic chromosomes. Virology 270, 124-134.

Bennett, N.J., May, J.S., and Stevenson, P.G. (2005). Gamma-herpesvirus latency requires T cell evasion during episome maintenance. PLoS Biol. 3, e120.

Berger, I., Fitzgerald, D.J., and Richmond, T.J. (2004). Baculovirus expression system for heterologous multiprotein complexes. Nat. Biotechnol. 22, 1583-1587.

Berndsen, C.E., and Wolberger, C. (2014). New insights into ubiquitin E3 ligase mechanism. Nat. Struct. Mol. Biol. 21, 301-307.

Bieniossek, C., Imasaki, T., Takagi, Y., and Berger, I. (2012). MultiBac: expanding the research toolbox for multiprotein complexes. Trends Biochem. Sci. 37, 49-57.

Bieniossek, C., Richmond, T.J., and Berger, I. (2008). MultiBac: multigene baculovirus-based eukaryotic protein complex production. Curr. Protoc. Protein Sci. Chapter 5, Unit 5 20.

Blackman, M.A., Flano, E., Usherwood, E., and Woodland, D.L. (2000). Murine gamma-herpesvirus-68: a mouse model for infectious mononucleosis? Mol. Med. Today 6, 488-490.

Blasdell, K., McCracken, C., Morris, A., Nash, A.A., Begon, M., Bennett, M., and Stewart, J.P. (2003). The wood mouse is a natural host for Murid herpesvirus 4. J. Gen. Virol. 84, 111-113.

Blasig, C., Zietz, C., Haar, B., Neipel, F., Esser, S., Brockmeyer, N.H., Tschachler, E., Colombini, S., Ensoli, B., and Sturzl, M. (1997). Monocytes in Kaposi's sarcoma lesions are productively infected by human herpesvirus 8. J. Virol. 71, 7963-7968.

Blaskovic, D., Stancekova, M., Svobodova, J., and Mistrikova, J. (1980). Isolation of five strains of herpesviruses from two species of free living small rodents. Acta Virol. 24, 468.

Bochkarev, A., Barwell, J.A., Pfuetzner, R.A., Bochkareva, E., Frappier, L., and Edwards, A.M. (1996). Crystal structure of the DNA-binding domain of the Epstein-Barr virus origin-binding protein, EBNA1, bound to DNA. Cell 84, 791-800.

Bochkarev, A., Barwell, J.A., Pfuetzner, R.A., Furey, W., Jr., Edwards, A.M., and Frappier, L. (1995). Crystal structure of the DNA-binding domain of the Epstein-Barr virus origin-binding protein EBNA 1. Cell 83, 39-46.

Bonnefoix, T., Bonnefoix, P., Callanan, M., Verdiel, P., and Sotto, J.J. (2001). Graphical representation of a generalized linear model-based statistical test estimating the fit of the single-hit Poisson model to limiting dilution assays. J. Immunol. 167, 5725-5730.

Borza, C.M., and Hutt-Fletcher, L.M. (2002). Alternate replication in B cells and epithelial cells switches tropism of Epstein-Barr virus. Na.t Med. 8, 594-599.

Bowden, R.J., Simas, J.P., Davis, A.J., and Efstathiou, S. (1997). Murine gammaherpesvirus 68 encodes tRNA-like sequences which are expressed during latency. J. Gen. Virol. 78 (Pt 7), 1675-1687.

Brooks, J.W., Hamilton-Easton, A.M., Christensen, J.P., Cardin, R.D., Hardy, C.L., and Doherty, P.C. (1999). Requirement for CD40 ligand, CD4(+) T cells, and B cells in an infectious mononucleosis-like syndrome. J. Virol. 73, 9650-9654.

Brostjan, C., Anrather, J., Csizmadia, V., Natarajan, G., and Winkler, H. (1997). Glucocorticoids inhibit E-selectin expression by targeting NF-kappaB and not ATF/c-Jun. J. Immunol. 158, 3836-3844.

Bubman, D., Guasparri, I., and Cesarman, E. (2007). Deregulation of c-Myc in primary effusion lymphoma by Kaposi's sarcoma herpesvirus latency-associated nuclear antigen. Oncogene 26, 4979-4986.

Cai, Q., Murakami, M., Si, H., and Robertson, E.S. (2007). A potential alpha-helix motif in the amino terminus of LANA encoded by Kaposi's sarcoma-associated herpesvirus is critical for nuclear accumulation of HIF-1alpha in normoxia. J. Virol. 81, 10413-10423.

Cai, Q., Verma, S.C., Lu, J., and Robertson, E.S. (2010). Molecular biology of Kaposi's sarcoma-associated herpesvirus and related oncogenesis. Adv. Virus Res. 78, 87-142.

Cai, Q.L., Knight, J.S., Verma, S.C., Zald, P., and Robertson, E.S. (2006). EC5S ubiquitin complex is recruited by KSHV latent antigen LANA for degradation of the VHL and p53 tumor suppressors. PLoS Pathog. 2, e116.

Cai, X., Lu, S., Zhang, Z., Gonzalez, C.M., Damania, B., and Cullen, B.R. (2005). Kaposi's sarcoma-associated herpesvirus expresses an array of viral microRNAs in latently infected cells. Proc. Natl. Acad. Sci. U. S. A. 102, 5570-5575.

Calado, D.P., Sasaki, Y., Godinho, S.A., Pellerin, A., Kochert, K., Sleckman, B.P., de Alboran, I.M., Janz, M., Rodig, S., and Rajewsky, K. (2012). The cell-cycle regulator c-Myc is essential for the formation and maintenance of germinal centers. Nat. Immunol. 13, 1092-1100.

Caldwell, R.G., Wilson, J.B., Anderson, S.J., and Longnecker, R. (1998). Epstein-Barr virus LMP2A drives B cell development and survival in the absence of normal B cell receptor signals. Immunity 9, 405-411.

Cardin, R.D., Brooks, J.W., Sarawar, S.R., and Doherty, P.C. (1996). Progressive loss of CD8+ T cell-mediated control of a gamma-herpesvirus in the absence of CD4+ T cells. J. Exp. Med. 184, 863-871.

Casola, S., Otipoby, K.L., Alimzhanov, M., Humme, S., Uyttersprot, N., Kutok, J.L., Carroll, M.C., and Rajewsky, K. (2004). B cell receptor signal strength determines B cell fate. Nat. Immunol. 5, 317-327.

Cesarman, E. (2014). Gammaherpesviruses and lymphoproliferative disorders. Annu. Rev. Pathol. 9, 349-372.

Cesarman, E., Chang, Y., Moore, P.S., Said, J.W., and Knowles, D.M. (1995). Kaposi's sarcoma-associated herpesvirus-like DNA sequences in AIDS-related body-cavity-based lymphomas. N. Engl. J. Med. 332, 1186-1191.

Chadburn, A., Hyjek, E.M., Tam, W., Liu, Y., Rengifo, T., Cesarman, E., and Knowles, D.M. (2008). Immunophenotypic analysis of the Kaposi sarcoma herpesvirus (KSHV; HHV-8)-infected B cells in HIV+ multicentric Castleman disease (MCD). Histopathology 53, 513-524.

Chandriani, S., and Ganem, D. (2010). Array-based transcript profiling and limiting-dilution reverse transcription-PCR analysis identify additional latent genes in Kaposi's sarcoma-associated herpesvirus. J. Virol. 84, 5565-5573.

Chang, Y., Cesarman, E., Pessin, M.S., Lee, F., Culpepper, J., Knowles, D.M., and Moore, P.S. (1994). Identification of herpesvirus-like DNA sequences in AIDS-associated Kaposi's sarcoma. Science 266, 1865-1869.

Collins, C.M., Boss, J.M., and Speck, S.H. (2009). Identification of infected B-cell populations by using a recombinant murine gammaherpesvirus 68 expressing a fluorescent protein. .J Virol. 83, 6484-6493.

Collins, C.M., and Speck, S.H. (2014). Expansion of murine gammaherpesvirus latently infected B cells requires T follicular help. PLoS Pathog. 10, e1004106.

Correia, B., Cerqueira, S.A., Beauchemin, C., Pires de Miranda, M., Li, S., Ponnusamy, R., Rodrigues, L., Schneider, T.R., Carrondo, M.A., Kaye, K.M.*, et al.* (2013). Crystal structure of the gamma-2 herpesvirus LANA DNA binding domain identifies charged surface residues which impact viral latency. PLoS Pathog. 9, e1003673.

Cruickshank, J., Shire, K., Davidson, A.R., Edwards, A.M., and Frappier, L. (2000). Two domains of the epstein-barr virus origin DNA-binding protein, EBNA1, orchestrate sequence-specific DNA binding. J. Biol. Chem. 275, 22273-22277.

Damania, B. (2004). Oncogenic gamma-herpesviruses: comparison of viral proteins involved in tumorigenesis. Nat. Rev. Microbiol. 2, 656-668.

Davison, A.J. (2002). Evolution of the herpesviruses. Vet. Microbiol. 86, 69-88.

Davison, A.J., Eberle, R., Ehlers, B., Hayward, G.S., McGeoch, D.J., Minson, A.C., Pellett, P.E., Roizman, B., Studdert, M.J., and Thiry, E. (2009). The order Herpesvirales. Arch. Virol. 154, 171-177.

De Leon Vazquez, E., and Kaye, K.M. (2011). The internal Kaposi's sarcoma-associated herpesvirus LANA regions exert a critical role on episome persistence. J. Virol. 85, 7622-7633.

De Silva, N.S., and Klein, U. (2015). Dynamics of B cells in germinal centres. Nat. Rev. Immunol. 15, 137-148.

Decalf, J., Godinho-Silva, C., Fontinha, D., Marques, S., and Simas, J.P. (2014). Establishment of murine gammaherpesvirus latency in B cells is not a stochastic event. PLoS Pathog. 10, e1004269.

Delgado-Eckert, E., and Shapiro, M. (2011). A model of host response to a multi-stage pathogen. J. Math. Biol. 63, 201-227.

Dell, G., Wilkinson, K.W., Tranter, R., Parish, J., Leo Brady, R., and Gaston, K. (2003). Comparison of the structure and DNA-binding properties of the E2 proteins from an oncogenic and a non-oncogenic human papillomavirus. J. Mol. Biol. 334, 979-991.

Dittmer, D., Lagunoff, M., Renne, R., Staskus, K., Haase, A., and Ganem, D. (1998). A cluster of latently expressed genes in Kaposi's sarcoma-associated herpesvirus. J. Virol. 72, 8309-8315.

Dittmer, D.P., and Damania, B. (2013). Kaposi sarcoma associated herpesvirus pathogenesis (KSHV)--an update. Curr. Opin. Virol. 3, 238-244.

Doherty, P.C., Tripp, R.A., Hamilton-Easton, A.M., Cardin, R.D., Woodland, D.L., and Blackman, M.A. (1997). Tuning into immunological dissonance: an experimental model for infectious mononucleosis. Curr. Opin. Immunol. 9, 477-483.

Dominguez-Sola, D., Victora, G.D., Ying, C.Y., Phan, R.T., Saito, M., Nussenzweig, M.C., and Dalla-Favera, R. (2012). The proto-oncogene MYC is required for selection in the germinal center and cyclic reentry. Nat. Immunol. 13, 1083-1091.

Domsic, J.F., Chen, H.S., Lu, F., Marmorstein, R., and Lieberman, P.M. (2013). Molecular basis for oligomeric-DNA binding and episome maintenance by KSHV LANA. PLoS Pathog. 9, e1003672.

Dupin, N., Fisher, C., Kellam, P., Ariad, S., Tulliez, M., Franck, N., van Marck, E., Salmon, D., Gorin, I., Escande, J.P*., et al.* (1999). Distribution of human herpesvirus-8 latently infected cells in Kaposi's sarcoma, multicentric Castleman's disease, and primary effusion lymphoma. Proc. Natl. Acad. Sci. U. S. A. 96, 4546-4551.

Dutia, B.M., Stewart, J.P., Clayton, R.A., Dyson, H., and Nash, A.A. (1999). Kinetic and phenotypic changes in murine lymphocytes infected with murine gammaherpesvirus-68 in vitro. J. Gen. Virol. 80 (Pt 10), 2729-2736.

Edelman, D.C. (2005). Human herpesvirus 8--a novel human pathogen. Virol. J. 2, 78.

Efstathiou, S., Ho, Y.M., and Minson, A.C. (1990). Cloning and molecular characterization of the murine herpesvirus 68 genome. J. Gen. Virol. 71 (Pt 6), 1355-1364.

Ehtisham, S., Sunil-Chandra, N.P., and Nash, A.A. (1993). Pathogenesis of murine gammaherpesvirus infection in mice deficient in CD4 and CD8 T cells. J. Virol. 67, 5247-5252.

Epstein, M.A., Achong, B.G., and Barr, Y.M. (1964). Virus Particles in Cultured Lymphoblasts from Burkitt's Lymphoma. Lancet 1, 702-703.

Fakhari, F.D., Jeong, J.H., Kanan, Y., and Dittmer, D.P. (2006). The latency-associated nuclear antigen of Kaposi sarcoma-associated herpesvirus induces B cell hyperplasia and lymphoma. J. Clin. Invest. 116, 735-742.

Feldman, E.R., Kara, M., Coleman, C.B., Grau, K.R., Oko, L.M., Krueger, B.J., Renne, R., van Dyk, L.F., and Tibbetts, S.A. (2014). Virus-encoded microRNAs facilitate gammaherpesvirus latency and pathogenesis in vivo. MBio 5, e00981-00914.

Flano, E., Husain, S.M., Sample, J.T., Woodland, D.L., and Blackman, M.A. (2000). Latent murine gamma-herpesvirus infection is established in activated B cells, dendritic cells, and macrophages. J. Immunol. 165, 1074-1081.

Flano, E., Jia, Q., Moore, J., Woodland, D.L., Sun, R., and Blackman, M.A. (2005). Early establishment of gamma-herpesvirus latency: implications for immune control. J. Immunol. 174, 4972-4978.

Flano, E., Kim, I.J., Moore, J., Woodland, D.L., and Blackman, M.A. (2003). Differential gamma-herpesvirus distribution in distinct anatomical locations and cell subsets during persistent infection in mice. J. Immunol. 170, 3828-3834.

Flano, E., Kim, I.J., Woodland, D.L., and Blackman, M.A. (2002). Gamma-herpesvirus latency is preferentially maintained in splenic germinal center and memory B cells. J. Exp. Med. 196, 1363-1372.

Fontinha, D., Lopes, F.B., Marques, S., and Simas, J.P. (2015). Murid Gammaherpesvirus Latency-Associated Protein M2 Promotes the Formation of Conjugates between Transformed B Lymphoma Cells and T Helper Cells. PLoS One 10, e0142540.

Forrest, J.C., Paden, C.R., Allen, R.D., 3rd, Collins, J., and Speck, S.H. (2007). ORF73-null murine gammaherpesvirus 68 reveals roles for mLANA and p53 in virus replication. J. Virol. 81, 11957-11971.

Fowler, P., Marques, S., Simas, J.P., and Efstathiou, S. (2003). ORF73 of murine herpesvirus-68 is critical for the establishment and maintenance of latency. J. Gen. Virol. 84, 3405-3416.

Francois, S., Vidick, S., Sarlet, M., Desmecht, D., Drion, P., Stevenson, P.G., Vanderplasschen, A., and Gillet, L. (2013). Illumination of murine gammaherpesvirus-68 cycle reveals a sexual transmission route from females to males in laboratory mice. PLoS Pathog. 9, e1003292.

Franklin, T.J., and Cook, J.M. (1969). The inhibition of nucleic acid synthesis by mycophenolic acid. Biochem. J. 113, 515-524.

Frederico, B., Chao, B., May, J.S., Belz, G.T., and Stevenson, P.G. (2014a). A murid gamma-herpesviruses exploits normal splenic immune communication routes for systemic spread. Cell Host Microbe 15, 457-470.

Frederico, B., May, J.S., Efstathiou, S., and Stevenson, P.G. (2014b). BAFF receptor deficiency limits gammaherpesvirus infection. J. Virol. 88, 3965-3975.

Frederico, B., Milho, R., May, J.S., Gillet, L., and Stevenson, P.G. (2012). Myeloid infection links epithelial and B cell tropisms of Murid Herpesvirus-4. PLoS Pathog. 8, e1002935.

Friborg, J., Jr., Kong, W., Hottiger, M.O., and Nabel, G.J. (1999). p53 inhibition by the LANA protein of KSHV protects against cell death. Nature 402, 889-894.

Fujimuro, M., and Hayward, S.D. (2003). The latency-associated nuclear antigen of Kaposi's sarcoma-associated herpesvirus manipulates the activity of glycogen synthase kinase-3beta. J. Virol. 77, 8019-8030.

Fujimuro, M., Wu, F.Y., ApRhys, C., Kajumbula, H., Young, D.B., Hayward, G.S., and Hayward, S.D. (2003). A novel viral mechanism for dysregulation of beta-catenin in Kaposi's sarcoma-associated herpesvirus latency. Nat. Med. 9, 300-306.

Gao, S.J., Kingsley, L., Li, M., Zheng, W., Parravicini, C., Ziegler, J., Newton, R., Rinaldo, C.R., Saah, A., Phair, J.*, et al.* (1996). KSHV antibodies among Americans, Italians and Ugandans with and without Kaposi's sarcoma. Nat. Med. 2, 925-928.

Garber, A.C., Hu, J., and Renne, R. (2002). Latency-associated nuclear antigen (LANA) cooperatively binds to two sites within the terminal repeat, and both sites contribute to the ability of LANA to suppress transcription and to facilitate DNA replication. J. Biol. Chem. 277, 27401-27411.

Gardella, T., Medveczky, P., Sairenji, T., and Mulder, C. (1984). Detection of circular and linear herpesvirus DNA molecules in mammalian cells by gel electrophoresis. J. Virol. 50, 248-254.

Gaspar, M., May, J.S., Sukla, S., Frederico, B., Gill, M.B., Smith, C.M., Belz, G.T., and Stevenson, P.G. (2011). Murid herpesvirus-4 exploits dendritic cells to infect B cells. PLoS Pathog. 7, e1002346.

Giffin, L., and Damania, B. (2014). KSHV: pathways to tumorigenesis and persistent infection. Adv. Virus Res. 88, 111-159.

Gires, O., Zimber-Strobl, U., Gonnella, R., Ueffing, M., Marschall, G., Zeidler, R., Pich, D., and Hammerschmidt, W. (1997). Latent membrane protein 1 of Epstein-Barr virus mimics a constitutively active receptor molecule. EMBO J. 16, 6131-6140.

Godinho-Silva, C., Marques, S., Fontinha, D., Veiga-Fernandes, H., Stevenson, P.G., and Simas, J.P. (2014). Defining immune engagement thresholds for in vivo control of virus-driven lymphoproliferation. PLoS Pathog. 10, e1004220.

Gramolelli, S., and Schulz, T.F. (2015). The role of Kaposi sarcoma-associated herpesvirus in the pathogenesis of Kaposi sarcoma. J. Pathol. 235, 368-380.

Grundhoff, A., and Ganem, D. (2003). The latency-associated nuclear antigen of Kaposi's sarcoma-associated herpesvirus permits replication of terminal repeat-containing plasmids. J. Virol. 77, 2779-2783.

Habison, A.C., Beauchemin, C., Simas, J.P., Usherwood, E.J., and Kaye, K.M. (2012). Murine gammaherpesvirus 68 LANA acts on terminal repeat DNA to mediate episome persistence. J. Virol. 86, 11863-11876.

Hadinoto, V., Shapiro, M., Sun, C.C., and Thorley-Lawson, D.A. (2009). The dynamics of EBV shedding implicate a central role for epithelial cells in amplifying viral output. PLoS Pathog. 5, e1000496.

Han, S.J., Hu, J., Pierce, B., Weng, Z., and Renne, R. (2010). Mutational analysis of the latency-associated nuclear antigen DNA-binding domain of Kaposi's sarcoma-associated herpesvirus reveals structural conservation among gammaherpesvirus origin-binding proteins. J. Gen. Virol. 91, 2203-2215.

Hassman, L.M., Ellison, T.J., and Kedes, D.H. (2011). KSHV infects a subset of human tonsillar B cells, driving proliferation and plasmablast differentiation. J. Clin. Invest. 121, 752-768.

Hawkins, J.B., Delgado-Eckert, E., Thorley-Lawson, D.A., and Shapiro, M. (2013). The cycle of EBV infection explains persistence, the sizes of the infected cell populations and which come under CTL regulation. PLoS Pathog. 9, e1003685.

He, B., Raab-Traub, N., Casali, P., and Cerutti, A. (2003). EBV-encoded latent membrane protein 1 cooperates with BAFF/BLyS and APRIL to induce T cell-independent Ig heavy chain class switching. J. Immunol. 171, 5215-5224.

Hegde, R.S., Grossman, S.R., Laimins, L.A., and Sigler, P.B. (1992). Crystal structure at 1.7 A of the bovine papillomavirus-1 E2 DNA-binding domain bound to its DNA target. Nature 359, 505-512.

Heise, N., De Silva, N.S., Silva, K., Carette, A., Simonetti, G., Pasparakis, M., and Klein, U. (2014). Germinal center B cell maintenance and differentiation are controlled by distinct NF-kappaB transcription factor subunits. J. Exp. Med. 211, 2103-2118.

Hellert, J., Weidner-Glunde, M., Krausze, J., Lunsdorf, H., Ritter, C., Schulz, T.F., and Luhrs, T. (2015). The 3D structure of Kaposi sarcoma herpesvirus LANA C-terminal domain bound to DNA. Proc. Natl. Acad. Sci. U. S. A. 112, 6694-6699.

Hellert, J., Weidner-Glunde, M., Krausze, J., Richter, U., Adler, H., Fedorov, R., Pietrek, M., Ruckert, J., Ritter, C., Schulz, T.F.*, et al.* (2013). A structural basis for BRD2/4-mediated host chromatin interaction and oligomer assembly of Kaposi sarcoma-associated herpesvirus and murine gammaherpesvirus LANA proteins. PLoS Pathog. 9, e1003640.

Henle, G., Henle, W., and Diehl, V. (1968). Relation of Burkitt's tumor-associated herpes-ytpe virus to infectious mononucleosis. Proc. Natl. Acad. Sci. U. S. A. 59, 94-101.

Herskowitz, J.H., Siegel, A.M., Jacoby, M.A., and Speck, S.H. (2008). Systematic mutagenesis of the murine gammaherpesvirus 68 M2 protein identifies domains important for chronic infection. J. Virol. 82, 3295-3310.

Hislop, A.D., Taylor, G.S., Sauce, D., and Rickinson, A.B. (2007). Cellular responses to viral infection in humans: lessons from Epstein-Barr virus. Annu. Rev. Immunol. 25, 587-617.

Hochberg, D., Middeldorp, J.M., Catalina, M., Sullivan, J.L., Luzuriaga, K., and Thorley-Lawson, D.A. (2004). Demonstration of the Burkitt's lymphoma Epstein-Barr virus phenotype in dividing latently infected memory cells in vivo. Proc. Natl. Acad. Sci. U. S. A. 101, 239-244.

Hsieh, D.J., Camiolo, S.M., and Yates, J.L. (1993). Constitutive binding of EBNA1 protein to the Epstein-Barr virus replication origin, oriP, with distortion of DNA structure during latent infection. EMBO J. 12, 4933-4944.

Hu, J., and Renne, R. (2005). Characterization of the minimal replicator of Kaposi's sarcoma-associated herpesvirus latent origin. J. Virol. 79, 2637-2642.

Hu, J., Yang, Y., Turner, P.C., Jain, V., McIntyre, L.M., and Renne, R. (2014). LANA binds to multiple active viral and cellular promoters and associates with the H3K4methyltransferase hSET1 complex. PLoS Pathog. 10, e1004240.

Husain, S.M., Usherwood, E.J., Dyson, H., Coleclough, C., Coppola, M.A., Woodland, D.L., Blackman, M.A., Stewart, J.P., and Sample, J.T. (1999). Murine gammaherpesvirus M2 gene is latency-associated and its protein a target for CD8(+) T lymphocytes. Proc. Natl. Acad. Sci. U. S. A. 96, 7508-7513.

Ilves, I., Kivi, S., and Ustav, M. (1999). Long-term episomal maintenance of bovine papillomavirus type 1 plasmids is determined by attachment to host chromosomes, which Is mediated by the viral E2 protein and its binding sites. J. Virol. 73, 4404-4412.

Inoue, H., Nojima, H., and Okayama, H. (1990). High efficiency transformation of Escherichia coli with plasmids. Gene 96, 23-28.

Jeong, J.H., Orvis, J., Kim, J.W., McMurtrey, C.P., Renne, R., and Dittmer, D.P. (2004). Regulation and autoregulation of the promoter for the latency-associated nuclear antigen of Kaposi's sarcoma-associated herpesvirus. J. Biol. Chem. 279, 16822-16831.

Joseph, A.M., Babcock, G.J., and Thorley-Lawson, D.A. (2000). EBV persistence involves strict selection of latently infected B cells. J. Immunol. 165, 2975-2981.

Kang, M.S., and Kieff, E. (2015). Epstein-Barr virus latent genes. Exp. Mol. Med. 47, e131.

Katano, H., Sato, Y., and Sata, T. (2001). Expression of p53 and human herpesvirus-8 (HHV-8)-encoded latency-associated nuclear antigen with inhibition of apoptosis in HHV-8-associated malignancies. Cancer 92, 3076-3084.

Kaul, R., Verma, S.C., and Robertson, E.S. (2007). Protein complexes associated with the Kaposi's sarcoma-associated herpesvirus-encoded LANA. Virology 364, 317-329.

Kedes, D.H., Operskalski, E., Busch, M., Kohn, R., Flood, J., and Ganem, D. (1996). The seroepidemiology of human herpesvirus 8 (Kaposi's sarcoma-associated herpesvirus): distribution of infection in KS risk groups and evidence for sexual transmission. Nat. Med. 2, 918-924.

Kelley-Clarke, B., Ballestas, M.E., Komatsu, T., and Kaye, K.M. (2007a). Kaposi's sarcoma herpesvirus C-terminal LANA concentrates at pericentromeric and peri-telomeric regions of a subset of mitotic chromosomes. Virology 357, 149-157.

Kelley-Clarke, B., Ballestas, M.E., Srinivasan, V., Barbera, A.J., Komatsu, T., Harris, T.A., Kazanjian, M., and Kaye, K.M. (2007b). Determination of Kaposi's sarcoma-associated herpesvirus C-terminal latency-associated nuclear antigen residues mediating chromosome association and DNA binding. J. Virol. 81, 4348-4356.

Kelley-Clarke, B., De Leon-Vazquez, E., Slain, K., Barbera, A.J., and Kaye, K.M. (2009). Role of Kaposi's sarcoma-associated herpesvirus C-terminal LANA chromosome binding in episome persistence. J. Virol. 83, 4326-4337.

Kerscher, O., Felberbaum, R., and Hochstrasser, M. (2006). Modification of proteins by ubiquitin and ubiquitin-like proteins. Annu. Rev. Cell Dev. Biol. 22, 159-180.

Kim, I.J., Flano, E., Woodland, D.L., Lund, F.E., Randall, T.D., and Blackman, M.A. (2003). Maintenance of long term gamma-herpesvirus B cell latency is dependent on CD40-mediated development of memory B cells. J. Immunol. 171, 886-892.

Komander, D., and Rape, M. (2012). The ubiquitin code. Annu. Rev. Biochem. 81, 203-229.

Krithivas, A., Young, D.B., Liao, G., Greene, D., and Hayward, S.D. (2000). Human herpesvirus 8 LANA interacts with proteins of the mSin3 corepressor complex and negatively regulates Epstein-Barr virus gene expression in dually infected PEL cells. J. Virol. 74, 9637-9645.

Kusano, S., and Eizuru, Y. (2010). Human I-mfa domain proteins specifically interact with KSHV LANA and affect its regulation of Wnt signaling-dependent transcription. Biochem. Biophys. Res. Commun. 396, 608-613.

Kutok, J.L., and Wang, F. (2006). Spectrum of Epstein-Barr virus-associated diseases. Annu. Rev. Pathol. 1, 375-404.

Lagunoff, M., and Ganem, D. (1997). The structure and coding organization of the genomic termini of Kaposi's sarcoma-associated herpesvirus. Virology 236, 147-154.

Laichalk, L.L., and Thorley-Lawson, D.A. (2005). Terminal differentiation into plasma cells initiates the replicative cycle of Epstein-Barr virus in vivo. J. Virol. 79, 1296-1307.

Lan, K., Kuppers, D.A., Verma, S.C., and Robertson, E.S. (2004). Kaposi's sarcoma-associated herpesvirus-encoded latency-associated nuclear antigen inhibits lytic replication by targeting Rta: a potential mechanism for virus-mediated control of latency. J. Virol. 78, 6585-6594.

Lawler, C., Milho, R., May, J.S., and Stevenson, P.G. (2015). Rhadinovirus host entry by co-operative infection. PLoS Pathog. 11, e1004761.

Lee, E.K., Kim, S.Y., Noh, K.W., Joo, E.H., Zhao, B., Kieff, E., and Kang, M.S. (2014). Small molecule inhibition of Epstein-Barr virus nuclear antigen-1 DNA binding activity interferes with replication and persistence of the viral genome. Antiviral Res. 104, 73-83.

Lee, K.S., Groshong, S.D., Cool, C.D., Kleinschmidt-DeMasters, B.K., and van Dyk, L.F. (2009). Murine gammaherpesvirus 68 infection of IFNgamma unresponsive mice: a small animal model for gammaherpesvirus-associated B-cell lymphoproliferative disease. Cancer Res. 69, 5481-5489.

Lehman, C.W., and Botchan, M.R. (1998). Segregation of viral plasmids depends on tethering to chromosomes and is regulated by phosphorylation. Proc. Natl. Acad. Sci. U. S. A. 95, 4338-4343.

Lerner, M.R., Andrews, N.C., Miller, G., and Steitz, J.A. (1981). Two small RNAs encoded by Epstein-Barr virus and complexed with protein are precipitated by antibodies from patients with systemic lupus erythematosus. Proc. Natl. Acad. Sci. U. S. A. 78, 805-809.

Li, S., Tan, M., Juillard, F., Ponnusamy, R., Correia, B., Simas, J.P., Carrondo, M.A., McVey, C.E., and Kaye, K.M. (2015). The Kaposi's sarcoma herpesvirus latency-associated nuclear antigen DNA binding domain dorsal positive electrostatic patch facilitates DNA replication and episome persistence. J. Biol. Chem.

Li, X., Liang, D., Lin, X., Robertson, E.S., and Lan, K. (2011). Kaposi's sarcoma-associated herpesvirus-encoded latency-associated nuclear antigen reduces interleukin-8 expression in endothelial cells and impairs neutrophil chemotaxis by degrading nuclear p65. J. Virol. 85, 8606-8615.

Liang, X., Collins, C.M., Mendel, J.B., Iwakoshi, N.N., and Speck, S.H. (2009). Gammaherpesvirus-driven plasma cell differentiation regulates virus reactivation from latently infected B lymphocytes. PLoS Pathog. 5, e1000677.

Liang, X., Paden, C.R., Morales, F.M., Powers, R.P., Jacob, J., and Speck, S.H. (2011). Murine gamma-herpesvirus immortalization of fetal liver-derived B cells requires both the viral cyclin D homolog and latency-associated nuclear antigen. PLoS Pathog. 7, e1002220.

Lieberman, P.M. (2014). Virology. Epstein-Barr virus turns 50. Science 343, 1323-1325.

Lim, C., Gwack, Y., Hwang, S., Kim, S., and Choe, J. (2001). The transcriptional activity of cAMP response element-binding protein-binding protein is modulated by the latency associated nuclear antigen of Kaposi's sarcoma-associated herpesvirus. J. Biol. Chem. 276, 31016-31022.

Lim, C., Sohn, H., Gwack, Y., and Choe, J. (2000). Latency-associated nuclear antigen of Kaposi's sarcoma-associated herpesvirus (human herpesvirus-8) binds ATF4/CREB2 and inhibits its transcriptional activation activity. J. Gen. Virol. 81, 2645-2652.

Liu, J., Martin, H.J., Liao, G., and Hayward, S.D. (2007). The Kaposi's sarcoma-associated herpesvirus LANA protein stabilizes and activates c-Myc. J. Virol. 81, 10451-10459.

Lopes, L.F., Ruiz Miyazawa, K.W., de Almeida, E.R., Serafim, K.G., de Almeida Gualtieri, K., Costa, I.C., Felipe, I., Pavanelli, W.R., and Watanabe, M.A. (2013). Epstein-Barr virus (EBV) microRNAs: involvement in cancer pathogenesis and immunopathology. Int. Rev. Immunol. 32, 271-281.

Lu, F., Tsai, K., Chen, H.S., Wikramasinghe, P., Davuluri, R.V., Showe, L., Domsic, J., Marmorstein, R., and Lieberman, P.M. (2012). Identification of host-chromosome binding sites and candidate gene targets for Kaposi's sarcoma-associated herpesvirus LANA. J. Virol. 86, 5752-5762.

Lu, J., Verma, S.C., Murakami, M., Cai, Q., Kumar, P., Xiao, B., and Robertson, E.S. (2009). Latency-associated nuclear antigen of Kaposi's sarcoma-associated herpesvirus (KSHV) upregulates survivin expression in KSHV-Associated B-lymphoma cells and contributes to their proliferation. J. Virol. 83, 7129-7141.

Lukac, D.M., Kirshner, J.R., and Ganem, D. (1999). Transcriptional activation by the product of open reading frame 50 of Kaposi's sarcoma-associated herpesvirus is required for lytic viral reactivation in B cells. J. Virol. 73, 9348-9361.

Lydeard, J.R., Schulman, B.A., and Harper, J.W. (2013). Building and remodelling Cullin-RING E3 ubiquitin ligases. EMBO Rep. 14, 1050-1061.

Marechal, V., Dehee, A., Chikhi-Brachet, R., Piolot, T., Coppey-Moisan, M., and Nicolas, J.C. (1999). Mapping EBNA-1 domains involved in binding to metaphase chromosomes. J. Virol. 73, 4385-4392.

Marques, S., Alenquer, M., Stevenson, P.G., and Simas, J.P. (2008). A single CD8+ T cell epitope sets the long-term latent load of a murid herpesvirus. PLoS Pathog. 4, e1000177.

Marques, S., Efstathiou, S., Smith, K.G., Haury, M., and Simas, J.P. (2003). Selective gene expression of latent murine gammaherpesvirus 68 in B lymphocytes. J. Virol. 77, 7308-7318.

Matsumura, S., Persson, L.M., Wong, L., and Wilson, A.C. (2010). The latency-associated nuclear antigen interacts with MeCP2 and nucleosomes through separate domains. J. Virol. 84, 2318-2330.

May, J.S., Coleman, H.M., Boname, J.M., and Stevenson, P.G. (2005). Murine gammaherpesvirus-68 ORF28 encodes a non-essential virion glycoprotein. J. Gen. Virol. 86, 919-928.

McBride, A.A. (2013). The papillomavirus E2 proteins. Virology 445, 57-79.

Mercier, A., Arias, C., Madrid, A.S., Holdorf, M.M., and Ganem, D. (2014). Site-specific association with host and viral chromatin by Kaposi's sarcoma-associated herpesvirus LANA and its reversal during lytic reactivation. J. Virol. 88, 6762-6777.

Mesri, E.A., Cesarman, E., and Boshoff, C. (2010). Kaposi's sarcoma and its associated herpesvirus. Nat. Rev. Cancer 10, 707-719.

Milho, R., Frederico, B., Efstathiou, S., and Stevenson, P.G. (2012). A heparan-dependent herpesvirus targets the olfactory neuroepithelium for host entry. PLoS Pathog. 8, e1002986.

Milho, R., Smith, C.M., Marques, S., Alenquer, M., May, J.S., Gillet, L., Gaspar, M., Efstathiou, S., Simas, J.P., and Stevenson, P.G. (2009). In vivo imaging of murid herpesvirus-4 infection. J. Gen. Virol. 90, 21-32.

Moorman, N.J., Willer, D.O., and Speck, S.H. (2003). The gammaherpesvirus 68 latency-associated nuclear antigen homolog is critical for the establishment of splenic latency. J. Virol. 77, 10295-10303.

Moser, J.M., Farrell, M.L., Krug, L.T., Upton, J.W., and Speck, S.H. (2006). A gammaherpesvirus 68 gene 50 null mutant establishes long-term latency in the lung but fails to vaccinate against a wild-type virus challenge. J. Virol. 80, 1592-1598.

Moser, J.M., Upton, J.W., Allen, R.D., 3rd, Wilson, C.B., and Speck, S.H. (2005). Role of B-cell proliferation in the establishment of gammaherpesvirus latency. J. Virol. 79, 9480-9491.

Mulligan, R.C., and Berg, P. (1981). Selection for animal cells that express the Escherichia coli gene coding for xanthine-guanine phosphoribosyltransferase. Proc. Natl. Acad. Sci. U. S. A. 78, 2072-2076.

Muromoto, R., Okabe, K., Fujimuro, M., Sugiyama, K., Yokosawa, H., Seya, T., and Matsuda, T. (2006). Physical and functional interactions between STAT3 and Kaposi's sarcoma-associated herpesvirus-encoded LANA. FEBS Lett. 580, 93-98.

Nash, A.A., Dutia, B.M., Stewart, J.P., and Davison, A.J. (2001). Natural history of murine gamma-herpesvirus infection. Philos. Trans. R. Soc. Lond. B. Biol. Sci. 356, 569-579.

Nicoll, M.P., Proenca, J.T., and Efstathiou, S. (2012). The molecular basis of herpes simplex virus latency. FEMS Microbiol. Rev. 36, 684-705.

Ottinger, M., Christalla, T., Nathan, K., Brinkmann, M.M., Viejo-Borbolla, A., and Schulz, T.F. (2006). Kaposi's sarcoma-associated herpesvirus LANA-1 interacts with the short variant of BRD4 and releases cells from a BRD4- and BRD2/RING3-induced G1 cell cycle arrest. J. Virol. 80, 10772-10786.

Ottinger, M., Pliquet, D., Christalla, T., Frank, R., Stewart, J.P., and Schulz, T.F. (2009). The interaction of the gammaherpesvirus 68 orf73 protein with cellular BET proteins affects the activation of cell cycle promoters. J. Virol. 83, 4423-4434.

Paden, C.R., Forrest, J.C., Moorman, N.J., and Speck, S.H. (2010). Murine gammaherpesvirus 68 LANA is essential for virus reactivation from splenocytes but not long-term carriage of viral genome. J. Virol. 84, 7214-7224.

Paden, C.R., Forrest, J.C., Tibbetts, S.A., and Speck, S.H. (2012). Unbiased mutagenesis of MHV68 LANA reveals a DNA-binding domain required for LANA function in vitro and in vivo. PLoS Pathog. 8, e1002906.

Pan, H.Y., Zhang, Y.J., Wang, X.P., Deng, J.H., Zhou, F.C., and Gao, S.J. (2003). Identification of a novel cellular transcriptional repressor interacting with the latent nuclear antigen of Kaposi's sarcoma-associated herpesvirus. J. Virol. 77, 9758-9768.

Panagopoulos, D., Victoratos, P., Alexiou, M., Kollias, G., and Mosialos, G. (2004). Comparative analysis of signal transduction by CD40 and the Epstein-Barr virus oncoprotein LMP1 in vivo. J. Virol. 78, 13253-13261.

Pauk, J., Huang, M.L., Brodie, S.J., Wald, A., Koelle, D.M., Schacker, T., Celum, C., Selke, S., and Corey, L. (2000). Mucosal shedding of human herpesvirus 8 in men. N. Engl. J. Med. 343, 1369-1377.

Pavlova, I.V., Virgin, H.W.t., and Speck, S.H. (2003). Disruption of gammaherpesvirus 68 gene 50 demonstrates that Rta is essential for virus replication. J. Virol. 77, 5731-5739.

Pearce, M., Matsumura, S., and Wilson, A.C. (2005). Transcripts encoding K12, v-FLIP, v-cyclin, and the microRNA cluster of Kaposi's sarcoma-associated herpesvirus originate from a common promoter. J. Virol. 79, 14457-14464.

Pfeffer, S., Sewer, A., Lagos-Quintana, M., Sheridan, R., Sander, C., Grasser, F.A., van Dyk, L.F., Ho, C.K., Shuman, S., Chien, M.*, et al.* (2005). Identification of microRNAs of the herpesvirus family. Nat. Methods 2, 269-276.

Piirsoo, M., Ustav, E., Mandel, T., Stenlund, A., and Ustav, M. (1996). Cis and trans requirements for stable episomal maintenance of the BPV-1 replicator. EMBO J. 15, 1-11.

Pires de Miranda, M., Alenquer, M., Marques, S., Rodrigues, L., Lopes, F., Bustelo, X.R., and Simas, J.P. (2008). The Gammaherpesvirus m2 protein manipulates the Fyn/Vav pathway through a multidocking mechanism of assembly. PLoS One 3, e1654.

Pires de Miranda, M., Lopes, F.B., McVey, C.E., Bustelo, X.R., and Simas, J.P. (2013). Role of Src homology domain binding in signaling complexes assembled by the murid gamma-herpesvirus M2 protein. J. Biol. Chem. 288, 3858-3870.

Ponnusamy, R., Petoukhov, M.V., Correia, B., Custodio, T.F., Juillard, F., Tan, M., Pires de Miranda, M., Carrondo, M.A., Simas, J.P., Kaye, K.M*., et al.* (2015). KSHV but not MHV-68 LANA induces a strong bend upon binding to terminal repeat viral DNA. Nucleic Acids Res.

Prinjha, R.K., Witherington, J., and Lee, K. (2012). Place your BETs: the therapeutic potential of bromodomains. Trends Pharmacol. Sci. 33, 146-153.

Purushothaman, P., McDowell, M.E., McGuinness, J., Salas, R., Rumjahn, S.M., and Verma, S.C. (2012). Kaposi's sarcoma-associated herpesvirus-encoded LANA recruits topoisomerase IIbeta for latent DNA replication of the terminal repeats. J. Virol. 86, 9983-9994.

Qiu, J., Cosmopoulos, K., Pegtel, M., Hopmans, E., Murray, P., Middeldorp, J., Shapiro, M., and Thorley-Lawson, D.A. (2011). A novel persistence associated EBV miRNA expression profile is disrupted in neoplasia. PLoS Pathog. 7, e1002193.

Radkov, S.A., Kellam, P., and Boshoff, C. (2000). The latent nuclear antigen of Kaposi sarcoma-associated herpesvirus targets the retinoblastoma-E2F pathway and with the oncogene Hras transforms primary rat cells. Nat. Med. 6, 1121-1127.

Rangaswamy, U.S., and Speck, S.H. (2014). Murine gammaherpesvirus M2 protein induction of IRF4 via the NFAT pathway leads to IL-10 expression in B cells. PLoS Pathog. 10, e1003858.

Rivas, C., Thlick, A.E., Parravicini, C., Moore, P.S., and Chang, Y. (2001). Kaposi's sarcoma-associated herpesvirus LANA2 is a B-cell-specific latent viral protein that inhibits p53. J. Virol. 75, 429-438.

Rodrigues, L., Filipe, J., Seldon, M.P., Fonseca, L., Anrather, J., Soares, M.P., and Simas, J.P. (2009). Termination of NF-kappaB activity through a gammaherpesvirus protein that assembles an EC5S ubiquitin-ligase. EMBO J. 28, 1283-1295.

Rodrigues, L., Pires de Miranda, M., Caloca, M.J., Bustelo, X.R., and Simas, J.P. (2006). Activation of Vav by the gammaherpesvirus M2 protein contributes to the establishment of viral latency in B lymphocytes. J. Virol. 80, 6123-6135.

Rodrigues, L., Popov, N., Kaye, K.M., and Simas, J.P. (2013). Stabilization of Myc through heterotypic poly-ubiquitination by mLANA is critical for gamma-herpesvirus lymphoproliferation. PLoS Pathog. 9, e1003554.

Roughan, J.E., and Thorley-Lawson, D.A. (2009). The intersection of Epstein-Barr virus with the germinal center. J. Virol. 83, 3968-3976.

Roupelieva, M., Griffiths, S.J., Kremmer, E., Meisterernst, M., Viejo-Borbolla, A., Schulz, T., and Haas, J. (2010). Kaposi's sarcoma-associated herpesvirus Lana-1 is a major activator of the serum response element and mitogen-activated protein kinase pathways via interactions with the Mediator complex. J. Gen. Virol. 91, 1138-1149.

Sato, K., Takeuchi, J.S., Misawa, N., Izumi, T., Kobayashi, T., Kimura, Y., Iwami, S., Takaori-Kondo, A., Hu, W.S., Aihara, K*., et al.* (2014). APOBEC3D and APOBEC3F potently promote HIV-1 diversification and evolution in humanized mouse model. PLoS Pathog. 10, e1004453.

Schulz, T.F., and Cesarman, E. (2015). Kaposi Sarcoma-associated Herpesvirus: mechanisms of oncogenesis. Curr. Opin. Virol. 14, 116-128.

Sears, J., Kolman, J., Wahl, G.M., and Aiyar, A. (2003). Metaphase chromosome tethering is necessary for the DNA synthesis and maintenance of oriP plasmids but is insufficient for transcription activation by Epstein-Barr nuclear antigen 1. J. Virol. 77, 11767-11780.

Sears, R., Nuckolls, F., Haura, E., Taya, Y., Tamai, K., and Nevins, J.R. (2000). Multiple Ras-dependent phosphorylation pathways regulate Myc protein stability. Genes Dev. 14, 2501-2514.

Shaffer, A.L., Rosenwald, A., Hurt, E.M., Giltnane, J.M., Lam, L.T., Pickeral, O.K., and Staudt, L.M. (2001). Signatures of the immune response. Immunity 15, 375-385.

Shi, J., and Vakoc, C.R. (2014). The mechanisms behind the therapeutic activity of BET bromodomain inhibition. Mol. Cell 54, 728-736.

Shrestha, P., and Sugden, B. (2014). Identification of properties of the Kaposi's sarcoma-associated herpesvirus latent origin of replication that are essential for the efficient establishment and maintenance of intact plasmids. J. Virol. 88, 8490-8503.

Si, H., and Robertson, E.S. (2006). Kaposi's sarcoma-associated herpesvirus-encoded latency-associated nuclear antigen induces chromosomal instability through inhibition of p53 function. J. Virol. 80, 697-709.

Si, H., Verma, S.C., Lampson, M.A., Cai, Q., and Robertson, E.S. (2008). Kaposi's sarcoma-associated herpesvirus-encoded LANA can interact with the nuclear mitotic apparatus protein to regulate genome maintenance and segregation. J. Virol. 82, 6734-6746.

Simas, J.P., and Efstathiou, S. (1998). Murine gammaherpesvirus 68: a model for the study of gammaherpesvirus pathogenesis. Trends Microbiol. 6, 276-282.

Simas, J.P., Swann, D., Bowden, R., and Efstathiou, S. (1999). Analysis of murine gammaherpesvirus-68 transcription during lytic and latent infection. J. Gen. Virol. 80 (Pt 1), 75-82.

Simpson, G.R., Schulz, T.F., Whitby, D., Cook, P.M., Boshoff, C., Rainbow, L., Howard, M.R., Gao, S.J., Bohenzky, R.A., Simmonds, P*., et al.* (1996). Prevalence of Kaposi's sarcoma associated herpesvirus infection measured by antibodies to recombinant capsid protein and latent immunofluorescence antigen. Lancet 348, 1133-1138.

Sin, S.H., and Dittmer, D.P. (2013). Viral latency locus augments B-cell response in vivo to induce chronic marginal zone enlargement, plasma cell hyperplasia, and lymphoma. Blood 121, 2952-2963.

Sin, S.H., Fakhari, F.D., and Dittmer, D.P. (2010). The viral latency-associated nuclear antigen augments the B-cell response to antigen in vivo. J. Virol. 84, 10653-10660.

Skaar, J.R., Pagan, J.K., and Pagano, M. (2013). Mechanisms and function of substrate recruitment by F-box proteins. Nat. Rev. Mol. Cell Biol. 14, 369-381.

Skiadopoulos, M.H., and McBride, A.A. (1998). Bovine papillomavirus type 1 genomes and the E2 transactivator protein are closely associated with mitotic chromatin. J. Virol. 72, 2079-2088.

Soulier, J., Grollet, L., Oksenhendler, E., Cacoub, P., Cazals-Hatem, D., Babinet, P., d'Agay, M.F., Clauvel, J.P., Raphael, M., Degos, L*., et al.* (1995). Kaposi's sarcoma-associated herpesvirus-like DNA sequences in multicentric Castleman's disease. Blood 86, 1276-1280.

Speck, S.H., and Ganem, D. (2010). Viral latency and its regulation: lessons from the gamma-herpesviruses. Cell Host Microbe 8, 100-115.

Stedman, W., Deng, Z., Lu, F., and Lieberman, P.M. (2004). ORC, MCM, and histone hyperacetylation at the Kaposi's sarcoma-associated herpesvirus latent replication origin. J. Virol. 78, 12566-12575.

Stevenson, P.G. (2004). Immune evasion by gamma-herpesviruses. Curr. Opin. Immunol. 16, 456-462.

Stevenson, P.G., and Doherty, P.C. (1999). Non-antigen-specific B-cell activation following murine gammaherpesvirus infection is CD4 independent in vitro but CD4 dependent in vivo. J. Virol. 73, 1075-1079.

Stevenson, P.G., May, J.S., Smith, X.G., Marques, S., Adler, H., Koszinowski, U.H., Simas, J.P., and Efstathiou, S. (2002). K3-mediated evasion of CD8(+) T cells aids amplification of a latent gamma-herpesvirus. Nat. Immunol. 3, 733-740.

Stevenson, P.G., Simas, J.P., and Efstathiou, S. (2009). Immune control of mammalian gamma-herpesviruses: lessons from murid herpesvirus-4. J. Gen. Virol. 90, 2317-2330.

Stewart, J.P., Usherwood, E.J., Ross, A., Dyson, H., and Nash, T. (1998). Lung epithelial cells are a major site of murine gammaherpesvirus persistence. J. Exp. Med. 187, 1941-1951.

Stoopler, E.T. (2005). Oral herpetic infections (HSV 1-8). Dent. Clin. North Am. 49, 15-29, vii.

Sun, Q., Tsurimoto, T., Juillard, F., Li, L., Li, S., De Leon Vazquez, E., Chen, S., and Kaye, K. (2014). Kaposi's sarcoma-associated herpesvirus LANA recruits the DNA polymerase clamp loader to mediate efficient replication and virus persistence. Proc. Natl. Acad. Sci. U. S. A. 111, 11816-11821.

Sunil-Chandra, N.P., Arno, J., Fazakerley, J., and Nash, A.A. (1994). Lymphoproliferative disease in mice infected with murine gammaherpesvirus 68. Am. J. Pathol. 145, 818-826.

Sunil-Chandra, N.P., Efstathiou, S., Arno, J., and Nash, A.A. (1992a). Virological and pathological features of mice infected with murine gamma-herpesvirus 68. J. Gen. Virol. 73 (Pt 9), 2347-2356.

Sunil-Chandra, N.P., Efstathiou, S., and Nash, A.A. (1992b). Murine gammaherpesvirus 68 establishes a latent infection in mouse B lymphocytes in vivo. J .Gen. Virol. 73 (Pt 12), 3275-3279.

Sunil-Chandra, N.P., Efstathiou, S., and Nash, A.A. (1993). Interactions of murine gammaherpesvirus 68 with B and T cell lines. Virology 193, 825-833.

Svobodova, J., Blaskovic, D., and Mistrikova, J. (1982). Growth characteristics of herpesviruses isolated from free living small rodents. Acta Virol. 26, 256-263.

Tarakanova, V.L., Suarez, F., Tibbetts, S.A., Jacoby, M.A., Weck, K.E., Hess, J.L., Speck, S.H., and Virgin, H.W.t. (2005). Murine gammaherpesvirus 68 infection is associated with lymphoproliferative disease and lymphoma in BALB beta2 microglobulin-deficient mice. J. Virol. 79, 14668-14679.

Thorley-Lawson, D.A. (2001). Epstein-Barr virus: exploiting the immune system. Nat. Rev. Immunol. 1, 75-82.

Thorley-Lawson, D.A. (2005). EBV the prototypical human tumor virus--just how bad is it? J. Allergy Clin. Immunol. 116, 251-261; quiz 262.

Thorley-Lawson, D.A., and Allday, M.J. (2008). The curious case of the tumour virus: 50 years of Burkitt's lymphoma. Nat. Rev. Microbiol. 6, 913-924.

Thorley-Lawson, D.A., and Gross, A. (2004). Persistence of the Epstein-Barr virus and the origins of associated lymphomas. N. Engl. J. Med. 350, 1328-1337.

Thorley-Lawson, D.A., Hawkins, J.B., Tracy, S.I., and Shapiro, M. (2013). The pathogenesis of Epstein-Barr virus persistent infection. Curr. Opin. Virol. 3, 227-232.

Thorley-Lawson, D.A., and Mann, K.P. (1985). Early events in Epstein-Barr virus infection provide a model for B cell activation. J. Exp. Med. 162, 45-59.

Tortorella, D., Gewurz, B.E., Furman, M.H., Schust, D.J., and Ploegh, H.L. (2000). Viral subversion of the immune system. Annu. Rev. Immunol. 18, 861-926.

Tripp, R.A., Hamilton-Easton, A.M., Cardin, R.D., Nguyen, P., Behm, F.G., Woodland, D.L., Doherty, P.C., and Blackman, M.A. (1997). Pathogenesis of an infectious mononucleosis-like disease induced by a murine gamma-herpesvirus: role for a viral superantigen? J. Exp. Med. 185, 1641-1650.

Trowitzsch, S., Bieniossek, C., Nie, Y., Garzoni, F., and Berger, I. (2010). New baculovirus expression tools for recombinant protein complex production. J. Struct. Biol. 172, 45-54.

Uldrick, T.S., Wang, V., O'Mahony, D., Aleman, K., Wyvill, K.M., Marshall, V., Steinberg, S.M., Pittaluga, S., Maric, I., Whitby, D.*, et al.* (2010). An interleukin-6-related systemic inflammatory syndrome in patients co-infected with Kaposi sarcoma-associated herpesvirus and HIV but without Multicentric Castleman disease. Clin. Infect. Dis. 51, 350-358.

Uldrick, T.S., and Whitby, D. (2011). Update on KSHV epidemiology, Kaposi Sarcoma pathogenesis, and treatment of Kaposi Sarcoma. Cancer Lett. 305, 150-162.

Uppal, T., Banerjee, S., Sun, Z., Verma, S.C., and Robertson, E.S. (2014). KSHV LANA--the master regulator of KSHV latency. Viruses 6, 4961-4998.

Usherwood, E.J., Ross, A.J., Allen, D.J., and Nash, A.A. (1996a). Murine gammaherpesvirus-induced splenomegaly: a critical role for CD4 T cells. J. Gen. Virol. 77 (Pt 4), 627-630.

Usherwood, E.J., Stewart, J.P., and Nash, A.A. (1996b). Characterization of tumor cell lines derived from murine gammaherpesvirus-68-infected mice. J, Virol. 70, 6516-6518.

Verma, S.C., Borah, S., and Robertson, E.S. (2004). Latency-associated nuclear antigen of Kaposi's sarcoma-associated herpesvirus up-regulates transcription of human telomerase reverse transcriptase promoter through interaction with transcription factor Sp1. J. Virol. 78, 10348-10359.

Verma, S.C., Choudhuri, T., Kaul, R., and Robertson, E.S. (2006). Latency-associated nuclear antigen (LANA) of Kaposi's sarcoma-associated herpesvirus interacts with origin recognition complexes at the LANA binding sequence within the terminal repeats. J. Virol. 80, 2243-2256.

Verma, S.C., Lu, J., Cai, Q., Kosiyatrakul, S., McDowell, M.E., Schildkraut, C.L., and Robertson, E.S. (2011). Single molecule analysis of replicated DNA reveals the usage of multiple KSHV genome regions for latent replication. PLoS Pathog. 7, e1002365.

Viejo-Borbolla, A., Ottinger, M., Bruning, E., Burger, A., Konig, R., Kati, E., Sheldon, J.A., and Schulz, T.F. (2005). Brd2/RING3 interacts with a chromatin-binding domain in the Kaposi's Sarcoma-associated herpesvirus latency-associated nuclear antigen 1 (LANA-1) that is required for multiple functions of LANA-1. J. Virol. 79, 13618-13629.

Vijayachandran, L.S., Viola, C., Garzoni, F., Trowitzsch, S., Bieniossek, C., Chaillet, M., Schaffitzel, C., Busso, D., Romier, C., Poterszman, A.*, et al.* (2011). Robots, pipelines, polyproteins: enabling multiprotein expression in prokaryotic and eukaryotic cells. J. Struct. Biol. 175, 198-208.

Vincentelli, R., and Romier, C. (2013). Expression in Escherichia coli: becoming faster and more complex. Curr. Opin. Struct. Biol. 23, 326-334.

Virgin, H.W.t., Latreille, P., Wamsley, P., Hallsworth, K., Weck, K.E., Dal Canto, A.J., and Speck, S.H. (1997). Complete sequence and genomic analysis of murine gammaherpesvirus 68. J. Virol. 71, 5894-5904.

Wang, C.Y., and Filippakopoulos, P. (2015). Beating the odds: BETs in disease. Trends Biochem. Sci. 40, 468-479.

Wang, Q.J., Jenkins, F.J., Jacobson, L.P., Kingsley, L.A., Day, R.D., Zhang, Z.W., Meng, Y.X., Pellett, P.E., Kousoulas, K.G., Baghian, A.*, et al.* (2001). Primary human herpesvirus 8 infection generates a broadly specific CD8(+) T-cell response to viral lytic cycle proteins. Blood 97, 2366-2373.

Wang, X., He, Z., Xia, T., Li, X., Liang, D., Lin, X., Wen, H., and Lan, K. (2014). Latency-associated nuclear antigen of Kaposi sarcoma-associated herpesvirus promotes angiogenesis through targeting notch signaling effector Hey1. Cancer Res. 74, 2026-2037.

Willer, D.O., and Speck, S.H. (2003). Long-term latent murine Gammaherpesvirus 68 infection is preferentially found within the surface immunoglobulin D-negative subset of splenic B cells in vivo. J. Virol. 77, 8310-8321.

Wong, L.Y., Matchett, G.A., and Wilson, A.C. (2004). Transcriptional activation by the Kaposi's sarcoma-associated herpesvirus latency-associated nuclear antigen is facilitated by an N-terminal chromatin-binding motif. J. Virol. 78, 10074-10085.

Wu, T.T., Blackman, M.A., and Sun, R. (2010). Prospects of a novel vaccination strategy for human gamma-herpesviruses. Immunol. Res. 48, 122-146.

Wu, T.T., Qian, J., Ang, J., and Sun, R. (2012). Vaccine prospect of Kaposi sarcoma-associated herpesvirus. Curr. Opin. Virol. 2, 482-488.

Wu, T.T., Usherwood, E.J., Stewart, J.P., Nash, A.A., and Sun, R. (2000). Rta of murine gammaherpesvirus 68 reactivates the complete lytic cycle from latency. J. Virol. 74, 3659-3667.

Xiao, B., Verma, S.C., Cai, Q., Kaul, R., Lu, J., Saha, A., and Robertson, E.S. (2010). Bub1 and CENP-F can contribute to Kaposi's sarcoma-associated herpesvirus genome persistence by targeting LANA to kinetochores. J. Virol. 84, 9718-9732.

Yates, J.L., Warren, N., and Sugden, B. (1985). Stable replication of plasmids derived from Epstein-Barr virus in various mammalian cells. Nature 313, 812-815.

Yoshimura, A., Naka, T., and Kubo, M. (2007). SOCS proteins, cytokine signalling and immune regulation. Nat. Rev. Immunol. 7, 454-465.

You, J., Srinivasan, V., Denis, G.V., Harrington, W.J., Jr., Ballestas, M.E., Kaye, K.M., and Howley, P.M. (2006). Kaposi's sarcoma-associated herpesvirus latency-associated nuclear antigen interacts with bromodomain protein Brd4 on host mitotic chromosomes. J. Virol. 80, 8909-8919.

Yu, X., Yu, Y., Liu, B., Luo, K., Kong, W., Mao, P., and Yu, X.F. (2003). Induction of APOBEC3G ubiquitination and degradation by an HIV-1 Vif-Cul5-SCF complex. Science 302, 1056-1060.

Zhu, J.Y., Strehle, M., Frohn, A., Kremmer, E., Hofig, K.P., Meister, G., and Adler, H. (2010). Identification and analysis of expression of novel microRNAs of murine gammaherpesvirus 68. J. Virol. 84, 10266-10275.

APPENDIX 1

OPEN ACCESS Freely available online

PLOS | PATHOGENS

Crystal Structure of the Gamma-2 Herpesvirus LANA DNA Binding Domain Identifies Charged Surface Residues Which Impact Viral Latency

Bruno Correia[1☯], Sofia A. Cerqueira[2☯], Chantal Beauchemin[3], Marta Pires de Miranda[2], Shijun Li[3], Rajesh Ponnusamy[1], Lénia Rodrigues[2], Thomas R. Schneider[4], Maria A. Carrondo[1]*, Kenneth M. Kaye[3]*, J. Pedro Simas[2]*, Colin E. McVey[1]*

1 Instituto de Tecnologia Química e Biológica, Universidade Nova de Lisboa, Oeiras, Portugal, **2** Instituto de Microbiologia e Instituto de Medicina Molecular, Faculdade de Medicina, Universidade de Lisboa, Lisboa, Portugal, **3** Departments of Medicine, Brigham and Women's Hospital and Harvard Medical School, Boston, Massachusetts, United States of America, **4** EMBL c/o DESY, Hamburg, Germany

Abstract

Latency-associated nuclear antigen (LANA) mediates γ2-herpesvirus genome persistence and regulates transcription. We describe the crystal structure of the murine gammaherpesvirus-68 LANA C-terminal domain at 2.2 Å resolution. The structure reveals an alpha-beta fold that assembles as a dimer, reminiscent of Epstein-Barr virus EBNA1. A predicted DNA binding surface is present and opposite this interface is a positive electrostatic patch. Targeted DNA recognition substitutions eliminated DNA binding, while certain charged patch mutations reduced bromodomain protein, BRD4, binding. Virus containing LANA abolished for DNA binding was incapable of viable latent infection in mice. Virus with mutations at the charged patch periphery exhibited substantial deficiency in expansion of latent infection, while central region substitutions had little effect. This deficiency was independent of BRD4. These results elucidate the LANA DNA binding domain structure and reveal a unique charged region that exerts a critical role in viral latent infection, likely acting through a host cell protein(s).

Citation: Correia B, Cerqueira SA, Beauchemin C, Pires de Miranda M, Li S, et al. (2013) Crystal Structure of the Gamma-2 Herpesvirus LANA DNA Binding Domain Identifies Charged Surface Residues Which Impact Viral Latency. PLoS Pathog 9(10): e1003673. doi:10.1371/journal.ppat.1003673

Editor: Shou-Jiang Gao, University of Southern California Keck School of Medicine, United States of America

Received April 26, 2013; **Accepted** August 16, 2013; **Published** October 17, 2013

Funding: The work was supported by grants from the Fundação para a Ciência e a Tecnologia (FCT) Harvard Medical School Portugal Program in Translational Research and Information (JPS, CEM, MAC and KMK) HMSP-ICT/0021/2010. This work was also supported by grants from the National Cancer Institute (CA082036) (KMK) and the U.S. Department of Defense (PR093491) (KMK). CEM is a holder of a Ciência 2008 position from the Portuguese Ministry of Science. The funders had no role in study design, data collection and analysis, decision to publish, or preparation of the manuscript.

Competing Interests: The authors have declared that no competing interests exist.

* E-mail: carrondo@itqb.unl.pt (MAC); kkaye@rics.bwh.harvard.edu (KMK); psimas@fm.ul.pt (JPS); mcvey@itqb.unl.pt (CEM)

☯ These authors contributed equally to this work.

Introduction

Herpesviruses are ubiquitous viruses, which infect many mammalian species and are a leading cause of human viral disease. There are two known human viruses from the gamma herpesvirus sub-family. The Epstein-Barr virus (EBV), a gamma-1 herpesvirus (Lymphocryptovirus), and the Kaposi's sarcoma-associated herpesvirus (KSHV), a gamma-2 herpesvirus (Rhadinovirus). KSHV has an etiologic role in Kaposi's Sarcoma, the leading AIDS malignancy, as well as primary effusion lymphoma and multicentric Castleman's disease. EBV is also associated with human cancers. These human viruses do not readily infect small laboratory animals. The murine gammaherpesvirus 68 (MHV-68 or murid herpesvirus 4), a rhadinovirus that was isolated from naturally infected rodents, is structurally and functionally related to human gamma-herpesviruses and readily infects mice, thus providing a mouse model for the investigation of gammaherpesvirus pathogenesis [1–3].

A key feature of herpesvirus infection is their lifelong persistence in the host in the form of latency. During latent infection, viral genomes persist as multi-copy, circularized, extrachromosomal episomes (plasmids). Only a small subset of viral genes is expressed during latency. In the case of gamma-herpesvirus sub-family members, latent infection is predominantly established in B lymphocytes. Intransal infection of mice with MHV-68 causes an acute self-limiting respiratory infection, followed by the establishment of splenic latency, which peaks 14 days after infection [4,5]. Splenic germinal centre (GC) B cells have a key role both in the establishment and maintenance of viral latency [6]. Like EBV [7], MHV-68 establishes latency predominantly in activated germinal centre B cells. This strategy favours physiological access of the virus to the memory B-cell pool, the major reservoir of long-term latency.

KSHV latency-associated nuclear antigen (kLANA), a 1,162 amino acid protein encoded by *ORF73* of the viral genome, is the predominant gene expressed in latent infection. LANA mediates persistence of episomal DNA and thus is required for long-term maintenance of viral genomes in dividing cells, a role central to viral latency. LANA promotes episomal replication and segregation to progeny nuclei after mitosis. The C-terminal region of kLANA harbours a DNA-binding domain (DBD) that self-associates and binds to terminal repeat (TR) DNA sequences of

Author Summary

Herpesviruses establish life-long latent infections. During latency, gammaherpesviruses, such as Kaposi's sarcoma-associated herpesvirus (KSHV), persist as multicopy, circularized genomes in the cell nucleus and express a small subset of viral genes. KSHV latency-associated nuclear antigen (LANA) is the predominant gene expressed during latent infection. C-terminal LANA binds KSHV terminal repeat (TR) DNA to mediate DNA replication. TR DNA binding also allows tethering of the viral genome to mitotic chromosomes to mediate DNA segregation to daughter nuclei. We describe here the crystal structure of the murine gammaherpesvirus 68 LANA DNA binding domain, which is homologous to that of KSHV LANA. The structure revealed a dimer and we identified residues involved in the interaction with viral DNA. Mutation of these residues abolished DNA binding and viable latency establishment in a mouse model of infection. We also identified a positively charged patch on the dimer surface opposite to the DNA binding region and found this patch exerts an important role in the virus's ability to expand latent infection in vivo. This work elucidates the structure of the LANA DNA binding domain and identifies a novel surface feature that is critical for viral latent infection, likely by acting through a host cell protein.

the viral episome [8–14]. LANA cooperatively binds to two sites within the TR DNA, LBS1 and LBS2. LBS1 is a high affinity site capable of facilitating the cooperative binding of LANA to LBS2. Both sites contribute to the ability of LANA to suppress transcription and to facilitate DNA replication [10]. An N-terminal region of kLANA is able to attach to chromosomes through binding to histones H2A and H2B [15]. Together, these binding properties allow kLANA to tether the viral genome to chromosomes during mitosis thus ensuring segregation of the episome to daughter nuclei [16,17]. Association of viral genomes with host mitotic chromosomes via a virus-encoded protein is a strategy employed by a number of different latent DNA viruses. Similar to the KSHV LANA, EBV EBNA1 and papillomavirus E2 proteins play a role in viral genome maintenance [18–22].

All gamma-2 herpesviruses encode homologs of KSHV LANA. The *ORF73* from MHV-68 encodes a much smaller, 314 amino acid, 50 kDa nuclear protein (termed mLANA thereafter) which lacks the extensive internal acidic and glutamine-rich repeat region of kLANA. The C-terminal region of mLANA, comprising amino acid residues 140 to 263, has amino acid similarity to the kLANA DNA-binding domain. Similar to kLANA, mLANA was recently shown to act on TR elements of the MHV-68 genome to mediate episome maintenance and to associate with mitotic chromosomes [23], and mLANA DNA-binding sites have been identified within MHV-68 TR DNA [24]. In a mouse model of infection, latency-associated nuclear antigen (LANA) protein is selectively expressed in infected GC B cells [25]. Recombinant viruses that do not express mLANA [26,27], or bear disruptive mutations in the predicted DNA-binding domain fail to establish viable latency [24]. mLANA therefore performs functions equivalent to those of kLANA regarding episomal maintenance and is essential for establishment of viable latency *in vivo*.

LANA proteins are also modulators of transcription from a variety of cellular and viral promoters and affect cellular growth [28,29]. Both kLANA and mLANA are able to regulate transcription through E3-ubiquitin ligase activity [30–32]. mLANA promotes the polyubiquitination and subsequent proteasomal-dependent nuclear degradation of host nuclear factor-kappa B (NF-κB) [31]. The mechanism involves the assembly of an Elongin C/Cullin5/SOCS (suppressors of cytokine signalling)-like complex, mediated by an unconventional viral SOCS-box motif (residues 199–206), homologous to the kLANA Cul5 box, present in the C-terminal domain of mLANA [30,31]. Another motif also within the C-terminal region of mLANA (QAKKLK motif, residues 226–231) has been shown to bind to several members of the BET (Bromodomain and Extra Terminal domain) family of proteins, including BRD2, BRD3 and BRD4 [33,34], that interact with acetylated histones. mLANA interaction with BET proteins leads to activation of cell cycle promoters.

Secondary structure predictions have suggested that the C-terminal regions of both mLANA and kLANA have similarity to the X-ray structure of the DNA-binding domain of the EBV nuclear antigen 1 protein (EBNA1) [35]. As a first step towards understanding the mechanism by which the C-terminal region of mLANA exerts its functions, we have determined the crystal structure of this mLANA domain (amino acids 140–272). $mLANA_{140–272}$ forms a β-barrel induced dimer and has an overall fold with an α-helix arrangement similar to that of the EBNA1 and E2 latency protein structures [36,37]. However, the structure reveals unique features that exert important effects on viral persistence in an animal model.

Results

X-ray crystal structure of C-terminal mLANA reveals an alpha+beta fold that assembles to form a dimer

The structure of the C-terminal domain of mLANA was determined at 2.2 Å resolution. Data collection and refinement statistics are reported in Table 1. The initial structure was solved using the coordinates of the EBV EBNA1 dimer, which has both functional and predicted secondary structure homology, as a molecular replacement model [36]. The crystallized domain contained residues 140–272, designated $mLANA_{140–272}$ (Figure S1). The refined electron density map was readily interpretable with exceptions only at the termini and loop regions. The tertiary structure of $mLANA_{140–272}$ exhibits an α+β ferredoxin-like fold (Figure 1A) which assembles to form a dimeric eight-stranded anti-parallel β-barrel that is central to its functional architecture. This dimer can be viewed from opposite sides of the β-barrel core which for clarity is termed the ventral (top) and the dorsal sides (bottom) (Figure 1B). Each monomer contributes an anti-parallel 4-stranded β-sheet "half-barrel" from which helix α2 and α3 pack onto the plaited sheet with their axis parallel to the strands of the sheet. The core of the barrel is occupied by large hydrophobic surface (Figure S2) that contributes to the stability of mLANA (Figure 1C). Size exclusion analysis confirms that $mLANA_{140–272}$ is also a dimer in solution (Figure S2B and C). When the dimer interface was disrupted by removal of residues 254–261, which lie below the β2–β3 loop of the adjacent monomer, the melting temperature of $mLANA_{140–253}$ decreased drastically (T_m 43°C), indicating the importance of these residues for stability (Figure 1D). The flanking helix α1 caps this helical arrangement and lies perpendicular to the central β-barrel. Helix α2, situated on the ventral side, is postulated to be the DNA recognition helix (see below).

LANA cooperatively binds to two adjacent sites within TR DNA, similar to the EBV DS element required for EBNA1 binding [38], suggesting a dimer-dimer interaction [39]. Analysis of the mLANA crystal packing shows that dimers pack so that the DNA-binding flanking helix α1 in each dimer is in position to interact with both the flanking helix α1 and helix α3 from the adjacent dimer (Figure 1E). Two phosphate ions on the ventral surface contribute and coordinate the binding of the α1–α3′

Table 1. Data collection and refinement statistics.

X-ray diffraction data	
Wavelength (Å)	1.129
Space group	C2
Cell dimensions: a, b, c (Å)	88.6 61.7 63.7
α, β, γ (°)	90.0, 99.4, 90.0
Resolution (Å)	37.6–2.2 (2.32–2.20)
R_{merge}	0.059 (0.64)
R_{meas}/R_{pim}	0.063 (0.69)/0.023 (0.25)
$I/\sigma I$	21.4 (3.3)
Completeness (%)	99.9 (98.5)
Redundancy	7.5 (7.4)
Total measured reflections	130,451
Unique reflections	17,333 (2,507)
Wilson B-factor (Å^2)	42.3
Refinement	
Resolution (Å)	30.8–2.2
R_{work}/R_{free}	0.1714/0.2032
Atoms: protein (chain A)/protein (chain B)/$PO4^{2-}$/water	1979/1946/35/62
B factors: chain A/chain B/PO4/water	49.4/50.7/51.8/41.9
Rmsd bond length (Å)	0.007
Rmsd bond angles (°)	1.168
Ramachandran analysis: favoured/allowed (%)	93.0/7.0

R_{work} and R_{free} are defined by $R = \sum hkl||F_{obs}|-|F_{calc}||/\sum hkl|F_{obs}|$, where hkl are the indices of the reflections (used in refinement for R_{work}; 5%, not used in refinement, for R_{free}), and F_{obs} and F_{calc} are the structure factors deduced from measured intensities and calculated from the model, respectively. Values in parentheses are for the highest resolution shell.

doi:10.1371/journal.ppat.1003673.t001

dimer-dimer interactions and suggest at least 2 or 3 nucleotides may span the spacer region between the LBS-1 and LBS-2 sites (Figure 1F). Consistent with this finding, size exclusion chromatography demonstrates that $mLANA_{140–314}$ forms tetramers in solution (Figure S2B). In addition, $mLANA_{140–272}$ dimer forms a tetramer to cooperatively bind adjacent mTR DNA binding sites (described below).

Despite functional conservation, mLANA and EBNA1 proteins do not exhibit amino acid similarity (Figure 2A). However, a PHYRE2 program [40] search predicts mLANA secondary structure homology between the C-terminal domains of mLANA and EBNA1 (not shown), similar to other predictions [35]. A superposition of both monomer structures is shown in Figure 2C.

Protruding perpendicular to the ventral face of mLANA lies a partially disordered β2–β3 loop (199–215) (Figure 2B) that harbours a motif required for the interaction of mLANA with Elongin B/C (EloBC)-cullin-SOCS box (ECS)-type E3 ubiquitin ligase, resulting in the polyubiquitination of NFκB [31]. Mutations at the base of this loop (^{199}VSCLPLVP^{206}, underlined residues mutated to Alanine) disrupt binding of mLANA to Elongin C and consequently mLANA's E3-ubiquitin ligase activity. A recombinant virus containing these mutations fails to establish latency *in vivo* [31].

Ventral face of mLANA – phosphate binding traces the site of DNA interaction

The structural basis for DNA recognition can be inferred from the observed phosphate binding pattern. In total, seven phosphates ions were located at the surface of mLANA. Five of these are situated on the ventral face (Figure 2D–F) while the remaining two cap the dorsal side of helix α1. Therefore, we consider the ventral face as the putative DNA binding site of mLANA. We modelled mLANA-DNA on the EBNA1-DNA structure (PDB ID: 1B3T) and the mLANA structure accommodated the DNA well (Figure 2G and Figure S3).

Mutation of predicted DNA phosphate contacts disrupts DNA binding to TR DNA

To directly assess mLANA DNA binding, we used an electrophoretic mobility shift assay (EMSA) to assess the ability of mLANA to bind DNA. DNAse I footprinting analysis with recombinant mLANA has shown three adjacent protected regions within the mTR sequence [24], (Figure 3A, green and blue regions). Two overlapping probes, mLBS1 or mLBS2, each containing a portion of the protected sequence, or control, overlapping adjacent sequence were used to assess mLANA binding (Figure 3B). After incubation with mLANA, a shifted complex was only observed after incubation with mLBS1, and not with mLBS2 or control adjacent sequence (Figure 3B). The mLBS1 complex was supershifted with anti-FLAG antibody and was effectively competed with excess, unlabelled mLBS1 or mLBS1-2 competitor (containing the entire DNAse I protected region), but not unlabelled mLBS2 (Figure 3B). Despite the inability of mLANA to shift mLBS2 probe, size exclusion chromatography analysis demonstrated that $mLANA_{140–272}$ bound adjacent mLBS1 and mLBS2 sites in mLBS1-2 oligonucleotide as a tetramer (Figure S6), consistent with cooperative binding to both sites. Therefore, similar to KSHV LANA DNA binding [10], mLANA cooperatively binds to adjacent high and low affinity TR DNA binding sites.

We then constructed mutations in the predicted mLANA recognition helix intended to decrease interactions with its cognate DNA. mLANA H186D/K187E contains substitutions predicted to disrupt phosphate interactions and abolish DNA binding, and this mutant was unable to complex with mLBS1 (Figure 3C). In contrast, mLANA K224A/K228A/K229A, mLANA K224E/K228E/K229E, mLANA K251A/K253A, and mLANA K251E/K253E, each contain substitutions within a dorsal positively charged patch (discussed below) opposite the predicted DNA interface, and each mLANA gel shifted the mLBS1 probe (Figure 3C). The mLANA K251E/K253E (Figure 3C, lane 7) complex was similar in intensity to that of mLANA (Figure 3C, lane 3), though the intensities of the mLANA K224A/K228/K229A and mLANA K251A/K253A complexes were each reduced (Figure 3C, comparing lane 4 and 6 with lane 3). The reduced mLANA K224A/K228A/K229A and mLANA K251A/K253A binding was likely in part due to modestly lower protein expression (Figure 3D). Notably, mLANA K224E/K228E/K229E demonstrated increased mLBS1 binding (comparing lane 5 with lane 3). Therefore, as predicted by the mLANA DNA binding domain structure, mLANA H186D/K187E substitutions abolished DNA binding, but DNA binding was preserved with dorsal mutations. The finding that dorsal alanine substitutions of lysine reduced DNA binding, while glutamate substitutions did not, suggests that substituting non charged residues may have subtle effects on DNA binding domain folding.

We characterised mLANA TR DNA binding by surface plasmon resonance (SPR) and isothermal titration calorimetry (ITC) to determine the dissociation constant (K_D) for mLBS1. The K_D for wild type and H186D/K187E were determined by

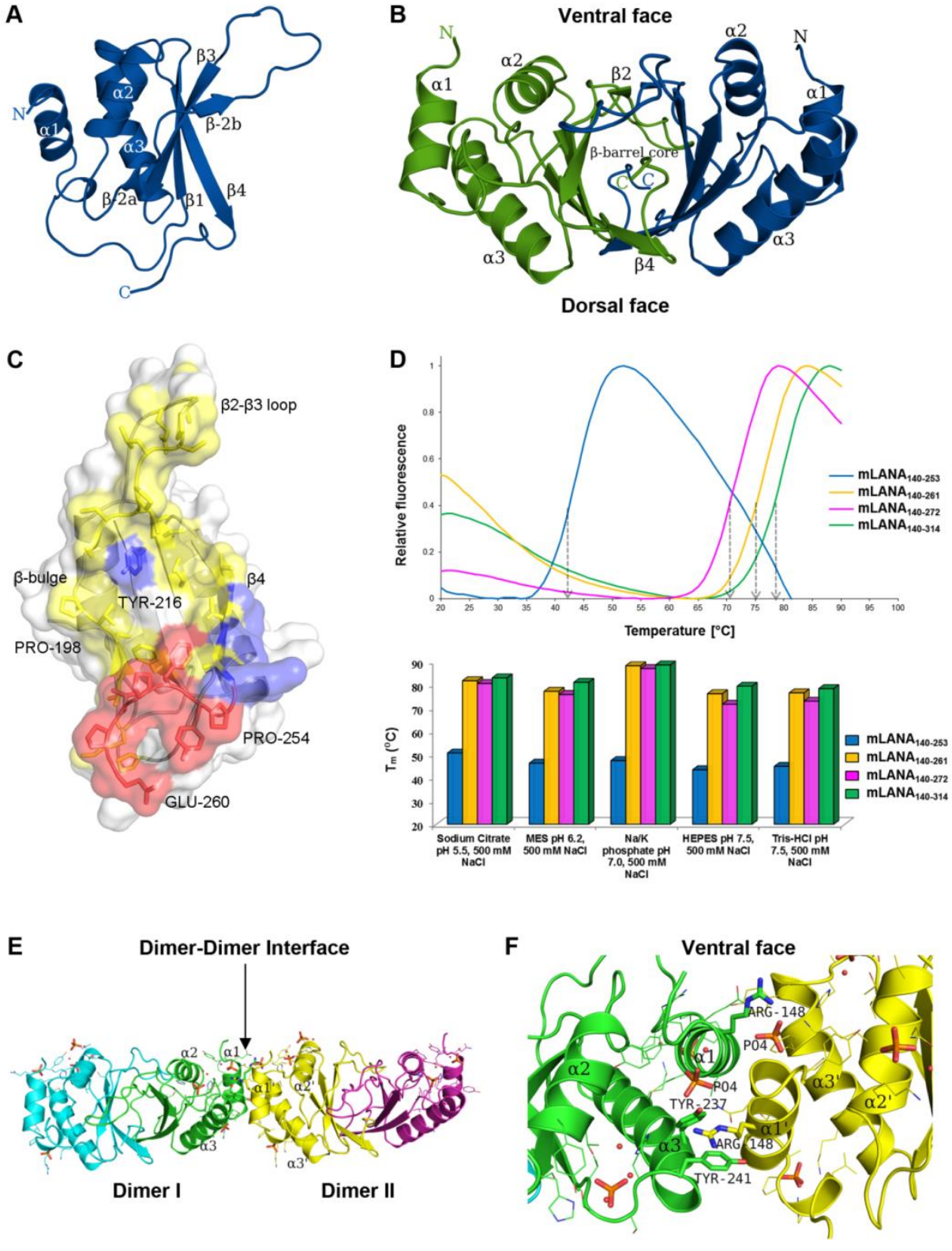

Figure 1. Structure of the C-terminal domain of mLANA. (**A**) A ribbon representation with secondary structure assignment for a monomer of the MHV-68 mLANA$_{140–272}$ DNA-binding domain (see also Figure S1). (**B**) A representation of the mLANA$_{140–272}$ quaternary structure and its dimeric conformation viewed along the non-crystallographic axis and illustrates the α-helical arrangement around the β-barrel core. The two chains are coloured in blue (chain A) and green (chain B). (**C**) Cross section of the dimer interface with coloured surface properties. A large area (~1440 Å^2) constituting the hydrophobic core is displayed in yellow with the hydrogen bonding residues displayed in blue. Deleting residues P254–P259 in red

from the C-terminus destabilizes the dimer, as it contributes to the hydrophobic stability of the dimer interface (see also Figure S2). (**D**) Fluorescence-based thermal shift analysis of mLANA truncations (arrows display the midpoint of the unfolding transitions). The midpoint melting temperatures of the protein-unfolding transition (T_m) for mLANA DBD truncations are shown for the optimal buffers. (**E**) mLANA tetramer assembly presumed for cooperative TR DNA binding as observed in the crystal packing with the symmetry equivalent dimer. Phosphate interactions coordinate the dimer-dimer interface. Two dimers form a tetramer stabilized by an interface with a surface area (~535 Å^2) per monomer that is approximately 12% of that of the total surface of a single subunit (~7,500 Å^2). (**F**) A ribbon representation of the dimer-dimer interface view from the ventral side. In the interface Arg-148 from dimer-2 stacks against Tyr-241, and makes a weak hydrogen bond with Tyr-237 from dimer-1. The arginine residue is conserved in both mLANA and kLANA proteins which has the ability to intercalate between hydrophobic aromatic amino acids on the second dimer.
doi:10.1371/journal.ppat.1003673.g001

titrating mLANA$_{124–272}$ against immobilized mLBS1 (Figure 3E and F). The K_D's were 169 nM and 960 nM for wild type and mLANA H186D/K187E, respectively (Table 2). Thermodynamics binding parameters in solution measured by ITC using the more soluble mLANA$_{124–314}$ fitted well to a one-site model, indicating one distinct mLANA binding site (Figure 3G), and provided a calculated K_D of 66 nM (Table 3). The discrepancy between the SPR and ITC dissociation constants was due to the inaccessibility of more than 50 percent of mLANA$_{124–314}$ for DNA binding as observed from the calculated N value from ITC (0.27 ± 0.03 dimer per TR-DNA)(Supporting Information, Text S1).

mLANA exhibits a novel positive patch on the dorsal face and interacts with BRD4

Electrostatic surface analysis of the mLANA protein reveals an extensive positive patch on the dorsal side which includes residues Arg-156, Lys-224, 225, 228, 229, 231, 251, 253, and Arg-232 (Figure 4A and B and S5B). Both Arg-156 and Lys-229 interact with a phosphate ion which is located on the dorsal face of helix α1. Lys-251 and 253 lie on the 2-fold non-crystallographic symmetry axis of the dimer interface (Figure 4B). The positive electrostatic surface also encompasses the identified ^{226}QAKKLK^{231} motif that is involved in binding to BET proteins [34]. Both mLANA and kLANA have been described to bind to the ET domain of BET proteins and the cluster of positive charges is energetically organized to establish charge-charge interactions with a negatively charged patch on the helical ET domain of the BET proteins BRD2 and BRD4. Four key Lysine residues are conserved in both mLANA (Lys-228, Lys-229, Lys-251, and Lys-253) and kLANA (Lys-1113, Lys-1114, Lys-1138 and Lys-1140) (Figure 2A).

Although mLANA was previously described to bind BRD4, a complete mapping of mLANA binding within BRD4 had not been performed. Therefore, we investigated mLANA binding to BRD4 (Figure 4C). GST mLANA 1–168 or GST mLANA 140–314 were used to assess binding to *in vitro* translated BRD4 or fragments spanning full length BRD4. GST mLANA$_{140–314}$ precipitated full length BRD4 more efficiently than did GST mLANA$_{1–168}$ (Figure 4D). Interestingly GST LANA mLANA$_{1–168}$ bound BRD4 at two sites, BRD4 1–470 and BRD4 1047–1362, while GST mLANA 140–314 bound BRD4 471–730 (Figure 4D). Since BRD4 471–730 contains the conserved ET domain in its C-terminal portion, we then assessed binding of mLANA to GST BRD4 471–594 (upstream of the ET domain) or GST BRD4 595–730 (ET domain and SEED motif). mLANA bound BRD4 471–594, upstream of the ET domain while consistent with previous results [41], kLANA bound the ET domain containing region in BRD4 595–730 (Figure 4E).

Since mLANA residues 226–231 were previously shown to be important for BRD4 binding [34], and since C-terminal mLANA bound the region upstream of the ET domain, we assessed the ability of mLANA, or mLANA mutated at positively charged residues, including within 226–331, to bind BRD4 471–594. mLANA K251E/K253E and mLANA K251A/K253A contain either negatively charged or neutral substitutions at residues in the central positive patch region, while mLANA K224E/K228E/K229E and mLANA K224A/K228A/K229A contain similar substitutions at the periphery of the positive patch. mLANA and each of the mutants bound BRD4 471–594 (Figure 4F). However, BRD4 binding was substantially reduced for mLANA K251E/K253E and modestly reduced for mLANA K224E/K228E/K229E (Figure 4F). In addition, we assessed the ability of GST mLANA 124–272, GST mLANA 124–272 mutated at dorsal positively charged residues, or GST mLANA 124–272 H186D/K187E, which is abolished for DNA binding (Figure 3), for the ability to bind BRD4 or fragments spanning BRD4. GST mLANA 124–272 bound BRD4 and BRD4 471–730 (Figure 4G), similar to GST mLANA 140–314 (Figure. 4D). Each of the mLANA mutants also bound both BRD4 and BRD4 471–730, although binding was reduced for mLANA 124–272 H186D/K187E, mLANA K224E/K228E/K229E, and mLANA K251E/K253E (Figure 4G). The finding that mLANA 124–272 H186D/K187E had reduced BRD4 binding suggests a potential role for these residues in interacting with Brd4. Therefore, substitution of negatively charged, but not neutral, residues for positively charged amino acids on the dorsal positive patch of C-terminal mLANA reduces BRD4 binding.

Loss of DNA binding abolishes virus persistence in mice

We assessed the role of mLANA binding to viral DNA on virus persistence in mice. A recombinant virus was generated bearing the mLANA H186D/K187E mutations in the predicted mLANA DNA recognition helix (designated vmLANA$_{H186D/K187E}$; Figure 5A). We first compared the kinetics of lytic viral replication *in vitro* and during the acute phase of infection in lungs. Lytic replication kinetics was essentially preserved, though changes in the pattern of lytic infection could be identified (Figure 5B and C; Supporting Information, Text S1). This result is consistent with mLANA having a predominant role in latency. We next proceeded to investigate the impact of the introduced mutations in the ability of MHV-68 to expand latent infection in GC B cells and establish persistent infection in mice. vmLANA$_{H186D/K187E}$ showed a marked defect in *in vitro* reactivation from latency (Figure 5D), and viable virus was barely detectable beyond the limit of detection of the assay as early as 14 dpi. This viral mutant also showed a clear defect in the frequency of viral-DNA positive splenocytes (Figure 5E and Table 4). Consistent with this deficit, the frequency of vmLANA$_{H186D/K187E}$ infection in GC B cells at the peak of virus latency (14 dpi) was three orders of magnitude lower (Figure 5F and Table 4). This result was confirmed by visualisation of latently infected cells within GCs in splenic sections (Figure 5G, a–b). Notably, analysis of vmLANA$_{H186D/K187E}$ at 21 and 50 dpi showed that loss of mLANA DNA binding severely diminished virus persistence in mice (Figure 5D and E). These results demonstrate that mLANA binding to its cognate DNA is essential for the expansion of latent infection in GC B cells and is critical for virus persistence.

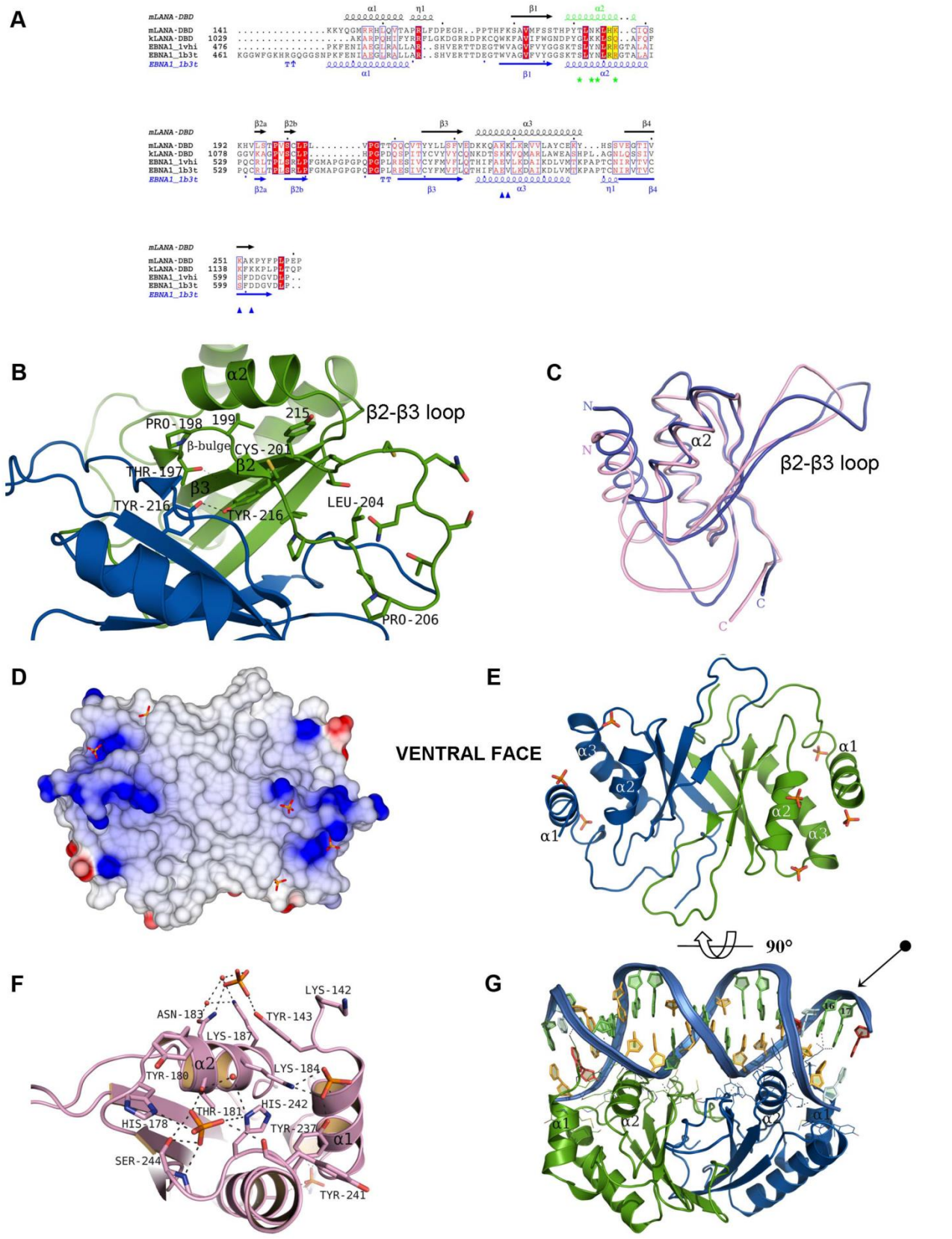
A
mLANA-DBD
mLANA-DBD 141 .....KKYQGMRHLQVTAPLFDPEGH..PPTHFKSAVMFSSTHPYTNKFHK..CIQS
kLANA-DBD 1029 .....AKANPFMHIFYRSFLGKDGRRDPKCQWKFAVIFWGNDFYGKKLSK..AFQF
EBNA1_1vhi 476 .....PKFENIAEGLRALLAR..SHVERTTDEGTWVAGVFVYGGSKTSLYNLRRGTALAI
EBNA1_1b3t 461 KGGWFGKHRGQGGGSNPKFENIAEGLRALLAR..SHVERTTDEGTWVAGVFVYGGSKTSLYNLRRGTALAI
EBNA1_1b3t
mLANA-DBD
mLANA-DBD 192 KHVLDTPSGLPL.....VPGTTQQVTYYLLSFVEDKKQAKKLKRVVLAYCEKY...HSSVEGTIV
kLANA-DBD 1078 GGVKAGPPSGLPL.....HPGPDQSPITYCVYYYCDNKDTSKKVQMANLAWEASHPL.AGNLQSGIV
EBNA1_1vhi 529 PQCRLTPFSGLLGFGMAPGPGPQPGPLRESIVCYFMVFLQTHIFAEVLKDAIKDLVMTKPAPTCNIRVTVC
EBNA1_1b3t 529 PQCRLTPFSGLLGFGMAPGPGPQPGPLRESIVCYFMVFLQTHIFAEVLKDAIKDLVMTKPAPTCNIRVTVC
EBNA1_1b3t
mLANA-DBD
mLANA-DBD 251 KAKPYFPDVEP
kLANA-DBD 1138 MFKKPLPETQP
EBNA1_1vhi 599 SFDDGVDEP..
EBNA1_1b3t 599 SFDDGVDEP..
EBNA1_1b3t
B
α2
215
β2-β3 loop
PRO-198
199
β-bulge
CYS-201
β2
THR-197
β3
TYR-216
TYR-216
LEU-204
PRO-206
C
N
N
α2
β2-β3 loop
C
C
D
VENTRAL FACE
E
α3
α1
α2
α2
α3
α1
F
LYS-142
ASN-183
TYR-143
LYS-187
α2
LYS-184
TYR-180
THR-181
HIS-242
HIS-178
TYR-237
α1
SER-244
TYR-241
G
90°
α1
α2
α2
α1

Figure 2. Conserved sequence and structural features of mLANA. (**A**) Structure based sequence alignment of the MHV-68 mLANA DBD with the DBD domains of KSHV kLANA, EBV EBNA1 (PDB ID: 1VHI), and EBNA1 DNA complex (PDB ID: 1B3T). The secondary structure of mLANA DBD is shown above the alignment while the secondary structure elements of EBNA1 structure are labelled below (blue). The recognition helix α2 is coloured in green with key residues highlighted. The recognition helix residues His-186 and Lys-187 are marked in yellow. Green stars indicate the residues of the recognition helix that interacted with phosphate ions. Conserved dorsal residues with positive charge are indicated by blue triangles. Figure is made with ESPript (http://espript.ibcp.fr/ESPript/ESPript/) Key: Red boxes and white characters indicate strict identity, red characters indicate similarity in a group and blue frames indicate similarity across groups. (**B**) Representation of the dimer interface on the ventral side highlighting the conformation of the β2–β3 SOCS box loop. The β2–β3 loop is the proposed hydrophobic interface for Elongin C interaction and shows the accessibility of residues Cys-201 and Leu-204 of the ^{199}VSCLPLVP^{206} SOCS motif, shown as sticks. The interface highlights the conserved hydrogen bond between chain A Tyr-216 (blue) and chain B Tyr-216 (green) and shows the Pro-198 β-bulge. (**C**) Structural superposition of mLANA$_{140–272}$ (chain B), in pink, with EBNA1 (PDB ID 1vhi; chain B), in blue (r.m.s deviation = 1.37 Å based on 82 equivalent Cα atoms). The recognition helix α2 in mLANA is shorter when compared to EBNA1 by 4 amino acids (1 helical turn), this has implications for both DNA binding and specificity. (**D**) mLANA dimer showing the electrostatic surface of the ventral side, the proposed DNA binding site and highlights five of the phosphate binding sites that trace DNA interactions. Electrostatic surface of mLANA was calculated and displayed using CCP4mg. The surface potentials displayed scale from −0.5 V (red, negatively charged) to +0.5 V (blue, positively charged). (**E**) A ribbon representation of the dimer in the same orientation, showing the secondary structure arrangement. (**F**) Representation of the recognition helix α2 and the key residues which interacts with 3 different phosphates through the side-chains of residues His-178, Thr-181, Asn-183, Lys-184 and Lys-187. (**G**) Structural model of a mLANA DBD DNA complex (rotated relative to panel E) using mLBS1 DNA docked onto the 18 bp EBNA1 DNA recognition sequence followed by energy minimisation using YASARA. The DNA shown was that which gave the best minimized score as indicated in Figure S3. In the structure each nucleotide is drawn in a different colour for clarity, adenine (red), guanine (green), cytosine (lightorange), and thymine (lightblue). The arrow indicates specific nucleotide interactions at sequence 16 and 17 of the modelled TR DNA.
doi:10.1371/journal.ppat.1003673.g002

Electrostatic surface residues on the dorsal face exert a role in expansion of latent infection in GC B cells

We investigated the role of the positive electrostatic surface residues on the pathogenesis of MHV-68 infection taking into account their charge and relative position on the dorsal face. Recombinant viruses were engineered to contain neutral or negatively charged mutations at the centre or periphery of the positive patch (Figure 5A). This set of mutations did not affect viral replication *in vitro* or affect lytic infection in lungs of mice (Figure 5B and C). However, when the latent phase of the infection was analysed a clear phenotype could be ascribed to mutations located at the periphery of the positively charged dorsal motif. Whereas vmLANA$_{K251A/K253A}$ and vmLANA$_{K251E/K253E}$ showed levels of latency comparable to wild type virus (Figure 5D, F and Table 4), viruses vmLANA$_{K224A/K228A/K229A}$ and vmLANA$_{K224E/K228E/K229E}$ showed a significant ($p<0.0001$) latency deficit at 14 dpi (Figure 5D). This deficit was confirmed by quantification of the frequency of viral DNA-positive cells in total splenocytes (Figure 5F and Table 4). This phenotype is unlikely to reflect inadvertant mutations introduced during the mutagenesis process since the equivalent phenotype was observed in both independently derived mutant viruses. Moreover, revertant viruses in which the mutated K224/K228/K229 residues were restored to wild type status did not show any defects in latent infection (Figure 5E), demonstrating that phenotypic changes observed were intrinsic to this locus and not a consequence of mutations elsewhere in the viral genome. Quantification of the frequency of infection in purified GC B cells (Figure 5G and Table 4) and visualisation of latently infected cells by *in situ* hybridisation (Figure 5H, c–d) revealed that replacing a positively charged lysine for the oppositely charged glutamate accentuated the attenuated phenotype when compared to replacement with a non-polar alanine. Notably, the attenuated latency phenotype ascribed to Lys-224, 228, 229 did not correlate with the activity of mLANA to bind BRD4. That conclusion is based on the result that BRD4 binding was reduced for mLANA K251E/K253E (Figure 4F and 4G), however vmLANA$_{K251E/K253E}$ showed no latent infection phenotype (Figure 5D, F, G and H, e–f). Further, mLANA K224A/K228A/K229A bound BRD4 normally (Figure 4F and 4G), yet vmLANA$_{K224A/K228A/K229A}$ was deficient for latent infection. Taken together these data demonstrate that Lys residues 224, 228 and 229 located at the periphery of the positively charged dorsal motif are required for the efficient expansion of infected GC B cells, likely acting through a host cell protein other than BRD4.

Discussion

C-terminal LANA is the most highly conserved LANA domain, and its ability to bind DNA is essential for viral DNA replication and episome persistence [12]. Here, we solve the X-ray crystal structure of the mLANA DNA binding domain. The overall fold comprises a rigid and thermostable β-barrel dimer flanked on either side by an α-helix arrangement. The structural features of mLANA are common to EBV EBNA1 and HPV E2 proteins, indicative of their conserved biological functions in episome maintenance and transcriptional activation.

This work identifies ventral C-terminal mLANA as the DNA binding interface and demonstrates its essential role in latent viral infection. The similarity in the protein folds of mLANA with EBNA1, the sites of mLANA phosphate ion binding, and the modelled superposition of the EBNA1-DNA complex all support that the ventral side interfaces with DNA. Furthermore, a high affinity TR DNA LANA binding site (mLBS1) was demonstrated by EMSA and shown by ITC to bind mLBS1 with nanomolar affinity, 66 nM, with enthalpy as the major driving force for binding. Similar to kLANA, mLANA cooperatively binds adjacent high and low affinity TR DNA binding sites. Disruption of targeted residues on the ventral surface abolished DNA binding (Figure 3), providing direct evidence that this surface is the DNA binding interface. Moreover, engineering the same disruptive mutations into the genome of MHV-68 abolished the ability of the virus to expand latent infection in GC B cells and eliminated persistence of virus that was capable of reactivation. This result was consistent with recent findings that virus containing mLANA incapable of binding DNA was highly deficient for virus *ex vivo* reactivation from splenocytes [24]. This work establishes that LANA binding to TR DNA is critical for viral persistence in proliferating GC B cells. Most importantly, it supports a model in which a strategy of expansion of virus infection in GC B cells to access persistence in long-lived memory B cells is vital for host colonisation. This establishes a parallel with EBV where the same strategy for virus persistence has been proposed based upon clinical investigation [7].

Prior genetic and functional analyses of the LANA DBD can now be interpreted in light of the solved mLANA structure. Consistent with their predicted contacts with DNA, mutations within α helices 1 and 2 affect DNA binding. mLANA Pro179Thr or Leu150Pro resulted in loss of the ability of mLANA to protect its binding site from DNase I cleavage [24,39,42]. Pro-179 is found

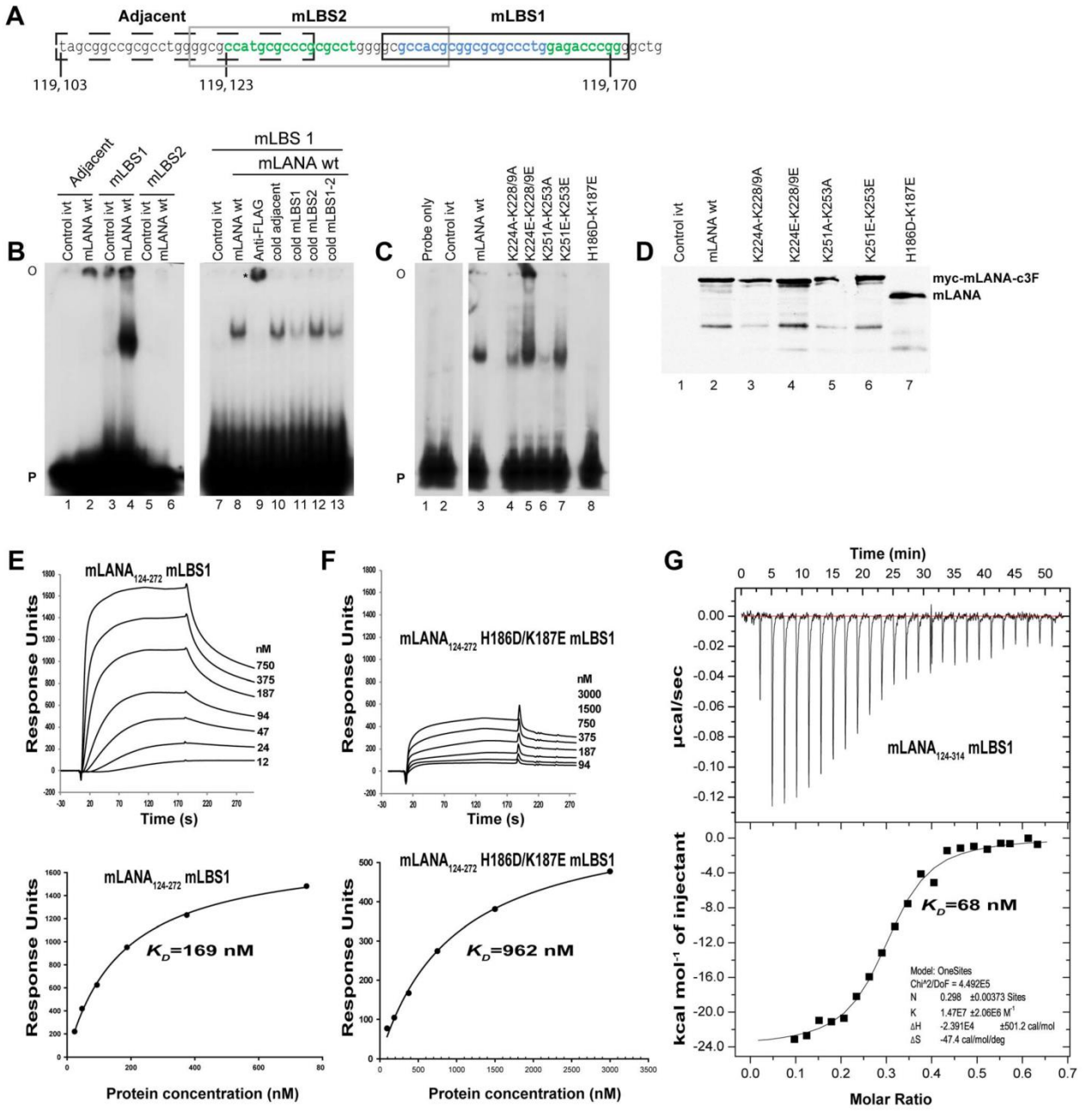

Figure 3. mLANA binds TR DNA with nanomolar affinity. (**A**) MHV-68 TR sequence with genomic coordinates is shown. Oligonucleotide sequences used for gel shift analyses are boxed. Sequence protected by DNAse I footprint analysis [24] is shown in blue and green. (**B**) mLBS1, mLBS2 or control adjacent ^{32}P-labeled oligonucleotides were each incubated with *in vitro*-translated mLANAc3F wt or control reticulocyte lysate (control ivt). Anti-FLAG antibody, or 50 fold excess unlabeled (cold) competitor were included in incubations where indicated. FLAG antibody supershifted complex is indicated by an asterisk. (**C**) mLBS1 ^{32}P-labeled oligonucleotide was incubated alone (lane 1), with control reticulocyte lysate (lane 2; control ivt), or the indicated *in vitro*-translated mLANA proteins. O, gel origin; P, free probe. (**D**) Western Blot is shown containing the same *in vitro*-translated mLANA proteins as in (C). (**E and F**) Panels show the SPR difference sensorgram with increasing concentrations of protein. Protein concentrations injected are as labelled. A 3-min association was followed by a 3-min dissociation phase. The bottom panels represent the K_D determination. The binding constant obtained by Langmuir fit of wild-type and mutant data sets using a 1:1 stoichiometry-binding model. (**G**) ITC binding profile of mLANA$_{124–314}$ with mLBS1 at 25°C. Top panel show raw differential power signals recorded versus time for 30 µM of mLBS1 titrations injected into a cell containing 8.5 µM of mLANA$_{124–314}$ dimer. Bottom panel show integrated injection heats versus the molar ratio of mLANA to mLBS1. Kinetic parameters obtained from the experiments are given in Table 3.

doi:10.1371/journal.ppat.1003673.g003

Table 2. Interaction of $mLANA_{124–272}$ and $mLANA_{124–272}$ H186D/K187E with TR-DNA.

K_D	WT	Mut H186D/K187E
EMSA*	Binding	No binding
SPR	169 nM	960 nM
ITC	66±12 nM	ND

*Full-length mLANA protein used in this experiment.
doi:10.1371/journal.ppat.1003673.t002

at the N-terminus turn of the α2-helix, and restricts the dihedral angles of the preceding amino acid His-178, diminishing the flexibility of His-178, a residue expected to be important for DNA interaction (Figure 2F). The Leu150Pro substitution in helix α1 causes helix disruption as proline is expected to destabilize the α-helix structure, causing a kink. Multiple mutations within α helices 1 and 2 of the kLANA DBD also disrupted DNA binding [24,39,42]. As some kLANA mutations located in regions other than α helix 1 and 2 also disrupted binding, it is likely that these disturb secondary structure and folding of the DBD. Consistent with the large surface area interface of the dimer, only larger deletions of ~10–15 amino acids were able to disrupt kLANA self-association [12,39,43].

Inhibition of NF-κB signalling is essential for MHV-68 latency [31]. mLANA recruits EC_5S E3 ubiquitin ligase complex to target NFκB for degradation by the ubiquitin-proteasome pathway by way of an unconventional SOCS box motif (^{199}**V**SC**LP**LV**P**^{206}). SOCS box containing proteins mediate interactions with elongins B and C to target substrates for degradation. The mLANA structure shows that this motif forms a loop perpendicular to the DNA binding interface, likely allowing accessibility for elongin binding without disrupting DNA binding. A strictly conserved leucine residue [44,45] is part of an essential hydrophobic interface required for Elongin C binding. This feature may be fulfilled by residues Leu-202, Pro-203 and/or Leu-204 that are positioned on the β2–β3 loop to accommodate an ElonginBC-Cul5 complex. A conserved cysteine is critical for SOCS-box interaction with Elongin C [44], and the LANA SOCS-box motif includes Cys-201 conserved in both mLANA and kLANA. The mLANA SOCS loop is an atypical structural motif since a typical SOCS-Elongin C interaction forms a "folded-leaf" four helix cluster. Since LANA does not display a standard SOCS box consensus sequence, it is likely that LANA has acquired a unique strategy to recruit an EC_5S ubiquitin ligase complex.

The most striking feature in the mLANA structure is the positive electrostatic charge on the dorsal face, which is absent in EBNA1 and E2. Residues ^{226}QAKKLK^{231}, within this charged region, were previously identified as binding the BET family of proteins, BRD2 and BRD4 by using BRD4 as a probe against an mLANA peptide array and these findings were confirmed in co-immunoprecipitation experiments with mLANA mutated at these residues [34]. Consistent with these results, we found that substitution of positively charged for negative residues in mLANA K224E/K228E/K229E reduced BRD4 binding, although substitution with neutral residues in mLANA K224A/K228A/K229A did not. Similarly, mLANA K251E/K253E, but not mLANA K251A/K251A, was reduced for BRD4 binding. These findings suggest possible electrostatic inhibition when positively charged residues were substituted for ones with a negative charge. Our results differ from other work [34] since the region immediately upstream of the BRD4 ET domain, rather than the ET domain itself, mediated C-terminal mLANA binding. Interestingly, in contrast to mLANA, and as previously reported [41], kLANA bound the ET domain rather than the upstream BRD4 region, suggesting independent evolution of this LANA binding. We also found that N-terminal mLANA binds to distinct BRD4 regions compared to C-terminal mLANA, although the C-terminal domain has the more prominent role in BRD4 binding (Figure 4). Interestingly EBNA1 and E2 each bind BRD4 through non C-terminal regions. EBNA1 binds BRD4 through N-terminal residues 61–83 [46], while the N-terminal E2 transactivation domain binds BRD2/4 [47]. Most importantly, our mouse infections with mutated viruses showed that this novel electrostatic charge patch on the mLANA dorsal face is required for efficient expansion of latently infected GC B cells. The charged patch could be divided into two components with different functional effects, consisting of a central region and a peripheral region. Unexpectedly, the attenuated latency phenotype ascribed to mutations in Lys-224, 228, 229 could not be attributed to BRD4. This finding suggests that this region is likely to be acting through a host cell protein other than BRD4, possibly a different BET protein.

Table 3. Kinetic values for $mLANA_{124–314}$ with TR-DNA by ITC.

	ΔH^0 kJ/mol	$-\Delta TS^0$ kJ/mol	ΔG^0 kJ/mol	K_D nM	n
WT	−103.9±3.4	63.0±3.4	−41.0±0.5	66±12	0.27±0.03

Standard deviations were calculated from three independent measurements. Gibbs free energy and entropy were calculated using these equations $\Delta G = RT \ln K_D$ and $\Delta G = \Delta H - T\Delta S$.
doi:10.1371/journal.ppat.1003673.t003

The resolution of the crystal structure of the DBD of mLANA provides advantages for pathogenesis studies in a mouse model. In this study, solving the mLANA DBD structure enabled the rational design of mutations in the DNA binding interface that resulted in loss of DNA binding and eliminated virus associated GC cell proliferation and persistence of viable virus in the host. In addition, the mLANA quaternary structure revealed a novel structural motif composed of a patch of positively charged lysine residues on the dorsal face. Results showed that this feature exerts a key role in the expansion of latently infected GC B cells. Thus, combining structural, in vitro and cellular studies with an animal model of infection offers a unique opportunity to investigate viral pathogenesis.

Materials and Methods

Ethics statement

This study was carried out in strict accordance with the recommendations of the Portuguese official Veterinary Directorate (Portaria 1005/92). The Portuguese Experiments on Animal Act strictly comply with the European Guideline 86/609/EEC and follow the FELASA. Animal experiments were approved by the Portuguese official veterinary department for welfare licensing under the protocol number AEC_2010_017_PS_Rdt_General and the IMM Animal Ethics Committee.

Cloning, expression and purification of mLANA

A series of C-terminal truncations of mLANA DBD were cloned into the pET-49b vector (Novagen) and the proteins expressed with an N-terminal GST-His-tag (Figure S1) in *Escherichia coli* BL21 Star (DE3) cells (Invitrogen) containing the pRARE2 plasmid (Novagen). Proteins were purified on an ÄKTA Explorer (GE Healthcare) FPLC system. Point mutations within mLANA

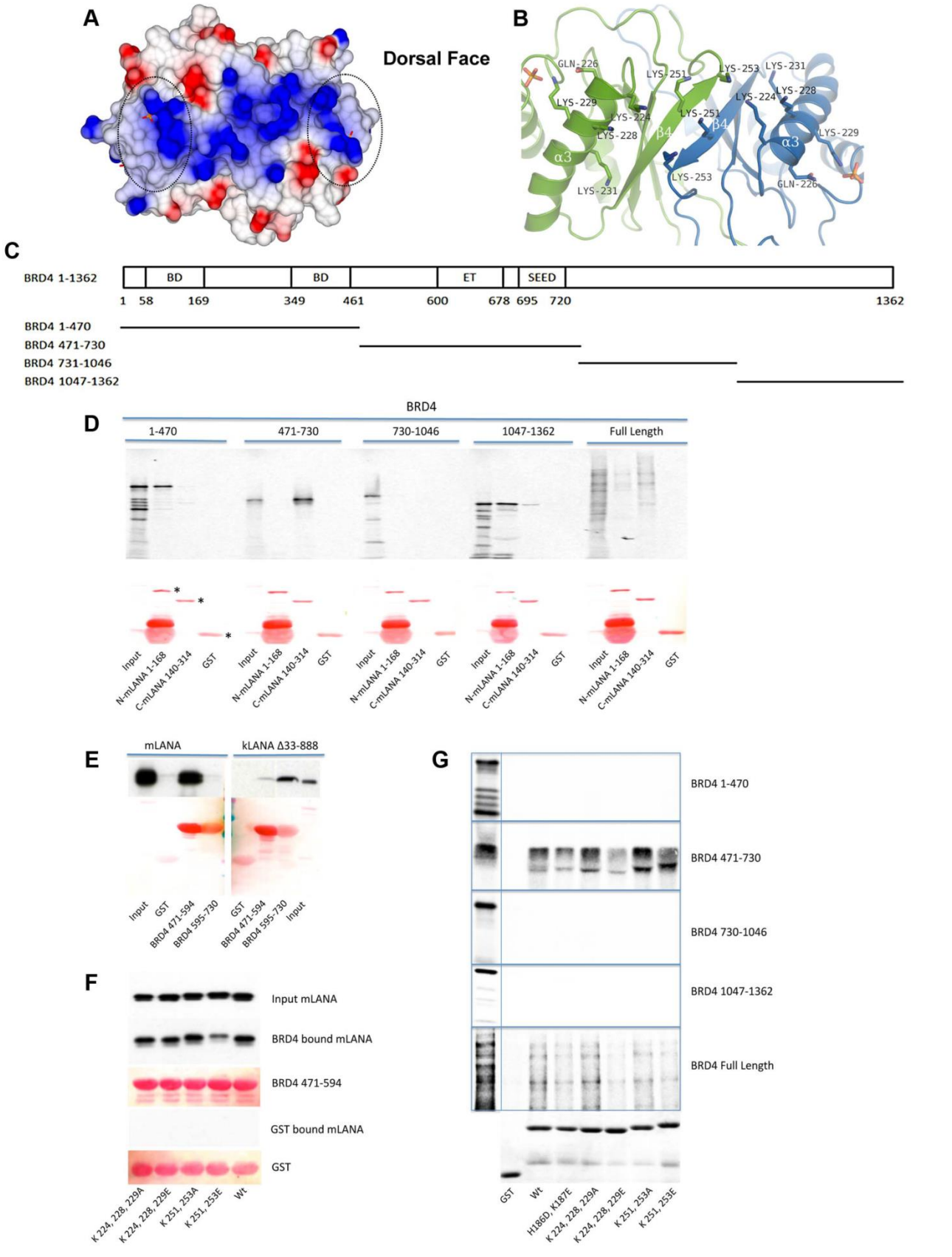
A
Dorsal Face
B
GLN-226
LYS-251
LYS-253
LYS-231
LYS-228
LYS-224
LYS-229
LYS-251
LYS-228
LYS-224
β4
β4
α3
α3
LYS-229
LYS-253
LYS-231
GLN-226
C
BRD4 1-1362
BD
BD
ET
SEED
1 58 169 349 461 600 678 695 720 1362
BRD4 1-470
BRD4 471-730
BRD4 731-1046
BRD4 1047-1362
D
BRD4
1-470
471-730
730-1046
1047-1362
Full Length
Input
N-mLANA 1-168
C-mLANA 140-314
GST
E
mLANA
kLANA Δ33-888
Input
GST
BRD4 471-594
BRD4 595-730
F
Input mLANA
BRD4 bound mLANA
BRD4 471-594
GST bound mLANA
GST
K 224, 228, 229A
K 224, 228, 229E
K 251, 253A
K 251, 253E
Wt
G
BRD4 1-470
BRD4 471-730
BRD4 730-1046
BRD4 1047-1362
BRD4 Full Length
GST
Wt
H186D, K187E
K 224, 228, 229A
K 224, 228, 229E
K 251, 253A
K 251, 253E

Figure 4. The dorsal face of mLANA and its role in BRD4 binding. (**A**) Electrostatic surface showing the residues that contribute to the positive electrostatic potential, Arg-156, Lys-224, 225, 228, 229, 231, and Arg-232, which run along the spine of the dorsal face. The QAKKLK motif is highlighted. The scale is from −0.5 V (red, negatively charged) to +0.5 V (blue, positively charged). (**B**) Ribbon diagram highlighting the key positively charged residues. (**C**) Schematic diagram of BRD4 and fragments used for mapping the mLANA binding. BD, bromodomain; ET, extra-terminal domain; SEED, conserved region consists of polyserine (S) residues interspersed with glutamic (E) and aspartic (D) acid residues [62,63]. (**D**) BRD4 fragments were labelled with [^{35}S]-methionine and assayed for binding to GST mLANA 1–168 or GST mLANA 140–314. Ponceau S detection of proteins (lower panel) is shown and full length GST, GST mLANA 1–168, or GST mLANA 140–314 are indicated with asterisks. (**E**) Western blots for mLANA and kLANA are shown in the upper panel; the Ponceau S stained GST and GST fusion proteins are displayed in the lower panel. Despite the lower intensity of the GST and GST BRD4 595–730 bands after Ponceau S staining, Coomassie blue staining (Figure S4) showed that similar amounts of fusion proteins were present. (**F**) After incubation with GST or GST BRD4 471–594, bound mLANA was detected by FLAG immunoblot. Ponceau S staining of fusion proteins is shown. (G) BRD4 or BRD4 fragments labelled with [^{35}S]-methionine were assayed for binding to GST mLANA 124–272 or GST mLANA 124–272 containing substitution mutations. Coomassie blue staining of fusion proteins is shown in the bottom panel.
doi:10.1371/journal.ppat.1003673.g004

were engineered using the QuikChange multisite-directed mutagenesis kit (Stratagene). Truncations of mLANA (Figure S1A) were PCR cloned into pET-49b as BamHI-NotI fragments using the appropriate primers (Figure S1B). All constructs were confirmed by DNA sequencing. The vector carries an N-terminal GST-tag and His-tag coding sequences followed by a recognition site for the human rhinovirus (HRV) 3C protease (LEVLFQ/GP). Cultures of BL21 Star (DE3) cells transformed with mLANA plasmids were grown until the mid-log phase (A600 nm = 1.8) in Terrific Broth medium supplemented with kanamycin (50 µg/ml) and chloramphenicol (30 µg/ml), induced with 0.5 mM isopropyl-1-thio-β-D-galactopyranoside, and grown for an additional 16 h at 18°C. Cells were harvested by centrifugation, resuspended in a buffer containing 50 mM Na/K phosphate (pH 7.0), 500 mM NaCl, 1 mM Tris (2-carboxyethyl) phosphine (TCEP), 10 mM imidazole, EDTA-free protease inhibitor cocktail (Roche) and 5 µg/ml OmniCleave, (Epicentre), and stored at −80°C. The cell pellet was disrupted using an APV-2000 continuous homogenizer (APV, Madrid, Spain) at 6000 psi. After centrifugation, the supernatant was loaded onto a HisTrap HP (GE Healthcare) column, pre-equilibrated in 50 mM Na/K phosphate (pH 7.0), 500 mM NaCl, 1 mM TCEP, 10 mM imidazole, and proteins eluted with a linear gradient from 10–500 mM imidazole in the same buffer using a ÄKTA Explorer (GE Healthcare) FPLC system (Figure S1C). The GST-Histidine tag was removed by overnight incubation with 3C protease at 4°C and the cleaved protein passed over a GSTPrep FF (GE Healthcare) column (to remove any uncleaved protein as well as the GST-tagged 3C protease) connected end to end to a HiPrep Heparin FF (GE Healthcare) column. The columns were disconnected and the heparin bound mLANA proteins eluted with a linear gradient from 0.3–2 M NaCl. Following 3C cleavage the recombinant protein contained the vector-derived sequence GPGYQKDP at the NH2-terminus. Finally, the protein was applied to a Superdex S75 16/60 filtration column (GE Healthcare) in 10 mM MES buffer, pH 6.5, 300 mM NaCl and 1 mM TCEP and stored at −80°C.

Differential scanning fluorimetry

Assays were performed on an iCycle IQ5 Real Time PCR Detection System (BioRad) with excitation and emission wavelengths of 490 and 575 nm, respectively. Reaction volumes of 20 µl contained 1 µg of protein and 10× of SYPRO orange (Invitrogen) previously diluted in 20 mM HEPES pH 7.5 from an initial 5000× stock. The reaction mix was prepared by adding 2.0 µl of protein-dye mixture solution to 18.0 µl of each buffer from the JBS Solubility kit (Jena Biosciences). For the thermal denaturation the plates were heated at a rate of 1°C/min from 20 to 90°C with a 10 s hold step for every point and fluorescence was measured in 1°C increments. Experiments were carried out in duplicate, and T_m values were calculated for each well using nonlinear regression analysis in the curve-fitting program GraphPad Prism. The T_m values were incorporated into a Microsoft Excel script (ftp://ftp.sgc.ox.ac.uk/pub/biophysics) for comparison of melting curves and thermal shifts.

Crystallization and structure determination

Screening of crystallization conditions was performed using four sparse matrix formulations from commercial screens (Structure Screen I+II, PACT-premier, JCSG-plus and Stura Footprint combination from Molecular Dimensions, UK) in round-bottom Greiner 96-well CrystalQuick plates (Greiner Bio-One) and performed using a Cartesian Crystallization Robot Dispensing System (Genomics Solutions). The sitting-drop vapour-diffusion method was used, with 100 nl protein sample (30 mg/ml) mixed with an equal volume of the reservoir screening solution. In less than 1 day at 21°C, $mLANA_{140–261}$ crystallized as small needle shaped crystals in condition E10 (0.1 M Tris-HCl pH 8.5, 20% w/v PEG 2000 MME, 0.01 M nickel chloride) of the Structure Screen and truncation $mLANA_{140–272}$ crystallized as thin, but large, plate-like crystals in condition F10 (0.1 M Tris-HCl pH 8.5, 25% w/v PEG 3350, 0.2 M lithium sulphate) of the Stura Footprint Combination Screen.

While crystal optimization by sitting-drop vapour diffusion technique failed for $mLANA_{140–261}$. Diffraction-quality crystals for $mLANA_{140–272}$ were obtained by exchanging the protein buffer to the optimal buffer system suggested by DSF assays (50 mM Na/K phosphate pH 7.0). $mLANA_{140–272}$ crystals were further optimized by serial streak-seeding in decreasing precipitant concentrations, with optimal growth to 0.05×0.05×0.15 mm in drops formed by mixing an equal volume of the protein solution with a reservoir solution that contained 0.1 M Na/K phosphate pH 7.0, 0.1 M lithium sulphate, 22% w/v PEG 3350 and 4% v/v 1,4 dioxane. Crystals were transferred to mother liquor supplemented with 20% v/v glycerol, and cryocooled in liquid nitrogen.

A diffraction data set was collected from EMBL beamline P14 at PETRA III (DESY, Germany), indexed and integrated with XDS [48], then merged and converted with Pointless [49] to mtz format for scaling in SCALA [49]. The structure was solved by molecular replacement using Phaser [50] with the EBNA1 dimer (PDB ID: 1VHI) as a search model. An initial model of the structure was autobuilt in PHENIX [51] with manual rebuilding of the model performed in Coot [52] and refined in PHENIX. The crystallographic data are summarized in Table 1. The structure was validated using MOLPROBITY [53] as implemented in PHENIX. The analysis of the dimer interface used the Protein interfaces, surfaces and assemblies service PISA at European Bioinformatics Institute [54]. Energy minimization for 3D structures of mLANA-DNA models was performed using YASARA [55]. Structural illustrations were prepared with PyMOL [56] and CCP4MG [57].

A

Virus	Mutations in mLANA
$vmLANA_{H186D/K187E}$	H186D, K187E
$vmLANA_{K224A/K228A/K2299A}$	K224A, K228A, K229A
$vmLANA_{K224E/K228E/K229E}$	K224E, K228E, K229E
$vmLANA_{K251A/K253A}$	K251A, K253A
$vmLANA_{K251E/K253E}$	K251E, K253E

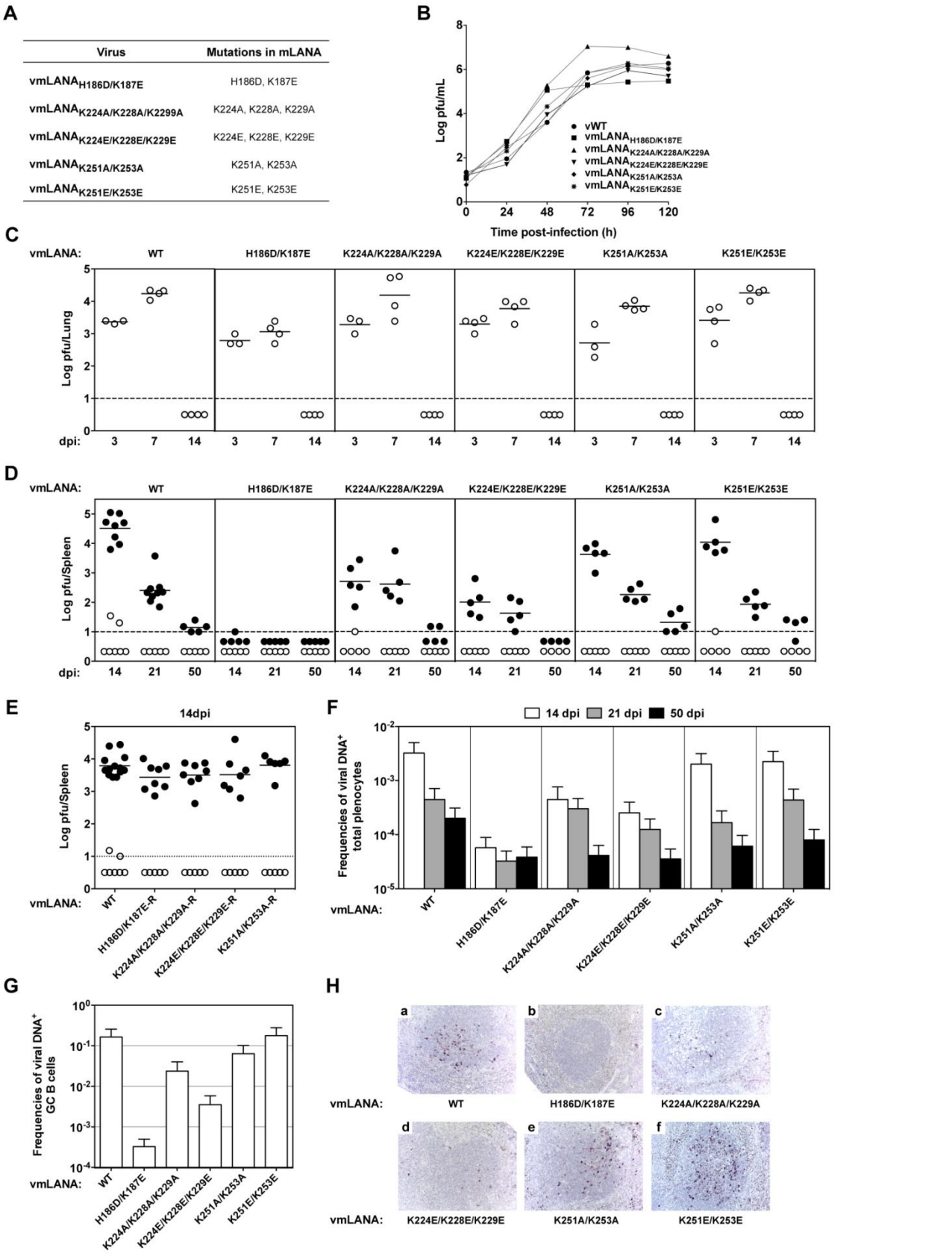

Figure 5. mLANA DNA binding is essential for virus persistence and the dorsal positive patch exerts a role in the expansion of GC B cells. (**A**) Amino acid substitutions in recombinant viruses (see also Figure S5). (**B**) Infection of BHK-21 cells at 0.01 p.f.u. per cell. Virus titres were determined by plaque assay. (**C**) Lungs from infected mice were removed and infectious viruses were titrated by plaque assay. (**D and E**) Quantification of latent infection in spleen by explant co-culture plaque assay (closed circles). Titres of infectious virus were determined in freeze/thawed splenocyte suspensions (open circles). Each circle represents the titre of an individual mouse. The dashed line represents the limit of detection of the assay. Mutant viruses are shown in panel D and revertant viruses in panel E. (**F and G**) Reciprocal frequencies of viral DNA-positive cells in total splenocytes (**F**) or GC B cells ($CD19^{+}CD95^{hi}GL7^{hi}$) (**G**) were determined by limiting dilution and real-time PCR. Data were obtained from pools of five spleens per group. Bars represent the frequency of viral DNA-positive cells with 95% confidence intervals. (**H**) Identification of latently infected cells in spleens by *in situ* hybridization. Representative splenic sections from each group of viruses are shown. All images are magnified ×200. Dark staining indicates cells positive for virally encoded miRNAs (see also Table 4).
doi:10.1371/journal.ppat.1003673.g005

Electrophoretic mobility shift assays

mLANA WT and mutants were in vitro-translated using TNT coupled Reticulocyte Systems (Promega # L4610) from pBS-mLANAc3F WT (Figure 3B), pBS mLANA H186D/K187E, pBS myc mLANAc3F wt (Figure 3C) and pBS mLANA K224A/K228/K229A, pBS mLANA K224E/K228/K229E, pBS mLANA K251A/K253A, or pBS mLANA K251E/K253E. mLBS probes were ^{32}P-labeled using Prime-It II (Agilent technology #300385). EMSAs were performed using 20,000 (panel B) or 30,000 (Figure 3C) cpm ^{32}P-labeled mLBS1, mLBS2, or control adjacent sequence, each also containing a GATC 5′ overhang. Probes were incubated 20 min. at RT with 5 to 10 µL of in vitro translated mLANA in EMSA buffer (20 mM Tris-HCl pH 7.5, 50 mM KCl, 10 mM MgCl2, 1 mM EDTA, 20 µg/mL polydI-dC [Amersham Bioscience #27-7880-02], 0.1 mM DTT and 10% glycerol). For competition controls, 50 fold excess unlabeled mLBS1, mLBS2, or mLBS1-2 were included in the incubation. To generate mLBS1-2 oligonucleotide, TATAATG-GATCCggcgccatgcgcccgcgcctggggcgccacgcggcg and TTATATG-GATccccgggtctccagggcgcgc-cgcgtggcgccccag primers were annealed and extended using Prime-It II kit (capital letters indicate additional non TR sequence). The resulting oligonucleotide was ligated into the EcoRV site of pBluescript. mLBS1-2 was then released after digestion with HindIII/XbaI and gel purified (Qiagen #28406). For the supershift, 1 µg anti-FLAG antibody (Sigma #F1804) was added to the reaction. Loading buffer (95% Formamide, 10 mM EDTA, 0.1% xylene cyanol and 0.1% bromophenol blue) was added to incubations prior to loading on a 3.5%/8% non-denaturing TBE-polyacrylamide gel. The gel was run in TBE buffer for 1 hour at 300 V and dried on Whatman paper before exposing to Kodak biomax MS film (Kodak #829 4985). *In vitro* translated mLANA wt and mutants were detected by

Table 4. Reciprocal frequency of MuHV-4 infection in total splenocytes and GC B-cells[a].

Cell subpopulation	Dpi	Virus	Reciprocal frequency[b] of viral DNA positive cells	
Total splenocytes	14	vWT	310	(198–707)
		$vmLANA_{H186D/K187E}$	17377	(11229–38406)
		$vmLANA_{K224A/K228A/K229A}$	2242	(1311–7712)
		$vmLANA_{K224E/K228E/K229E}$	3953	(2502–9373)
		$vmLANA_{K251A/K253A}$	499	(317–1170)
		$vmLANA_{K251E/K253E}$	448	(287–1019)
	21	vWT	2243	(1405–5545)
		$vmLANA_{H186D/K187E}$	30949	(20094–67314)
		$vmLANA_{K224A/K228A/K229A}$	3322	(2148–7334)
		$vmLANA_{K224E/K228A/K229E}$	7985	(5134–17955)
		$vmLANA_{K251A/K253A}$	5979	(3653–16461)
		$vmLANA_{K251E/K253E}$	2296	(1442–5630)
	50	vWT	4976	(3220–10952)
		$vmLANA_{H186D/K187E}$	24175	(15796–51478)
		$vmLANA_{K224A/K228A/K229A}$	28081	(18461–58638)
		$vmLANA_{K224E/K228E/K229E}$	16282	(10332–38380)
		$vmLANA_{K251A/K253A}$	12444	(8010–27880)
GC B-cells[c]	14	vWT	6	(4–14)
		$vmLANA_{H186D/K187E}$	3079	(2006–6619)
		$vmLANA_{K224A/K228A/K229A}$	30	(20–59)
		$vmLANA_{K224E/K228E/K229E}$	284	(171–841)
		$vmLANA_{K251A/K253A}$	16	(10–39)
		$vmLANA_{K251E/K253E}$	6	(4–13)

[a]Data were obtained from pools of at least five spleens. WT, wild type.
[b]Frequencies were calculated by limiting-dilution analysis with 95% confidence intervals (numbers in parentheses).
[c]The purity of sorted cells was determined by fluorescence-activated cell sorting (FACS) analysis, and was always greater 95%.
doi:10.1371/journal.ppat.1003673.t004

western blot. mLANA was resolved by 10% SDS-PAGE and after transfer to nitrocellulose membrane, the protein detected using monoclonal anti-mLANA (6A3) followed by HRP conjugated goat anti-mouse secondary antibody (Southern Biotech #1031-05).

SPR and ITC analysis

SPR binding experiments were performed on a BIACORE ×100 instrument (GE Healthcare) at 25°C. Single stranded DNA oligonucleotides, mLBS1 with an addition of five thymine's in the 5′ end as a spacer were annealed to its pair before injected over a streptavidin-coated sensor chip (SA chip, GE Healthcare) at 1 nM concentration at 10 µl min^{-1} up to 590 RU. A flow cell was left blank to allow background signal subtraction.

Purified recombinant $mLANA_{124–272}$ protein dilution series from higher to lower concentration were injected at a flow rate of 10–30 µL min^{-1} for 3 min and the regeneration of the binding surface was achieved by 4M NaCl. All the experiments were performed in duplicates. Data were processed using BiaEvaluation (GE Healthcare) and analyzed using SigmaPlot. The equilibrium dissociation constant, K_D, was determined by non-linear fitting of the data using a 1:1 Langmuir isotherm.

We further examined mLANA-DNA binding using ITC. Purified $mLANA\ protein_{124–314}$ and mLBS1 DNA (without biotin-TTTTT spacer) were dialyzed against 25 mM Na/K phosphate pH 7.0, 150 mM NaCl, and 5% glycerol. ITC titrations were performed with a MicroCal iTC200 Isothermal Titration Calorimeter (MicroCal) at 25°C. Protein and DNA absorbance were measured after dialysis by NanoDrop (NanoDrop Technologies) and their concentrations were determined with their respective extinction coefficients. Twenty-five injections of 1.5 µl each of 30 µM mLBS1 DNA were titrated into 8.5 µM protein solution. Data were corrected for nonspecific heats and analysed using MicroCal Origin 7.0 software using a one-site binding model. The experiments were performed in triplicate and showed similar results.

In vitro binding of mLANA and BRD4

BRD4, BRD4 1–470, 471–730, 731–1046, or 1047–1362 [41] were *in vitro* translated and labelled with [^{35}S]-methionine using TNT Coupled Reticulocyte Lysate System (Promega). mLANA K224A/K228A/K229A, mLANA K224E/K228E/K229E, mLANA K251A/K253A or mLANA K251E/K253E each were engineered to include three tandem C-terminal FLAG epitope tags and were in vitro translated from pBluescript. GST, GST-N-$mLANA_{1–168}$ or GST-C-$mLANA_{140–314}$ were expressed from pGEX-2T. GST mLANA 124–272, GST mLANA 124–272 H186D/K187E, GST mLANA 124–272 K224A/K228A/K229A, GST mLANA 124–272 K224E/K228E/K229E, GST mLANA 124–272 K251A/K253A and GST mLANA 124–272 K251E/K253E fusion proteins were expressed from pET-49. GST, GST mLANA or GST BRD4 [41] fusion proteins were expressed in BL21 (DE3) bacteria and collected on Glutathione Sepharose 4B (GE Healthcare) beads. GST fusion binding assays were performed as described [41]. Proteins were resolved by SDS-PAGE using 10% polyacrylamide, and transferred to nitrocellulose membrane. ^{35}S labelled BRD4 proteins were detected after exposure to film, KSHV LANAΔ33-888 [58] was detected with anti-T7•Tag antibody (Novagen), and mLANA was detected with anti-FLAG M2 antibody (Sigma).

Generation of recombinant viruses

MuHV-4 recombinant viruses were independently generated by mutagenesis of the viral genome cloned as a bacterial artificial chromosome (BAC) [59]. The point mutations were introduced by PCR on the mLANA gene cloned into pCMV-Myc. pCMV-Myc-mLANA was digested with HindIII and PciI or BstEII and PciI to isolate the fragment harbouring the desired mutations, which were inserted into the BamHI-G genomic clone. Recombinant BamHI-G mutant fragments were subcloned into the BamHI site of a pST76K-SR shuttle plasmid and transformed into an *Escherichia coli* strain (DH10B) containing the wild-type MuHV-4 BAC (pHA3). Following a multistep selection procedure, recombinant BAC clones were identified by DNA sequencing. To generate revertant viruses the wild type BamHI-G pST76K-SR shuttle plasmid was transformed into DH10B cells containing each of the mutant BAC genomes. The integrity of each BAC was confirmed by restriction digestion with BamHI and EcoRI. All viruses were reconstituted by transfection of BAC DNA into BHK-21 cells using X-tremeGENE HP (Roche). The *loxP*-flanked BAC cassette was removed by viral passage through NIH Cre 3T3 cells and limiting dilution to obtain GFP-negative viruses.

Analysis of recombinant viruses

We performed five independent animal infections, which were analyzed by five complementary experiments; *ex vivo* explant co-culture assays to measure virus latency in total splenocytes, flow cytometry coupled to limiting dilution and real-time PCR to quantify the frequency of viral DNA-positive in total splenocytes or to quantify GC B cells, and *in situ* hybridisation to identify virally infected cells within the spleen. *In situ* hybridisation for transcripts corresponding to the MHV-68-encoded miRNAs permits the detection of latently infected cells in splenic sections. Quantification of viral infection in GC B cells is highly relevant since mLANA is selectively expressed in proliferating GC B cells [25]. Revertant viruses were analysed at 14 days post-infection by *ex vivo* explant co-culture assay by three independent animal infections. C57BL/6 mice (Charles River, Spain) with 6–8 weeks of age were intranasally inoculated with 10^4 p.f.u. in 20 µl of PBS under isofluorane anaesthesia. At 3, 7, 14, 21 and 50 days post-infection, lungs or spleens were removed and processed for subsequent analysis. Infectious virus titers in freeze-thawed lung homogenates were determined by suspension assay using BHK-21 cells. Latent viruses were examined using explant co-cultures of single-cell suspension splenocytes with BHK-21 cells. Plates were incubated for 4 (suspension assay) or 5 days (co-culture assay), fixed with 10% formal saline and counterstained with toluidine blue. Viral plaques were counted with a plate microscope. Frequencies of virus-genome-positive cells were determined by limiting dilution combined with real-time PCR, as described earlier [25]. Total splenocytes suspensions were prepared from pools of five spleens. GC B-cell ($CD19^+CD95^{hi}GL7^{hi}$) populations were purified from pools of five spleens using a BD FACSAria Flow Cytometer (BD Biosciences). The purity of sorted populations was always >95%, as analysed by flow cytometry. Real-time PCR reactions were performed as reported [60]. To determine multistep growth curves, BHK-21 cells were infected with MuHV-4 recombinant viruses, at a low multiplicity of infection (0.01 p.f.u. per cell). After 1 hour of virus adsorption, cells were washed in PBS and at the indicated times post-infection virus titers were determined by plaque assay. p values were determined using ordinary one-way ANOVA (GraphPad Prism). *In situ* hybridisation was performed on formalin-fixed, paraffin-embedded splenic sessions using digoxigenin-labelled riboprobes, generated by T7 transcription of pEH1.4 [61]. *In situ* hybridisation for transcripts corresponding to the MHV-68-encoded miRNAs (encoded within pEH1.4) permits the detection of latently infected cells in splenic sessions, specifically within GC reactions.

Accession codes

mLANA DNA AF105037; Uniprot accession numbers for mLANA O41974 and kLANA Q76SB0; The atomic coordinates and structure factors have been deposited in the Protein Data Bank under accession number PDB ID: 4blg.

Supporting Information

Figure S1 Construct design of mLANA. (**A**) Schematic of mLANA truncations. (**B**) list of primer sequences used for cloning into the expression vector pET-49b(+); restriction enzyme sites are shown in bold (BamHI used in forward primers and NotI in reverse primers), extra bases to ensure the correct reading frame in red and stop codons are underlined. (**C**) Coomassie blue stained SDS-PAGE of GST-6XHis-mLANA constructs purified by Ni^{2+}-sepharose beads.
(TIF)

Figure S2 mLANA DBD homodimer analysis. (**A**) The residues that constitute the hydrophobic core and hydrogen-bonding network of the dimer interface are coloured by amino acid group. The interactions are composed of 83 non-bonded contacts (where the interaction distance is $\leq$3.9 Å) with only 7 direct hydrogen bonds involved. The figure was generated by PDBSUM. (**B**) Purified mLANA DBD truncations were analysed by size exclusion chromatography. The majority of the mLANA truncations elute as a dimer, however, the elution profile of $mLANA_{140–314}$ is consistent with a tetramer. (**C**) Biophysical characterization of mLANA protein truncations, showing the theoretical and calculated molecular weight (M_r) of each truncation. The calculated oligomerization state and protein stability profiles are also shown. Ve – elution volume, K_{av} - partition coefficient.
(TIF)

Figure S3 Sequence analysis of MHV-68 and KSHV LANA Binding Sites (LBS). KSHV LBS1 and LBS2 are highlighted in blue and orange (which includes the 16 bp core) and the putative MHV-68 DNA footprints underlined in green and red [24]. Several potential mLANA LBS DNA sequences tested for energy minimization and respective result values (z-score in brackets). Energy minimization for 3D structures of mLANA-DNA models was performed using YASARA.
(TIF)

Figure S4 Coomassie blue staining of BRD4 fusion proteins. GST, GST-BRD4 471–594 or GST-BRD4 595–730 proteins used for binding mLANA. Similar amounts of protein used in the mLANA binding assay are shown despite staining differently with Ponceau S in Figure 4, panel E.
(TIF)

Figure S5 Sequence comparison of the ventral and dorsal face of LANA, EBV EBNA1 and HPV6 E2 proteins. (**A**) Table comparing the key residues of mLANA involved in DNA interactions on the ventral face showing the equivalent residues in kLANA, E2 and EBNA1 proteins. (**B**) Table comparing the key residues that contribute to the contrasting electrostatic surfaces on the dorsal face of LANA, EBNA1 and E2 proteins.
(TIF)

Figure S6 The mLANA dimer binds cooperatively to mLBS1-2. (**A**) The elution profile of $mLANA_{140–272}$ dimer from size-exclusion chromatography (predicted size 31.8 kDa) in the absence of DNA. (**B**) The elution profile of $mLANA_{140–272}$ after incubation with mLBS1, (predicted size of $mLANA_{140–272}$ dimer-mLBS1 complex 49.4 kDa). (**C**) The elution profile of $mLANA_{140–272}$ after incubation with mLBS1-2, (predicted size of $mLANA_{140–272}$-mLBS1-2 complex 92.8 kDa). Samples were analysed on a Superdex 200 10/300 GL column. Peak fractions were analysed by SDS-PAGE (4–20% gradient gel) and stained for both protein (Coomassie blue) and mLBS DNA (Sybr Safe). SEC analysis confirms the binding of one $mLANA_{140–272}$ dimer to the mLBS1 site (estimated size 51.8 kDa, V_e 15.8 ml) and two $mLANA_{140–272}$ dimers to the mLBS1-2 sites (estimated size 93.6 kDa, V_e 13.9 ml). For panels B and C, the $A_{280\ nm}$ signal indicating protein is amplified due to the contribution of DNA in the complex, V_e is the sample elution volume and M represents protein standards (Supporting Information, Text S1).
(TIF)

Text S1 Supporting data including a supporting method and supporting results.
(DOCX)

Acknowledgments

Diffraction data were collected on EMBL beamline P14 at PETRA III (DESY, Germany) and we would like to thank Gleb Bourenkov for support with data collection.

Author Contributions

Conceived and designed the experiments: CEM JPS KMK MAC. Performed the experiments: BC CEM MPdM SAC RP TRS SL CB LR. Analyzed the data: BC CEM MPdM LR RP CB SL. Wrote the paper: CEM MAC KMK JPS MPdM SL CB LR. X-ray synchrotron data collection: TRS.

References

1. Simas JP, Efstathiou S (1998) Murine gammaherpesvirus 68: a model for the study of gammaherpesvirus pathogenesis. Trends Microbiol 6: 276–282.
2. Speck SH, Ganem D (2010) Viral latency and its regulation: lessons from the gamma-herpesviruses. Cell Host Microbe 8: 100–115.
3. Nash AA, Dutia BM, Stewart JP, Davison AJ (2001) Natural history of murine gamma-herpesvirus infection. Philos Trans R Soc Lond B Biol Sci 356: 569–579.
4. Cardin RD, Brooks JW, Sarawar SR, Doherty PC (1996) Progressive loss of CD8+ T cell-mediated control of a gamma-herpesvirus in the absence of CD4+ T cells. J Exp Med 184: 863–871.
5. Sunil-Chandra NP, Efstathiou S, Nash AA (1992) Murine gammaherpesvirus 68 establishes a latent infection in mouse B lymphocytes in vivo. J Gen Virol 73 (Pt 12): 3275–3279.
6. Flano E, Kim IJ, Woodland DL, Blackman MA (2002) Gamma-herpesvirus latency is preferentially maintained in splenic germinal center and memory B cells. J Exp Med 196: 1363–1372.
7. Thorley-Lawson DA (2001) Epstein-Barr virus: exploiting the immune system. Nat Rev Immunol 1: 75–82.
8. Ballestas ME, Kaye KM (2001) Kaposi's sarcoma-associated herpesvirus latency-associated nuclear antigen 1 mediates episome persistence through cis-acting terminal repeat (TR) sequence and specifically binds TR DNA. J Virol 75: 3250–3258.
9. Cotter MA, II, Subramanian C, Robertson ES (2001) The Kaposi's sarcoma-associated herpesvirus latency-associated nuclear antigen binds to specific sequences at the left end of the viral genome through its carboxy-terminus. Virology 291: 241–259.
10. Garber AC, Hu J, Renne R (2002) Latency-associated nuclear antigen (LANA) cooperatively binds to two sites within the terminal repeat, and both sites contribute to the ability of LANA to suppress transcription and to facilitate DNA replication. J Biol Chem 277: 27401–27411.
11. Hu J, Garber AC, Renne R (2002) The latency-associated nuclear antigen of Kaposi's sarcoma-associated herpesvirus supports latent DNA replication in dividing cells. J Virol 76: 11677–11687.
12. Komatsu T, Ballestas ME, Barbera AJ, Kelley-Clarke B, Kaye KM (2004) KSHV LANA1 binds DNA as an oligomer and residues N-terminal to the oligomerization domain are essential for DNA binding, replication, and episome persistence. Virology 319: 225–236.
13. Lim C, Sohn H, Lee D, Gwack Y, Choe J (2002) Functional dissection of latency-associated nuclear antigen 1 of Kaposi's sarcoma-associated herpesvirus

involved in latent DNA replication and transcription of terminal repeats of the viral genome. J Virol 76: 10320–10331.
14. Schwam DR, Luciano RL, Mahajan SS, Wong L, Wilson AC (2000) Carboxy terminus of human herpesvirus 8 latency-associated nuclear antigen mediates dimerization, transcriptional repression, and targeting to nuclear bodies. J Virol 74: 8532–8540.
15. Barbera AJ, Chodaparambil JV, Kelley-Clarke B, Joukov V, Walter JC, et al. (2006) The nucleosomal surface as a docking station for Kaposi's sarcoma herpesvirus LANA. Science 311: 856–861.
16. Ballestas ME, Chatis PA, Kaye KM (1999) Efficient persistence of extrachromosomal KSHV DNA mediated by latency-associated nuclear antigen. Science 284: 641–644.
17. Cotter MA, II, Robertson ES (1999) The latency-associated nuclear antigen tethers the Kaposi's sarcoma-associated herpesvirus genome to host chromosomes in body cavity-based lymphoma cells. Virology 264: 254–264.
18. Hung SC, Kang MS, Kieff E (2001) Maintenance of Epstein-Barr virus (EBV) oriP-based episomes requires EBV-encoded nuclear antigen-1 chromosome-binding domains, which can be replaced by high-mobility group-I or histone H1. Proc Natl Acad Sci U S A 98: 1865–1870.
19. Ilves I, Kivi S, Ustav M (1999) Long-term episomal maintenance of bovine papillomavirus type 1 plasmids is determined by attachment to host chromosomes, which Is mediated by the viral E2 protein and its binding sites. J Virol 73: 4404–4412.
20. Lehman CW, Botchan MR (1998) Segregation of viral plasmids depends on tethering to chromosomes and is regulated by phosphorylation. Proc Natl Acad Sci U S A 95: 4338–4343.
21. Yates JL, Warren N, Sugden B (1985) Stable replication of plasmids derived from Epstein-Barr virus in various mammalian cells. Nature 313: 812–815.
22. Bastien N, McBride AA (2000) Interaction of the papillomavirus E2 protein with mitotic chromosomes. Virology 270: 124–134.
23. Habison AC, Beauchemin C, Simas JP, Usherwood EJ, Kaye KM (2012) Murine Gammaherpesvirus 68 LANA Acts on Terminal Repeat DNA To Mediate Episome Persistence. J Virol 86: 11863–11876.
24. Paden CR, Forrest JC, Tibbetts SA, Speck SH (2012) Unbiased Mutagenesis of MHV68 LANA Reveals a DNA-Binding Domain Required for LANA Function In Vitro and In Vivo. PLoS Pathog 8: e1002906.
25. Marques S, Efstathiou S, Smith KG, Haury M, Simas JP (2003) Selective gene expression of latent murine gammaherpesvirus 68 in B lymphocytes. J Virol 77: 7308–7318.
26. Fowler P, Marques S, Simas JP, Efstathiou S (2003) ORF73 of murine herpesvirus-68 is critical for the establishment and maintenance of latency. J Gen Virol 84: 3405–3416.
27. Moorman NJ, Willer DO, Speck SH (2003) The gammaherpesvirus 68 latency-associated nuclear antigen homolog is critical for the establishment of splenic latency. J Virol 77: 10295–10303.
28. An FQ, Compitello N, Horwitz E, Sramkoski M, Knudsen ES, et al. (2005) The latency-associated nuclear antigen of Kaposi's sarcoma-associated herpesvirus modulates cellular gene expression and protects lymphoid cells from p16 INK4A-induced cell cycle arrest. J Biol Chem 280: 3862–3874.
29. Shamay M, Krithivas A, Zhang J, Hayward SD (2006) Recruitment of the de novo DNA methyltransferase Dnmt3a by Kaposi's sarcoma-associated herpesvirus LANA. Proc Natl Acad Sci U S A 103: 14554–14559.
30. Cai QL, Knight JS, Verma SC, Zald P, Robertson ES (2006) EC5S ubiquitin complex is recruited by KSHV latent antigen LANA for degradation of the VHL and p53 tumor suppressors. PLoS Pathog 2: e116.
31. Rodrigues L, Filipe J, Seldon MP, Fonseca L, Anrather J, et al. (2009) Termination of NF-kappaB activity through a gammaherpesvirus protein that assembles an EC5S ubiquitin-ligase. EMBO J 28: 1283–1295.
32. Li X, Liang D, Lin X, Robertson ES, Lan K (2011) Kaposi's sarcoma-associated herpesvirus-encoded latency-associated nuclear antigen reduces interleukin-8 expression in endothelial cells and impairs neutrophil chemotaxis by degrading nuclear p65. J Virol 85: 8606–8615.
33. Ottinger M, Christalla T, Nathan K, Brinkmann MM, Viejo-Borbolla A, et al. (2006) Kaposi's sarcoma-associated herpesvirus LANA-1 interacts with the short variant of BRD4 and releases cells from a BRD4- and BRD2/RING3-induced G1 cell cycle arrest. J Virol 80: 10772–10786.
34. Ottinger M, Pliquet D, Christalla T, Frank R, Stewart JP, et al. (2009) The interaction of the gammaherpesvirus 68 orf73 protein with cellular BET proteins affects the activation of cell cycle promoters. J Virol 83: 4423–4434.
35. Grundhoff A, Ganem D (2003) The latency-associated nuclear antigen of Kaposi's sarcoma-associated herpesvirus permits replication of terminal repeat-containing plasmids. J Virol 77: 2779–2783.
36. Bochkarev A, Barwell JA, Pfuetzner RA, Furey W, Jr., Edwards AM, et al. (1995) Crystal structure of the DNA-binding domain of the Epstein-Barr virus origin-binding protein EBNA 1. Cell 83: 39–46.
37. Dell G, Wilkinson KW, Tranter R, Parish J, Leo Brady R, et al. (2003) Comparison of the structure and DNA-binding properties of the E2 proteins from an oncogenic and a non-oncogenic human papillomavirus. J Mol Biol 334: 979–991.
38. Reisman D, Yates J, Sugden B (1985) A putative origin of replication of plasmids derived from Epstein-Barr virus is composed of two cis-acting components. Mol Cell Biol 5: 1822–1832.
39. Han SJ, Hu J, Pierce B, Weng Z, Renne R (2010) Mutational analysis of the latency-associated nuclear antigen DNA-binding domain of Kaposi's sarcoma-associated herpesvirus reveals structural conservation among gammaherpesvirus origin-binding proteins. J Gen Virol 91: 2203–2215.
40. Kelley LA, Sternberg MJ (2009) Protein structure prediction on the Web: a case study using the Phyre server. Nat Protoc 4: 363–371.
41. You J, Srinivasan V, Denis GV, Harrington WJ, Jr., Ballestas ME, et al. (2006) Kaposi's sarcoma-associated herpesvirus latency-associated nuclear antigen interacts with bromodomain protein Brd4 on host mitotic chromosomes. J Virol 80: 8909–8919.
42. Kelley-Clarke B, De Leon-Vazquez E, Slain K, Barbera AJ, Kaye KM (2009) Role of Kaposi's sarcoma-associated herpesvirus C-terminal LANA chromosome binding in episome persistence. J Virol 83: 4326–4337.
43. Kelley-Clarke B, Ballestas ME, Srinivasan V, Barbera AJ, Komatsu T, et al. (2007) Determination of Kaposi's sarcoma-associated herpesvirus C-terminal latency-associated nuclear antigen residues mediating chromosome association and DNA binding. J Virol 81: 4348–4356.
44. Stebbins CE, Kaelin WG, Jr., Pavletich NP (1999) Structure of the VHL-ElonginC-ElonginB complex: implications for VHL tumor suppressor function. Science 284: 455–461.
45. Stanley BJ, Ehrlich ES, Short L, Yu Y, Xiao Z, et al. (2008) Structural insight into the human immunodeficiency virus Vif SOCS box and its role in human E3 ubiquitin ligase assembly. J Virol 82: 8656–8663.
46. Lin A, Wang S, Nguyen T, Shire K, Frappier L (2008) The EBNA1 protein of Epstein-Barr virus functionally interacts with Brd4. J Virol 82: 12009–12019.
47. Baxter MK, McPhillips MG, Ozato K, McBride AA (2005) The mitotic chromosome binding activity of the papillomavirus E2 protein correlates with interaction with the cellular chromosomal protein, Brd4. J Virol 79: 4806–4818.
48. Kabsch W (2010) Xds. Acta Crystallogr D Biol Crystallogr 66: 125–132.
49. Evans P (2006) Scaling and assessment of data quality. Acta Crystallogr D Biol Crystallogr 62: 72–82.
50. McCoy AJ, Grosse-Kunstleve RW, Adams PD, Winn MD, Storoni LC, et al. (2007) Phaser crystallographic software. J Appl Crystallogr 40: 658–674.
51. Adams PD, Afonine PV, Bunkoczi G, Chen VB, Davis IW, et al. (2010) PHENIX: a comprehensive Python-based system for macromolecular structure solution. Acta Crystallogr D Biol Crystallogr 66: 213–221.
52. Emsley P, Cowtan K (2004) Coot: model-building tools for molecular graphics. Acta Crystallogr D Biol Crystallogr 60: 2126–2132.
53. Chen VB, Arendall WB, . (2010) MolProbity: all-atom structure validation for macromolecular crystallography. Acta Crystallogr D Biol Crystallogr 66: 12–21.
54. Krissinel E, Henrick K (2007) Inference of macromolecular assemblies from crystalline state. J Mol Biol 372: 774–797.
55. Krieger E, Joo K, Lee J, Raman S, Thompson J, et al. (2009) Improving physical realism, stereochemistry, and side-chain accuracy in homology modeling: Four approaches that performed well in CASP8. Proteins 77 Suppl 9: 114–122.
56. Schrödinger, LLC (2010) The PyMOL Molecular Graphics System, Version 1.5.0.3.
57. McNicholas S, Potterton E, Wilson KS, Noble ME (2011) Presenting your structures: the CCP4mg molecular-graphics software. Acta Crystallogr D Biol Crystallogr 67: 386–394.
58. De Leon Vazquez E, Kaye KM (2011) The internal Kaposi's sarcoma-associated herpesvirus LANA regions exert a critical role on episome persistence. J Virol 85: 7622–7633.
59. Adler H, Messerle M, Wagner M, Koszinowski UH (2000) Cloning and mutagenesis of the murine gammaherpesvirus 68 genome as an infectious bacterial artificial chromosome. J Virol 74: 6964–6974.
60. Pires de Miranda M, Alenquer M, Marques S, Rodrigues L, Lopes F, et al. (2008) The Gammaherpesvirus m2 protein manipulates the Fyn/Vav pathway through a multidocking mechanism of assembly. PLoS One 3: e1654.
61. Simas JP, Bowden RJ, Paige V, Efstathiou S (1998) Four tRNA-like sequences and a serpin homologue encoded by murine gammaherpesvirus 68 are dispensable for lytic replication in vitro and latency in vivo. J Gen Virol 79 (Pt 1): 149–153.
62. Wu SY, Chiang CM (2007) The double bromodomain-containing chromatin adaptor Brd4 and transcriptional regulation. J Biol Chem 282: 13141–13145.
63. Belkina AC, Denis GV (2012) BET domain co-regulators in obesity, inflammation and cancer. Nat Rev Cancer 12: 465–477.

APPENDIX 2

LANA E3 Ubiquitin-Ligase Activity Impacts Gammaherpesvirus Latent Infection

Sofia A. Cerqueira[1¶], Min Tan[2¶], Shijun Li[2], Franceline Juillard[2], Colin E. McVey[3], Kenneth M. Kaye[2&*], J. Pedro Simas[1&*]

[1] Instituto de Medicina Molecular, Faculdade de Medicina, Universidade de Lisboa, Lisboa, Portugal

[2] Departments of Medicine, Brigham and Women's Hospital and Harvard Medical School, Boston, Massachusetts, United States of America

[3] Instituto de Tecnologia Química e Biológica, Universidade Nova de Lisboa, Oeiras, Portugal

[*] Corresponding authors

E-mail: kkaye@bwh.harvard.edu (KMK); psimas@medicina.ulisboa.pt (JPS)

[¶]These authors contributed equally to this work.

[&]These authors also contributed equally to this work.

Running title: mLANA E3 Ligase Activity Impacts Latency

Abstract

Viruses have evolved mechanisms to hijack components of cellular E3 ubiquitin-ligases, thus modulating the ubiquitination pathway. However, the biological relevance of such mechanisms for viral pathogenesis *in vivo* remains largely unknown. Here, we use murid herpesvirus-4 (MuHV-4) infection of mice as a model system to address the role of latency-associated nuclear antigen (mLANA) E3 ligase activity in gammaherpesvirus latent infection. We show that specific mutations in the mLANA SOCS-box (V199A, V199A/L202A or P203A/P206A) disrupted mLANA's ability to recruit ElonginC and Cullin5, thereby impairing the formation of the EC_5S^{mLANA} complex and mLANA's E3 ligase activity on host NF-κB and Myc. Although these mutations resulted in considerably reduced binding to viral terminal repeat DNA as assessed by EMSA, the mutations did not disrupt mLANA's ability to mediate episome persistence. *In vivo*, MuHV-4 recombinant viruses bearing these mLANA SOCS-box mutations exhibited reduced numbers of latently infected B cells. These findings demonstrate that the E3 ligase activity of mLANA contributes to gammaherpesvirus latency expansion *in vivo*. Hence, pharmacological inhibition of viral E3 ligase activity through targeting SOCS-box motifs is a putative strategy to control gammaherpesvirus-driven lymphoproliferation.

Author Summary

The gammaherpesviruses (γHVs) Epstein-Barr virus (EBV) and Kaposi´s sarcoma-associated herpesvirus (KSHV) cause life-long persistent infection and exert causative roles in several human malignancies. Colonization of B cells is crucial for virus persistence, and access to the B cell compartment is felt to be gained by virus-driven proliferation in germinal center (GC) B cells. Hence, identification of viral proteins with functions that are vital for infection in GC B cells is key to elucidate the mechanisms underlying these infections. Infection of B cells is predominantly latent, with the viral genome persisting as a multi-copy episome, and expressing only a small subset of viral genes. Here, we focused on the latency-associated nuclear antigen (mLANA) encoded by murid herpesvirus-4 (MuHV-4), which exhibits homology in sequence, structure and function to KSHV LANA (kLANA), thereby allowing the study of LANA pathogenesis in the mouse. Our experiments show that mLANA's E3 ubiquitin-ligase activity is necessary for efficient expansion of latent infection in B cells. This finding suggests that the development of pharmacological inhibitors of LANA E3 ubiquitin-ligase activity may allow strategies to interfere with γHV-driven lymphoproliferation and persistent infection.

Introduction

As obligatory intracellular parasites, viruses have evolved mechanisms to modulate ubiquitination, which is an essential regulatory mechanism in eukaryotes, controlling a wide range of cellular pathways. Ubiquitination occurs through a three-enzyme cascade, involving an E1 ubiquitin-activating enzyme, an E2 ubiquitin-conjugating enzyme and an E3 ubiquitin-ligase enzyme [1]. E3 ligases bind to the

E2~ubiquitin intermediate and the substrate, catalyzing the transfer of ubiquitin to the substrate target lysine. Many E3 ligases have been described such as Cullin5-RING E3 ligases (CRL5), also known as ElonginBC/Cullin5/SOCS (EC_5S) E3 ligases. These are multisubunit complexes containing a scaffold protein (Cullin5) attached to a RING finger protein (Rbx) (Cullin5-Rbx module), an adaptor heterodimer (ElonginB/C), and a substrate recognition protein [suppressor of cytokine signaling (SOCS)-box protein]. The latter component bridges the substrate of ubiquitination to the E3 ligase complex, by interacting with ElonginB/C and Cullin5 through a SOCS-box motif [2-4]. Certain viruses encode proteins with SOCS-box motifs to hijack the components of cellular E3 ligases, thus modulating the ubiquitination pathway. Examples include latency-associated nuclear antigen (LANA) of Kaposi's sarcoma-associated herpesvirus (KSHV) [5, 6] and murid herpesvirus-4 (MuHV-4) [7, 8], BZLF1 of Epstein-Barr virus (EBV) [9], Vif of human immunodeficiency virus-1 (HIV-1) [10-12] and E4orf6/E1B55K of adenovirus [13]. Several studies have shown that these viral proteins target multiple cellular substrates for poly-ubiquitination. However, determining the relevance of a viral protein acting as a SOCS protein and exhibiting E3 ligase activity within the physiological context of viral pathogenesis *in vivo* remains a challenge.

In this study, we used MuHV-4, a gammaherpesvirus that is genetically related to the human virus KSHV and which readily infects laboratory mice, thus providing a model to study gammaherpesvirus pathogenesis *in vivo* [14]. Gammaherpesviruses infect a variety of mammalian species and are associated with lymphoproliferative disease and several tumors [14]. These viruses induce proliferation of latently infected B cells in germinal center (GC) reactions to expand latency and to gain access to memory B cells, the major reservoir of gammaherpesvirus latency [15-17]. Therefore, gammaherpesviruses establish life-long latent infections in the host, during which the viral DNA genome persists as a multi-copy, circularized, extrachromosomal episome [18]. During latent infection, only a small subset of viral genes is expressed, including *ORF73* [19, 20]. LANA, the product of *ORF73*, mediates viral episome maintenance by binding to terminal repeat (TR) DNA sequences of the viral episome and tethering the viral genome to mitotic chromosomes, thus ensuring segregation of the episome to daughter nuclei [21-23]. LANA is also known as a modulator of cellular transcription, including through E3 ligase activity [5-8]. MuHV-4 LANA protein (mLANA) exhibits homology in sequence, structure and function to KSHV LANA (kLANA), thereby allowing the study of LANA pathogenesis in the mouse [23-26]. mLANA assembles an E3 ligase complex (EC_5S^{mLANA}) by recruiting ElonginB/C and Cullin5, through an unconventional SOCS-box motif (amino acid residues 199-206) present in mLANA C-terminal domain [7]. mLANA also acts as the substrate recognition component of the EC_5S^{mLANA} complex, interacting with cellular substrates through motifs independent of the SOCS-box, as yet unidentified [7, 8]. Two cellular targets of mLANA E3 ligase activity are known: NF-κB and Myc. mLANA mediates poly-ubiquitination-dependent proteasomal degradation of the NF-κB family member p65, thus inhibiting NF-κB transcriptional activity [7]. In contrast, mLANA stabilizes Myc through heterotypic poly-ubiquitination, thus increasing Myc transcriptional activity and promoting virus-driven lymphoproliferation [8]. To clarify the contribution of mLANA E3 ligase activity for latent infection, we generated MuHV-4 recombinant viruses bearing mutations in mLANA SOCS-box which impaired E3 ligase activity without compromising episome

maintenance function, using structure-based [25] design. Our results provide evidence that the E3 ligase activity of mLANA protein contributes to gammaherpesvirus latency expansion. This study is novel in assessing the impact of an E3 ubiquitin-ligase complex assembly by a gammaherpesvirus protein in the context of latency *in vivo*.

Results

Extensive mutation of the mLANA SOCS-box abolishes DNA binding and episome persistence

We have previously shown that the mLANA-SOCS mutant, with mutations at the base of β2-β3 loop (^{199}VSCLPLVP^{206}, underlined residues mutated to alanine), fails to bind ElonginC, resulting in disruption of mLANA E3 ligase activity [7]. A recombinant MuHV-4 virus containing these mutations (vSOCS) exhibits a severe latency deficit, and is unable to expand in GC B cells or persist in mice. Subsequent to the publication of this work, mLANA was demonstrated to bind mTR DNA to mediate MuHV-4 episome maintenance [23], and the structure of the mLANA DNA binding domain (DBD) was solved [25, 26]. Notably, the structure revealed that the mLANA SOCS-box lies within a loop (β2-β3 loop, residues 199-215), which protrudes perpendicularly to the DNA binding interface [25] (Fig. 1A), raising the possibility that the four mLANA-SOCS mutations (V199A, L202A, P203A and P206A) [7] might interfere with mLANA DNA binding. Therefore, we assessed the mLANA-SOCS mutant for the ability to bind mTR DNA.

Fig. 1. The effect of SOCS motif mutations on mLANA TR DNA binding. (A) Structural model of the mLANA DNA binding domain complexed with DNA (using mLBS1 DNA docked onto the 18 bp EBNA1 DNA recognition sequence followed by energy minimisation using YASARA [25]). V199, L202, P203 and P206 are highlighted in stick representation coloured yellow. The left view is rotated 180° about the x axis, and +45° about the y axis relative to the view on the right. (B & C) ^{32}P-labeled (B) mLBS1 or (C) mLBS1-2 oligonucleotides were incubated with *in vitro*-translated mLANA or mLANA mutants and complexes detected after resolution by gel electrophoresis. Longer exposure is shown at right. (D) Anti-FLAG Western blot of *in vitro* translated mLANA used in EMSAs. IB, immunoblot.

We used electrophoretic mobility shift assays (EMSAs) to assess mLANA DNA binding. Each mTR contains two adjacent DNA binding sites: mLBS1, a high affinity site, and mLBS2, a low affinity site, to which mLANA cooperatively binds. As expected, after incubation with mLBS1 or mLBS1-2 probe, *in vitro* translated mLANA generated shifted complexes that were absent in the control reticulocyte lysate. LBS1 formed a single complex with mLANA, while LBS1-2 formed two complexes. The faster migrating mLBS1-2 "lower" band (Fig. 1C, L) is due to occupation of only the LBS1 site, while the slower migrating "upper" band (Fig. 1C, U), detected in mLANA mLBS1-2 (but not mLBS1) incubations, is due to mLANA occupation of both LBS1 and LBS2 binding sites. The LBS1 and LBS1-2 complexes were effectively competed with excess, unlabeled competitor mLBS1, and were supershifted with anti-FLAG antibody which binds to the C-terminal mLANA epitope tag (Fig. 1B and C). In contrast, mLANA-SOCS did not form a shifted complex with mLBS1 or mLBS1-2 probe, consistent with loss of the ability to bind

mTR DNA (Fig. 1B and C). The absence of DNA binding was not due to insufficient mLANA-SOCS protein as mLANA-SOCS was expressed at a similar level to mLANA (Fig. 1D). Since mLANA DNA binding is required for episome maintenance function, this result suggested that mLANA-SOCS may be deficient for episome maintenance.

Therefore, we assessed mLANA-SOCS for the ability to mediate episome persistence. mLANA-SOCS-m4TR contains mLANA-SOCS and four mTR elements. mLANA acts on mTR elements to mediate episome persistence. Mouse embryonic fibroblasts (MEF) cells were seeded in tissue culture dishes and transfected with mLANA-m4TR, mLANA-SOCS-m4TR, or m4TR. Transfected cell were placed under G418-selection, for which resistance is encoded by the plasmid vector. Greater than 100 G418-resistant colonies grew out in the mLANA-m4TR dish and eleven of these were independently expanded. In contrast, only ~20-30 G418-resistant colonies grew out and could be expanded from the m4TR transfected MEF cells. The lower rate of G418-resistant outgrowth of the m4TR transfected cells compared to the mLANA-m4TR transfected cells is consistent with the need for mTR integration to persist, which is generally an uncommon event compared to episome persistence. Notably, only five mLANA-SOCS-4TR G418-resistant colonies grew out. The low mLANA-SOCS-4TR G418 outgrowth was consistent with deficiency in mLANA-SOCS ability to mediate episome persistence.

G418-resistant cell lines were expanded and assessed for the presence of episomes by Gardella gel analysis. In a Gardella gel, episomes as large as several hundred kb migrate into the gel whereas cellular DNA remains at the gel origin [27]. As expected, m4TR cell lines, which lack mLANA, did not contain episomes (Fig. 2A). In contrast, ten of eleven (91%) mLANA-4TR cell lines contained episomal DNA. None of the five mLANA-SOCS-4TR cell lines contained episomes (Fig. 2A). The absence of episomal DNA was not due to lack of protein expression since all mLANA-SOCS-m4TR cell lines expressed mLANA-SOCS (Fig. 2B). Therefore, mLANA-SOCS is abolished for the ability to mediate episome persistence.

Fig. 2. mLANA-SOCS is abolished for episome persistence. (A & B) MEF cells were transfected with mLANA-m4TR, SOCS-m4TR or m4TR. Forty-eight hours later, cells were trypsinized, re-seeded into 15-cm dishes and placed under G418 selection. G418-resistant colonies were picked and expanded. (A) Gardella gel containing G418-resistant MEF cells transfected with mLANA-m4TR (lanes 1 to 11), mLANA SOCS-m4TR (lanes 12 to 17) or m4TR (lanes 18 to 20). ~2×10^6 cells were loaded per lane. Input plasmid mLANA-4mTR, mLANA-SOCS-m4TR or m4TR DNA are in the lanes at left. O, gel origin. (B) Western blot of mLANA and tubulin for cells in panel (A). Letters above lanes correspond to the lower case letters in panel (A). IB, immunoblot.

We also assessed mLANA distribution within cells. In mLANA-m4TR episome containing cells, mLANA (green) concentrated to dots along mitotic chromosomes (red) and in the nuclei of interphase cells (overlay of green and red generates yellow) (Fig. 3). LANA dots are a result of mLANA concentration at sites of episomes. In contrast, mLANA-SOCS-4TR (green) distributed broadly over mitotic chromosomes, and within interphase nuclei (Fig. 3), consistent with an absence of episomes.

Fig. 3. Distribution of mLANA or mLANA mutants in interphase and mitosis. mLANA-m4TR or mLANA-m4TR containing SOCS-box mutations stably expressed in MEF cells was detected in interphase or metaphase. mLANA or mLANA mutants (green) was detected with antibody directed against the mLANA C-terminal FLAG epitope. DNA was counterstained with propidium iodide (red). The overlay of green and red results in yellow. Brightness and contrast were uniformly adjusted for some panels from the same field with Adobe Photoshop. Magnification, ×630.

Altogether, these results demonstrate that the mutations introduced in the mLANA-SOCS mutant compromised not only mLANA E3 ligase activity, but also its ability to bind mTR DNA and to mediate episome maintenance. Given the central role of mLANA episome persistence for viral latency expansion in GC B cells and virus persistence in mice [25], the severe latency deficit of vSOCS recombinant virus cannot exclusively be attributed to the loss of mLANA E3 ligase activity.

$mLANA_{V199A}$, $mLANA_{V199A/L202A}$ and $mLANA_{P203A/P206A}$ mutants exhibit impaired E3 ubiquitin-ligase activity

Taking into account the finding that mLANA-SOCS mutant did not mediate episome persistence, the contribution of mLANA E3 ligase activity for latent infection remains to be clarified. To this end, we proposed to identify mutations in mLANA SOCS-box which abolished E3 ligase activity without compromising episome maintenance function, using a structure-based [25] approach. The mLANA-SOCS mutant contained four mutations: V199A, L202A, P203A and P206A [7]. To minimize the interference with the DNA binding interface, we generated six mLANA constructs containing different combinations of these mutations: $mLANA_{V199A}$, $mLANA_{L202A}$, $mLANA_{V199A/L202A}$, $mLANA_{P203A}$, $mLANA_{P206A}$ and $mLANA_{P203A/P206A}$.

To evaluate E3 ligase activity of mLANA mutants towards NF-κB and Myc, reporter gene assays were performed. HEK 293T cells were transiently transfected with a NF-κB or Myc reporter plasmid containing tandem copies of κB or E-box consensus sequences (respectively) regulating the expression of luciferase, and a plasmid encoding mLANA (WT or mutants). TNF was used as a stimulus leading to NF-κB activation. These experiments revealed that $mLANA_{V199A}$, $mLANA_{V199A/L202A}$ and $mLANA_{P203A/P206A}$ mutants had impaired ability to both inhibit TNF-driven NF-κB activation (Fig. 4A) and to increase MYC transcriptional activity (Fig. 4B). In contrast, $mLANA_{L202A}$, $mLANA_{P203A}$ and $mLANA_{P206A}$ mutants behaved similarly to mLANA-WT, inhibiting NF-κB (Fig. 4A) and promoting MYC (Fig. 4B) transcriptional activities. Taken together, these data show that mutations at residues V199, V199/L202 and P203/P206 compromise E3 ligase activity of mLANA, turning them into good candidates to study mLANA E3 ligase function *in vivo*.

Fig. 4. $mLANA_{V199A}$, $mLANA_{V199A/L202A}$ and $mLANA_{P203A/P206A}$ exhibit impaired ability to inhibit NF-κB and activate Myc transcriptional activities. (A & B) HEK 293T cells were transiently transfected with a NF-κB (A) or Myc (B) luciferase reporter vector and a plasmid encoding mLANA (WT or mutants), as indicated at the bottom. In (A), transfected cells were either stimulated with 50 ng/ml of TNF (filled bars) or left unstimulated (open bars). NF-κB (A) and Myc (B) transcriptional activities associated with each sample were assayed using a luminometer.

Results are shown as the fold induction relative to luciferase activity measured in unstimulated cells (A) or in cells that did not express mLANA (B). Error bars represent SEM from triplicates from two independent transfection experiments. (C & D) HEK 293T cells were transiently transfected with plasmids encoding mLANA (WT or mutants), p65 (C) or Myc (D) and histidine-tagged ubiquitin, as indicated on top. After 48 h, total cellular lysates were subjected to a Ni-NTA pull-down, allowing the purification of ubiquitinated proteins. The levels of ubiquitinated p65 (C) or Myc (D) in each condition were assayed using an anti-p65 or anti-Myc antibody (first panel), respectively. Representative aliquots of the total cellular lysates were used to detect the appropriate expression of p65 (C) or Myc (D) (second panel) and mLANA (third panel). Graphs at the bottom show densitometry analysis of ubiquitinated p65 (C) and ubiquitinated Myc (D) levels present in each experimental condition, expressed as fold induction relative to cells not expressing mLANA. -, without; +, with; PD, pull-down; TCL, total cellular lysates; Ub, ubiquitinated.

mLANA targets nuclear p65 for poly-ubiquitination and subsequent proteasomal degradation, leading to a down-modulation of NF-κB transcriptional activity [7]. In contrast, mLANA stabilizes Myc through heterotypic poly-ubiquitination, thus promoting Myc transcriptional activity [8]. Therefore, we investigated if the impaired ability of mLANA mutants to modulate NF-κB and Myc was dependent on poly-ubiquitination. With this objective, we performed poly-ubiquitination assays, in which ubiquitinated proteins were pulled-down using nickel-nitrilotriacetic acid (Ni-NTA) agarose beads, in the presence of histidine-tagged ubiquitin. The levels of ubiquitinated p65 and Myc present in each condition were then analyzed by Western blot. We observed that $mLANA_{V199A}$, $mLANA_{V199A/L202A}$ and $mLANA_{P203A/P206A}$ mutants had diminished capability to promote both p65 and Myc poly-ubiquitination, whereas $mLANA_{L202A}$, $mLANA_{P203A}$ and $mLANA_{P206A}$ enhanced p65 and Myc poly-ubiquitination as efficiently as mLANA-WT (Fig. 4C and D). These data demonstrate that the defective modulation of NF-κB and Myc transcriptional activities observed for $mLANA_{V199A}$, $mLANA_{V199A/L202A}$ and $mLANA_{P203A/P206A}$ mutants can be attributed to inefficient substrate poly-ubiquitination mediated by these mutants.

Next, we investigated poly-ubiquitination activity of mLANA mutants on the basis of reconstitution of an E3 ubiquitin-ligase complex. To this end, we tested the ability of mLANA mutants to associate with ElonginC and Cullin5, which are part of the EC_5S^{mLANA} E3 ligase complex [7]. Immunoprecipitation experiments revealed that $mLANA_{V199A}$, $mLANA_{V199A/L202A}$ and $mLANA_{P203A/P206A}$ mutants were unable to recruit ElonginC and weakly associated with Cullin5, whereas $mLANA_{L202A}$, $mLANA_{P203A}$ and $mLANA_{P206A}$ efficiently recruited both ElonginC and Cullin5 (Fig. 5A and B). These results demonstrate that $mLANA_{V199A}$, $mLANA_{V199A/L202A}$ and $mLANA_{P203A/P206A}$ mutants have impaired ability to assemble an E3 ligase complex, thus compromising their poly-ubiquitination activity towards p65 and Myc.

Fig. 5. $mLANA_{V199A}$, $mLANA_{V199A/L202A}$ and $mLANA_{P203A/P206A}$ are unable to recruit ElonginC and weakly associate with Cullin5. (A & B) HEK 293T cells were transiently transfected with plasmids encoding mLANA (WT or mutants) and ElonginC (A) or Cullin5 (B), as indicated on top. After 48 h, cells were lysed and total cellular lysates were subjected to immunoprecipitation using an anti-ElonginC (A) or anti-Cullin5 (B) antibody. Immunoprecipitates were analyzed by Western blot (first and second panels). Representative aliquots of the total

cellular lysates were used to detect the appropriate expression of mLANA (third panel). -, without; +, with; α, anti; IP, immunoprecipitation; TCL, total cellular lysates; EloC, ElonginC; Cul5, Cullin5.

Taken together, the data obtained demonstrate that mutations at residues V199, V199/L202 or P203/P206 disrupt recruitment of ElonginC and, to a lesser extent, Cullin5, thus impairing the formation of EC_5S^{mLANA} E3 ligase complex and, consequently, mLANA function as a mediator of p65 and Myc poly-ubiquitination. Hence, these mutations impair mLANA E3 ligase activity, which impacts its ability to modulate NF-κB and Myc transcriptional activities.

$mLANA_{V199A}$ and $mLANA_{P203A/P206A}$, but not $mLANA_{V199A/L202A}$, mediate episome persistence

Since $mLANA_{V199A}$, $mLANA_{V199A/L202A}$ and $mLANA_{P203A/P206A}$ mutants were deficient for E3 ligase activity, we assessed their ability to bind mTR DNA by EMSA. $mLANA_{L202A}$, $mLANA_{P203A}$ and $mLANA_{P206A}$, which retained E3 ligase activity, were also assessed. $mLANA_{P202A}$ and $mLANA_{P206A}$ bound mLBS1 or mLBS1-2 probes similar to mLANA (Fig. 1B and C), while $mLANA_{P203A}$ was modestly reduced in its ability to bind mLBS1 or mLBS1-2. $mLANA_{V199A}$, which has an alanine substitution of the SOCS loop residue that is closest to the predicted mLANA DNA binding surface (Fig. 1A), and $mLANA_{P203A/P206A}$ were both substantially reduced for binding to mLBS1 or mLBS1-2 (Fig. 1B and C). The finding that P203A/P206A significantly impacted mLBS-1 binding despite the individual mutations exerting only minor (P203A) or no (P206A) effect, suggests that the rigidity provided by these two prolines is important for mTR DNA binding. $mLANA_{V199A/L202A}$ was most severely affected and did not complex with mLBS1 probe. However, after incubation with mLBS1-2, a faint signal was evident, especially on longer exposure (Fig. 1C, vertical lines, longer exposure at right). Notably, compared to mLANA and the other mLANA mutants, binding to both LBS1 and LBS2 binding sites of LBS1-2 was favoured for $mLANA_{V199A/L202A}$. Whereas the intensity of the faster migrating, LBS1 bound, "lower" complex was much greater than that of the slower migrating LBS1 and LBS2 bound "upper" complex for mLANA and the other mutants, both complexes were of similar intensity for $mLANA_{V199A/L202A}$ (Fig. 1C), indicating preferential binding to both LBS1 and LBS2. The lower level of DNA binding for $mLANA_{P203A}$, $mLANA_{V199A}$, $mLANA_{P203A/P206A}$ and $mLANA_{V199A/L202A}$ was not due to insufficient protein since similar amounts of mLANA protein were used in all incubations (Fig. 1D). Therefore, the E3 ligase deficient mLANA mutants were also deficient for mTR DNA binding.

Next, we assessed the abilities of $mLANA_{V199A}$, $mLANA_{L202A}$, $mLANA_{V199A/L202A}$, $mLANA_{P203A}$, $mLANA_{P206A}$ and $mLANA_{P203A/P206A}$ to mediate episome persistence. mLANA-m4TR, mTR, $mLANA_{V199A}$-m4TR, $mLANA_{L202A}$-m4TR, $mLANA_{V199A/L202A}$-m4TR, $mLANA_{P203A}$-m4TR, $mLANA_{P206A}$-m4TR or $mLANA_{P203A/P206A}$-m4TR were each transfected into MEF cells, and cells placed under G418 selection. As previously observed, greater than 100 G418-resistant colonies grew out in the mLANA-4TR plate. Only ~20 colonies grew from the m4TR plate, consistent with the absence of mLANA episome persistence. Similar to mLANA, greater than 100 G418-resistant colonies grew from the $mLANA_{V199A}$-m4TR, $mLANA_{L202A}$-m4TR, $mLANA_{P203A}$-m4TR, $mLANA_{P206A}$-m4TR and $mLANA_{P203A/P206A}$-m4TR plates. In contrast, only six G418-resistant clones grew from the

294 mLANA$_{V199A/L202A}$-m4TR plate, which was notable since mLANA$_{V199A/L202A}$ was also highly deficient for
295 mTR DNA binding. The robust G418-resistant outgrowth of mLANA$_{V199A}$-m4TR, mLANA$_{L202A}$-m4TR,
296 mLANA$_{P203A}$-m4TR, mLANA$_{P206A}$-m4TR and mLANA$_{P203A/P206A}$-m4TR plates suggests these mutants
297 have the ability to mediate episome persistence, while the low mLANA$_{V199A/L202A}$-m4TR G418 outgrowth
298 is consistent with episome maintenance deficiency.
299 We assessed G418-resistant cell lines for the presence of episomes by Gardella gel. As expected,
300 none of the m4TR lanes contained episomes, while all four mLANA-4TR lanes had episomal DNA.
301 Episomal DNA was also present in all mLANA$_{P206A}$-m4TR lanes, and in all but one lane for
302 mLANA$_{V199A}$-m4TR, mLANA$_{L202A}$-m4TR, mLANA$_{P203A}$-m4TR and mLANA$_{P203A/P206A}$-m4TR (Fig. 6A
303 and B). In contrast, mLANA$_{V199A/L202A}$ did not contain episomes in any lanes (Fig. 6B). When including
304 additional Gardella gel results (not shown) mLANA$_{V199A}$-m4TR had episomes in 7/11 (64%) of cell lines,
305 mLANA$_{L202A}$-m4TR had episomes in 7/11 (64%) of cell lines, mLANA$_{P203A}$-m4TR had episomes in 9/10
306 (90%) of cell lines, mLANA$_{P206A}$-m4TR had episomes in 8/11 (73%) of cell lines, mLANA$_{P203A/P206A}$-
307 m4TR had episomes in 10/11 (91%) of cell lines, and mLANA-4TR had episomes in 14/15 (93%) of cell
308 lines. In contrast, only six G418-resistant mLANA$_{V199A/L202A}$ clones could be expanded, and all lacked
309 episomes. The lack of episomal DNA was not due to absence of mLANA$_{V199A/L202A}$ expression since
310 protein levels were similar to those of mLANA (Fig. 6C). Therefore, mLANA$_{V199A}$, mLANA$_{L202A}$,
311 mLANA$_{P203A}$, mLANA$_{P206A}$ and mLANA$_{P203A/P206A}$ each maintained episomes, while mLANA$_{V199A/L202A}$
312 did not.
313
314 **Fig. 6. The effect of SOCS motif mutations on mLANA episome persistence.** (A & B) MEF cells were
315 transfected with mLANA-4TR, m4TR, or mLANA mutants. Forty-eight hours later, cells were trypsinized, re-seeded
316 into 15-cm dishes and placed under G418 selection. G418-resistant clones were picked and expanded. ~2×10^6 cells
317 were loaded per lane for Gardella gels. (A) Gardella gel containing G418-resistant MEF cells transfected with
318 mLANA-4TR (lanes 1 to 4), mLANA$_{V199A}$-4TR (lanes 5 to 10), mLANA$_{L202A}$-m4TR (lanes 11 to 16) or
319 mLANA$_{P203A}$-m4TR (lanes 17 to 22). Input plasmid mLANA-4mTR or m4TR DNA are in the lanes at left. O, gel
320 origin. (B) Gardella gel containing G418-resistant MEF cells transfected with m4TR (lanes 1 to 4), mLANA$_{P206A}$-
321 4TR (lanes 5 to 10), mLANA$_{V199A/L202A}$-4TR (lanes 11 to 16) or mLANA$_{P203A/P206A}$-4TR (lanes 17 to 22). O, gel
322 origin. (C) Immunoblot of mLANA or tubulin for mLANA-m4TR or mLANA$_{V199A/L202A}$-m4TR cells in panels (A)
323 and (B). IB, immunoblot.
324
325 We also assessed mLANA distribution within cells. In episome containing cells, mLANA$_{V199A}$,
326 mLANA$_{L202A}$, mLANA$_{P203A}$, mLANA$_{P206A}$ and mLANA$_{P203A/P206A}$ (green) concentrated to dots along
327 mitotic chromosomes (red) and in the nuclei of interphase cells (overlay of green and red generates
328 yellow), similar to mLANA (Fig. 3). In contrast, mLANA$_{V199A/L202A}$ (green) distributed broadly over
329 mitotic chromosomes, and within interphase nuclei (Fig. 3), consistent with its lack of ability to maintain
330 episomes.

mLANA E3 ubiquitin-ligase activity deficiency reduces MuHV-4 latency amplification

We next assessed the impact of mLANA E3 ligase impairment on the physiological context of latency *in vivo*. To accomplish this, we generated MuHV-4 recombinant viruses containing E3 ligase-deficient mLANA with mutation V199A (vmLANA$_{V199A}$) or mutations P203A and P206A (vmLANA$_{P203A/P206A}$). Recombinant viruses bearing mLANA mutations P203A (vmLANA$_{P203A}$), which exerts WT E3 ligase activity, or V199A/L202A (vmLANA$_{V199A/L202A}$), which is E3 ligase-deficient, but did not maintain episome persistence, were generated as controls. These viruses were used to infect mice and the effect of the introduced mutations on latent infection was assessed by two complementary experiments: *ex vivo* co-culture assays of total splenocytes with permissive BHK-21 cells to determine latent load in spleen; and limiting dilution analysis coupled to real-time PCR to quantify the frequency of viral DNA-positive cells in total splenocytes.

MuHV-4 latent infection in the spleen is characterized by an initial proliferation of infected B cells and consequent amplification of the latent virus, reaching maximum levels around 14 dpi and decreasing thereafter to low levels, which remain stable throughout the entire life of the host [14, 20, 28, 29]. Therefore, mice were assessed at 14 or 21 days post-infection (dpi). As expected, the splenic latency levels established by virus vmLANA$_{P203A}$ were identical to vWT (Fig. 7). This is in good agreement with our previous observations that E3 ligase and episome maintenance functions of mLANA$_{P203A}$ mutant were intact (Figs. 1, 3-6). In contrast, viruses vmLANA$_{V199A}$ and vmLANA$_{P203A/P206A}$ exhibited an attenuation of latency at 14 dpi, the peak of viral latency expansion (Fig. 7A, closed circles). Consistent with this result, the frequency of vmLANA$_{V199A}$ and vmLANA$_{P203A/P206A}$ infection in total splenocytes at 14 dpi was about 1-log lower than vWT infection (Fig. 7B and Table 1). No preformed infectious viruses were detected by suspension assay of frozen/thawed spleen homogenates, showing that splenic infection was only latent (Fig. 7A, open circles). At 21 dpi, when the viral latent load is declining, levels of latent infection were similar for vmLANA$_{V199A}$, vmLANA$_{P203A/P206A}$ and vWT (Fig. 7C). Altogether, these data demonstrate that the impairment of mLANA E3 ligase activity impacts MuHV-4 latent infection at the peak of latency amplification.

Fig. 7. Impairment of mLANA E3 ubiquitin-ligase activity impacts MuHV-4 latency amplification. (A & C) Quantification of latent infection in spleen by *ex vivo* co-culture assay. BALB/c mice were intranasally infected with 10^4 PFU of the indicated viruses. At days 14 (A) and 21 (C) post-infection, latent viruses in spleens were titrated by *ex vivo* co-culture assay (closed circles). Titers of infectious viruses were determined in frozen/thawed splenocyte suspensions (open circles). Each circle represents the titer of an individual mouse. The dashed line represents the limit of detection of the assay. (B) Quantification of viral DNA-positive cells in total splenocytes. BALB/c mice were intranasally infected with 10^4 PFU of the indicated viruses. At 14 dpi, reciprocal frequencies of viral infection in total splenocytes were determined by limiting dilution and real-time PCR. Data were obtained from pools of three to four spleens per group. Bars represent the frequency of viral DNA-positive cells with 95% confidence intervals. PFU, plaque forming unit; dpi, days post-infection.

Table 1. Reciprocal frequency of MuHV-4 infection in total splenocytes.

Cell subpopulation	Dpi	Virus	Reciprocal frequency of viral DNA positive cells	
Total splenocytes	14	vWT	151	(95-367)
		vmLANA$_{P203A}$	98	(63-219)
		vmLANA$_{V199A}$	1877	(998-15734)
		vmLANA$_{P203A/P206A}$	1544	(855-7916)
		vmLANA$_{V199A/L202A}$	663	(411-1710)

Data were obtained from pools of 3 to 4 spleens. Frequencies of virus-genome-positive cells were determined by limiting dilution combined with real-time PCR, with 95% confidence intervals (numbers in parentheses).

Unexpectedly, vmLANA$_{V199A/L202A}$, which lacked episome maintenance activity (Fig. 6B), was capable of establishing infection and exhibited an attenuation of latency at 14 dpi (Fig. 7A and B), similar to vmLANA$_{V199A}$ and vmLANA$_{P203A/P206A}$. This result was not anticipated since the absence of vmLANA$_{V199A/L202A}$ episome maintenance activity was expected to lead to loss of the ability to establish latent infection.

mLANA$_{V199A/L202A}$ mutant efficiently mediates episome persistence in virus

mLANA episome maintenance is critical for MuHV-4 establishment and expansion of latent infection *in vivo* [24, 25, 30, 31]. Specifically, it has been established that LANA binding to TR DNA is essential for episome persistence [32] and mLANA lacking the ability to bind mTR DNA cannot establish viable latent infection [25, 30].

Since mLANA episome persistence is necessary for latent MuHV-4 infection, we reasoned that mLANA$_{V199A/L202A}$ likely mediates MuHV-4 episome maintenance despite the absence of mLANA$_{V199A/L202A}$-m4TR episome persistence (Fig. 6B). One possibility is that since mLANA$_{V199A/L202A}$-m4TR contains only four mTR elements, mLANA$_{V199A/L202A}$ might exert episome maintenance function in the setting of a higher number of mTR elements. We previously observed that mLANA episome maintenance efficiency was increased with eight compared to two or four mTR elements [23]. If MuHV-4 contains ~40 TR elements (similar to KSHV), it is possible that this number may be necessary for mLANA$_{V199A/L202A}$ episome maintenance function.

To investigate whether mLANA$_{V199A/L202A}$ could mediate MuHV-4 episome persistence in a whole-virus context, we used MuHV-4 ORF50-deficient virus [33], which is abolished for lytic infection and therefore latently infects otherwise permissive cells. MuHV-4 ORF50-deficient virus contains a deletion of *ORF50* exon 2 [33], preventing the expression of ORF50, the major lytic transactivator protein of MuHV-4 [34, 35] (Fig. 8A). We generated an ORF50-deficient virus recombinant for mLANA$_{V199A/L202A}$ (vORF50^{-} mLANA$_{V199A/L202A}$). As a negative control, we constructed an ORF50-deficient recombinant virus bearing mutations V199A/L202A/P203A/P206A in mLANA (vORF50^{-} mLANA-SOCS). ORF50-deficient virus containing mLANA-WT (vORF50^{-} mLANA-WT) was used as a positive control for episome maintenance. Next, we infected MEF cells with vORF50^{-} mLANA-WT, vORF50^{-} mLANA-SOCS or vORF50^{-} mLANA$_{V199A/L202A}$ at a multiplicity of infection of 3 plaque forming units (PFU) per

cell, to ensure that nearly all cells were infected. Cells were seeded at low density and placed under drug selection with mycophenolic acid (MPA) and xanthine. Bacterial artificial chromosome (BAC)-derived MuHV-4 viruses retain the BAC cassette [36], which contains *gpt* (guanosine phosphoribosyl transferase) gene from *Escherichia coli* (Fig. 8B). MPA inhibits *de novo* synthesis of cellular purines, however *E. coli* enzyme GPT is able to synthesize purine precursors from xanthine [37], allowing selection of cells latently infected with ORF50-deficient viruses in the presence of these drugs. Since mLANA is essential for viral episome maintenance [23, 25, 30], only MEF cells latently infected with an ORF50-deficient virus containing mLANA able to mediate episome persistence are expected to efficiently persist under drug selection.

Fig. 8. mLANA$_{V199A/L202A}$ efficiently mediates MuHV-4 episome persistence. (A) Schematic diagram showing the insertion of eGFP in place of the removed ORF50 gene, and the insertion of a M3 promoter-luciferase-polyA cassette between ORFs 57 and 58, as described by Milho *et al.*, 2009 [33]. Relevant restrictions sites are shown. (B) Schematic diagram showing the left end of BAC-cloned MuHV-4 genome, with viral terminal repeats and *gpt* gene, BAC sequences and *gfp* gene, flanked by *loxP* sites, as described by Adler *et al.*, 2000 [36]. (C) Schematic diagram showing the experimental setting of establishment of MEF cell lines latently infected with ORF50-deficient viruses. MEF-1 cells were infected with ORF50-deficient viruses at a multiplicity of infection of 3 PFU per cell. Two days after infection, cells were trypsinized, counted and seeded at low cell density. Fresh medium containing MPA and xanthine was added. Resistant clones were picked, expanded under continued drug selection and analyzed in Gardella gels for the presence of viral genomes. (D) After 98 days of MPA selection, ~5x10^6 cells were loaded per lane for Gardella gel analysis. Gardella gel containing uninfected MEF cells (lanes 1, 2), vORF50$^-$ mLANA-WT (lanes 3-8) or vORF50$^-$ mLANA$_{V199A/L202A}$ (lanes 9-16) infected MEF cells. O, gel origin, E, episomal DNA, L, linear MuHV-4 DNA resulting from low level lytic replication. GFP, green fluorescent protein; Luc, luciferase; TR, terminal repeats; *gpt*, guanosine phosphoribosyl transferase; BAC, bacterial artificial chromosome; MPA, mycophenolic acid.

The same number of MEF cells was infected with each virus (Fig. 8C). Infection with vORF50$^-$ mLANA-SOCS resulted in only five MPA-resistant clones, whereas the number of MPA-resistant clones for vORF50$^-$ mLANA-WT or vORF50$^-$ mLANA$_{V199A/L202A}$ were too numerous to count (Table 2). The high rate of MPA outgrowth for vORF50$^-$ mLANA$_{V199A/L202A}$ (similar to ORF50$^-$ mLANA-WT) suggested that mLANA$_{V199A/L202A}$ mediates episome maintenance, whereas the low outgrowth of vORF50$^-$ mLANA-SOCS was consistent with absence of episome maintenance. LANA mediated episome persistence generally has a much higher efficiency compared to integration, which is required for virus persistence in the absence of episome maintenance. Ten vORF50$^-$ mLANA-WT or vORF50$^-$ mLANA$_{V199A/L202A}$ clones, and all five vORF50$^-$ mLANA-SOCS clones were picked for expansion. Six of ten (60%) vORF50$^-$ mLANA-WT and 8/10 (80%) vORF50$^-$ mLANA$_{V199A/L202A}$ clones could be expanded after 98 days (Table 2). In contrast, all five vORF50$^-$ mLANA-SOCS clones failed to expand and cells died. We directly assessed the MPA-resistant cells for the presence of episomal DNA by Gardella gel analysis. All six vORF50$^-$ mLANA-WT and all eight vORF50$^-$ mLANA$_{V199A/L202A}$ cell lines contained episomes (Fig. 8D and Table 2). Therefore, mLANA$_{V199A/L202A}$ mediates MuHV-4 episome persistence.

Table 2. Number of resistant clones obtained from infection of MEF cells with ORF50-deficient viruses.

Virus	Number of resistant clones	Number of resistant clones after 98 days of drug selection	Number of resistant clones containing viral episomes
vORF50$^-$ mLANA-WT	TNTC	6/10	6/6
vORF50$^-$ mLANA-SOCS	5	0/5	NA
vORF50$^-$ mLANA$_{V199A/L202A}$	TNTC	8/10	8/8

TNTC, Too Numerous To Count; NA, Not Applicable.

The finding that mLANA$_{V199A/L202A}$ mediates episome persistence is consistent with our observations that recombinant vmLANA$_{V199A/L202A}$ was able to establish viable latency in mice (Fig. 7A and B). Notably, mLANA$_{V199A/L202A}$ mediated episome persistence as efficiently as did vORF50$^-$ mLANA-WT. Therefore, the attenuation of latency expansion exhibited by vmLANA$_{V199A/L202A}$ can be attributed to the impairment of mLANA E3 ligase activity (Figs. 4-5).

Discussion

In this study, we were able to establish a link between the E3 ubiquitin-ligase activity of mLANA and murid gammaherpesvirus pathogenesis *in vivo*. MuHV-4 recombinant viruses with mutations in mLANA SOCS-box compromising E3 ligase activity, without abrogating episome maintenance function, exhibited an attenuation of latency. Therefore, mLANA E3 ligase activity contributes to gammaherpesvirus latency expansion. This work also demonstrates that mLANA is capable of episome maintenance despite mutations that result in considerably reduced mTR DNA binding.

It is likely that cooperative binding in the setting of multiple mTR elements compensates for mLANA DNA binding deficiencies. Four mTR elements proved to be sufficient to overcome the mLANA$_{P203A/P206A}$ and mLANA$_{V199A}$ DNA binding reductions as this number permitted a WT level of episome maintenance. However, even four mTR elements do not provide optimal episome maintenance efficiency. We previously observed increased episome persistence efficiency with eight mTR elements as compared to two or four mTR elements [23]. Notably, Gardella gels demonstrated that episomes with mLANA-m4TR migrated slower than input plasmid. This slower migration was also observed for each of the mutants that maintained episomes. We previously observed similar increases in episome size for mLANA or kLANA episomes, even when using plasmids containing eight TR elements [22, 23, 38]. The large, slowly migrating KSHV episomes are due to TR duplication and recombination of input plasmids into multimers [22, 38]. KSHV contains ~40 TR elements and MuHV-4 may contain a similar number. It is likely that there is strong selection for recombination events that lead to a TR number similar to that in the virus. At least 16 TR elements are likely necessary for optimal KSHV episome maintenance [39].

It is particularly noteworthy that despite a severe DNA binding deficiency and the failure to mediate episome maintenance with four mTR elements, mLANA$_{V199A/L202A}$ efficiently mediated episome persistence in the setting of a full complement of mTRs in MuHV-4. Only a very low level of mLANA$_{V199A/L202A}$ DNA binding was detected for mLBS1-2, and compared with mLANA or the other

mutants, the migration of the EMSA complexes indicated preferential occupation of both the mLBS1 and mLBS2 sites. The fact that no binding was observed to mLBS1 alone combined with the preferential occupation of both the LBS1 and LBS2 sites suggests that cooperative binding is necessary to overcome $mLANA_{V199A/L202A}$ binding deficiency. Although $mLANA_{V199A/L202A}$ mediated episome persistence in the setting of a full complement of MuHV-4 mTR elements, such compensation by an increased mTR number is not without limit, as MuHV-4 with mLANA-SOCS or other mLANA mutants that are completely abolished for DNA binding cannot establish viable latent infection [7, 25, 30]. It is possible that higher order mLANA structures may exert compensatory roles to overcome DNA binding deficiency through avidity, or even matricity-driven interactions. Notably, it was recently shown that the positively charged patch opposite of the DNA binding surface on the kLANA DBD can interact with DNA, independently of DNA sequence [40], and mLANA has a similar positively charged patch [25, 26, 40, 41].

Mouse infection experiments in this study showed that a reduction of mLANA E3 ligase activity sufficed to impair MuHV-4 latency amplification in B cells. To demonstrate an unequivocal effect a complete ablation of E3 ligase activity would be required. In a previous study, we generated an mLANA-SOCS mutant virus, containing four SOCS-box mutations (V199A/L202A/P203A/P206A) [7]. Although, this mutant exhibited a knockout of E3 ligase activity, in the current study we demonstrated that this mutant could not bind mTR DNA nor maintain viral episomes. Despite several efforts to identify residues in mLANA SOCS-box which are essential to E3 ligase activity, we did not succeed in finding a set of mutations that completely disrupted E3 ligase activity without compromising episome maintenance function. Recently, we resolved the crystal structure of mLANA C-terminal domain that revealed that the SOCS-box lies within a loop (β2-β3 loop, residues 199-215), which protrudes perpendicular to the DNA binding interface [25]. Given the spatial proximity of these two functional regions, it is possible that the introduction of certain mutations in the SOCS-box impact on DNA recognition helix α2, disrupting the DNA binding interface and, consequently, mLANA-mediated episome persistence. In any case, the finding that deficient mLANA E3 ligase activity reduced viral latency suggests that complete inhibition of this activity could result in an even more severe effect on the ability of virus to establish latent infection, perhaps abolishing it.

The property of a viral protein assembling an EC_5S E3 ligase complex through a SOCS-box motif is not unique to LANA proteins. However, the biological significance of such a mechanism for viral pathogenesis *in vivo* is only beginning to be characterized. A recent study showed that HIV-1 Vif-mediated degradation of APOBEC3 proteins, the targets of Vif E3 ligase activity, is important for viral propagation *in vivo* [42]. The authors infected a humanized mouse model with HIV-1 mutants, which contained mutations in Vif motifs involved in interaction with APOBEC3 proteins. Although those mutations did not specifically inhibit Vif E3 ligase activity, since they were introduced in Vif substrate binding motifs rather than in its SOCS-box, this study highlights the importance of Vif E3 ligase activity *in vivo*, at least on APOBEC3 proteins.

Our study demonstrates that the E3 ligase activity of mLANA impacts the expansion of latent infection in B cells in an animal model of infection. mLANA has two known cellular targets for poly-

ubiquitination, Myc and NF-κB. These results do not distinguish the contribution of NF-κB modulation from that of Myc modulation to the proliferation of latently infected GC B cells and consequent viral latency expansion. In addition, it is possible that mLANA may target other cellular proteins for poly-ubiquitination, so that impairing E3 ligase activity may hamper mLANA-mediated modulation of other proteins relevant to MuHV-4 latency expansion. However, these data are compatible with stabilization of Myc and inhibition of NF-κB by mLANA mediated poly-ubiquitination playing essential roles for virus induced B cell proliferation in GC B cells, as previously proposed [7, 8].

Given the importance of the ubiquitin system, it is not surprising that gammaherpesviruses have developed a strategy to hijack host proteins involved in the ubiquitination pathway. Herein, we provide evidence for the *in vivo* importance of the E3 ligase complex, through which mLANA modulates at least two cellular proteins whose regulation is critical for GC reaction, NF-kB and Myc, thus promoting virus expansion during latency. Although mLANA E3 ligase activity was not completely ablated, the partial impairment of this function was sufficient to reduce viral latency levels. Thus, pharmacological inhibition of LANA E3 ligase activity through targeting of SOCS-box motifs is a putative strategy to control gammaherpesvirus infection.

Materials and Methods

Ethics statement

This study was carried out in strict accordance with the recommendations of the Portuguese official Veterinary Directorate (Portaria 1005/92). The Portuguese Experiments on Animal Act strictly comply with the European Directive 2010/63/EU and follow the Federation of European Laboratory Animal Science Associations (FELASA) guidelines on laboratory animal welfare. Animal experiments were approved by the Portuguese official veterinary department for welfare licensing (protocol AEC_2010_017_PS_Rdt_General) and by the Instituto de Medicina Molecular (IMM) Animal Ethics Committee.

Plasmids

pRepCK-mLANAF-m4TR (mLANA-4TR) was previously described [23]. To introduce SOCS-box mutations into mLANAF-4TR, the region within mLANA between the *Pci*I and *Hind*III restriction enzyme sites was PCR amplified using "forward" primers, each of which contained the relevant mutation (capital letters and underlined in sequence below). The forward primers for each mutation were the following: V199A: gcaaACATGTactctcaacaccaGCTagctg; L202A: gcaaACATGTactctcaacaccagttagctgtGCAcccttg; P203A: gcaaACATGTactctcaacaccagttagctgttta GCCttggtac; P206A: gcaaACATGTactctcaacaccagttagctgtttaCCCttggtaGCAggc; V199A/L202A: gcaaACATGTactctcaacaccaGCTagctgtGCAcccttg; P203A/P206A: gcaaACATGTactctcaacaccag ttagctgtttaGCCttggtaGCAggc; SOCS: gcaaACATGTactctcaacaccaGCTagctgtGCAGCCttggtaGC Aggc. The sequence of the reverse primer used for all amplifications was ccag*AAGCTT*gtgtacttgtggatggctgctcggggtctgtag. The *Pci*I (capital letters) and *Hind*III (capital letters and in italics) restriction sites are indicated. Purified PCR products were digested with *Pci*I and *Hind*III and inserted into *Pci*I and *Hind*III digested mLANA-4TR to generate the final mutated constructs. Mutations were cloned into pBS-myc-LANA-C3F [25] using the QuikChange II XL Site-Directed Mutagenesis Kit (Agilent Technologies) according to the manufacturer's instructions. All constructs were confirmed by sequencing. pCMV-Myc plasmids encoding wild-

type mLANA and mLANA-SOCS mutant were described previously [7]. pCMV-Myc constructs encoding $mLANA_{V199A}$, $mLANA_{L202A}$, $mLANA_{V199A/L202A}$, $mLANA_{P203A}$, $mLANA_{P206A}$ and $mLANA_{P203A/P206A}$ were generated by site-directed mutagenesis, using QuikChange II XL Site-Directed Mutagenesis Kit (Agilent Technologies) according to the manufacturer's instructions. All constructs were verified by DNA sequencing. pCMV-Myc plasmid encoding p65 and pC45 (κB-Luc) plasmid, which contains three copies of κB consensus sequence regulating the expression of firefly luciferase, were described earlier [43, 44]. pMyc-TA-Luc vector, containing six tandem copies of the E-box consensus sequence driving the expression of firefly luciferase, was purchased from Clontech. *Renilla* expression plasmid was kindly provided by Xosé R. Bustelo. pCMV-HA plasmid encoding Myc was described earlier [8]. Histidine-tagged ubiquitin, Flag-tagged ElonginC and Myc-tagged Cullin5 plasmids were provided by Dr. D. Bohmann, Dr. E. Burstein and Dr. X.F. Yu, respectively.

Immunological reagents

mLANA monoclonal antibody and mLANA polyclonal antiserum were described previously [7, 8]. Anti-p65 (F-6) monoclonal antibody and anti-c-Myc (N-262), anti-EloC (R-20) and anti-Cul5 (H-300) polyclonal antibodies were purchased from Santa Cruz Biotechnology. Monoclonal antibodies directed to c-Myc (9E10) and FLAG (M2) epitope tags were from Clontech and Sigma, respectively. Horseradish peroxidase (HRP)-conjugated secondary antibodies were from Jackson Immunoresearch, GE Healthcare and Southern Biotech.

Tissue culture and DNA transfection

HEK 293T, NIH-3T3-CRE [45], 3T3-ORF50 [33] and MEF-1 cells were cultured in Dulbecco's modified Eagle's medium (DMEM) supplemented with 10% fetal bovine serum, 2 mM glutamine and 100 U/ml penicillin–streptomycin. BHK-21 cells were grown in Glasgow's modified Eagle's medium (GMEM) supplemented as described above plus 10% tryptose phosphate broth. HEK 293T cells were transiently transfected with X-tremeGENE HP DNA Transfection Reagent (Roche) according to the manufacturer's instructions. In all transfections, an empty vector was used to normalize the total amount of plasmid DNA.

Electrophoretic mobility shift assays (EMSAs)

mLANA-WT or mLANA SOCS-box mutants were *in vitro*-translated using TNT coupled Reticulocyte Systems (Promega # L4610) from pBS-Myc-mLANAc3F or pBS-Myc-mLANAc3F containing each SOCS-box mutation. *In vitro* mLANA protein expression was confirmed by Western blot using monoclonal anti-FLAG (M2) followed by HRP conjugated goat anti-mouse secondary antibody. mLBS1 or mLBS1-2 ^{32}P radiolabeled probe was prepared as previously described [25]. Probe was incubated with 10 µl of *in vitro* translated mLANA or mLANA mutant, or reticulocyte lysate control in EMSA buffer (20 mM Tris-HCl pH 7.5, 50 mM KCl, 10 mM $MgCl_2$, 1 mM EDTA, 20 µg/ml polydI-dC [Amersham Bioscience #27-7880-02], 0.1 mM DTT and 10% glycerol) for 30 minutes at 4°C. Fifty-fold excess unlabeled mLBS1, or 50x excess unlabeled mLBS1-2 were included in incubations for competition experiments. For supershift assays, 1 µg of anti-FLAG monoclonal antibody was included in the incubation. Loading buffer (95% formamide, 10 mM EDTA, 0.1% xylene cyanol and 0.1% bromophenol blue) was added to incubations followed by loading into a 3.5%/8% non-denaturing TBE-polyacrylamide gel. Electrophoresis was performed in TBE buffer for 1 hour at 300 V, the gel dried on Whatman paper, and exposed to Kodak Biomax MS film (Kodak #829 4985).

Episome maintenance assays

Two µg of mLANA-4TR or mLANA-4TR containing SOCS-box mutations were transfected into MEF cells (at ~75% confluence) in 6-cm dishes, using Effectene transfection reagent (Qiagen) according to the manufacturer's instructions. Two days post-transfection, cells were trypsinized, counted, and seeded at $1x10^5$ cells in a 15-cm dish. The next day, cells were rinsed with PBS, and fresh medium containing G418 (1 mg/ml) (Gemini) was added. G418-resistant clones were picked and transferred to 12-well plates for expansion.

Gardella gel analysis [27] was performed on G418-resistant clones. $1\text{-}2\times10^6$ cells were loaded into gel wells composed of agarose containing DNase-free protease (Sigma) and sodium dodecyl sulfate (SDS). *In situ* lysis of cells occurs as electrophoresis begins in TBE buffer. After the gel run, DNA was transferred to a nylon membrane and detected with a ^{32}P-labeled MuHV-4 TR (mTR) probe. mTR DNA was generated from pRepCK-m4TR [23] after *Not*I digestion.

Immunofluorescence microscopy

MEF cells were grown in 6-well dishes to ~75% confluence and then incubated overnight in 1 µg/ml of colcemid (Calbiochem) to induce arrest in metaphase. Cells were then swollen in hypotonic buffer (1% sodium citrate, 10 mM $CaCl_2$, 10 mM $MgCl_2$) for 20 min, spread onto slides by cytospin (Thermoshandon), fixed for 10 minutes in 4% paraformaldehyde (Polysciences) in PBS, and permeabilized for 5 minutes using 0.5% Triton X-100 in PBS. Slides were incubated with M2 anti-FLAG monoclonal antibody (Sigma) at a 1:1000 dilution followed by incubation with secondary anti-mouse–Alexa Fluor 488 (Molecular Probes). Counterstaining was performed with propidium iodide (Molecular Probes) (1 µg/ml) to detect DNA. Coverslips were applied using Aqua-Poly mounting reagent (Polysciences). Microscopy was performed using a Zeiss Axioskop microscope, PCM2000 hardware, and C-imaging software (Compix, Inc.).

Reporter gene assays

For NF-κB reporter gene assays, HEK 293T cells were transiently transfected with 150 ng of reporter plasmid (pC45) and 1 µg of plasmid encoding mLANA (WT or mutants). A *Renilla* luciferase expression plasmid (20 ng) was used to normalize luciferase activity. After 48 h in culture, cells were left unstimulated or stimulated with TNF-α (50 ng/ml) for 7 h. Cells were washed in PBS and lysed in 200 µl of passive lysis buffer (Promega). Firefly luciferase and *Renilla* luciferase activities were assayed using Dual-Luciferase Reporter Assay System (Promega). Light emission in each sample was quantified in a luminometer. Results are shown as fold induction relative to luciferase activity measured in unstimulated cells. Myc reporter gene assays were performed essentially as described before [8]. Briefly, HEK 293T cells were transiently transfected with 500 ng of reporter plasmid (pMyc-TA-Luc) and 1 µg of plasmid encoding mLANA (WT or mutants). A *Renilla* luciferase expression plasmid (20 ng) was used to normalize luciferase activity. After 48 h in culture, cells were washed in PBS and lysed in 200 µl of passive lysis buffer (Promega). Results are shown as fold induction relative to luciferase activity measured in cells not expressing mLANA.

Poly-ubiquitination assays

Levels of ubiquitinated p65 or Myc were determined by pull-down using Ni-NTA agarose beads (Qiagen), essentially as described earlier [7, 8]. Briefly, HEK 293T cells were transiently transfected with expression plasmids encoding p65 (2 µg) or Myc (2 µg), mLANA (WT or mutants) (2 µg), and His_6–ubiquitin (4 µg). After 48 h in culture, cells were lysed in urea buffer containing 8 M urea, 50 mM Tris–HCl (pH 7.5), 300 mM NaCl, 1% Triton X-

100, 10 mM imidazole, 1 mM Na_3VO_4 and a cocktail of protease inhibitors (cOmplete, Roche). Cleared lysates were incubated with Ni-NTA beads for 2 h at 4ºC. After incubation, beads were washed three times with urea buffer. Proteins were eluted and denatured by boiling in Laemmli's buffer and analyzed by Western blot.

Immunoprecipitations

HEK 293T cells were transiently transfected with expression plasmids encoding ElonginC (2 µg) or Cullin5 (4 µg), and mLANA (WT or mutants) (2 µg). After 48 h in culture, cells were disrupted in ice-cold lysis buffer containing 10 mM Tris–HCl (pH 7.5), 150 mM NaCl, 1% Triton X-100, 1 mM NaF, 100 mM Na_3VO_4 and a cocktail of protease inhibitors (cOmplete, Roche), and processed for immunoprecipitation essentially as described [46].

Generation of MuHV-4 recombinant viruses

MuHV-4 recombinant viruses were independently generated by mutagenesis of the viral genome cloned as a BAC [36]. pCMV-Myc constructs encoding $mLANA_{P203A}$, $mLANA_{V199A}$, $mLANA_{P203A/P206A}$ and $mLANA_{V199A/L202A}$ were digested with *Hind*III and *Pci*I to isolate the fragment harboring the desired mutations, which was inserted into the *Bam*HI-G genomic clone. Recombinant *Bam*HI-G mutant fragments were subcloned into the *Bam*HI site of a pST76K-SR shuttle plasmid and transformed into *E. coli* DH10B containing wild-type MuHV-4 BAC (pHA3). Following a multistep selection procedure, recombinant BAC clones were identified by DNA sequencing and the integrity of each BAC was confirmed by restriction digestion with *Bam*HI and *Eco*RI. All viruses were reconstituted by transfection of BAC DNA into BHK-21 cells using X-tremeGENE HP DNA Transfection Reagent (Roche). The *loxP*-flanked BAC cassette was removed by viral passage through NIH-3T3-CRE cells and limiting dilution to obtain GFP-negative viruses. The stability of the introduced mutations was confirmed by viral DNA sequencing across *ORF73* gene using viruses recovered from infected mice.

Analysis of MuHV-4 recombinant viruses

BALB/c mice (Charles River Laboratories) with 6–8 weeks of age were intranasally inoculated with 10^4 PFU of MuHV-4 recombinant viruses in 20 µl of PBS under isofluorane anesthesia. At 14 and 21 dpi spleens were removed and processed for subsequent analysis. Titers of infectious viruses were determined by suspension assays of frozen/thawed spleen homogenates using BHK-21 cells. Latent viruses were titrated by *ex vivo* co-culture of splenocytes with BHK-21 cells. Plates were incubated for 5 days, then fixed with 4% formaldehyde and stained with toluidine blue. Viral plaques were counted with a plate microscope. Frequencies of virus-genome-positive cells were determined by limiting dilution combined with real-time PCR, as reported earlier [20, 47]. Total splenocytes suspensions were prepared from pools of three to four spleens per group.

Generation of MuHV-4 ORF50-deficient viruses

MuHV-4 ORF50-deficient (MuHV-4 M3 Luc/ORF50$^-$ eGFP) recombinant viruses were independently generated by mutagenesis of the viral genome cloned as a BAC [36]. pST76K-SR shuttle plasmids encoding mLANA-SOCS [7] or $mLANA_{V199A/L202A}$ (described above) were transformed into *E. coli* DH10B containing MuHV-4 M3 Luc/ORF50$^-$ eGFP BAC [33]. Following a multistep selection procedure, recombinant BAC clones encoding mLANA-SOCS or $mLANA_{V199A/L202A}$ were identified by DNA sequencing and the integrity of each BAC was confirmed by restriction digestion with *Bam*HI and *Eco*RI. BAC of MuHV-4 ORF50-deficient virus encoding mLANA-WT was extracted from *E. coli* DH10B containing MuHV-4 M3 Luc/ORF50$^-$ eGFP BAC [33]. All viruses were reconstituted by

transfection of BAC DNA into 3T3-ORF50 cells [33] using X-tremeGENE HP DNA Transfection Reagent (Roche) and treating cells with doxycycline (1µg/ml).

Episome maintenance assays of MuHV-4 ORF50-deficient viruses

MEF-1 cells were infected with ORF50-deficient viruses at a multiplicity of infection of 3 PFU per cell in 10-cm dishes at about 80% confluence. Two days after infection, cells were trypsinized, counted and seeded at $2x10^4$ or $2x10^5$ cells in a 10-cm dish. On the next day, fresh medium containing MPA (25 µM) and xanthine (25 µM) was added. Resistant clones were picked and, after expansion under continued drug selection, their content in viral genomes was analyzed in Gardella gels as described above.

Acknowledgments

We would like to thank Stacey Efstathiou and Philip Stevenson for providing ORF50-deficient viruses. We thank Lénia Rodrigues for help constructing plasmids encoding mLANA mutants and Janet S. May for support growing ORF50-deficient viruses. We also thank Marta Pires de Miranda for thoughtful discussion.

References

1. Berndsen CE, Wolberger C. New insights into ubiquitin E3 ligase mechanism. Nat Struct Mol Biol. 2014;21(4):301-7. doi: 10.1038/nsmb.2780. PubMed PMID: 24699078.

2. Lydeard JR, Schulman BA, Harper JW. Building and remodelling Cullin-RING E3 ubiquitin ligases. EMBO Rep. 2013;14(12):1050-61. doi: 10.1038/embor.2013.173. PubMed PMID: 24232186; PubMed Central PMCID: PMC3849489.

3. Skaar JR, Pagan JK, Pagano M. Mechanisms and function of substrate recruitment by F-box proteins. Nat Rev Mol Cell Biol. 2013;14(6):369-81. doi: 10.1038/nrm3582. PubMed PMID: 23657496; PubMed Central PMCID: PMC3827686.

4. Yoshimura A, Naka T, Kubo M. SOCS proteins, cytokine signalling and immune regulation. Nat Rev Immunol. 2007;7(6):454-65. doi: 10.1038/nri2093. PubMed PMID: 17525754.

5. Cai QL, Knight JS, Verma SC, Zald P, Robertson ES. EC5S ubiquitin complex is recruited by KSHV latent antigen LANA for degradation of the VHL and p53 tumor suppressors. PLoS Pathog. 2006;2(10):e116. doi: 10.1371/journal.ppat.0020116. PubMed PMID: 17069461; PubMed Central PMCID: PMC1626105.

6. Li X, Liang D, Lin X, Robertson ES, Lan K. Kaposi's sarcoma-associated herpesvirus-encoded latency-associated nuclear antigen reduces interleukin-8 expression in endothelial cells and impairs neutrophil chemotaxis by degrading nuclear p65. J Virol. 2011;85(17):8606-15. doi: 10.1128/JVI.00733-11. PubMed PMID: 21697472; PubMed Central PMCID: PMC3165807.

7. Rodrigues L, Filipe J, Seldon MP, Fonseca L, Anrather J, Soares MP, et al. Termination of NF-kappaB activity through a gammaherpesvirus protein that assembles an EC5S ubiquitin-ligase. EMBO J. 2009;28(9):1283-95. doi: 10.1038/emboj.2009.74. PubMed PMID: 19322197; PubMed Central PMCID: PMC2664658.

8. Rodrigues L, Popov N, Kaye KM, Simas JP. Stabilization of Myc through heterotypic poly-ubiquitination by mLANA is critical for gamma-herpesvirus lymphoproliferation. PLoS Pathog. 2013;9(8):e1003554. doi: 10.1371/journal.ppat.1003554. PubMed PMID: 23950719; PubMed Central PMCID: PMC3738482.

9. Sato Y, Kamura T, Shirata N, Murata T, Kudoh A, Iwahori S, et al. Degradation of phosphorylated p53 by viral protein-ECS E3 ligase complex. PLoS Pathog. 2009;5(7):e1000530. doi: 10.1371/journal.ppat.1000530. PubMed PMID: 19649319; PubMed Central PMCID: PMC2712087.

10. Yu X, Yu Y, Liu B, Luo K, Kong W, Mao P, et al. Induction of APOBEC3G ubiquitination and degradation by an HIV-1 Vif-Cul5-SCF complex. Science. 2003;302(5647):1056-60. doi: 10.1126/science.1089591. PubMed PMID: 14564014.

11. Yu Y, Xiao Z, Ehrlich ES, Yu X, Yu XF. Selective assembly of HIV-1 Vif-Cul5-ElonginB-ElonginC E3 ubiquitin ligase complex through a novel SOCS box and upstream cysteines. Genes Dev. 2004;18(23):2867-72. doi: 10.1101/gad.1250204. PubMed PMID: 15574593; PubMed Central PMCID: PMC534647.

12. Mehle A, Goncalves J, Santa-Marta M, McPike M, Gabuzda D. Phosphorylation of a novel SOCS-box regulates assembly of the HIV-1 Vif-Cul5 complex that promotes APOBEC3G degradation. Genes Dev. 2004;18(23):2861-6. doi: 10.1101/gad.1249904. PubMed PMID: 15574592; PubMed Central PMCID: PMC534646.

13. Querido E, Blanchette P, Yan Q, Kamura T, Morrison M, Boivin D, et al. Degradation of p53 by adenovirus E4orf6 and E1B55K proteins occurs via a novel mechanism involving a Cullin-containing complex. Genes Dev. 2001;15(23):3104-17. doi: 10.1101/gad.926401. PubMed PMID: 11731475; PubMed Central PMCID: PMC312842.

14. Simas JP, Efstathiou S. Murine gammaherpesvirus 68: a model for the study of gammaherpesvirus pathogenesis. Trends Microbiol. 1998;6(7):276-82. PubMed PMID: 9717216.

15. Thorley-Lawson DA. Epstein-Barr virus: exploiting the immune system. Nat Rev Immunol. 2001;1(1):75-82. doi: 10.1038/35095584. PubMed PMID: 11905817.

16. Flano E, Kim IJ, Woodland DL, Blackman MA. Gamma-herpesvirus latency is preferentially maintained in splenic germinal center and memory B cells. J Exp Med. 2002;196(10):1363-72. PubMed PMID: 12438427; PubMed Central PMCID: PMC2193987.

17. Dittmer DP, Damania B. Kaposi sarcoma associated herpesvirus pathogenesis (KSHV)--an update. Curr Opin Virol. 2013;3(3):238-44. doi: 10.1016/j.coviro.2013.05.012. PubMed PMID: 23769237; PubMed Central PMCID: PMC3716290.

18. Collins CM, Medveczky PG. Genetic requirements for the episomal maintenance of oncogenic herpesvirus genomes. Adv Cancer Res. 2002;84:155-74. PubMed PMID: 11883526.

19. Dittmer D, Lagunoff M, Renne R, Staskus K, Haase A, Ganem D. A cluster of latently expressed genes in Kaposi's sarcoma-associated herpesvirus. J Virol. 1998;72(10):8309-15. PubMed PMID: 9733875; PubMed Central PMCID: PMC110196.

20. Marques S, Efstathiou S, Smith KG, Haury M, Simas JP. Selective gene expression of latent murine gammaherpesvirus 68 in B lymphocytes. J Virol. 2003;77(13):7308-18. PubMed PMID: 12805429; PubMed Central PMCID: PMC164786.

21. Ballestas ME, Chatis PA, Kaye KM. Efficient persistence of extrachromosomal KSHV DNA mediated by latency-associated nuclear antigen. Science. 1999;284(5414):641-4. PubMed PMID: 10213686.

22. Ballestas ME, Kaye KM. Kaposi's sarcoma-associated herpesvirus latency-associated nuclear antigen 1 mediates episome persistence through cis-acting terminal repeat (TR) sequence and specifically binds TR DNA. J Virol. 2001;75(7):3250-8. doi: 10.1128/JVI.75.7.3250-3258.2001. PubMed PMID: 11238851; PubMed Central PMCID: PMC114118.

23. Habison AC, Beauchemin C, Simas JP, Usherwood EJ, Kaye KM. Murine gammaherpesvirus 68 LANA acts on terminal repeat DNA to mediate episome persistence. J Virol. 2012;86(21):11863-76. doi: 10.1128/JVI.01656-12. PubMed PMID: 22915819; PubMed Central PMCID: PMC3486315.

24. Fowler P, Marques S, Simas JP, Efstathiou S. ORF73 of murine herpesvirus-68 is critical for the establishment and maintenance of latency. J Gen Virol. 2003;84(Pt 12):3405-16. doi: 10.1099/vir.0.19594-0. PubMed PMID: 14645921.

25. Correia B, Cerqueira SA, Beauchemin C, Pires de Miranda M, Li S, Ponnusamy R, et al. Crystal structure of the gamma-2 herpesvirus LANA DNA binding domain identifies charged surface residues which impact viral latency. PLoS Pathog. 2013;9(10):e1003673. doi: 10.1371/journal.ppat.1003673. PubMed PMID: 24146618; PubMed Central PMCID: PMC3798461.

26. Hellert J, Weidner-Glunde M, Krausze J, Richter U, Adler H, Fedorov R, et al. A structural basis for BRD2/4-mediated host chromatin interaction and oligomer assembly of Kaposi sarcoma-associated herpesvirus and murine gammaherpesvirus LANA proteins. PLoS Pathog. 2013;9(10):e1003640. doi: 10.1371/journal.ppat.1003640. PubMed PMID: 24146614; PubMed Central PMCID: PMC3798688.

27. Gardella T, Medveczky P, Sairenji T, Mulder C. Detection of circular and linear herpesvirus DNA molecules in mammalian cells by gel electrophoresis. J Virol. 1984;50(1):248-54. PubMed PMID: 6321792; PubMed Central PMCID: PMC255605.

28. Cardin RD, Brooks JW, Sarawar SR, Doherty PC. Progressive loss of CD8+ T cell-mediated control of a gamma-herpesvirus in the absence of CD4+ T cells. J Exp Med. 1996;184(3):863-71. PubMed PMID: 9064346; PubMed Central PMCID: PMC2192775.

29. Sunil-Chandra NP, Efstathiou S, Nash AA. Murine gammaherpesvirus 68 establishes a latent infection in mouse B lymphocytes in vivo. J Gen Virol. 1992;73 (Pt 12):3275-9. doi: 10.1099/0022-1317-73-12-3275. PubMed PMID: 1469366.

30. Paden CR, Forrest JC, Tibbetts SA, Speck SH. Unbiased mutagenesis of MHV68 LANA reveals a DNA-binding domain required for LANA function in vitro and in vivo. PLoS Pathog. 2012;8(9):e1002906. doi: 10.1371/journal.ppat.1002906. PubMed PMID: 22969427; PubMed Central PMCID: PMC3435236.

31. Moorman NJ, Willer DO, Speck SH. The gammaherpesvirus 68 latency-associated nuclear antigen homolog is critical for the establishment of splenic latency. J Virol. 2003;77(19):10295-303. PubMed PMID: 12970414; PubMed Central PMCID: PMC228443.

32. Komatsu T, Ballestas ME, Barbera AJ, Kelley-Clarke B, Kaye KM. KSHV LANA1 binds DNA as an oligomer and residues N-terminal to the oligomerization domain are essential for DNA binding, replication, and episome persistence. Virology. 2004;319(2):225-36. doi: 10.1016/j.virol.2003.11.002. PubMed PMID: 14980483.

33. Milho R, Smith CM, Marques S, Alenquer M, May JS, Gillet L, et al. In vivo imaging of murid herpesvirus-4 infection. J Gen Virol. 2009;90(Pt 1):21-32. doi: 10.1099/vir.0.006569-0. PubMed PMID: 19088269; PubMed Central PMCID: PMC2885022.

34. Wu TT, Usherwood EJ, Stewart JP, Nash AA, Sun R. Rta of murine gammaherpesvirus 68 reactivates the complete lytic cycle from latency. J Virol. 2000;74(8):3659-67. PubMed PMID: 10729142; PubMed Central PMCID: PMC111876.

35. Pavlova IV, Virgin HWt, Speck SH. Disruption of gammaherpesvirus 68 gene 50 demonstrates that Rta is essential for virus replication. J Virol. 2003;77(10):5731-9. PubMed PMID: 12719566; PubMed Central PMCID: PMC154050.

36. Adler H, Messerle M, Wagner M, Koszinowski UH. Cloning and mutagenesis of the murine gammaherpesvirus 68 genome as an infectious bacterial artificial chromosome. J Virol. 2000;74(15):6964-74. PubMed PMID: 10888635; PubMed Central PMCID: PMC112213.

797 37. Mulligan RC, Berg P. Selection for animal cells that express the Escherichia coli gene coding for xanthine-
798 guanine phosphoribosyltransferase. Proc Natl Acad Sci USA. 1981;78(4):2072-6. PubMed PMID: 7017722; PubMed
799 Central PMCID: PMC319285.
800 38. De Leon Vazquez E, Kaye KM. The internal Kaposi's sarcoma-associated herpesvirus LANA regions exert
801 a critical role on episome persistence. J Virol. 2011;85(15):7622-33. doi: 10.1128/JVI.00304-11. PubMed PMID:
802 21593163; PubMed Central PMCID: PMC3147901.
803 39. Shrestha P, Sugden B. Identification of properties of the Kaposi's sarcoma-associated herpesvirus latent
804 origin of replication that are essential for the efficient establishment and maintenance of intact plasmids. J Virol.
805 2014;88(15):8490-503. doi: 10.1128/JVI.00742-14. PubMed PMID: 24829342; PubMed Central PMCID:
806 PMC4135972.
807 40. Hellert J, Weidner-Glunde M, Krausze J, Lunsdorf H, Ritter C, Schulz TF, et al. The 3D structure of Kaposi
808 sarcoma herpesvirus LANA C-terminal domain bound to DNA. Proc Natl Acad Sci USA. 2015;112(21):6694-9. doi:
809 10.1073/pnas.1421804112. PubMed PMID: 25947153; PubMed Central PMCID: PMC4450395.
810 41. Domsic JF, Chen HS, Lu F, Marmorstein R, Lieberman PM. Molecular basis for oligomeric-DNA binding
811 and episome maintenance by KSHV LANA. PLoS Pathog. 2013;9(10):e1003672. doi:
812 10.1371/journal.ppat.1003672. PubMed PMID: 24146617; PubMed Central PMCID: PMC3798644.
813 42. Sato K, Takeuchi JS, Misawa N, Izumi T, Kobayashi T, Kimura Y, et al. APOBEC3D and APOBEC3F
814 potently promote HIV-1 diversification and evolution in humanized mouse model. PLoS Pathog.
815 2014;10(10):e1004453. doi: 10.1371/journal.ppat.1004453. PubMed PMID: 25330146; PubMed Central PMCID:
816 PMC4199767.
817 43. Brostjan C, Anrather J, Csizmadia V, Natarajan G, Winkler H. Glucocorticoids inhibit E-selectin expression
818 by targeting NF-kappaB and not ATF/c-Jun. J Immunol. 1997;158(8):3836-44. PubMed PMID: 9103451.
819 44. Anrather J, Csizmadia V, Soares MP, Winkler H. Regulation of NF-kappaB RelA phosphorylation and
820 transcriptional activity by p21(ras) and protein kinase Czeta in primary endothelial cells. J Biol Chem.
821 1999;274(19):13594-603. PubMed PMID: 10224130.
822 45. Stevenson PG, May JS, Smith XG, Marques S, Adler H, Koszinowski UH, et al. K3-mediated evasion of
823 CD8(+) T cells aids amplification of a latent gamma-herpesvirus. Nat Immunol. 2002;3(8):733-40. doi:
824 10.1038/ni818. PubMed PMID: 12101398.
825 46. Pires de Miranda M, Alenquer M, Marques S, Rodrigues L, Lopes F, Bustelo XR, et al. The
826 Gammaherpesvirus m2 protein manipulates the Fyn/Vav pathway through a multidocking mechanism of assembly.
827 PloS one. 2008;3(2):e1654. doi: 10.1371/journal.pone.0001654. PubMed PMID: 18301737; PubMed Central
828 PMCID: PMC2244710.
829 47. Godinho-Silva C, Marques S, Fontinha D, Veiga-Fernandes H, Stevenson PG, Simas JP. Defining immune
830 engagement thresholds for in vivo control of virus-driven lymphoproliferation. PLoS Pathog. 2014;10(6):e1004220.
831 doi: 10.1371/journal.ppat.1004220. PubMed PMID: 24967892; PubMed Central PMCID: PMC4072806.

Figure 1

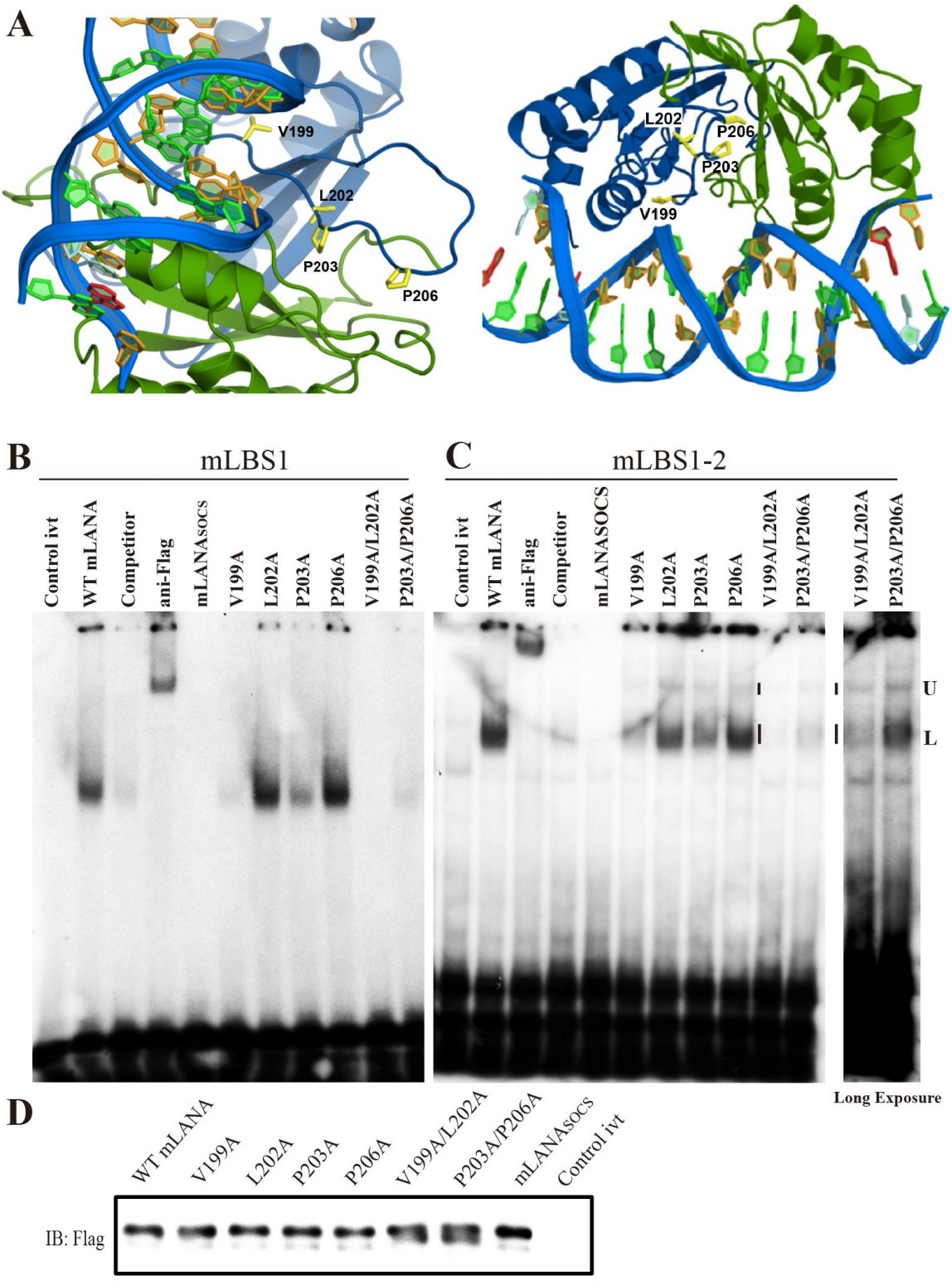
A
V199
L202
P203
P206
L202
P206
P203
V199
B
mLBS1
Control ivt
WT mLANA
Competitor
ani-Flag
mLANAsocs
V199A
L202A
P203A
P206A
V199A/L202A
P203A/P206A
C
mLBS1-2
Control ivt
WT mLANA
ani-Flag
Competitor
mLANASOCS
V199A
L202A
P203A
P206A
V199A/L202A
P203A/P206A
V199A/L202A
P203A/P206A
U
L
Long Exposure
D
WT mLANA
V199A
L202A
P203A
P206A
V199A/L202A
P203A/P206A
mLANAsocs
Control ivt
IB: Flag

Figure 2

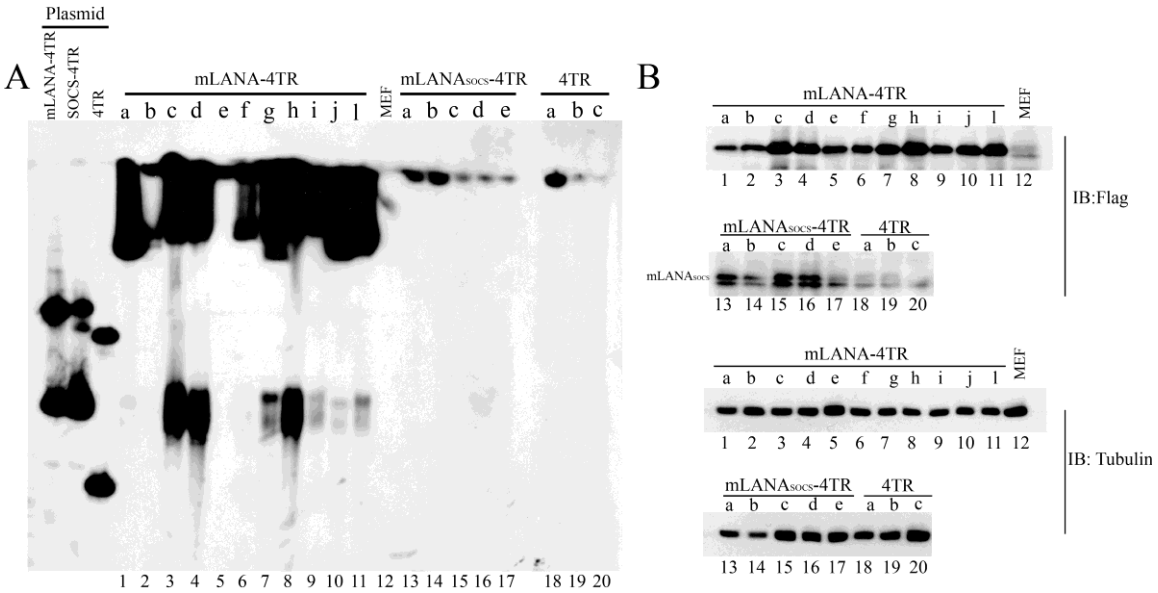
A
Plasmid
mLANA-4TR
SOCS-4TR
4TR
mLANA-4TR
a b c d e f g h i j l
MEF
mLANAsocs-4TR
a b c d e
4TR
a b c
1 2 3 4 5 6 7 8 9 10 11 12 13 14 15 16 17 18 19 20
B
mLANA-4TR
a b c d e f g h i j l MEF
1 2 3 4 5 6 7 8 9 10 11 12
IB:Flag
mLANAsocs-4TR
a b c d e
4TR
a b c
mLANAsocs
13 14 15 16 17 18 19 20
mLANA-4TR
a b c d e f g h i j l MEF
1 2 3 4 5 6 7 8 9 10 11 12
IB: Tubulin
mLANAsocs-4TR
a b c d e
4TR
a b c
13 14 15 16 17 18 19 20

Figure 3

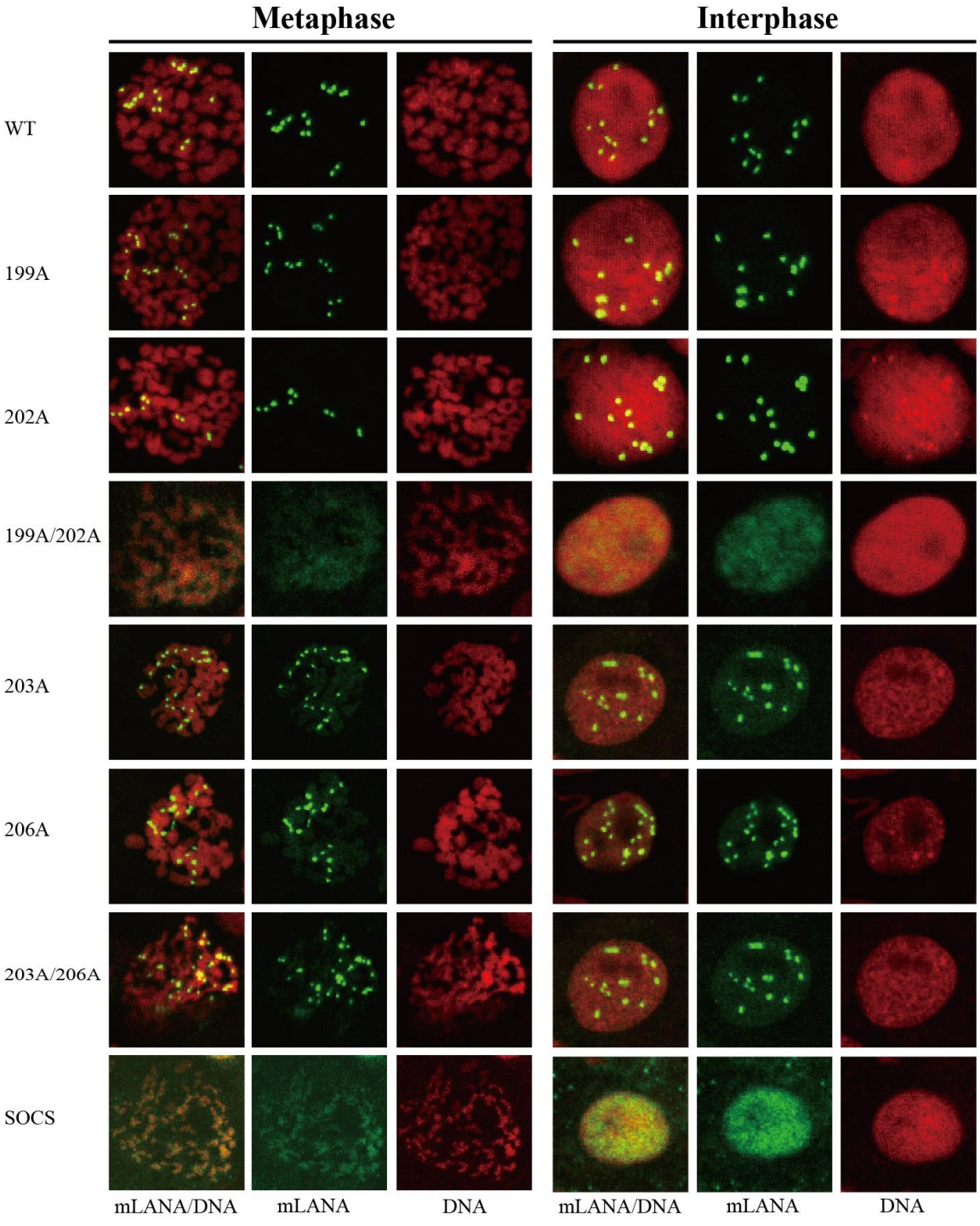
Metaphase
Interphase
WT
199A
202A
199A/202A
203A
206A
203A/206A
SOCS
mLANA/DNA
mLANA
DNA
mLANA/DNA
mLANA
DNA

Figure 4

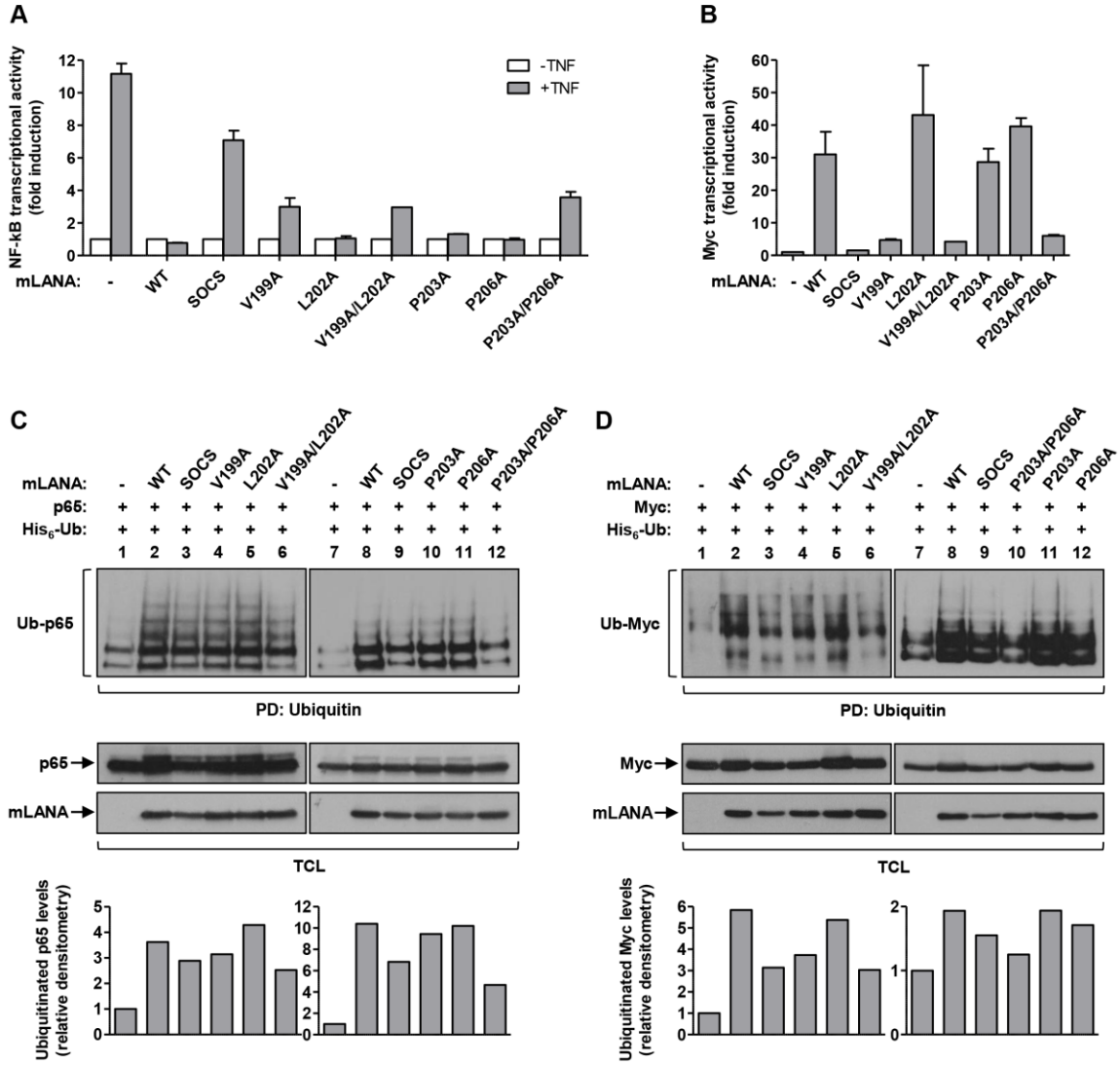
A
NF-kB transcriptional activity (fold induction)
-TNF
+TNF
mLANA: - WT SOCS V199A L202A V199A/L202A P203A P206A P203A/P206A
B
Myc transcriptional activity (fold induction)
mLANA: - WT SOCS V199A L202A V199A/L202A P203A P206A P203A/P206A
C
mLANA: - WT SOCS V199A L202A V199A/L202A - WT SOCS P203A P206A P203A/P206A
p65: + + + + + + + + + + + +
His6-Ub: + + + + + + + + + + + +
1 2 3 4 5 6 7 8 9 10 11 12
Ub-p65
PD: Ubiquitin
p65
mLANA
TCL
Ubiquitinated p65 levels (relative densitometry)
D
mLANA: - WT SOCS V199A L202A V199A/L202A - WT SOCS P203A/P206A P203A P206A
Myc: + + + + + + + + + + + +
His6-Ub: + + + + + + + + + + + +
1 2 3 4 5 6 7 8 9 10 11 12
Ub-Myc
PD: Ubiquitin
Myc
mLANA
TCL
Ubiquitinated Myc levels (relative densitometry)

Figure 5

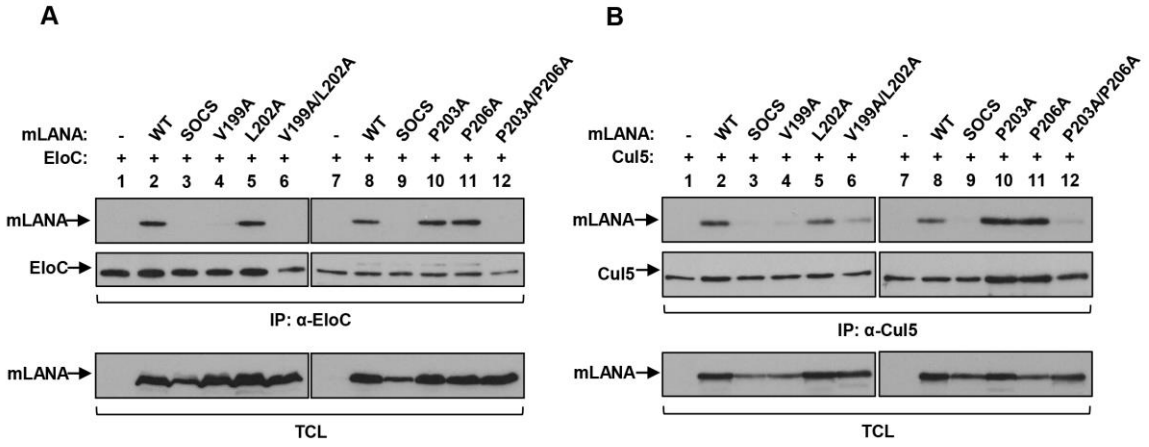
A
mLANA: - WT SOCS V199A L202A V199A/L202A - WT SOCS P203A P206A P203A/P206A
EloC: + + + + + + + + + + + +
1 2 3 4 5 6 7 8 9 10 11 12
mLANA
EloC
IP: α-EloC
mLANA
TCL
B
mLANA: - WT SOCS V199A L202A V199A/L202A - WT SOCS P203A P206A P203A/P206A
Cul5: + + + + + + + + + + + +
1 2 3 4 5 6 7 8 9 10 11 12
mLANA
Cul5
IP: α-Cul5
mLANA
TCL

Figure 6

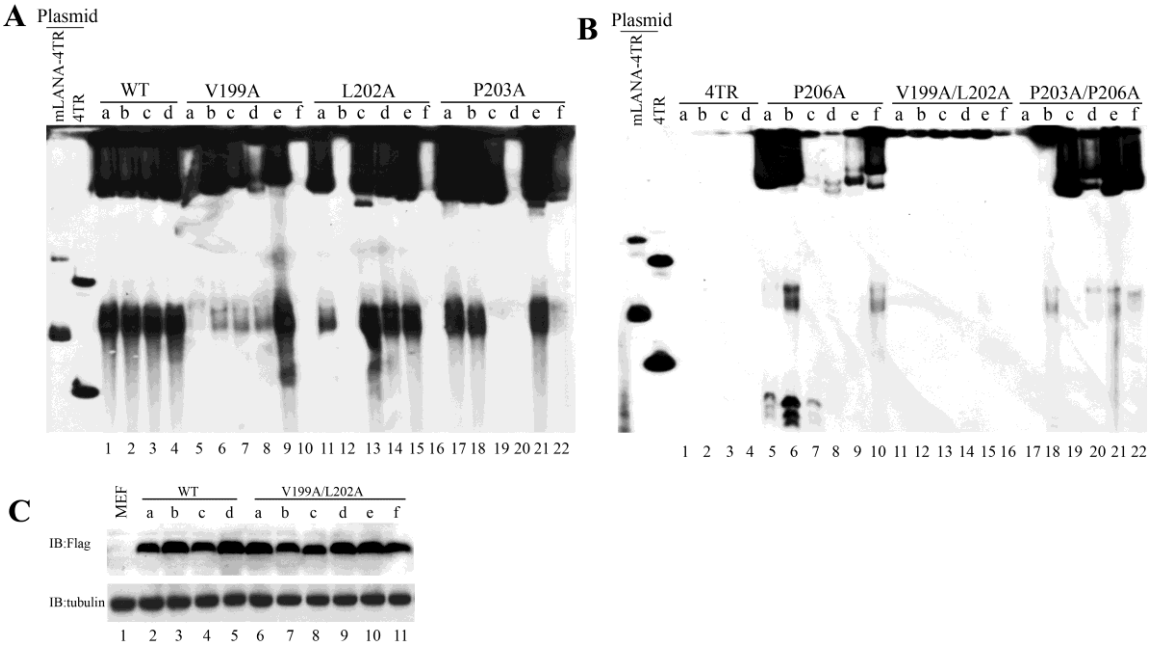
A
Plasmid
mLANA-4TR
4TR
WT
V199A
L202A
P203A
a b c d a b c d e f a b c d e f a b c d e f
1 2 3 4 5 6 7 8 9 10 11 12 13 14 15 16 17 18 19 20 21 22
B
Plasmid
mLANA-4TR
4TR
4TR
P206A
V199A/L202A
P203A/P206A
a b c d a b c d e f a b c d e f a b c d e f
1 2 3 4 5 6 7 8 9 10 11 12 13 14 15 16 17 18 19 20 21 22
C
MEF
WT
V199A/L202A
a b c d a b c d e f
IB:Flag
IB:tubulin
1 2 3 4 5 6 7 8 9 10 11

Figure 7

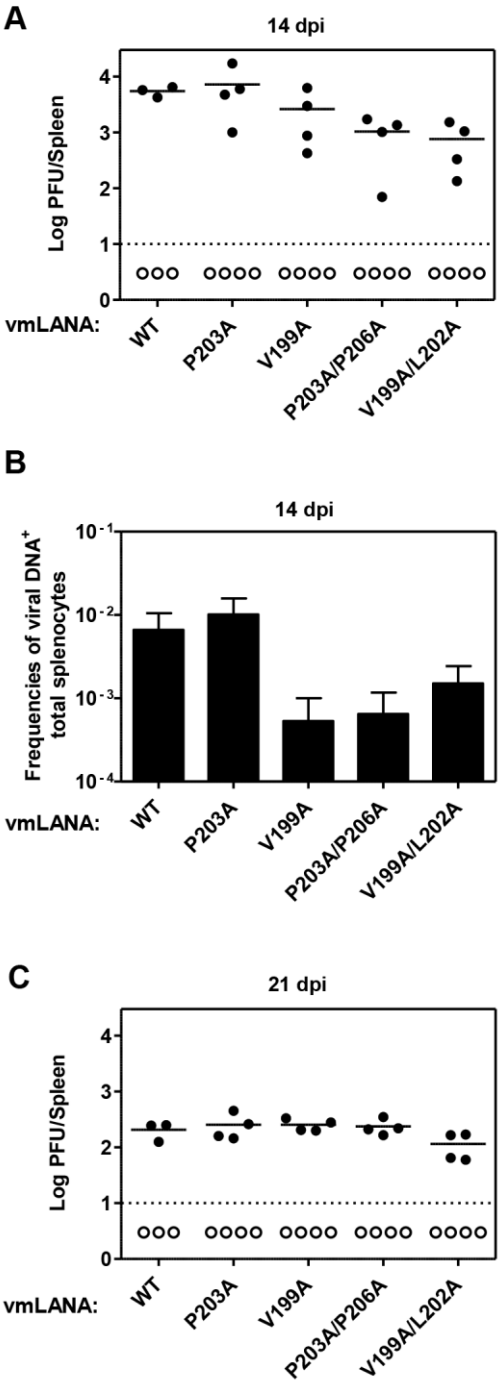
A
14 dpi
Log PFU/Spleen
4
3
2
1
0
vmLANA:
WT
P203A
V199A
P203A/P206A
V199A/L202A
B
14 dpi
Frequencies of viral DNA+ total splenocytes
10-1
10-2
10-3
10-4
vmLANA:
WT
P203A
V199A
P203A/P206A
V199A/L202A
C
21 dpi
Log PFU/Spleen
4
3
2
1
0
vmLANA:
WT
P203A
V199A
P203A/P206A
V199A/L202A

Figure 8

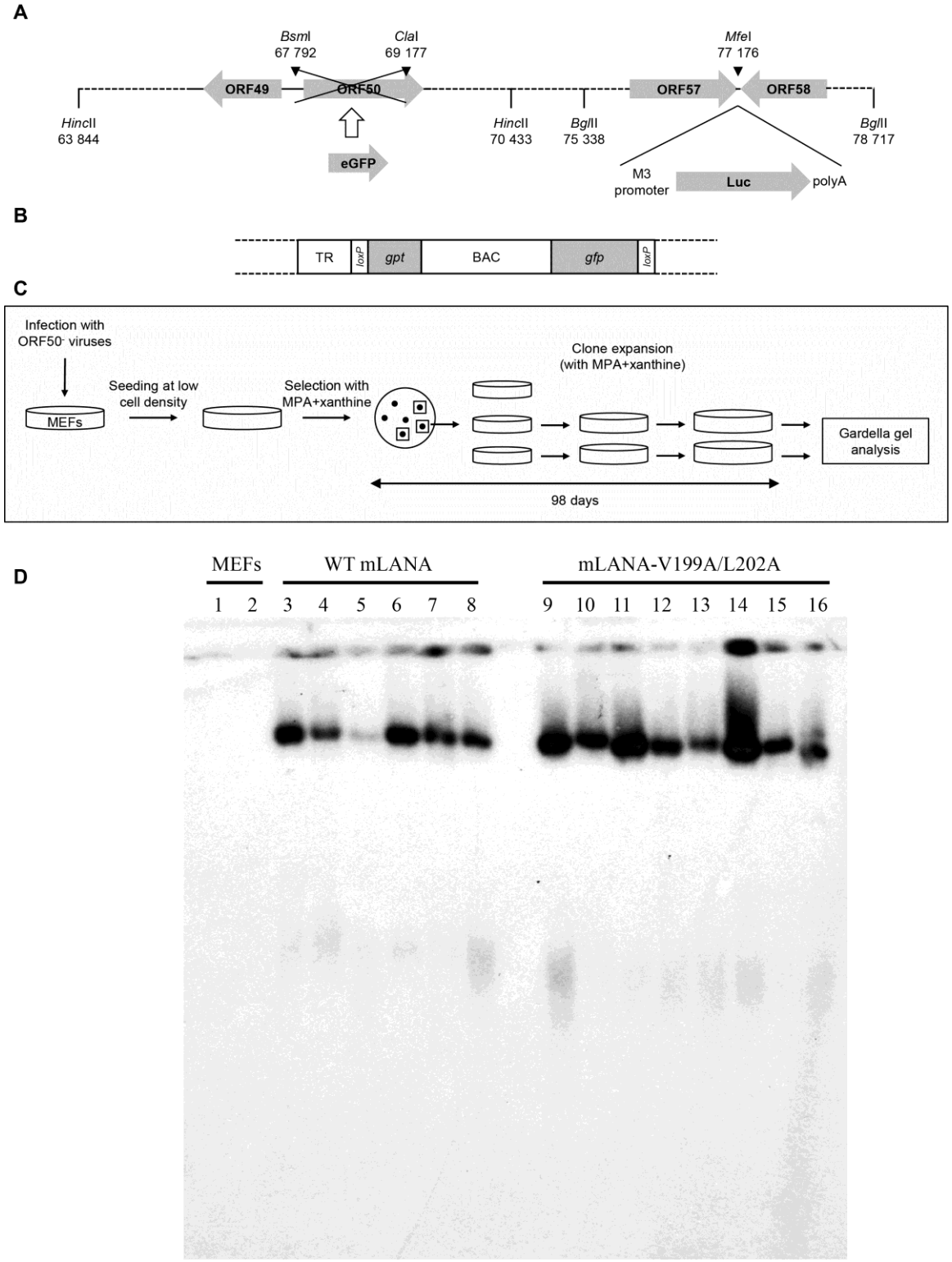
A
BsmI
67 792
ClaI
69 177
MfeI
77 176
ORF49
ORF50
ORF57
ORF58
HincII
63 844
HincII
70 433
BglII
75 338
BglII
78 717
eGFP
M3
promoter
Luc
polyA
B
TR
loxP
gpt
BAC
gfp
loxP
C
Infection with
ORF50- viruses
MEFs
Seeding at low
cell density
Selection with
MPA+xanthine
Clone expansion
(with MPA+xanthine)
Gardella gel
analysis
98 days
D
MEFs
WT mLANA
mLANA-V199A/L202A
1 2 3 4 5 6 7 8 9 10 11 12 13 14 15 16